UNIWERSYTET ŚLĄSKI W KATOWICACH

WYDZIAŁ NAUK PRZYRODNICZYCH

Instytut Nauk o Ziemi

MGR INŻ. KRZYSZTOF KUPCZAK

REKONSTRUKCJA HISTORYCZNYCH (V WIEK P.N.E. - XIX WIEK N.E.) METOD WYTOPU METALI NA TERENIE POLSKI

Rozprawa doktorska

Promotor: prof. dr hab. Aleksandra Gawęda

Promotor pomocniczy: dr Rafał Warchulski, prof. UŚ

SOSNOWIEC 2025

Pragnę wyrazić serdeczne podziękowania
mojej Pani promotor,
prof. dr hab. Aleksandrze Gawędzie, za
nieocenione wsparcie, inspirację i cenne
wskazówki, które były kluczowe na
każdym etapie realizacji niniejszej pracy
doktorskiej.

Szczególne podziękowania kieruję także do
mojego promotora pomocniczego,
dr Rafała Warchulskiego, prof. UŚ,
za wszechstronną pomoc, cierpliwość
i życzliwość, które towarzyszyły mi
w trakcie pracy.

Dziękuje również za wsparcie finansowe udzielone przez Narodowe Centrum Nauki
w ramach grantu PRELUDIUM BIS 1 o numerze 2019/35/O/ST10/00313.

Publikacje wchodzące w skład rozprawy doktorskiej:

- Warchulski, R., Szczuka, M., Kupczak, K. 2020. Reconstruction of 16th–17th century lead smelting processes on the basis of slag properties: A case study from Sławków, Poland. Minerals, 10(11), 1039. DOI: 10.3390/min10111039. 100 pkt MNiSW.
- Kupczak, K., Warchulski, R., Gawęda, A. 2023. Reconstruction of smelting conditions during 16th-to 18th-century copper ore processing in the Kielce region (Old Polish Industrial District) based on slags from Miedziana Góra, Poland. Archaeometry, 65(3), 547-569. DOI: 10.1111/arcm.12837. 200 pkt MNiSW.
- Warchulski, R., Kupczak, K., Gawęda, A., Sitko, R. 2022. Complete reconstruction of the process and conditions during gold smelting in the 15th–17th centuries in Złoty Stok based on metallurgical slags. Archaeometry, 64(4), 916-934. DOI: 10.1111/arcm.12752. 200 pkt MNiSW.
- Kupczak, K., Warchulski, R., Gawęda, A., Janiec, J. 2024. Bloomery iron production in the Holy Cross Mountains (Poland) area during the Roman period: conditions during the metallurgical process and their uniformity between locations. Heritage Science, 12(1), 147. DOI: 10.1186/s40494-024-01266-6. 140 pkt MNiSW.
- Kupczak, K., Warchulski, R., Gawęda, A., Ślęzak, M., Migas, P. 2024. The use of predominance area diagrams (PAD) to determine the oxygen and sulfur fugacities prevailing during historical metallurgical processes: the case of fifteenth to seventeenth century copper slags from Polichno (Old Polish industrial district). Heritage Science, 12(1), 49. DOI: 10.1186/s40494-024-01171-y. 140 pkt MNiSW.
- Kupczak, K., Warchulski, R., Dulski, M., Środek, D. 2020. Chemical and phase reactions on the contact between refractory materials and slags, a case from the 19th century Zn-Pb smelter in Ruda Śląska, Poland. Minerals, 10(11), 1006. DOI: 10.3390/min10111006. 100 pkt MNiSW.
- Kupczak, K., Warchulski, R. 2024. SLAG—software for reconstruction of historical smelting processes based on slag properties. Archaeometry. 66(4), 803-823. DOI: 10.1111/arcm.12940. 200 pkt MNiSW.

Streszczenie w języku angielskim

The study focuses on reconstructing historical metal production techniques in the area of present-day Poland, where the earliest evidence of metallurgy dates to the turn of the Common Era. While there are numerous records documenting past metallurgical activities, considerable gaps persist in our understanding of the specific conditions and methods employed in metal smelting. The primary goal of this research was to employ advanced geochemical (ICP-MS/OES, XRF), mineralogical (SEM, EPMA, XRD), and experimental methods to analyze smelting conditions, enabling the reconstruction of historical metallurgical techniques. Key aspects of the research included determining smelting temperatures, melt viscosity, oxygen fugacity, and in some cases cooling rates, sulfur fugacity and reactions occurring in smelting furnaces. The research was conducted based on the slags from Sławków (Pb), Miedziana Góra (Cu), Złoty Stok (Au), Bloomery Fe production (in the Holy Cross Mountains), Polichno (Cu), and Ruda Śląska (Zn).

Metallurgical activities in Sławków took place during the 16th and 17th centuries, using Mississippi Valley types ores, containing Pb and Zn sulfides. Slags from Sławków were composed mainly of SiO_2 (26,18-46,50 wt.%), CaO (4,48-30,39 wt.%), and Fe_2O_3 (9,81-22,83 wt.%) with high concentrations of Pb (>10 wt.%) and Zn (up to 21 wt.%). In terms of phase composition, slags contained mainly glass, augite $(Ca,Mg,Fe)(Mg,Fe)Si_2O_6$), willemite (Zn_2SiO_4), melilite ($Ca_2M(XSiO_7)$), olivine ($(Mg,Fe)_2SiO_4$), wollastonite ($CaSiO_3$), quartz (SiO_2), wüstite (FeO), K-feldspar ($K(AlSi_3O_8)$, lead oxide (PbO), cerussite ($PbCO_3$), galena (PbS), and Zn sulfides. Experimental studies revealed the liquidus temperature of slags was at least 1150°C, with a solidus range of 900-1000°C. Oxygen fugacity (logP O_2) was determined using mineral buffers, indicating values between −4.5 and −12 atm. Viscosity calculations showed a viscosity (logη) ranging from 1.34 to 1.48 Pa·s.

Copper production in Miedziana Góra (Holy Cross Mountains) was conducted from the 16th to the 18th century, utilizing local deposits, including chalcopyrite ($CuFeS_2$), chalcocite (Cu_2S), bornite (Cu_5FeS_4), and tetrahedrite ($[Cu,Fe]_{12}Sb_4S_{13}$). Chemically, the analyzed slags primarily contained SiO_2 (49.81-57.14 wt.%), CaO (11.25-21.64 wt.%), FeO (8.42-11.03 wt.%), and Al_2O_3 (7.54-9.14 wt.%). The slags also contained Pb (0.50-5.91 wt.%) and Cu (0.40-4.98 wt.%). Phase composition analysis showed that slags were mainly composed of glass, SiO_2 polymorphs, wollastonite, anorthite ($Ca(Al_2Si_2O_8)$), metallic Cu, lead oxides (PbO), clinopyroxene, Cu

sulfides/arsenides, The liquidus temperature of the slag was from 1150-1200 °C, while solidus temperature was around 1100 °C. The viscosity of the metallurgical melt (logη) was from 1.19 to 4.42 Pa·s. The smelting process in Miedziana Góra took place under oxygen fugacity conditions (logP O_2) ranging from -4 to -12 atm.

Gold smelting in Złoty Stok occurred during the 16th-17th centuries based on ore mineralization found in pyroxenites, amphibolites, serpentinites, dolomitic marls, and limestone-silica rocks. The most important gold-bearing minerals in the deposit were löllingite ($FeAs_2$) and arsenopyrite (FeAsS). The slags were characterized by a chemical composition dominated by SiO_2 (52.12-56.60 wt.%), MgO (7.43-18.36 wt.%), CaO (10.84-15.19 wt.%), and FeO (9.08-15.36 wt.%). The phase composition of the slags showed the presence of olivine, pyroxene, glass, sulfides, and Fe arsenides. The liquidus temperature was determined to be between 1300-1350 °C, while the solidus temperature was approximately 1200 °C. The cooling rate of slags was from 5 to 300 °C/h. Melt viscosity (logη) at 1350 °C ranged from 0.26 to 0.90 Pa·s. It was found that the smelting process occurred under oxygen fugacity conditions (log P O_2) in the range of −10.5 to −11.5 atm.

The research on bloomery iron production focused on comparing smelting conditions across different locations (Suchedniów, Skarżysko-Kamienna, and Starachowice) in the Holy Cross Mountains. The analyzed slags primarily consisted of FeO (43.97-75.32 wt.%) and SiO_2 (18.04-47.14 wt.%). The dominant phases in the slags included olivine, wüstite, spinel from the magnetite ($Fe^{2+}Fe^{3+}{}_2O_4$)-hercynite ($Fe^{2+}Al_2O_4$) series, and leucite ($KAlSi_2O_6$). Isotopic dating confirmed the ancient (196 BC–4 AD) age of slags. The liquidus temperature of slags was from 1150 to 1200 °C and the cooling rate was 5-300 °C/h. The viscosity of the melt was from 0.15 to 1.02 Pa·s. The maximum oxygen fugacity (logP O_2) during smelting ranged from -12.53 to -13.20 atm.

The analysis of slags from Polichno (Holy Cross Mountains) were focused on applying a more precise method for determining the oxygen fugacity during smelting. The chemical composition of the analyzed slags mainly consisted of SiO_2 (34.88-49.69 wt.%), FeO (12.62-17.71 wt.%), and CaO (12.57-29.95 wt.%). The most important phases observed in slags were: glass (containing PbO and ZnO), wollastonite, calcite ($CaCO_3$), SiO_2 polymorphs, clinopyroxene, barite ($BaSO_4$), cerussite, metallic Cu and Fe, chalcocite (Cu_2S), Cu arsenides, Pb and Fe oxide, pyrrhotite ($Fe_{1-x}S$), and galena. The liquidus temperature of the slags ranged from 1100 to 1200 °C, while the solidus

temperature fell between 800 and 1100 °C. Based on thermodynamic calculations the oxygen and sulfur fugacities during slag formation were determined. The slags from Polichno were formed under an oxygen fugacity range of logP O_2 = −4.30 to −14.08 atm., and the sulfur fugacity during slag formation ranged from logP S_2 = −2.50 to −6.92 atm.

The study of slags from Ruda Śląska were focused on the chemical and phase reactions in the contact between the metallurgical melt and the refractory materials. Analysis showed that the slags consisted mainly of SiO_2 (38.17 wt.%), Fe_2O_3 (22.71 wt%), Al_2O_3 (15.81 wt.%), and CaO (10.56 wt.%). The refractory material was primarily composed of SiO_2 (65.70 wt.%) and Al_2O_3 (29.08 wt.%). Phase analysis of the slags revealed the presence of feldspar, clinopyroxene, melilite, spinel, and zincite (ZnO). The refractory materials were dominated by mullite ($3Al_2O_3 \cdot 2SiO_2$) and SiO_2 polymorphs. Microscopic observations revealed the presence of K-feldspars enriched in Pb and Ba, glass with high As and Pb content, and alumohematite ($(Fe,Al)_2O_3$) in the contact zone. The first type of reactions involved reactions between the gaseous/fluidal phases and the refractory material, where some components of the metallurgical charge (PbO, K, As, Zn, and Na_2O) migrated in the gaseous (or fluid) form into the refractory material. The second type of reaction involved reactions between the liquid melt and the refractory material. In this process, certain components of the charge (primarily PbO_2, As_2O_3, FeO, and ZnO) moved toward the bottom of the retort. As a result, K-feldspar with Pb substitutions, Fe-rich pyroxene, and glass containing As_2O_3 and PbO formed in the contact zone.

A notable component of the dissertation involved developing methodological approaches for reconstructing historical metallurgical processes. This included creating dedicated software (SLAG) for modeling the basic smelting parameters. The software allows for the determination of liquidus temperature, slag viscosity, and oxygen and sulfur fugacities during smelting. The main goal in developing software was to enable individuals without specialized knowledge in thermodynamics and rheological studies to reconstruct smelting processes.

Komentarz wprowadzający w tematykę rozprawy doktorskiej

1. Wstęp

Hutnictwo od wieków odgrywa kluczową rolę w rozwoju cywilizacji, będąc fundamentem postępu technologicznego i gospodarczego. Umiejętność produkcji metali była na tyle istotna dla rozwoju ludzkości, że podział prehistorii na epoki został dokonany na podstawie przełomów w metalurgii (epoka miedzi, brązu, żelaza; Tylecote, 1992; Milisauskas, 2011). Początkowo przedmioty wykonane z metalu najczęściej wykorzystywane były do produkcji ozdób oraz w celach religijnych (Leusch i inni, 2015; Alconini i Covey, 2018; Napierała, 2022). Wyjątkowe właściwości otrzymywanych metali jak np. wytrzymałość i plastyczność umożliwiły wykorzystanie ich do produkcji przedmiotów użytecznych (m.in. narzędzi i broni). Wprowadzanie do gospodarki wyrobów metalowych oraz umiejętność łączenia różnych metali w stopy znacząco podnosiło poziom rozwoju społeczeństw (Tylecote, 1992; Milisauskas, 2011).

Na ziemiach polskich występuje szeroki zakres rud wykorzystywanych w przeszłości do produkcji metali. Były one eksploatowane w różnych epokach historycznych, świadcząc o bogatej tradycji hutniczej i innowacyjności technologicznej naszych przodków (Orzechowski, 2018; Warchulski i inni, 2022; Kupczak i inni, 2023). Historyczna produkcja hutnicza na terenie obecnej Polski obejmowała głównie metale takie jak żelazo, ołów, miedź, cynk, srebro oraz złoto (Bielenin, 1992; Rozmus, 2014; Derkowska i inni, 2021; Warchulski i inni 2020, 2022; Kupczak i inni, 2020, 2023, 2024a). Produkcja żelaza prowadzona była co najmniej od okresu wpływów rzymskich (od początku naszej ery do 4 w. n.e). m.in. na terenie Gór Świętokrzyskich, Mazowsza i Śląska (Orzechowski, 2018). Ołów, srebro i cynk wytapiane były przede wszystkim na obszarze Śląsko-Krakowskim. Początkowo produkcja opierała się jedynie na wytopie ołowiu i srebra i prowadzona była najprawdopodobniej od XI wieku (Rozmus, 2014). Hutnictwo cynku rozwinęło się dopiero od przełomu wieków XVIII i XIX, wraz z wynalezieniem przez Jana Ruberga metody produkcji metalicznego cynku (Dębicki, 1927). W mniejszym stopniu ołów i srebro wytapiane były z wykorzystaniem złóż znajdujących się w Górach Świętokrzyskich (Wróblewski, 2014). Historyczna produkcja miedzi prowadzona była na obszarze Gór Świętokrzyskich oraz na Dolnym Śląsku i mogła być prowadzona już od XIII wieku (Derkowska i inni, 2021). Na Dolnym Śląsku co najmniej od XIII wieku prowadzono również prace hutnicze w celu wytopu złota (Dziekoński, 1972).

Pomimo tak istotnego znaczenia hutnictwa dla rozwoju ludzkości w większości przypadków informacje o przebiegu i warunkach panujących podczas procesu produkcji metali w czasach historycznych są słabo dostępne. Przeważnie jedynymi pozostałościami po dawnych pracach hutniczych są żużle, które jako materiał odpadowy były składowane w pobliżu hut (np. Kupczak i inni, 2023). Obecnie, wykorzystując metody analityczne, możemy na ich podstawie odtworzyć schemat przebiegu wytopu oraz warunki, w jakich był on prowadzony (Derkowska i inni, 2021). Niestety, od czasów historycznych po współczesność żużle stanowiły atrakcyjny materiał do ponownej przeróbki lub wykorzystania jako materiał budowlany (Potysz i inni, 2018; Wowkonowicz i inni, 2018). Z tego względu rozliczne stanowiska składowania historycznych żużli hutniczych zostały zniszczone (Kowalczewski i Szczecińska, 1977; Bielenin, 1992). Możliwość komercyjnego wykorzystania historycznych żużli hutniczych jest przedmiotem stale rosnącego zainteresowania badaczy również współcześnie (Ettler i inni, 2020; Kuhn i inni, 2022). Z tego powodu istnieje ryzyko, że z biegiem lat kolejne pozostałości po dawnych procesach hutniczych zostaną utracone. W związku z tym przeprowadzenie szczegółowych badań dotyczących metod produkcji metali, które w tak znacznym stopniu przyczyniły się do rozwoju naszego społeczeństwa, staje się pilnym problemem.

Głównym celem pracy było odtworzenie historycznych metod wytopu metali na terenie obecnej Polski. Cel ten został zrealizowany poprzez:

- odtworzenie schematu przebiegu procesu hutniczego oraz stosowanych technik wytopu;
- określenie podstawowych parametrów wytopu jak;
  - temperatura wytopu – uwzględniając temperaturę likwidusu (minimalną temperaturę, w której wszystkie składniki ulegają przetopieniu) i solidusu (temperaturę, w której rozpoczyna się topienie);
  - lepkość stopu hutniczego;
  - lotność tlenu;
  - prędkość chłodzenia stopu;
- opracowanie graficznych rekonstrukcji urządzeń wykorzystywanych w przeszłości.

Dodatkowym celem pracy było określenie reakcji zachodzących w piecu hutniczym podczas produkcji Zn oraz opracowanie nowych rozwiązań metodycznych, ułatwiających prowadzenie rekonstrukcji historycznych procesów hutniczych w przyszłości. Cel ten został osiągnięty poprzez:

- określenie reakcji chemicznych i fazowych zachodzących pomiędzy stopem a materiałami ogniotrwałymi;
- udoskonalenie metody określania lotności tlenu oraz zaproponowanie metody określania lotności siarki podczas wytopu;
- stworzenie oprogramowania, które umożliwi określanie podstawowych parametrów wytopu na podstawie obliczeń termodynamicznych oraz tworzonych diagramów.

Lokalizacje objęte badaniami zostały dobrane tak, aby uwzględniały maksymalne zróżnicowanie czasowe (zakres wieków) oraz rodzaj produkowanego metalu. W tym celu zdecydowano się przeanalizować żużle z następujących lokalizacji (Rys. 1):

- obszar Gór Świętokrzyskich – hutnictwo żelaza w okresie wpływów rzymskich (od II w. p.n.e do IV w. n.e.; Kupczak i inni, 2024b);
- Złoty Stok – hutnictwo złota prowadzone od XV do XVII wieku (Warchulski i inni, 2022);
- Miedziana Góra oraz Polichno – hutnictwo miedzi (XV-XVIII wiek; Kupczak i inni, 2023, 2024a);
- Sławków – hutnictwo ołowiu w okresie od XVI do XVII wieku (Warchulski i inni, 2020);
- Ruda Śląska – hutnictwo cynku w XIX wieku (Kupczak i inni, 2020).

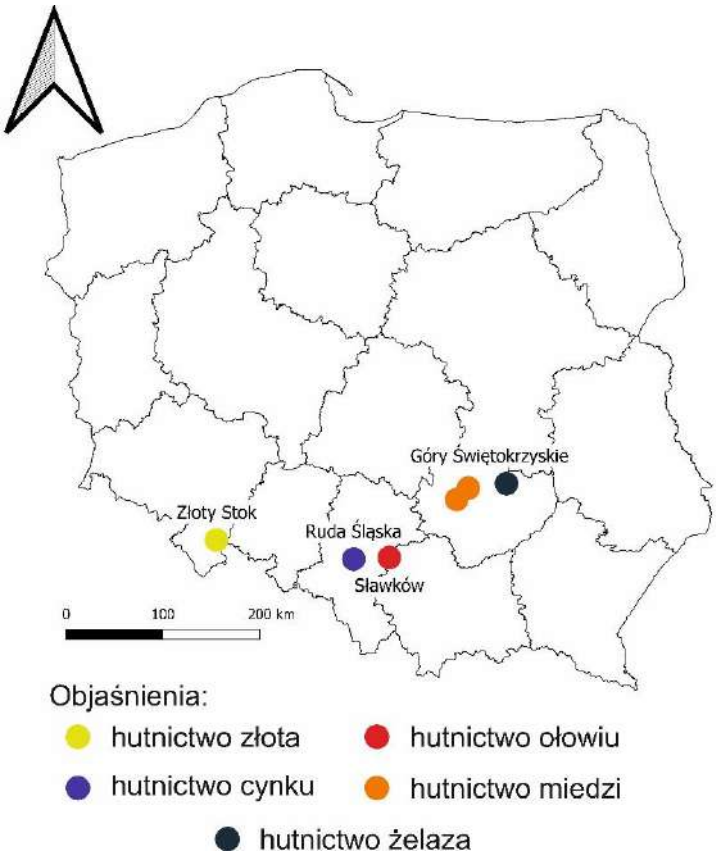

Rysunek 1 Mapa lokalizacyjna miejsc poboru prób

W każdej z analizowanych lokalizacji położono nacisk na różne aspekty procesu hutniczego, co wynikało z dostępności danych historycznych oraz specyfiki badanych materiałów:

- w Miedzianej Górze i Sławkowie ze względu na brak szczegółowych informacji o procesach produkcyjnych, analiza żużli miała na celu kompleksową rekonstrukcję procesów hutniczych;
- w Złotym Stoku proces produkcji był już opisany w literaturze (np. Dziekoński, 1972), dlatego badania żużli koncentrowały się na pełnej charakterystyce chemicznej i fazowej materiału i na tej podstawie korekty tych opisów oraz ich uzupełnieniu o nowe szczegóły;
- w Polichnie analizy żużli skupiały się na zaproponowaniu metody wykorzystania diagramów obszarów przewagi (Predominance Area Diagrams – PAD) w celu określenia lotności gazowych składników procesu hutniczego, takich jak tlen i siarka;
- w Rudzie Śląskiej ze względu na dostępność szczegółowych opisów procesów produkcyjnych (np. Domański i Krupkowski, 1954), analizy żużli skupiły się na określeniu w jaki sposób w żużlach powstawały fazy wzbogacone w metale i metaloidy, w tym nietypowe fazy arsenowo-ołowiowe;
- żużle z dymarkowej produkcji żelaza zostały zbadane pod kątem oceny jednolitości procesu pomiędzy różnymi lokalizacjami na terenie Gór Świętokrzyskich.

2. Dotychczasowy stan wiedzy

2.1. Techniki odtwarzania historycznych procesów hutniczych

Badania dotyczące hutnictwa w czasach historycznych są prowadzone w wielu miejscach na świecie, wykorzystując dane historyczne, archeologiczne oraz nowoczesne metody analityczne (np. Maldonado i Rehren, 2009; Thondhlana i inni, 2016; Xiao i inni, 2021). Badania historyczne i archeologiczne skupiają się zwykle na aspektach gospodarczych oraz społecznych (Orzechowski, 2018). Z kolei metody analityczne są wykorzystywane do badań nad technicznymi aspektami procesu produkcji metali (np. Xiao i inni, 2021). Wykorzystanie metod analitycznych pozwala uzyskać informacje o składzie fazowym i chemicznym (w tym izotopowym) pozostałości po dawnych procesach hutniczych. W tym celu najczęściej wykorzystuje się żużle hutnicze, ponieważ ich własności są silnie powiązane z warunkami, w jakich prowadzono wytop (np. Derkowska i inni, 2021; Xiao i inni, 2021).

Najważniejszymi parametrami określanymi podczas rekonstrukcji historycznych procesów hutniczych są temperatura wytopu, lepkość stopu hutniczego, lotność tlenu oraz w niektórych przypadkach prędkość chłodzenia stopu krzemianowego (Ettler i inni, 2009; Kądziołka i inni, 2020; Derkowska i inni, 2021). Temperatura wytopu jest najważniejszym czynnikiem, jaki należy wziąć pod uwagę, analizując dawne metody hutnicze. Wynika to z faktu, że jedynie w odpowiednio wysokiej temperaturze możliwe jest przetopienie materiału wsadowego, z którego ma być oddzielona faza metaliczna, jednocześnie warunki temperaturowe wpływają na pozostałe wymienione parametry (Barin, 1993; Davenport i inni, 2002). Do określenia temperatury wytopu najczęściej wykorzystuje się temperaturę likwidusu żużli hutniczych (Kądziołka i inni, 2020). W dotychczasowych badaniach m.in. w Capattoli Valley (Włochy; Manasse i inni, 2001), Itziparátzico (Meksyk; Maldonado i Rehren, 2009) i Shankare Hill (Południowa Afryka; Thondhlana i inni, 2016) do jej określenia wykorzystywano diagramy fazowe. Dostępne diagramy fazowe są jednak najczęściej ograniczone do układów 2-4 składnikowych przez co stosowanie ich w przypadku skomplikowanych pod względem składu chemicznego żużli hutniczych może być obarczone dużym błędem. Temperatura likwidusu może być również określana za pomocą oprogramowania komputerowego (np. MELTS-Rhyolite), które zostało wykorzystane m.in. podczas analiz hutnictwa Cu w Sudetach (Kądziołka i inni, 2020). Ograniczenia oprogramowania MELTS-Rhyolite wiążą się z faktem, że zostało ono zaprojektowane do analiz skał

naturalnych, o wyższej zawartości krzemionki, co znacząco ogranicza możliwość ich zastosowania w przypadku żużli hutniczych, w których zawartość Cu, Zn, Pb może dochodzić do kilkudziesięciu procent (Potysz i inni, 2015).

Alternatywną metodą oceny warunków temperaturowych są geotermometry, które mogą być wykorzystane do określenia temperatury krystalizacji poszczególnych faz. Geotermometry były dotychczas stosowane do określenia warunków temperaturowych podczas analiz żużli po produkcji m.in. Cu z Misérègne (Włochy; Toffolo i inni, 2018) oraz Zn-Pb na Górnym Śląsku (Warchulski, 2016). Zastosowanie geotermometrów jest jednak ograniczone jedynie do faz, dla których zostały one opracowane (np. oliwiny, pirokseny, skalenie; Warchulski, 2016). Skuteczne zastosowanie geotermometrów wymaga również wysokiej znajomości petrologicznej badanego materiału. W przypadku historycznych żużli hutniczych często mamy do czynienia z materiałem szklistym, w którym występują jedynie fazy metaliczne (np. Derkowska i inni, 2021), co wówczas wyklucza możliwość ich zastosowania.

Z termodynamicznego punktu widzenia, im wyższa temperatura, tym efektywniej można prowadzić wytop (Ettler i inni, 2009; Kekkonen i inni, 2012). Należy jednak pamiętać, że wyższa temperatura znacząco wpływała na koszt produkcji. Z tego powodu w czasach historycznych hutnicy manipulowali składem chemicznym wsadu hutniczego poprzez dodawanie topników, tak aby możliwe było efektywne oddzielenie pożądanego metalu w możliwie najniższej temperaturze (Davenport i inni, 2002).

Lepkość stopu hutniczego jest kolejnym parametrem wpływającym na proces wytopu. Im niższa, tym łatwiej dochodzi do oddzielenia się fazy metalicznej (lub półproduktów) od stopu krzemianowego (Davenport i inni, 2002; Ettler i inni, 2009). Lepkość stopu jest uzależniona od składu chemicznego oraz warunków temperaturowych (Seetharaman i inni, 2005; Persikov i Bukhtiyarov, 2020). Pod względem składu chemicznego na lepkość wpływa wielkość jonów oraz oddziaływania elektrostatyczne (Kekkonen i inni, 2012). Niektóre tlenki występujące w żużlach (SiO_2, P_2O_5) ze względu na kowalencyjny charakter wiązania pomiędzy metalem a tlenem prowadzą do zwiększania lepkości stopu (Giordano i inni, 2006; Kekkonen i inni, 2012). W hutnictwie lepkość stopu może zostać obniżona poprzez dodanie do wsadu hutniczego składników modyfikujących sieć krystaliczną (np. K_2O, Na_2O, MnO, FeO, MgO, CaO; Giordano i inni, 2006; Kekkonen i inni, 2012). W żużlach hutniczych obserwuje się również składniki amfoteryczne, które mogą w zależności od konkretnego przypadku

zwiększać lub zmniejszać lepkość stopu (Al_2O_3, Fe_2O_3; Kekkonen i inni, 2012). Lepkość historycznych żużli hutniczych może być określona za pomocą indeksu lepkości zaproponowanego przez Bachmanna (1982) jak to miało miejsce w przypadku m.in. żużli po produkcji żelaza w Sarnena Sredna Gora (Bułgaria; Kostova i inni, 2023). W przypadku indeksu lepkości im wyższa wartość tym mniejsza lepkość stopu. Ta metoda jest jednak ograniczona, ponieważ uwzględnia jedynie stosunek składników budujących sieć krystaliczną do składników ją modyfikujących, pomijając wpływ warunków temperaturowych. Lepszym rozwiązaniem jest zastosowanie modelu zaproponowanego przez Giordano i współpracowników (2006), który został wykorzystany podczas analiz żużli po produkcji Pb-Ag w Bohutín (Czechy; Ettler i inni, 2009) lub modelu opracowanego przez Bachmanna i współpracowników (1989) zastosowanego podczas analiz żużli po produkcji Cu w Luserna (Włochy; Addis i inni, 2016). W przypadku modelu Giordano i inni (2006) ograniczeniem jest skład chemiczny żużli, ponieważ model był zaprojektowany dla skał naturalnych. W literaturze dostępne są również inne modele, które mogą być wykorzystane podczas analiz lepkości. Projektowane są one na podstawie analiz reologicznych materiałów o składzie chemicznym mieszczącym się w określonym zakresie (Zhang i Reddy, 2002; Mantha i Reddy, 2005; Giordano i inni, 2006, 2008) a wpływ temperatury uwzględnia się, wykorzystując zależność przedstawioną równaniem Arrheniusa (Persikov i Bukhtiyarov, 2020):

$$\eta = n_0 \exp\left(\frac{E}{RT}\right)$$

Gdzie: η – lepkość; E – energia aktywacji; R – stała gazowa; T – temperatura; n_0 – czynnik przedwykładniczy. W ostatnich latach pojawiają się również modele uwzględniające właściwości strukturalne stopów (Giordano i Russell, 2018; Persikov i Bukhtiyarov, 2020), jednak nie są one stosowane do historycznych żużli hutniczych.

Istotnym czynnikiem wpływającym na możliwość produkcji metali jest lotność tlenu panująca podczas wytopu. Jedynie przy odpowiednio redukcyjnym środowisku możliwa jest redukcja tlenków do formy metalicznej (Davenport i inni, 2002; Bassiakos i Catapotis, 2006; Addis i inni, 2016; Derkowska i inni, 2021). W dotychczasowych badaniach warunki utleniająco redukcyjne były najczęściej określane z wykorzystaniem buforów mineralnych np. podczas analiz żużli po produkcji Pb-Ag w Rio Tinto (Hiszpania; Anguilano, 2012) oraz Cu w Val Malenco (Włochy; Giacometti, i inni, 2014).

Jednak ze względu na fakt, że są one projektowane dla skał naturalnych i uwzględniają jedynie fazy zawierające żelazo precyzja z jaką można określić lotność tlenu jest ograniczona. W przypadku historycznej produkcji niektórych metali (Cu, Au) ważne było również utrzymywanie odpowiednio wysokiej lotności siarki lub arsenu. Ich wysoka lotność umożliwiała tworzenie w początkowych etapach procesu stopu siarczkowego (matte) lub arsenkowego (speiss), który kumulował w sobie pożądany metal. Następnie matte i speiss w kolejnym kroku technologicznym były ponownie przetapiane aby otrzymać produkt końcowy (Davenport i inni, 2002; Davis, 2001).

Bazując na właściwościach żużla możliwe jest również określenie prędkości chłodzenia stopu hutniczego, która może być oszacowana na podstawie pokroju faz występujących w żużlach. Tego typu analizy były wykonywane m.in. dla żużli po produkcji Fe ze stanowiska archeologicznego Oiola (Hiszpania; Portillo-Blanco i inni, 2020) oraz dla żużli po produkcji Pb-Ag w Bohutín (Czechy; Ettler i inni, 2009). Niestety w związku z tym, że dane dotyczące morfologii faz i prędkości chłodzenia są dostępne jedynie dla oliwinów metoda ta jest ograniczona jedynie do żużli zawierających te fazy (Warchulski, 2016).

2.2. Dotychczasowe badania nad historycznym hutnictwem w Polsce

Badania nad historią działalności hutniczej w Polsce sięgają co najmniej XVI-XVII wieku. Do pierwszych badaczy zajmujących się polskim hutnictwem należeli Walenty Roździeński, Stanisław Staszic i Hieronim Łabędzki (Roździeński, 1612; Staszic, 1815; Łabęcki, 1841). Praca Walentego Roździeńskiego (1612) dotyczyła hutnictwa żelaza, a prowadzone w XIX wieku badania skupiały się głównie na opisie występowania rud i zakładów hutniczych (Staszic, 1815). W XX wieku prace dotyczące historycznego hutnictwa były prowadzone na szerszą skalę i obejmowały zarówno historyczne hutnictwo żelaza, jak i wytop innych metali (Dębicki, 1927; Radwan, 1956; Dziekoński, 1972; Kowalczewski i Szczecińska, 1977; Bielenin, 1992; Paulewicz, 1992). Badania prowadzone w XX wieku obejmowały analizę dokumentów historycznych, inwentaryzację stanowisk hutniczych i eksperymentalne próby rekonstrukcji procesów hutniczych (Radwan, 1956; Dziekoński, 1972; Kowalczewski i Szczecińska, 1977). Część badań obejmowała także analizę składu chemicznego żużli oraz określenie temperatury wytopu (Kowalczewski i Szczecińska, 1977; Bielenin, 1992).

Najbardziej zaawansowane badania były prowadzone nad żużlami pochodzącymi z okresu wpływów rzymskich. Badaniami nad dymarkowym hutnictwem w Górach Świętokrzyskich zajmowali się Mieczysław Radwan (np. Radwan, 1956), Kazimierz Bielenin (np. Bielenin, 1992), Szymon Orzechowski (np. Orzechowski, 2018) i inni (np. Przychodni i Suliga, 2016). Badania nad starożytnymi żużlami po produkcji żelaza prowadzone były również w innych rejonach Polski, m.in. na Mazowszu (Janiszewski, 2018) i Śląsku (Lehnhardt i inni, 2019). Zakrojone na szeroką skalę badania starożytnych żużli obejmowały między innymi datowania izotopowe, rekonstrukcje stosowanych pieców, odtwarzanie metod wytopu, a także analizę społeczno-ekonomicznych uwarunkowań życia w przeszłości (Bielenin, 1992; Orzechowski, 2018).

Ze względu na wysoką zawartość metali/metaloidów obecnie prowadzone badania skupiają się najczęściej na aspektach środowiskowych (np. Warchulski i inni, 2019). Prowadzone są badania nad żużlami po produkcji ołowiu (np. Cabała i inni, 2020), miedzi (np. Kądziołka i inni, 2020; Derkowska i inni, 2021) oraz cynku (np. Tyszka i inni, 2014). Badania te obejmują analizę składu chemicznego i fazowego (Cabała i inni, 2020; Kierczak i Pietranik, 2011; Warchulski i inni, 2015; Warchulski i inni, 2016; Tyszka i inni, 2018), testy wymywania metali/metaloidów (np. Kierczak i inni, 2013) oraz możliwości ponownego wykorzystania żużli (np. Potysz i Kierczak, 2019). W ostatnich latach przeprowadzono również badania mające na celu rekonstrukcje warunków, w jakich prowadzono wytop (np. Derkowska i inni, 2021), przy czym część badań uwzględniała jedynie warunki temperaturowe (Kądziołka i inni, 2020).

Jak do tej pory nie prowadzono badań nad rekonstrukcją procesu produkcji Cu na terenie Gór Świętokrzyskich. Istniejące analizy skupiały się przede wszystkim na opisach makroskopowych oraz składzie chemicznym żużli (np. Kowalczewski i Szczecińska, 1977). W literaturze dostępne są prace dotyczące hutnictwa złota w Złotym Stoku, które zawierają opis procesu produkcji oraz analizę żużli hutniczych (Dziekoński, 1972; Garbacz-Klempka, 2014). Proces hutniczy był oparty głównie na przekazach historycznych i nie obejmował szczegółowej charakterystyki żużli hutniczych. Z kolei badania nad składem żużli po produkcji Au nie były prowadzone w celu określenia warunków wytopu, lecz skupiały się na analizie składu chemicznego i fazowego żużli (Garbacz-Klempka, 2014). Podobnie badania nad historycznym hutnictwem prowadzono w przypadku żużli po dymarkowej produkcji Fe m.in. na terenie Gór Świętokrzyskich. Skupiano się w nich przede wszystkim na określeniu wieku żużli oraz odtworzeniu

warunków temperaturowych i metod wytopu. Nie podejmowano szczegółowych analiz dotyczących warunków utleniająco redukcyjnych oraz lepkości stopu (m.in. Radwan, 1956; Bielenin, 1992; Orzechowski, 2018). Szczegółowo proces hutniczy był opisany w przypadku produkcji Zn na Górnym Śląsku (Domański i Krupkowski, 1954; Warchulski, 2016). Badania nad tymi żużlami były również prowadzone w celu określenia ich składu chemicznego i fazowego, w których zwracano uwagę na występowanie faz o wysokiej zawartości As oraz Pb (Puziewicz i inni, 2007). Jednak badania nie obejmowały procesów prowadzących do powstania tych istotnych środowiskowo faz.

3. Metodyka

3.1. Prace kameralne, terenowe i preparatyka

Pierwszym etapem badań nad żużlami był przegląd literatury dotyczący lokalizacji zakładów hutniczych w czasach historycznych. W lokalizacjach wytypowanych na podstawie dostępnych danych były następnie prowadzone prace terenowe mające na celu pobór prób.

W przypadku Rudy Śląskiej próbki do analiz były pobierane z eksploatowanej hałdy co umożliwiło pobranie materiału, który w ograniczonym zakresie został poddany procesom wietrzeniowym (Kupczak i inni, 2020). Podczas poboru prób wyselekcjonowano jedynie te fragmenty, na których widoczny był kontakt żużla z materiałem ogniotrwałym (fragmentem retorty). W Sławkowie pobierano próbki z warstwy żużla znajdującej się w profilu glebowym (Warchulski i inni, 2020). Żużle ze Złotego Stoku były pobierane w obrębie składowiska, które uległo naturalnej sukcesji roślinnej i obecnie jest pokryte roślinnością (Warchulski i inni, 2022). W Miedzianej Górze, podobnie jak w przypadku Sławkowa, pobierano próbki z warstwy żużla w obrębie profilu glebowego (Kupczak i inni, 2023). W Polichnie żużle również zostały pobrane z profilu glebowego, jednak nie tworzyły one jednorodnej warstwy lecz były rozproszone, co wynikało z faktu, że podczas budowy drogi pomiędzy Chęcinami a Miedzianką oryginalna hałda odpadów pohutniczych została zlikwidowana i pozostały jedynie rozproszone fragmenty żużla (Kupczak i inni, 2024a). W przypadku Złotego Stoku, Miedzianej Góry, Polichna oraz Sławkowa podczas poboru prób starano się wybierać żużle różniące się pod względem makroskopowym (kolor, struktura, tekstura) aby podczas analiz mieć wgląd w całe spektrum żużli powstałych w danej lokalizacji. Podczas badań nad dymarkowym hutnictwem żelaza w Górach Świętokrzyskich próbki do analiz zostały dostarczone przez Muzeum Przyrody i Techniki w Starachowicach oraz jednego ze współautorów artykułu, który posiada prywatną kolekcję żużli (Kupczak i inni, 2024b). Kolejnym etapem badań było przygotowanie próbek do dalszych analiz, obejmujące kruszenie, mielenie, przygotowywanie szlifów cienkich oraz zgładów.

3.2. Metody analityczne

Analizy laboratoryjne rozpoczęto od obserwacji mikroskopowych z wykorzystaniem mikroskopu optycznego (Olympus BX-51) i skaningowego (Phenom XL) będących na wyposażeniu Instytutu Nauk o Ziemi w Uniwersytecie Śląskim. Obserwacje mikroskopowe pozwalały na wstępną ocenę żużli pod kątem: tekstury i struktury, składu fazowego oraz morfologii faz. W obszarach wytypowanych wstępnie podczas obserwacji mikroskopowych wykonano analizy składu chemicznego z wykorzystaniem elektronowej mikroanalizy rentgenowskiej (EPMA). Analizy EPMA były wykonywane przy pomocy mikrosondy Cameca SX 100 w Laboratorium Mikroskopii Elektronowej, Mikroanalizy i Dyfrakcji Rentgenowskiej na Wydziale Geologii Uniwersytetu Warszawskiego.

Skład chemiczny próbek określono z wykorzystaniem metod XRF (X-ray Fluorescence) oraz ICP-MS/OES (Inductively Coupled Plasma Mass Spectrometry/Optical Emission Spectroscopy). Połącznie metod XRF oraz ICP pozwoliło na ocenę składu chemicznego w możliwie najszerszym zakresie, uwzględniając zarówno pierwiastki główne, jak i śladowe. Analizy chemiczne były wykonywane przez Bureau Veritas Mineral Laboratories (Vancouver, Kanada). Skład fazowy próbek był określany za pomocą proszkowej dyfrakcji rentgenowskiej z wykorzystaniem dyfraktometrów PANalytical X'PERT PRO-PW 3040/60 (anoda Co, filtr Fe) oraz PANalytical X'Pert PW 3710 (anoda Cu, filtr Ni) znajdujących się na wyposażeniu Instytutu Nauk o Ziemi w Uniwersytecie Śląskim. Podczas analiz dyfraktogramów przeprowadzano analizę Rietvelda, z wykorzystaniem bazy danych PDF4+ (Fawcett i inni, 2005).

Wiek żużla po produkcji żelaza określono na podstawie wyników datowania izotopowego węgla drzewnego znalezionego w żużlu z wykorzystaniem metody AMS (Accelerator Mass Spectrometer AMS) w Centrum Metod Izotopowych CEMIZ (Instytut Fizyki Politechniki Śląskiej). Na podstawie informacji o stosunku izotopów ^{14}C do ^{12}C określono wiek węgla, następnie uzyskana data została skalibrowana z wykorzystaniem oprogramowania OxCal 4.4 (Bronk Ramsey 2009) korzystając z krzywej kalibracyjnej IntCal20 (Reimer i inni, 2020).

3.3. Metody określania poszczególnych parametrów wytopu

3.3.1. Temperatura

Temperatura likwidusu podczas prowadzonych badań była określana na podstawie kombinacji kilku niezależnych metod, co pozwalało na uzyskanie możliwie najdokładniejszego wyniku. Szerokie spektrum wykorzystanych metod umożliwiło określenie zarówno temperatury likwidusu jak i solidusu badanych żużli. Do wykorzystywanych metod należały eksperymenty wysokotemperaturowe (Warchulski i inni, 2020, 2022; Kupczak i inni; 2023; 2024a) diagramy fazowe (Warchulski i inni, 2022; Kupczak i inni, 2023, 2024a, 2024b) oraz oprogramowanie MELTS-Rhyolite (Warchulski i inni, 2022; Kupczak i inni, 2023). Eksperymenty wysokotemperaturowe prowadzone były z wykorzystaniem pieca laboratoryjnego PLF 160/5 wyposażonego w kontroler PC 442/18, grzałki wykonane z węglika krzemu (SiC), oraz termoparę typu S znajdującego się w Instytucie Nauk o Ziemi w Uniwersytecie Śląskim (Warchulski i inni, 2020, 2022; Kupczak i inni, 2023; 2024a) oraz mikroskopu wysokotemperaturowego (Leitz) znajdującego się na wydziale Inżynierii Metali i Informatyki Przemysłowej (Akademia Górniczo-Hutnicza; Kupczak i inni, 2024a) .

3.3.2. Lepkość

Lepkość stopu wyznaczana była na podstawie modeli matematycznych. Podczas określania lepkości stopu hutniczego wykorzystywano indeks lepkości (Warchulski i inni, 2020, 2022; Kupczak i inni, 2023) oraz modele uwzględniające skład chemiczny i temperaturę. Podczas badań zastosowano m.in. modele zaproponowane przez następujących autorów: Utigrad i Warczok (1995; Kupczak i inni, 2023), Giordano i inni (2006; Warchulski i inni, 2020; Kupczak i inni, 2023) oraz Browning i inni (2003; Kupczak i inni, 2024b).

3.3.3. Lotność składników gazowych

Warunki utleniająco redukcyjne określano wykorzystując diagramy wykonane na podstawie danych termodynamicznych. Wykorzystano bufory mineralne zaproponowane przez Zhao i współpracowników (1999; Warchulski i inni, 2020; Kupczak i inni, 2023), diagram Ellinghama z publikacji Chirikure (2015; Kupczak i inni, 2023) oraz diagram obszarów przewagi zaproponowany przez Yazawę (1974; Kupczak i inni, 2023). W toku prowadzonych prac, w szczególności nad próbkami, w których składzie poza fazami zawierającymi żelazo obserwowano ołów oraz miedź (Kupczak

i inni, 2023; 2024a) zdecydowano się wykorzystać obliczenia termodynamiczne do konstrukcji własnych diagramów obszarów przewagi (Kupczak i inni, 2024a; Kupczak i inni, 2024c).

3.3.4. Prędkość chłodzenia stopu

Prędkość chłodzenia żużli szacowano analizując morfologię oliwinów krystalizujących ze stopu (Donaldson, 1976). Ze względu na konieczność występowania tej fazy w żużlu parametr ten został określony jedynie dla materiału po produkcji żelaza oraz złota (Warchulski i inni, 2022; Kupczak i inni 2024b).

3.4. Oprogramowanie

W celu graficznej obróbki danych wykorzystywano pakiety CorelDRAW, QGIS (dane wektorowe) oraz Adobe (dane rastrowe). Ponadto podczas wykonywania graficznych rekonstrukcji urządzeń stosowano oprogramowanie AutoCAD. Aplikacja SLAG została napisana w języku programowania Python, korzystając z następujących bibliotek: cmath, re, math, matplotlib, numpy, cProfile, setuptools, tkinter oraz ttkbootstrap. Statystyczna obróbka danych była wykonywana głównie z wykorzystaniem pakietu Office (Excel) i obejmowała przede wszystkim obliczenia średnich oraz odchyleń standardowych.

4. Wyniki

4.1. Rekonstrukcja procesu produkcji Pb w Sławkowie

Z dostępnych źródeł wynika, że w Sławkowie prowadzono działalność hutniczą w XVI i XVII wieku a obecność infrastruktury hutniczej do prażenia rud świadczy o stosowaniu technologii przystosowanych do przetwarzania rud siarczkowych (Witkowski i Krajniewski, 2013). Dane geologiczne wskazują, że na analizowanym obszarze powszechnie występują epigenetyczne złoża typu Mississippi Valley (Cabała i inni, 2020). Najważniejszymi minerałami rudonośnymi tych złóż są galena (PbS) oraz sfaleryt (ZnS; Cabała, 2001), które najprawdopodobniej były przedmiotem eksploatacji w omawianym okresie.

Podczas prac terenowych w Sławkowie stwierdzono występowanie trzech rodzajów żużli hutniczych: szkliste, krystaliczne oraz zwietrzałe. Pod względem składu chemicznego żużle składały się przede wszystkim z SiO_2 (26,18-46,50 % wag.), CaO (4,48-30,39 % wag.) oraz Fe_2O_3 (9,81-22,83 % wag.). W żużlach szklistych i zwietrzałych stwierdzono również wysokie koncentracje Pb (>10 % wag.) i Zn (do ok. 21 % wag.). Głównymi składnikami fazowymi żużli szklistych były: szkło, augit $(Ca,Mg,Fe)(Mg,Fe)Si_2O_6$), willemit (Zn_2SiO_4), oliwin ($(Mg,Fe)_2SiO_4$), wüstyt (FeO), galena oraz tlenek ołowiu (PbO). Żużle krystaliczne zbudowane były głównie z minerałów z grupy melilitu ($Ca_2M(XSiO_7)$), kwarcu (SiO_2), wollastonitu ($CaSiO_3$), oraz skalenia potasowego ($K(AlSi_3O_8)$. Żużle zwietrzałe składały się głównie z willemitu, oliwinu, skalenia potasowego, klinopiroksenu, cerusytu ($PbCO_3$), galeny, sfalerytu i wurcytu (ZnS).

Wykorzystując otrzymane dane oraz źródła historyczne pochodzące z omawianego okresu (Agricola, 1556) wykonano interpretację sposobu postępowania podczas produkcji Pb w Sławkowie. Po wydobyciu i wzbogaceniu rud proces hutniczy rozpoczynano od prażenia, którego celem było utlenienie siarczków. Następnie wyprażony materiał mieszano z węglem drzewnym i piaskiem kwarcowym, po czym przetapiano go w piecu szybowym (Rys. 2). Węgiel drzewny pełnił funkcję zarówno źródła energii, jak i reduktora, zaś piasek kwarcowy obniżał temperaturę likwidusu. Podczas wytopu ze względu na dużą gęstość ołów spływał na dno, gdzie był akumulowany (Rys. 2b). Po przeprowadzonym wytopie hutnicy otwierali otwór w piecu, którędy wypływał przetopiony materiał, i separowali żużel od metalicznego ołowiu.

Badania eksperymentalne wykazały, że temperatura likwidusu żużli wynosiła co najmniej 1150 °C, natomiast solidusu mieściła się w przedziale 900–1000 °C (Tabela 1). Ze względu na złożony skład żużli i nierównowagową krystalizację niemożliwe było zastosowanie diagramów fazowych, oprogramowania MELTS-Rryolite i geotermometrów, dlatego posłużono się jedynie metodami eksperymentalnymi.

Lotność tlenu określono przy użyciu buforów mineralnych. Współwystępowanie wüstytu (FeO), magnetytu ($FeFe_2O_4$) i hematytu (Fe_2O_3) wskazywało na wartość log P O_2 w zakresie od −4,5 do −12 atm. Analizując lepkość stopu obliczono indeks lepkości oraz lepkość stopu dla temperatury likwidusu żużli. Indeks lepkości żużli mieścił się w przedziale 0,83-1,00, natomiast lepkość wynosiła od 1,34 do 1,48 Pa·s.

Ponadto, podczas prac terenowych odkryto fragmenty cegieł z przyklejonymi resztkami szklistego żużla. Analiza chemiczna wykazała, że skład szkliwa odpowiada składowi żużli, co potwierdziło, że w Sławkowie stosowano piece zbudowane z cegieł.

Tabela 1 Zestawienie podstawowych parametrów wytopu w analizowanych lokalizacjach

Lokalizacja	**Produkowany metal**	**Okres produkcji**	**Temperatura likwidusu [°C]**	**Temperatura solidusu [°C]**	**Lepkość (logη [Pa·s])**	**Lotność tlenu (logP O_2 [atm.])**
Sławków (Warchulski i inni, 2020)	ołów	16-17 wiek	1150	900-1000	1,34-1,48	od -4,5 do -12
Miedziana Góra (Kupczak i inni, 2023)	miedź	16-18 wiek	1150-1200	ok. 1100	1,19-4,42	od -4 do -12
Złoty Stok (Warchulski i inni, 2022)	złoto	15-17 wiek	1300-1350	1100-1200	0,26-0,90	od -10,5 do -11,5
Góry Świętokrzyskie (Kupczak i inni, 2024b)	żelazo	Okres wpływów rzymskich	1150-1200	-	-0,82–0,01	od -12,53 do -13,20
Polichno (Kupczak i inni, 2024a)	miedź	15-17 wiek	1100-1200	800-1100	-	od -4,3 do -14,08
Ruda Śląska (Kupczak i inni, 2020)	cynk	19 wiek	-	-	-	-

4.2. Rekonstrukcja procesu produkcji Cu w Miedzianej Górze

Na podstawie danych literaturowych wiadomo, że proces produkcji prowadzony był w Miedzianej Górze w okresie od XVI do XVIII wieku z wykorzystaniem lokalnych złóż (Wojciechowski, 2002). Do najważniejszych minerałów miedziowych (pierwotnych) występujących w złożu Miedziana Góra należą chalkopiryt ($CuFeS_2$), chalkozyn (Cu_2S), bornit (Cu_5FeS_4) oraz tetraedryt ($[Cu,Fe]_{12}Sb_4S_{13}$). W strefie mineralizacji wtórnej dodatkowo występują malachit ($Cu_2(CO_3)(OH)_2$), azuryt ($Cu_3(CO_3)_2(OH)_2$) oraz chryzokola ($(Cu, Al)_2H_2Si_2O_5(OH)_4 \cdot n(H_2O)$) (Piekarski, 1961). Analizy żużli wykazały obecność rozproszonych siarczków w żużlach co sugeruje wykorzystywanie podczas produkcji mineralizacji pierwotnej.

Podczas analiz żużli wyodrębniono sześć typów (MG1-6) różniących się cechami makroskopowymi, takimi jak barwa i stopień krystaliczności. Pod względem składu chemicznego analizowane żużle zawierały głównie SiO_2 (49,81-57,14 % wag.), CaO (11,25-21,64 % wag.), FeO (8,42-11,03 % wag.) oraz Al_2O_3 (7,54-9,14 % wag.). W żużlach stwierdzono również obecność Pb (0,50-5,91 % wag.) oraz Cu (0,40-4,98 % wag.). Analiza składu fazowego wykazała, że żużle MG1-5 zbudowane były głównie ze szkła z rozproszonymi polimorfami SiO_2, metaliczną miedzią, tlenkami ołowiu (PbO), klinopiroksenami oraz sporadycznie obserwowanymi siarczkami/arsenkami Cu oraz metalicznym Pb. Natomiast żużle typu MG6 składały się głównie ze szkła, wollastonitu, skalenia potasowego, siarczków Cu oraz metalicznej miedzi.

Ze względu na zbliżony okres rekonstrukcja metod stosowanych podczas wytopu w Miedzianej Górze również opierała się na źródłach historycznych (Agricola, 1556). W tym przypadku wykorzystano również dane literaturowe dotyczące procesu produkcji miedzi (m.in. Davenport i inni, 2002). Na podstawie danych literaturowych oraz różnic w składzie fazowym i chemicznym żużli stwierdzono, ze proces produkcji w Miedzianej Górze był dwuetapowy. W trakcie badań wyodrębniono żużle powstałe w pierwszym (MG1-5) oraz drugim etapie procesu hutniczego (MG6). W przeciwieństwie do Sławkowa, w Miedzianej Górze siarczkowa ruda nie była poddawana prażeniu, gdyż hutnikom zależało na uzyskaniu półproduktu w formie stopu siarczkowego lub siarczkowo-arsenkowego w pierwszym etapie procesu. W tym celu do pieca hutniczego wprowadzano wzbogaconą rudę wraz z dodatkami, takimi jak węgiel drzewny oraz pokruszone piaskowce i wapienie. Węgiel drzewny dostarczał niezbędną energię oraz redukował lotność tlenu w piecu. Z kolei piaskowce i wapienie ułatwiały separację

stopu krzemianowego od siarczkowego oraz skutecznie obniżały temperaturę likwidusu, poprawiając efektywność procesu. W trakcie wytopu powstawał stop siarczkowy/arsenkowy (matte/speiss), który osadzał się w dolnych partiach pieca (Rys. 2c). Stop ten składał się głównie z siarczków miedzi, ołowiu i żelaza. W górnych partiach pieca gromadził się żużel, który po zakończeniu procesu był usuwany (Rys. 2c). Możliwe było, że już na tym etapie powstawała pewna ilość metalicznej miedzi, która akumulowała się na samym dnie pieca (Rys. 2c).

W drugim etapie stop siarczkowy/arsenkowy był ponownie przetapiany, tym razem w atmosferze utleniającej. Celem tego etapu było usunięcie ze stopu zanieczyszczeń, pozostawiając jedynie metaliczną miedź. Czysty metal uzyskiwano dzięki dodawaniu do pieca materiałów, które wiązały utlenione żelazo i ołów, tworząc żużel systematycznie usuwany podczas procesu. Materiały te stanowiły odpady z procesów wzbogacania rud oraz skały pochodzące z powierzchni ziemi. Po usunięciu zanieczyszczeń w formie żużla w piecu utrzymywano atmosferę utleniającą aż do całkowitego utlenienia siarki i jej usunięcia w postaci SO_x.

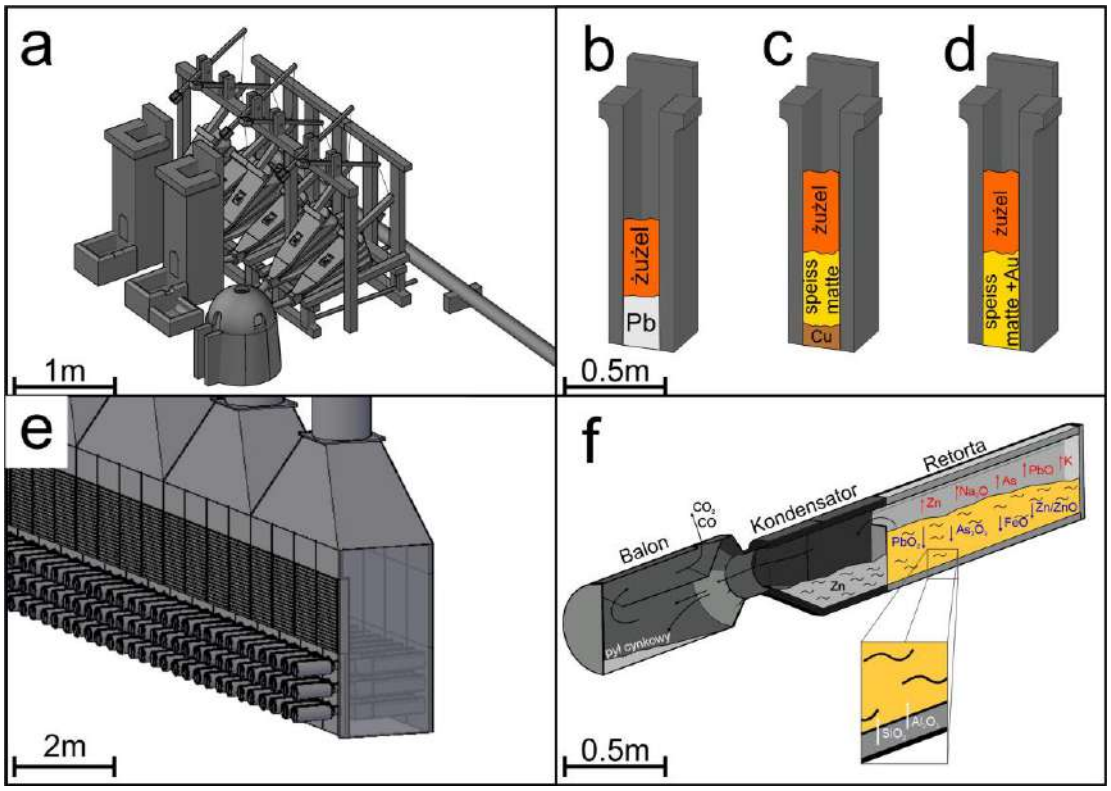

Rysunek 2 Graficzne rekonstrukcje historycznych urządzeń stosowanych do wytopu: piece szybowe oraz piec kupelacyjny wraz z urządzeniami do nadmuchu (miechami; a); piec szybowy ze schematem oddzielania się faz podczas wytopu ołowiu (c), miedzi (d) i złota; (e) piec do wytopu cynku; f) schemat retorty stosowanej podczas produkcji cynku.

Temperaturę likwidusu żużli z Miedzianej Góry określono na podstawie diagramów fazowych, oprogramowania MELTS-Rhyolite oraz eksperymentów wysokotemperaturowych. Wyniki uzyskane za pomocą diagramów fazowych mieściły się w przedziale 1300-1500 °C, natomiast temperatura uzyskana z wykorzystaniem oprogramowania wynosiła 1118-1155 °C. Ponieważ diagramy fazowe oraz MELTS-Rhyolite nie uwzględniają metali takich jak Pb, Cu czy Zn, których udział w żużlach wynosił do 8 % wagowych, jako temperaturę likwidusu przyjęto wartość określoną eksperymentalnie w zakresie 1150–1200 °C. Temperatura solidusu żużli została wyznaczona również eksperymentalnie na około 1100 °C.

Lepkość stopu (logη) oszacowano według modeli Giordano i innych (2006) oraz Utigarda i Warczoka (1995), uzyskując wartości od 1,19 do 4,42 Pa·s (Tabela 1). Najwyższa lepkość (logη = 4,42 Pa·s) była charakterystyczna dla żużli powstałych w drugim etapie produkcji, w którym niska lepkość nie była priorytetem hutników. W pierwszym etapie produkcji lepkość (logη) była niższa i wynosiła od 1,19 do 2,52 Pa·s. Dodatkowo określono również indeks lepkości żużli, który wynosił od 0,37 do 0,62.

Warunki utleniająco-redukcyjne wyznaczono z wykorzystaniem buforów mineralnych (Zhao i inni, 1999), diagramu Ellinghama (Chirikure, 2015) oraz diagramów zaprojektowanych przez Yazawę (1974). Podczas określania zakresu lotności tlenu uwzględniono występowanie w żużlach metalicznej miedzi oraz tlenków żelaza i ołowiu. Ustalono, że wytop w Miedzianej Górze przebiegał w warunkach lotności tlenu (logP O_2) od -4 do -12 atm., przy czym w pierwszym etapie wytopu utrzymywała się w zakresie od -5 do -12 atm. Z uwagi na utleniający charakter 2 etapu podczas przetapiania speiss/matte lotność tlenu wynosiła od -4 do -7 atm.

4.3. Rekonstrukcja procesu produkcji Au w Złotym Stoku

Hutnictwo złota w lokalizacji, z której pobrano żużle do analiz w Złotym Stoku prowadzone było w XVI-XVII wieku (Dziekoński, 1972). Prace prowadzone były w oparciu o mineralizacje rudną występującą w piroksenitach, amfibolitach, serpentynitach, marglach dolomitycznych oraz w skałach wapienno krzemionkowych (Gil i inni, 2015; Mikulski i Speczik, 2016). Złoto występuje w tych skałach w postaci drobnodyspersyjnych wrostków w strukturze minerałów, głównie w siarczkach i arsenkach. Kluczowymi minerałami złotonośnymi w złożu są löllingit ($FeAs_2$) oraz arsenopiryt (FeAsS).

Żużle pobrane podczas badań zostały podzielone ze względu na różnice makroskopowe oraz stopień zmian wietrzeniowych na siedem typów (ZS-1-7). Żużle charakteryzowały się składem chemicznym zdominowanym przez SiO_2 (52,12-56,60 % wag.), MgO (7,43-18,36 % wag.), CaO (10,84-15,19 % wag.) oraz FeO (9,08-15,36 % wag.). Pod względem składu fazowego w żużlach obserwowano oliwin, piroksen, szkło, siarczki oraz arsenki Fe.

Proces produkcji złota w Złotym Stoku, pierwotnie opisany w literaturze jako czteroetapowy (Dziekoński, 1972), został zweryfikowany na podstawie analizy składu chemicznego, fazowego oraz danych literaturowych (Agricola, 1556; Garbacz-Klempka, 2014). Wyniki badań wykazały, że etap prażenia, wcześniej uznawany za drugi etap wytopu, nie był częścią procesu produkcji. W związku z tym stwierdzono, że proces wytopu złota w Złotym Stoku obejmował jedynie trzy etapy. Pierwszy etap miał na celu stworzenie speiss/matte, drugi stop Pb-Au a trzeci oddzielenie Pb od Au. W pierwszym etapie do wzbogaconego złoża dodawano łupki, gnejsy oraz produkty powstałe w kolejnych etapach, takie jak speiss/matte oraz część żużli. Łupki i gnejsy obniżały temperaturę wytopu, natomiast speiss/matte zapewniały odpowiednio wysoką lotność arsenu i siarki, co umożliwiało uzyskanie odpowiedniej ilości stopu siarczkowo-arsenkowego (Rys. 2d). Powtórne przetapianie żużli, zawierających niewielkie ilości złota, zwiększało efektywność procesu hutniczego.

W drugim etapie stop siarczkowo-arsenkowy był przetapiany z dodatkiem ołowiu, który wiązał złoto i gromadził się na dnie pieca. W tym procesie w górnych partiach pieca pozostawał stop siarczkowo-arsenkowy, który był następnie dodawany do pierwszego etapu wytopu. Ostatni etap, tzw. kupelacja, polegał na przetapianiu stopu Pb-Au

w warunkach utleniających. W trakcie tego procesu ołów ulegał utlenieniu do PbO, a następnie w formie płynnej był oddzielany od złota.

Warunki wytopu w Złotym Stoku określono dla żużli powstałych w pierwszym etapie procesu produkcyjnego. Wynika to z faktu, że materiały po kolejnych etapach były powtórnie przerabiane w związku z zawartością pożądanych pierwiastków (Au, S, As, Pb). Do określenia temperatury wytopu w Złotym Stoku zastosowano diagramy fazowe oraz oprogramowanie MELTS-Rhyolite. Z uwagi na skład chemiczny żużli zbliżony do składu piroksenów, do oszacowania temperatury likwidusu wykorzystano diagram zaprojektowany dla tych faz, który wskazał zakres temperatury likwidusu na 1200-1400 °C. Ponadto, zastosowanie diagramów opracowanych dla piroksenów umożliwiło również określenie temperatury solidusu, która mieściła się w przedziale 1100-1225 °C. Podobne wyniki dla temperatur likwidusu (1220-1410 °C) i solidusu (1070-1270 °C) otrzymano na podstawie obliczeń wykonanych oprogramowaniem MELTS-Rhyolite. Warunki temperaturowe zweryfikowano następnie eksperymentami wysokotemperaturowymi oraz geotermometrami. Eksperymenty wysokotemperaturowe wskazały temperaturę likwidusu w zakresie 1300-1350 °C oraz temperaturę solidusu wynoszącą ok. 1200 °C.

Występowanie w żużlach oliwinów umożliwiło zastosowanie geotermometrów w celu określenia temperatury ich krystalizacji. Obliczenia wykazały, że krystalizacja oliwinów rozpoczęła się w temperaturze 1280-1320 °C. Dodatkowo wykorzystując inkluzje szkła w obrębie oliwinów stwierdzono, że proces krystalizacji trwał co najmniej do momentu osiągnięcia temperatury niższej niż 1200 °C. Obecność oliwinów umożliwiła również oszacować prędkości chłodzenia. Żużle ze Złotego Stoku były chłodzone z gradientem temperaturowym wynoszącym od 5 °C/h do 300 °C/h.

Lepkość stopu została określona z wykorzystaniem indeksu lepkości oraz modelu zaproponowanego przez Giordano i współpracowników (2006). Indeks lepkości analizowanych żużli wynosił 0,61-0,76, z kolei lepkość stopu (logη) w temperaturze 1350 °C wynosiła od 0,26 do 0,90 Pa·s. Warunki utleniająco redukcyjne określono na podstawie buforów mineralnych (Zhao i inni, 1999) na podstawie stopnia utlenienia żelaza w żużlach. Stwierdzono, ze proces wytopu prowadzony był w warunkach lotności tlenu ($\log P O_2$) w zakresie od −10,5 do −11,5 atm. (Tabela 1).

4.4. Ocena jednorodności procesu produkcji żelaza w okresie wpływów rzymskich

Ze względu na szeroką dostępność danych literaturowych dotyczących dymarkowej produkcji żelaza w Górach Świętokrzyskich (np. Bielenin, 1992), uwzględniających skład chemiczny żużli, temperatury likwidusu oraz stosowane metody hutnicze, przeprowadzone badania skoncentrowano na porównaniu warunków wytopu między różnymi lokalizacjami. W tym celu przeanalizowano żużle pochodzące z Suchedniowa, Skarżyska-Kamiennej i Starachowic.

Analizowane żużle składały się głównie z FeO (43.97-75.32 % wag.) oraz SiO_2 (18.04-47.14 % wag.). Pozostałe składniki występowały w ilościach poniżej 5 % wagowych tlenku. Wśród faz obecnych w żużlach dominowały: oliwin, wüstyt, spinel z szeregu magnetyt ($Fe^{2+}Fe^{3+}{}_2O_4$)-hercynit ($Fe^{2+}Al_2O_4$) oraz leucyt ($KAlSi_2O_6$). W zależności od próbki obserwowano również polimorfy SiO_2, iskoryt ($Fe^{2+}{}_5Fe^{3+}{}_2SiO_{10}$), skaleń oraz cyrkon ($Zr(SiO_4$). Aby potwierdzić wiek próbek, przeanalizowano również fragmenty węgla drzewnego znalezionego w jednym z żużli. Wyniki datowania izotopowego wskazały na lata 196 p.n.e.–4 n.e., co potwierdziło, że badane żużle pochodzą z dymarkowej produkcji żelaza opisywanej dotychczas przez archeologów (Bielenin, 1992).

W trakcie badań zidentyfikowano kluczowe parametry procesu hutniczego i nie stwierdzono znaczących różnic pomiędzy analizowanymi lokalizacjami. Temperatura likwidusu została określona na podstawie diagramów fazowych i wynosiła od 1150 do 1200 °C. Lepkość stopu obliczono na podstawie modelu BBHLW (Browning i in., 2003), uzyskując wartości w zakresie 0,15-1,02 Pa·s. Lotność tlenu (logP O_2) oszacowano za pomocą oprogramowania SLAG, wykorzystując stopień utlenienia żelaza w żużlach. Maksymalna lotność tlenu podczas wytopu wynosiła od -12,53 do -13,20 atm. (Tabela 1). Warunki utleniająco-redukcyjne określono również na podstawie wskaźnika RII (Reducible Iron Index), opracowanego przez Charltona i współpracowników (2010). Analizowane żużle wykazywały wartości RII w przedziale 0,57–1,13. Najniższa wartość wskaźnika, odpowiadająca najbardziej redukcyjnemu środowisku, została zaobserwowana w przypadku żużla z Suchedniowa, natomiast najwyższa, wskazująca na największą lotność tlenu, charakteryzowała żużel STAR1 ze Starachowic. Biorąc pod uwagę, że żużle składały się głównie z oliwinów oszacowano, że proces ich chłodzenia przebiegał z prędkością od 5 do 300 °C/h w zależności od próbki.

4.5. Wykorzystanie diagramów obszarów przewagi do określenia lotności składników gazowych

Poza rekonstrukcją warunków panujących podczas historycznego hutnictwa celem pracy było również zaproponowanie nowych metod, które mogą być stosowane podczas badań archeometrycznych. Badania prowadzone na podstawie żużli z Polichna ukierunkowane były na zastosowaniu bardziej precyzyjnej metody określania lotności tlenu panującej podczas wytopu. W tym celu przeanalizowano żużle z Polichna pod względem składu chemicznego i fazowego oraz zaproponowano wykorzystanie danych termodynamicznych do obliczenia lotności tlenu oraz siarki podczas wytopu.

Podczas analiz wyodrębniono pięć typów żużli (POL1-5), różniących się makroskopowo (barwa, stopień krystaliczności). Analizowane żużle pod względem chemicznym składały się głównie z SiO_2 (34,88-49,69 % wag.), FeO (12,62-17,71 % wag.) oraz CaO (12.57-29.95 % wag.) z pozostałymi składnikami nie przekraczającymi 5 % wagowych. Z punktu widzenia prowadzonych badań istotna była również obecność Pb (7 104-39 941 $mg \cdot kg^{-1}$), Zn (6 921-31 970 $mg \cdot kg^{-1}$) oraz Cu (415-27 746 $mg \cdot kg^{-1}$) w analizowanych żużlach. Najczęściej występującymi fazami w żużlach z Polichna były: szkło, wollastonit, kalcyt ($CaCO_3$), polimorfy SiO_2, klinopiroksen, baryt ($BaSO_4$) oraz cerusyt. W kontekście określania lotności tlenu i siarki istotne było również występowanie w żużlach szkła zawierającego utleniony Pb oraz Zn, metalicznej miedzi oraz żelaza, chalkozynu (Cu_2S), arsenków Cu, tlenku Pb, tlenku Fe, pirotynu ($Fe_{1-x}S$) oraz galeny.

Przeprowadzone badania uwidoczniły kluczowe znaczenie precyzyjnego określenia temperatury wytopu, ponieważ zdolność do redukcji metali silnie zależy od warunków temperaturowych. W badaniach wykorzystano zarówno metody teoretyczne (diagramy fazowe), jak i eksperymentalne. Na podstawie diagramów fazowych oszacowano temperaturę likwidusu żużli w zakresie 1060-1600 °C. Zrealizowano dwa rodzaje eksperymentów wysokotemperaturowych. W pierwszym próbki podgrzewano w piecu laboratoryjnym, a następnie analizowano zmiany, jakie zaszły pod wpływem wysokiej temperatury. Wykorzystanie tej metody pozwoliło oszacować temperaturę likwidusu w zakresie 1100-1200 °C a temperaturę solidusu na 800-1100 °C. W drugim podejściu zastosowano mikroskop wysokotemperaturowy, który pozwalał na bezpośrednią obserwację powierzchni próbki podczas jej ogrzewania i

topienia. Temperatura likwidusu określona tą metodą wynosiła od 1126 do 1263 °C a temperatura solidusu od 821 do 1100 °C.

Na podstawie obliczeń termodynamicznych oraz opracowanych diagramów określono wartości lotności tlenu (logP O_2) oraz siarki panujące podczas wytopu w Polichnie. W związku z obecnością metalicznej miedzi oraz sporadycznie występującego metalicznego żelaza, lotność tlenu w trakcie procesu wytopu wynosiła od -4,30 do -14,08 atm. Z kolei na podstawie obecności siarczków miedzi, żelaza i ołowiu ustalono, że lotność siarki (logP S_2) podczas wytopu mieściła się w zakresie od -2,50 do -6,92 atm.

Przeprowadzone badania potwierdziły, że zastosowanie obliczeń termodynamicznych umożliwia określenie lotności składników gazowych z większą dokładnością w porównaniu do powszechnie stosowanych buforów mineralnych. Jest to związane z faktem, że bufory mineralne projektowane były głównie dla skał naturalnych, w związku z czym uwzględniają głównie informacje o lotności tlenu przy przejściu pomiędzy minerałami zawierającymi żelazo (najczęściej hematyt, magnetyt, fajalit, metaliczne żelazo). Z kolei podczas produkcji metali, szczególnie poprzez przeróbkę rud polimetalicznych, w stopie hutniczym występuje szereg pierwiastków, które mogą ulegać redukcji oraz utlenianiu (np. Zn, Cu, Pb). Wykorzystanie informacji o tym, z jakimi fazami są związane poszczególne metale w stopie, może nam dać bardziej precyzyjną informację o zakresie lotności składników gazowych w piecu hutniczym.

4.6. Określenie reakcji chemiczno-fazowych podczas produkcji cynku w XIX wieku

W przypadku procesu produkcji cynku w związku z dostępnością literatury dotyczącej samego procesu produkcji zdecydowano się skupić na reakcjach, jakie zachodziły podczas wytopu. Uwzględniając fakt, że proces produkcji odbywał się w retortach (Dębicki, 1927; Rys. 2e-f), podczas badań skupiono się na reakcjach chemiczno-fazowych w strefie kontaktowej pomiędzy stopem a elementami retorty (materiału okładziny; Rys. 2f). Aspekt ten w historycznym hutnictwie cynku był kluczowy z uwagi na konieczność częstej wymiany zużytych retort (Dębicki, 1927). Istotnym punktem badań było również odtworzenie reakcji prowadzących do powstawania faz wzbogaconych w pierwiastki potencjalnie toksyczne (głównie Pb i As).

Analiza materiału pobranego z Rudy Śląskiej wykazała, ze żużle składały się głównie z SiO_2 (38,17 % wag.), Fe_2O_3 (22,71 % wag.), Al_2O_3 (15,81 % wag.) oraz CaO (10,56 % wag.) W żużlach stwierdzono również wysoką (powyżej 1 % wag) zawartość Zn. Z kolei materiał ogniotrwały zbudowany był głównie z SiO_2 (65,70 % wag.) oraz Al_2O_3 (29,08 % wag.). Pod względem fazowym w analizowanych żużlach stwierdzono obecność głównie skalenia, klinopiroksenu, polimorfów SiO_2, melilitu, spineli i cynkitu (ZnO). W materiały ogniotrwałych dominował mulit ($3Al_2O_3 \cdot 2SiO_2$) oraz polimorfy SiO_2. Dodatkowo podczas obserwacji mikroskopowych oraz analiz EPMA stwierdzono występowanie w strefie kontaktowej skaleni potasowych wzbogaconych w Pb i Ba, szkła o wysokiej zawartości As i Pb oraz alumohematytu ($(Fe,Al)_2O_3$).

Podczas badań wyszczególniono dwa główne rodzaje reakcji zachodzących pomiędzy materiałami ogniotrwałymi a wsadem hutniczym. Pierwszym z nich są reakcje pomiędzy fazami gazowymi/fluidalnymi a materiałem ogniotrwałym. W wyniku tych reakcji część składników wsadu hutniczego (PbO, K, As, Zn, i Na_2O) przechodziła do formy gazowej (lub fluidalnej) i migrowała w głąb materiału ogniotrwałego przetapiając częściowo fazy budujące retortę. Powstały w tym procesie stop w dalszym ciągu migrował w głąb retorty, a następnie zastygał, tworząc fazy szkliste wzbogacone w pierwiastki pochodzące ze stopu hutniczego (Rys. 2f). Drugi rodzaj reakcji, jakie zachodziły w stopie hutniczym, dotyczył reakcji pomiędzy fazą płynną a materiałem ogniotrwałym. W tym przypadku główną rolę odgrywała dyferencjacja stopu ze względu na właściwości poszczególnych składników. Część składników wsadu hutniczego (głównie PbO_2 oraz As_2O_3) ze względu na stosunkowo niską temperaturę topnienia ulegała upłynnieniu wcześniej niż pozostałe składniki i migrowała w kierunku dna retorty. Po upłynnieniu wsadu hutniczego również inne składniki o wyższej gęstości (FeO, ZnO) migrowały w kierunku dna retorty. W ten sposób w strefie kontaktowej powstawał stop wzbogacony o Fe, As, Zn oraz Pb, który reagując z retortą powodował powstawanie skaleni potasowych z podstawieniami Pb, piroksenów o wysokiej zawartości Fe oraz szkieł zawierających As_2O_3 i PbO. W wyniku reakcji pomiędzy ciekłym stopem a okładziną również składniki budujące materiał okładziny migrowały do stopu, tworząc następnie fazy wzbogacone materiałem ogniotrwałym jak alumohematyt.

4.7. Wytworzenie programu ułatwiającego wykonywanie rekonstrukcji historycznych procesów hutniczych

Kolejnym etapem prowadzonych badań było stworzenie jednego narzędzia, które w prosty sposób będzie umożliwiać określenie najważniejszych parametrów wytopu. Wykorzystując język programowania Python oraz biblioteki pozwalające na tworzenie aplikacji z graficznym interfejsem opracowano oprogramowanie SLAG 1.0. Umożliwia ono określanie podstawowych parametrów wytopu jak temperatura likwidusu, lepkość stopu oraz lotności tlenu i siarki podczas wytopu. Głównym celem podczas tworzenia tego oprogramowania była chęć udostępnienia osobom niemającym specjalistycznej wiedzy z zakresu termodynamiki oraz badań reologicznych narzędzia do dokonywania rekonstrukcji procesów hutniczych.

Do zaprezentowania możliwości oprogramowania wykorzystano wyniki analiz składu chemicznego i fazowego żużli hutniczych pochodzących z historycznej produkcji Cu oraz Pb. Rezultaty wykazały, że oprogramowanie SLAG przy wykorzystaniu odpowiednich dla analizowanego materiału modeli może być skutecznie stosowane podczas rekonstrukcji procesów hutniczych. Ograniczeniem stosowalności oprogramowania zarówno podczas określania temperatury likwidusu, jak i lepkości stopu hutniczego są składy chemiczne materiałów, mieszczące się w zakresach, dla których poszczególne modele były zaprojektowane. Brak ograniczeń stosowalności widoczny był jedynie w przypadku określania lotności tlenu i siarki.

5. Podsumowanie

Badania przeprowadzone w ramach rozprawy doktorskiej umożliwiły wykonanie rekonstrukcji procesu produkcji najczęściej wytwarzanych na terenie obecnej Polski metali. W każdej z badanych lokalizacji kładziono nacisk na unikatowe dla nich własności żużli oraz konieczność zapełniania odmiennych luk w wiedzy. Wykorzystanie nowoczesnych metod analitycznych pozwoliło odtworzyć warunki temperaturowe, lepkość stopu oraz lotność tlenu panującą podczas wytopu żelaza, miedzi, ołowiu oraz złota.

Z kolejnymi publikacjami szczególną uwagę zwracano udoskonalanie precyzji określania warunków podczas wytopu. Kwestia ta ma wyjątkowe znaczenie w przypadku określenia temperatury w procesie, ponieważ jedynie przy jej poprawnym określeniu możliwe jest dokładne wyznaczenie lepkości i warunków utleniająco redukcyjnych. Z tego powodu w zależności od lokalizacji do wyznaczenia temperatury likwidusu wykorzystywano połączenie eksperymentów wysokotemperaturowych, diagramów fazowych, oprogramowania MELTS-Rhyolite oraz geotermometrów.

Do poprawnego określenia lepkość stopu hutniczego wykorzystywano odpowiednie dla analizowanego materiału modele matematyczne. Wykorzystywano zarówno modele uwzględniające jedynie skład chemiczny żużli oraz modele uwzględniające również temperaturę wytopu. Podczas badań żużli po produkcji żelaza i miedzi z Gór Świętokrzyskich zwrócono uwagę, że efektywność wytopu nie zawsze jest uzależniona jedynie od lepkości stopu hutniczego. Jest to szczególnie widoczne w przypadku żużli po dymarkowej produkcji żelaza, gdzie pomimo niskiej lepkości stopu w żużlach pozostawała stosunkowo duża ilość żelaza. Podobnie w przypadku konwersji speiss/matte do metalicznej miedzi niska lepkość stopu nie była kluczowym czynnikiem wpływającym na poprawność procesu.

Warunki utleniająco redukcyjne w omawianych lokalizacjach były uzależnione od produkowanego metalu oraz od stosowanej technologii. Obserwacje składu fazowego próbek wykazały, że w przypadku produkcji metali niewymagających ekstremalnie niskiej lotności tlenu (ołów, miedź) zastosowanie paliwa w postaci węgla drzewnego umożliwiało otrzymanie bardziej redukcyjnego środowiska, niż było to wymagane z termodynamicznego punktu widzenia. Najlepiej widoczne jest to na przykładnie żużli z Polichna, gdzie w niektórych strefach stopu warunki były na tyle redukcyjne,

że możliwe było otrzymanie metalicznego żelaza. Największe znaczenie pod względem efektywności procesu miała lotność tlenu właśnie podczas produkcji tego metalu. Niewystarczająco redukcyjne środowisko i/lub zbyt krótki czas wytopu powodowały, że część żelaza nie ulegała redukcji i przechodziła do żużla.

Istotnym punktem przedstawionej rozprawy są zaproponowane narzędzia do rekonstrukcji procesów hutniczych. Zarówno wykorzystanie diagramów obszarów przewagi jak i oprogramowania SLAG może pozytywnie wpłynąć na ilość i jakość publikacji dotyczących historycznych procesów hutniczych.

6. Literatura

Agricola, G. 1556. De Re metallica libri XII (Ed Muzeum Karkonoskie w Jeleniej Górze, 2000), Jelenia Góra.

Anguilano, L. 2012. Roman lead silver smelting at Rio Tinto: the case study of Corta Lago (Doctoral dissertation, UCL (University College London)).

Addis, A., Angelini, I., Nimis, P., Artioli, G. 2016. Late Bronze Age copper smelting slags from Luserna (Trentino, Italy): Interpretation of the metallurgical process. Archaeometry, 58(1), 96–114.

Bachmann, H.G. 1982. The Identification of Slags from Archeological Sites; Occasional Publication No. 6; Institute of Archeology: London, UK,; pp. 1–37.

Bachmann, H. G., Lutz, C., Thiemann, U. (1989). Schlackenviskositäten. In A. Hauptmann, E. Pernicka, G. A. Wagner, Archäometallurgie in der Alten Welt – Old World archaeometallurgy. Der Anschnitt, Beiheft 7; pp. 137–140. Bochum: Verlag Glückauf GmbH.

Barin, I., 1993. Thermochemical data of pure substances. VCH 2, 1523.

Bielenin, K., 1992. Starożytne górnictwo i hutnictwo żelaza w Górach Świętokrzyskich., Wyd. 2 poszerzone i poprawione. ed. Kieleckie Towarzystwo Naukowe, Towarzystwo Przyjaciół Górnictwa, Hutnictwa i Przemysłu Staropolskiego w Kielcach, Kielce.

Bronk Ramsey, C. 2009. Bayesian analysis of radiocarbon dates. Radiocarbon, 51(1), 337-360.

Browning, G.J., Bryant, G.W., Hurst, H.J., Lucas, J.A., Wall, T.F., 2003. An empirical method for the prediction of coal ash slag viscosity. Energy & Fuels 17, 731–737.

Cabała, J., 2001. Development of oxidation in Zn-Pb deposits in Olkusz area. Mineral Deposits at the Beginning of the 21st Century. Balkema. Publ, 121–124.

Cabała, J., Warchulski, R., Rozmus, D., Środek, D., Szełęg, E., 2020. Pb-Rich Slags, Minerals, and Pollution Resulted from a Medieval Ag-Pb Smelting and Mining Operation in the Silesian-Cracovian Region (Southern Poland). Minerals 10, 28.

Charlton MF, Crew P, Rehren T, Shennan SJ. Explaining the evolution of ironmaking recipes—an example from northwest Wales. J Anthropol Archaeol. 2010; 29:352–67.

Davenport, W.G., King, M., Schlesinger, M., Biswas, A.K., 2002. Extractive Metallurgy of Copper 460.

Dębicki, J., 1927. Przemysł cynkowy: szkic historyczno-gospodarczy. Skł. gł. Gebethner i Wolff.

Derkowska, K., Świerk, M., Nowak, K., 2021. Reconstruction of Copper Smelting Technology Based on 18–20th-Century Slag Remains from the Old Copper Basin, Poland. Minerals 11, 926.

Domański, W., Krupkowski, A., 1954: Metalurgia cynku i kadmu. Państwowe Wydawnictwo Naukowe. Warszawa

Donaldson, C.H., 1976. An experimental investigation of olivine morphology. Contributions to Mineralogy and Petrology 57, 187–213.

Dziekoński, T., 1972. Wydobywanie rud i metalurgia złota i arsenu w Złotym Stoku. Zakład Narodowy im. Ossolińskich, Wrocław, pp. 133–202.

Ettler, V., Červinka, R., Johan, Z., 2009. Mineralogy of medieval slags from lead and silver smelting (Bohutín, Příbram district, Czech Republic): towards estimation of historical smelting conditions. Archaeometry 51, 987–1007.

Ettler, V., Mihaljevič, M., Jarošíková, A., Culka, A., Kříbek, B., Majer, V., Vaněk, A., Penížek, V., Sracek, O., Mapani, B., Kamona, F., 2020. Vanadium-rich slags from the historical processing of Zn–Pb–V ores at Berg Aukas (Namibia): Mineralogy and environmental stability. Applied Geochemistry 114, 104473.

Fawcett, T.G., Faber, J., Kabbekodu, S., McClune, F., Rafaja, D., 2005. 4+, the material identification database. Microstruct. Anal. Mater. Sci. 1–3.

Garbacz-Klempka, A., Wardas-Lason, M., Rzadkosz, S. 2014. Odpady hutnicze z rejonu Złotego Stoku. Archieves of Foundry Engineering, 14, 23–28

Giacometti, F., Rebay, G., Riccardi, M. P., Tarantino, S. C., Tizzoni, C. C.,Tizzoni, M. 2014. Iron Age silicate slags from Val Malenco (Italy): the role of textural and compositional studies in the reconstruction of smelting conditions. Periodico di Mineralogia, 83(3).

Gil, G., Barnes, J.D., Boschi, C., Gunia, P., Raczyński, P., Szakmány, G., Bendő, Z., Péterdi, B., 2015. Nephrite from Złoty Stok (Sudetes, SW Poland): Petrological, geochemical, and isotopic evidence for a dolomite-relate origin. Can Mineral 53, 533–556. https://doi.org/10.3749/canmin.1500018

Giordano, D., Mangiacapra, A., Potuzak, M., Russell, J.K., Romano, C., Dingwell, D.B., Di Muro, A., 2006. An expanded non-Arrhenian model for silicate melt viscosity: A treatment for metaluminous, peraluminous and peralkaline liquids. Chemical Geology 229, 42–56.

Giordano, D., Russell, J.K., Dingwell, D.B., 2008. Viscosity of magmatic liquids: a model. Earth and Planetary Science Letters 271, 123–134.

Godzik, B.; Woch, M.W. 2015. History of mining in the Olkusz region. In Natural and Historical Values of the Olkusz Ore-Bearing Region; Polish Academy of Sciences: Krakow, Poland, pp. 29–37.

Janiszewski, R., 2018. Before or after? Stratigraphic relations of Iron Age slag-pit furnaces in the Mazovian Centre of Metallurgy. Archeologické rozhledy 381.

Kądziołka, K., Pietranik, A., Kierczak, J., Potysz, A., Stolarczyk, T., 2020. Towards better reconstruction of smelting temperatures: Methodological review and the case of historical K-rich Cu-slags from the Old Copper Basin, Poland. Journal of Archaeological Science 118, 105142.

Kekkonen, M., Oghbasilasie, H., Louhenkilpi, S., 2012. Viscosity models for molten slags.

Kierczak, J., Pietranik, A., 2011. Mineralogy and composition of historical Cu slags from the Rudawy Janowickie Mountains, southwestern Poland. The Canadian Mineralogist 49, 1281–1296.

Kierczak, J., Potysz, A., Pietranik, A., Tyszka, R., Modelska, M., Néel, C., Ettler, V., Mihaljevič, M., 2013. Environmental impact of the historical Cu smelting in the

Rudawy Janowickie Mountains (south-western Poland). Journal of Geochemical Exploration 124, 183–194.

Kostova, B., Paneva, D., Cherkezova-Zheleva, Z., Mihaylova, K.,Dumanov, B. 2023. Ancient Metallurgical Iron Slags—Chemical, Powder X-ray Diffraction and Mössbauer Spectroscopic Study. Crystals, 13(6), 888.

Kowalczewski, Z., Szczecińska, A., 1977. Wyniki badań nad żużlami z kilku stanowisk dawnego hutnictwa metali nieżelaznych w Górach Świętokrzyskich. Rocznik Świętokrzyski 5, 151–168.

Kuhn, K., Goldmann, S., Rammlmair, D., Goldmann, D., Qiu, H., 2022. Quantitative metal and metaloid distribution in primary and secondary phases in historical lead-silver smelting slags from Rammelsberg ore deposit (Germany) and implications for their recovery. Journal of Geochemical Exploration 240, 107044.

Kupczak, K., Warchulski, R., Dulski, M., Środek, D. 2020. Chemical and phase reactions on the contact between refractory materials and slags, a case from the 19th century Zn-Pb smelter in Ruda Śląska, Poland. Minerals, 10(11), 1006.

Kupczak, K., Warchulski, R., Gawęda, A. 2023. Reconstruction of smelting conditions during 16th-to 18th-century copper ore processing in the Kielce region (Old Polish Industrial District) b ased on slags from Miedziana Góra, Poland. Archaeometry, 65(3), 547-569.

Kupczak, K., Warchulski, R., Gawęda, A., Ślęzak, M., Migas, P. 2024a. The use of predominance area diagrams (PAD) to determine the oxygen and sulfur fugacities prevailing during historical metallurgical processes: the case of fifteenth to seventeenth century copper slags from Polichno (Old Polish industrial district). Heritage Science, 12(1), 49.

Kupczak, K., Warchulski, R., Gawęda, A., Janiec, J. 2024b. Bloomery iron production in the Holy Cross Mountains (Poland) area during the Roman period: conditions during the metallurgical process and their uniformity between locations. Heritage Science, 12(1), 147.

Kupczak, K., Warchulski, R. 2024c. SLAG—software for reconstruction of historical smelting processes based on slag properties. Archaeometry.

Łabęcki, H., 1841. Górnictwo w Polsce: zapis kopalnictwa i hutnictwa Polskiego, pod względem technicznym, historycznostatystycznym i prawnym.

Lehnhardt, E., Błażejewski, A., Madera, P., Meister, J., 2019. Pielgrzymowice–A Przeworsk culture iron smelting site from the Roman period in Silesia. Przegląd Archeologiczny 177–230.

Leusch, V., Armbruster, B., Pernicka, E., Slavčev, V., 2015. On the Invention of Gold Metallurgy: The Gold Objects from the Varna I Cemetery (Bulgaria)—Technological Consequence and Inventive Creativity. CAJ 25, 353–376.

Maldonado, B., Rehren, T. 2009. Early copper smelting at Itziparátzico, Mexico. Journal of Archaeological Science, 36(9), 1998-2006.

Manasse, A., Mellini, M., Viti, C., 2001. The copper slags of the Capattoli Valley, Campiglia Marittima, Italy. Eur. J. Mineral. 13, 946–960

Mikulski, S.Z., Speczik, S., 2016. The auriferous ore mineralisation and its zonal distribution around the Variscan Kłodzko–Złoty Stok granitoid pluton in the Sudetes (SW Poland)–an overview. Geological Quarterly 60, 650–674.

Napierała, M. 2022. Wykorzystanie żelaza w starożytnym Egipcie do początku Okresu Późnego. Folia Praehistorica Posnaniensia, 27(1), 131-161.

Orzechowski, S., 2018. Socio-economic determinants of iron production on Polish lands during antiquity The phenomenon of metallurgical smelting centres of the Przeworsk culture. Archeologické Rozhledy 391.

Paulewicz, M., 1992. Chęcińskie górnictwo kruszcowe (XIV do poł. XVII wieku). Kieleckie towarzystwo naukowe, Kielce.

Persikov, E.S., Bukhtiyarov, P.G., 2020. Viscosity of magmatic melts: Improved structural-chemical model. chemical Geology 556, 119820.

Piekarski, K., 1961. W sprawie genezy złoża rud miedzi w Miedzianej Górze koło Kielc. Prace Geologiczne 3, 43–58.

Potysz, A., van Hullebusch, E.D., Kierczak, J., Grybos, M., Lens, P.N., Guibaud, G., 2015. Copper metallurgical slags–current knowledge and fate: a review. Critical reviews in environmental science and technology 45, 2424–2488.

Potysz, A., Kierczak, J., Pietranik, A., Kądziołka, K. 2018. Mineralogical, geochemical, and leaching study of historical Cu-slags issued from processing of the Zechstein formation (Old Copper Basin, southwestern Poland). Applied Geochemistry, 98, 22-35.

Potysz, A., Kierczak, J., 2019. Prospective (bio) leaching of historical copper slags as an alternative to their disposal. Minerals 9, 542.

Portillo-Blanco, H., Zuluaga, M.C., Ortega, L.A., Alonso-Olazabal, A., Cepeda-Ocampo, J.J., Martínez Salcedo, A., 2020. Mineralogical characterization of slags from the Oiola Site (Biscay, Spain) to assess the development in bloomery iron smelting technology from the Roman Period to the Middle Ages. Minerals 10, 321.

Przychodni, A., Suliga, I., 2016. Charakterystyka łupki żelaznej i kloca żużlowego z doświadczalnego procesu dymarskiego. Wiadomości Archeologiczne 67, 147–173.

Puziewicz, J., Zainoun, K., Bril, H. 2007. Primary phases in pyrometallurgical slags from a zinc-smelting waste dump, Swietochłowice, Upper Silesia, Poland. The Canadian Mineralogist, 45(5), 1189-1200.

Radwan, M., 1956. O śladach hutnictwa żelaza we wschodniej części zagłębia staropolskiego. Przegląd Geologiczny 4, 344.

Reimer, P., Austin, W., Bard, E., Bayliss, A., Blackwell, P., Bronk Ramsey, C., Butzin, M., Cheng, H., Edwards, R., Friedrich, M., Grootes, P., Guilderson, T., Hajdas, I., Heaton, T., Hogg, A., Hughen, K., Kromer, B., Manning, S., Muscheler, R., Palmer, J., Pearson, C., van der Plicht, J., Reimer, R., Richards, D., Scott, E., Southon, J., Turney, C., Wacker, L., Adolphi, F., Büntgen, U., Capano, M., Fahrni, S., Fogtmann-Schulz, A., Friedrich, R., Köhler, P., Kudsk, S., Miyake, F., Olsen, J., Reinig, F., Sakamoto, M., Sookdeo, A., Talamo, S. 2020. The IntCal20 Northern Hemisphere radiocarbon age calibration curve (0–55 cal kBP). Radiocarbon, 62.

Rozdzieński, W., 1612. Officina ferraria, ábo, Hutá i wárstát z kuźniámi szláchetnego dziełá żeláznego. Drukarnia Symona Kempiniego, Kraków.

Rozmus, D., 2014. Wczesnośredniowieczne zagłębie hutnictwa srebra i ołowiu na obszarach obecnego pogranicza Śląska i Małopolski (druga połowa XI–XII/XIII wiek). Kraków.

Seetharaman, S., Mukai, K., Sichen, D., 2005. Viscosities of Slags - an Overview. steel research international 76, 267–278.

Staszic, S., 1815. O ziemiorództwie Karpatów i innych gór i równin Polski.Drukarnia Rządowa, Warszawa

Thondhlana, T.P., Martinón-Torres, M., Chirikure, S., 2016. The archaeometallurgical reconstruction of early second-millennium AD metal production activities at Shankare Hill, northern Lowveld, South Africa. Azania: Archaeological Research in Africa 51, 327–361.

Toffolo, L., Addis, A., Martin, S., Nimis, P., Rottoli, M., Godard, G. 2018. The Misérègne slag deposit (Valle d'Aosta, Western Alps, Italy): Insights into (pre-) Roman copper metallurgy. Journal of Archaeological Science: Reports, 19, 248-260.

Tyszka, R., Kierczak, J., Pietranik, A., Ettler, V., Mihaljevič, M., 2014. Extensive weathering of zinc smelting slag in a heap in Upper Silesia (Poland): Potential environmental risks posed by mechanical disturbance of slag deposits. Applied Geochemistry 40, 70–81.

Tyszka, R., Pietranik, A., Kierczak, J., Zieliński, G., Darling, J., 2018. Cadmium distribution in Pb-Zn slags from Upper Silesia, Poland: Implications for cadmium mobility from slag phases to the environment. Journal of Geochemical Exploration 186, 215–224.

Warchulski, R., Gawęda, A., Kądziołka-Gaweł, M., Szopa, K. 2015. Composition and element mobilization in pyrometallurgical slags from the Orzeł Biały smelting plant in the Bytom–Piekary Śląskie area, Poland. Mineralogical Magazine, 79(2), 459-483.

Warchulski, R. 2016. Zn-Pb slag crystallization: evaluating temperature conditions on the basis of geothermometry. European Journal of Mineralogy, 28(2), 375-384.

Warchulski, R., Gawęda, A., Janeczek, J., Kądziołka-Gaweł, M. 2016. Mineralogy and origin of coarse-grained segregations in the pyrometallurgical Zn-Pb slags from Katowice-Wełnowiec (Poland). Mineralogy and Petrology, 110, 681-692.

Warchulski, R., Mendecki, M., Gawęda, A., Sołtysiak, M., Gadowski, M. 2019. Rainwater-induced migration of potentially toxic elements from a Zn–Pb slag dump in Ruda Śląska in light of mineralogical, geochemical and geophysical investigations. Applied Geochemistry, 109, 104396.

Warchulski, R., Szczuka, M., Kupczak, K. 2020. Reconstruction of 16th–17th century lead smelting processes on the basis of slag properties: A case study from Sławków, Poland. Minerals, 10(11), 1039.

Warchulski, R., Kupczak, K., Gawęda, A., Sitko, R. 2022. Complete reconstruction of the process and conditions during gold smelting in the 15th–17th centuries in Złoty Stok based on metallurgical slags. Archaeometry, 64(4), 916-934.

Witkowski, S.; Krajniewski, J. 2013. Inwentarz i Lustracje Klucza Sławkowskiego z XVII i XVIII Wieku; Muzeum Miejskie “Sztygarka”: Dąbrowa Górnicza, Poland

Wojciechowski, A. 2002. Hałdy dawnego górnictwa świętokrzyskiego jako źródło metali kolorowych i szlachetnych. Przegląd Geologiczny, 50(3), 240–244.

Wowkonowicz, P., Bojanowicz-Bablok, A., Gworek, B. 2018. Wykorzystanie odpadów z przemysłu wydobywczego i hutnictwa w drogownictwie. Rocznik Ochrona Środowiska, 20.

Wróblewski, T., 2014. Kruszce Karczówki i ich kopalnie. Studia muzealno-historycznes 6, 11–28.

Xiao, Y., Zhou, W., Mo, L., Chen, J., Li, M., Liu, S., 2021. Microstructure, Mineralogical Characterization and the Metallurgical Process Reconstruction of the Zinc Calcine Relics from the Zinc Smelting Site (Qing Dynasty). Materials 14, 2087.

Yazawa, A., 1974. Thermodynamic considerations of copper smelting. Canadian Metallurgical Quarterly 13, 11.

Zhao, D., Essene, E.J., Zhang, Y., 1999. An oxygen barometer for rutile–ilmenite assemblages: oxidation state of metasomatic agents in the mantle. Earth and Planetary Science Letters 166, 127–137.

minerals

MDPI

Article

Reconstruction of 16th–17th Century Lead Smelting Processes on the Basis of Slag Properties: A Case Study from Sławków, Poland

Rafał Warchulski [1,*], Monika Szczuka [2] and Krzysztof Kupczak [1]

[1] Institute of Earth Sciences, Faculty of Natural Sciences, University of Silesia, Będzińska 60, 41-200 Sosnowiec, Poland; krzysztof.kupczak@us.edu.pl
[2] Department of General Geology and Geotourism, Faculty of Geology, Geophysics and Environmental Protection, AGH, Al. Mickiewicza 30, 30-059 Kraków, Poland; szczuka@agh.edu.pl
* Correspondence: rafal.warchulski@us.edu.pl

Received: 3 November 2020; Accepted: 19 November 2020; Published: 20 November 2020

Abstract: The study focuses on the reconstruction of the technological process in the 16th–17th century lead smelter in Sławków based on chemical and petrographic analyzes of slags. There are three main types of material at the landfill: glassy, crystalline, and weathered. Glassy slags are made of amorphous phase in which crystals of pyroxene, willemite, olivine, wüstite, and lead oxide appear. Crystalline slags are composed of wollastonite, rankinite, melilite, anorthite, quartz, and Fe oxides. Weathered slags have a composition similar to glassy slags, but they also contain secondary phases: anglesite and cerussite. Chemical analyzes confirmed that the smelter used sulphide ores, which were roasted, and the main addition to the charge was quartz sand. The smelting process took place in a brick-built furnace, under reducing conditions, with varied oxygen fugacity ranging from WM to MH buffer. The slag characteristics show a knowledge of the workers in the field of smelting methods. The addition of SiO_2 allowed for the binding of elements that could contaminate the obtained lead, and at the same time, the low melting point of the material (1150 °C) and the melt viscosity ($\log\eta$ = 1.34 for 1150 °C) was maintained, enabling the effective separation of liquid lead.

Keywords: slags; archaeometry; archaeology; lead; zinc; silver; smelting; reconstruction; melt modelling

1. Introduction

Due to the ease of processing, a wide range of applications and the coexistence with silver, lead deposits have played an important role in historical times [1]. The oldest (from 7th–6th millennium BC) known center related to lead metallurgy is the Anatolian settlement of Catal Hüjük, where the remains of jewelry made of this metal have been preserved [2]. An impressive metallurgical complex from the Late Chalcolithic period (5th millennium BC) was discovered in a cave in the northern Negev desert (Israel) [3]. In this complex a biconical object made of pure metallic lead was found logged onto a wooden shaft [3]. In Europe, the oldest objects containing metallic lead are biconical vessels from Pietrele on the Lower Danube dated to ca. 4400–4300 BC [4]. In antiquity, lead compounds were commonly used, e.g., as dyes (red lead—Pb_3O_4; lead white—$PbCO_3$) [2,5], cosmetics (e.g., mascara or lipstick in ancient Egypt (ZnS)) [1,2,5] and as alloy additives [6]. The ancient Romans began to use lead on an industrial scale, including for the construction of aqueducts [1,2]. In Rome, lead acetate was also widely used as a substance for improving the taste of wine [5,6], although this application of lead was invented by the Egyptians and the Greeks [7]. Later, lead began to be used for the production of shooting balls, printing inks, and toys (lead soldiers) [5]. Despite the knowledge about

its harmfulness, lead is still a widely used metal nowadays. It is used in the production of sulfuric acid, in the construction industry, as well as in the production of batteries and nuclear reactors [5]. In the centers of the historical metallurgical industry, we can observe remnants of metallurgical activities in the form of slags. They are a research topic in Poland [8,9] and in other European countries [10–14].

Due to the presence of potentially toxic elements (PTEs) in slags, they are most often analyzed in terms of their impact on the environment [9,15,16]. Slag analysis also helps to understand the mechanism of the formation of mineral phases with an unusual chemical composition [17]. They are also used to understand geological processes, as they can be treated as analogs of natural rocks (e.g., paralavas, melilitolites) which are formed under similar pressure and temperature conditions [18]. Their commercial use is also widely researched [17,19,20]. Slags are often the only tool for the reconstruction of historical metallurgical processes [10,12,21].

During such reconstructions, the important sources of information are historical documents and production remains. Based on descriptions contained in such works as *De Re Metallica*, the methods and devices used for the production of metals can be reconstructed [22]. Production remains such as slags are significant because, in the absence of historical documents on their basis, it is possible to reconstruct the smelting conditions [10,12,13,23–28]. By analyzing their chemical and phase composition, we can recreate the conditions in the historical furnaces. One of them is temperature during smelting process. Geochemical, petrological and experimental methods can be used to approximate it. Numerous slag studies determined the smelting temperature based on phase diagrams [10,18,23,25,27], geothermometers [21,29,30], or laboratory experiments [8,18,31]. Other method require the construction of furnaces, similar to those used in historical times [11,12]. During smelting experiments in such, it is possible to measure the actual temperature inside the furnace [12]. It also allows the observation of the reactions taking place during the smelting [11,12]. Another factor that should be considered in the studies of historical smelting process is the melt viscosity [10,17,27,31,32]. Low melt viscosity facilitated the process of separating of the metallic phase from the slag, which makes the metallurgical process more effective [31]. Geochemical and petrological studies can also approximate the furnace atmosphere [31] and addition in the smelting process [8,24,32–34]. The charcoal fragments occasionally occurring in historical slags can be used to determine the type of wood used [12,28], and also by dendrochronological [35] and radiocarbon [12,28,35] methods to determine their age.

Little is known about the slag and smelting processes of the early modern period. The existing studies focus mainly on medieval (e.g., [11,12,14,24]) or contemporary times (e.g., [16,21,26]). It creates an almost 300-year (1500–1800) gap in the research on slags and metallurgical processes. This study aims to fill this gap by recreating the historic metallurgical process in the 16th–17th century lead smelter in Sławków. Process reconstruction is based on mineralogical and geochemical studies, taking into account the temperature in the furnace, the viscosity of the metallurgical melt, and the type of additives added to the ore. This research will allow for a better understanding of metal production in this period in Poland and Europe.

2. Location and Ore Exploitation

Sławków is one of the oldest centers related to lead metallurgy in Poland. It is located in southern Poland (Figure 1), between Dąbrowa Górnicza and Sosnowiec in the west and Olkusz in the east. The town was an important economic center in the Middle Ages. Apart from mining and metallurgy, Sławków was an important trade center, situated on the route connecting the east and west of Europe [36]. In the Middle Ages, the administration of industry in the Sławków region was carried out by the Archbishop of Cracow [9]. We can be certain that Ag-Pb ores were exploited and processed from the 15th to the 19th century, but it is assumed that a metallurgical industry existed in the Sławków region much earlier [9,37]. The ore mineralization in this area is associated with Mississippi Valley type deposits. These are low-temperature epigenetic deposits occurring in the Middle Triassic dolomites [38]. Primary ore mineralization consists mainly of galena (PbS), sphalerite and wurtzite (ZnS), pyrite and marcasite (FeS_2) [38]. However, due to weathering processes, the ore minerals

should also include smithsonite ($ZnCO_3$), monheimite ($FeZnCO_3$), hydrozincite ($Zn[(OH)_3CO_3]_2$), cerussite ($PbCO_3$), Fe-oxides, and hemimorphite ($Zn_4(Si_2O_7)(OH)_2 \cdot H_2O$) [39]. Initially, exploitation was limited to shallow deposits. After the resources above the groundwater table were exhausted, attempts were made to deepen and drain the mines. However, due to the lack of appropriate technology, these activities were limited [9]. Lead smelting in Sławków was carried out in the smelter located on Quaternary sands and muds [9]. It was placed in the south-eastern part of the city, near the left bank of the Przemsza River (Figure 1). Historical information [40] describes the existence of two independent "Old" and "New" smelters in this area. Both functioned in the 17th century, and at least the old smelter also in the 16th century [40]. Currently, there are no traces of the smelters' buildings in the area. Their location can only be identified by elevated terrain and slags appearing on the surface.

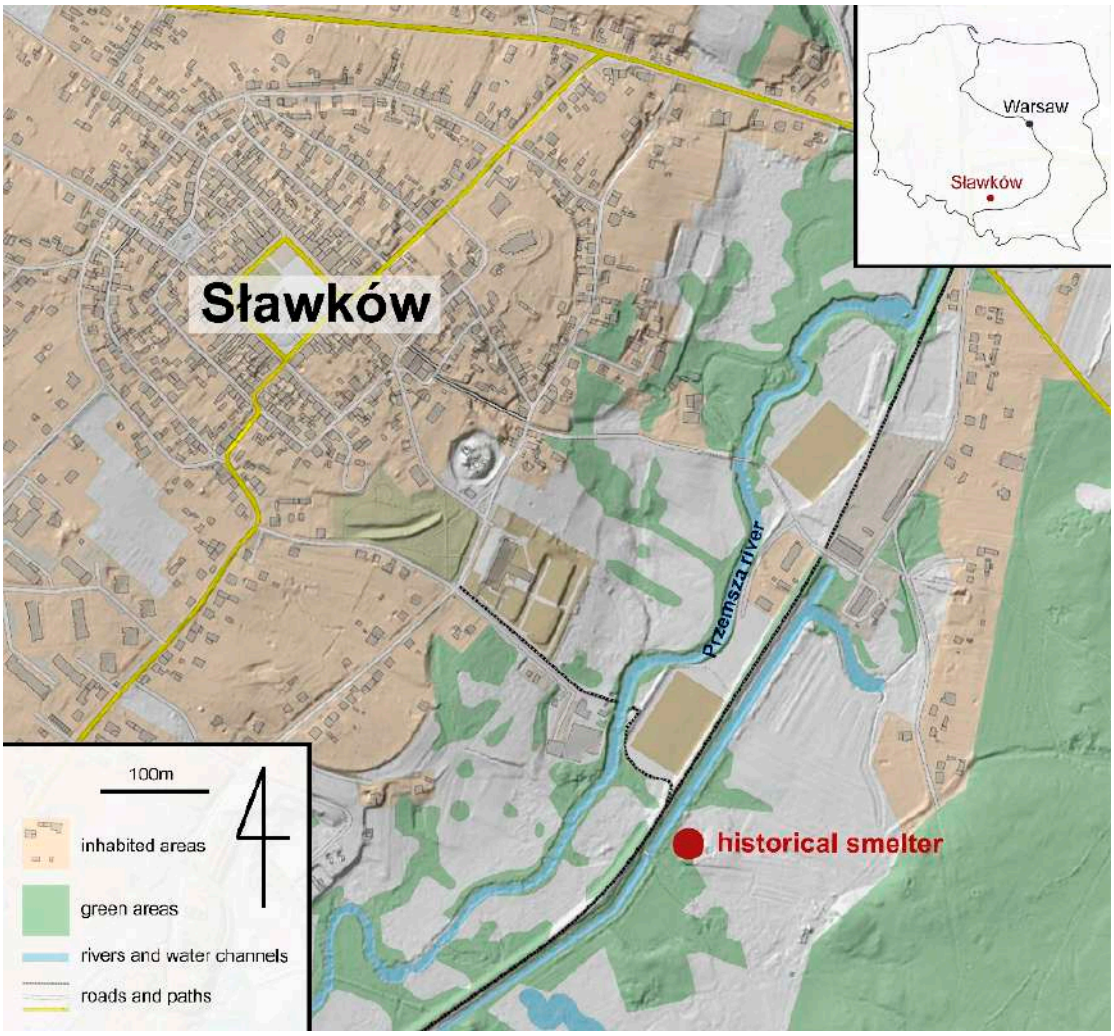

Figure 1. Location of the historical smelter in Sławków (based on data from [41,42]).

3. Materials and Methods

3.1. Sampling

Forty-two slag and eleven brick samples were collected from the surface and in excavations related to the bicycle path carried out in the historical landfill. Based on the macroscopic differentiation and the degree of weathering, three main types of slags were distinguished, from which representative fragments were subjected to preparation and geochemical and petrological analyses. Two brick

samples were selected for preparations and SEM-EDS analyses to confirm their relationship to the smelting process.

3.2. Furnace Experiments

Experiments were performed in PLF 160/5 chamber furnace (Protherm, Ankara, Turkey) with a PC 442/18 controller, SiC heaters, and a thermocouple S with a maximum working temperature of 1550 °C. Samples were melted in alumina pots. To determine the melting temperature of the slag samples we performed successive experiments with rising temperatures and fast cooling until a complete melting of the sample (ca. 1 cm^3) had occurred.

3.3. Geochemical and Petrological Analyses

For quantitative and qualitative phase composition of samples, samples were examined using the Olympus BX-51 (Tokyo, Japan) polarizing microscope, scanning electron microscope (SEM; Thermo Fisher Scientific Phenom XL, Waltham, MA, USA), equipped with an energy-dispersive spectrometer (EDS) at the Faculty of Natural Sciences, University of Silesia and Electron probe micro-analyzer (EPMA) CAMECA SX 100 (Gennevilliers, France) at the Inter-Institutional Laboratory of Microanalysis of Minerals and Synthetic Materials, University of Warsaw. EPMA analyses were performed at 15 keV accelerating voltage, a 10–20.1 nA beam current, and a beam diameter of up to 5 μm. Standards included: Al—$KAlSi_3O_8$; As—GaAs; Ba—$BaSO_4$; Ca—$CaSiO_3$; Fe—Fe_2O_3; K—$KAlSi_3O_8$; Mg—$MgCaSi_2O_6$; Mn—$MnCO_3$; Na—$NaAlSi_3O_8$; P—$Ca_5(PO_4)_3$(F,Cl,OH); Pb—PbS, $PbCrO_4$; S—$BaSO_4$, $CuFeS_2$, ZnS; Si—$CaSiO_3$; Ti—TiO_2; V—V; Zn—ZnS.

X-ray powder diffraction data were obtained using an X'PERT PRO—PW 3040/60 diffractometer (PANalytical Malvern, UK; CoKα1 source radiation, Fe-filter to reduce the Kβ radiation, and X'Celerator detector), at the Faculty of Natural Sciences, the University of Silesia in Katowice. Quantitative data processing was performed using the X'PERT High Score Plus software using the latest PDF4+ database and applying the Rietveld method. The Rietveld method applies the least-squares approach to match the theoretical profile line with a measured peak intensity of a powder sample, thus minimizing the residual function, and refining the crystal structure of the compound.

Considering insignificant differences of glassy slag in SEM and EPMA analyses for the bulk chemical compositions we used large (ca. 7.5 kg) and averaged sample of this slag type to better reflect their mean composition. It was supplemented by two samples of crystalline and weathered slags and analysed by a combination of X-ray fluorescence (XRF) spectrometry and inductively coupled plasma mass spectrometry (ICP-MS) for a broader spectrum of major, minor, and trace elements. Analyses were performed by the Bureau Veritas Minerals Laboratories. Sample preparation consisted of $LiBO_2$ fusion for XRF and lithium tetraborate decomposition and aqua regia digestion for ICP-MS. Loss on ignition was determined before XRF at 1000 °C.

3.4. Software

The furnace design was developed using Autodesk AutoCAD 2021 (San Rafael, CA, USA) and Adobe Photoshop 2021 software (San Jose, CA, USA).

4. Results

4.1. Slag Types at Sławków Landfill

Based on macroscopic observations it is possible to distinguish three main types of slags occurring at the landfill (Figure 2): (i) glassy slag with commonly incorporated grains of sand; (ii) crystalline slags; (iii) slags showing signs of weathering processes. Glassy slag is most common (33 samples from 42 gathered). It is black and gray with a yellow coating and is characterized by flow structures (Figure 2a) and incorporated grains of sand (Figure 2b). Crystalline slag is less common (five among 42 samples). This type of slag is gray, porous and in the section, partly melted grains are visible

(Figure 2c). Weathered slags are uncommon at the landfill (four among 42 samples). They are porous, yellow to brow, with coatings of secondary mineralization (Figure 2d).

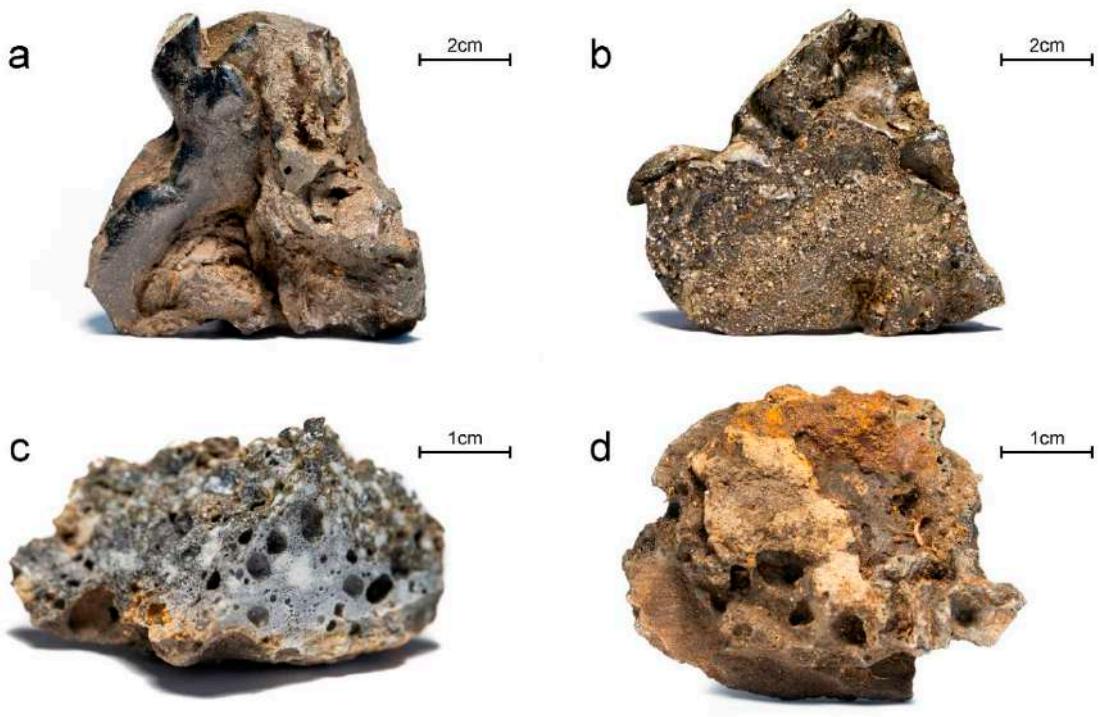

Figure 2. Macroscopic images of slag types distinguished at Sławków landfill: (**a**) glassy slag; (**b**) glassy slag with incorporated sand grains; (**c**) crystalline slag; (**d**) slag with signs of weathering processes.

4.2. Phase Composition and Chemistry of Phases

4.2.1. Glassy Slag

According to the XRD data (Figure 3) the glassy slag is dominated (42 vol.%) by petedunnite ($Ca(Zn,Mn^{2+},Mg,Fe^{2+})Si_2O_6$), accompanied by the willemite (31 vol.%; Zn_2SiO_4), fayalite (16 vol.%; Fe_2SiO_4), quartz (5 vol.%; SiO_2), galena (3 vol.%; PbS) and wüstite (3 vol.%; FeO). The diffractogram shows the hump characteristic for samples containing amorphous phases (Figure 3). Within the glassy slag, we observed areas that are composed of an amorphous phase with only singular crystallites (Figure 4a,d) and more crystalline zones (Figure 4b,c). Considering the phase dependencies in glassy slag we can determine that crystallization was started by the star-shaped pyroxene up to 100 μm, followed by dendritic crystals of willemite (Figure 4a,d). With an increasing level of crystallinity of zone, pyroxene gains subhedral morphology with crystals up to 200 μm (Figure 4a–c), while willemite forms laths up to 200 μm in length (Figure 4a–c). Occasionally they are accompanied by olivine up to 20 μm across (Figure 4c).

Based on the EPMA data we can distinguish two generations of pyroxenes within glassy slag. The proportion of Ca:Mg:Fe makes both generations augite, although the first is Mg-enriched ($Wo_{32}En_{57}Fs_{11}$), while the second Ca and Fe-enriched ($Wo_{44}En_{19}Fs_{37}$) (Table 1). In opposition to Mg-rich augite, Fe-augite concentrates also Zn (up to 7.34 wt.% of ZnO; Table 1) moving its composition closer to the petedunnite. Willemite in glassy slag is characterized by the significant addition of Fe (up to 18.29 wt.% of FeO) and lower concentrations of Mg, Mn, and P (Table 1). Olivine has close to ideal, forsterite dominated (Fo_{84}) composition (Table 1). Lead oxide phases are enriched in minor amounts of Zn (up to 0.40 wt.% of ZnO) and Fe (0.37 wt.% of FeO) (Table 1). Amorphous phase in glassy slag has a diverse composition consisting mainly of Pb (8.88–39.51 wt.% of PbO), Si (30.89–38.55 wt.% of SiO_2), Fe (11.46–21.27 wt.% of Fe_2O_3), Zn (4.92–12.61 wt.% of ZnO) and Ca (3.19–11.15 wt.% of CaO) (Table 1).

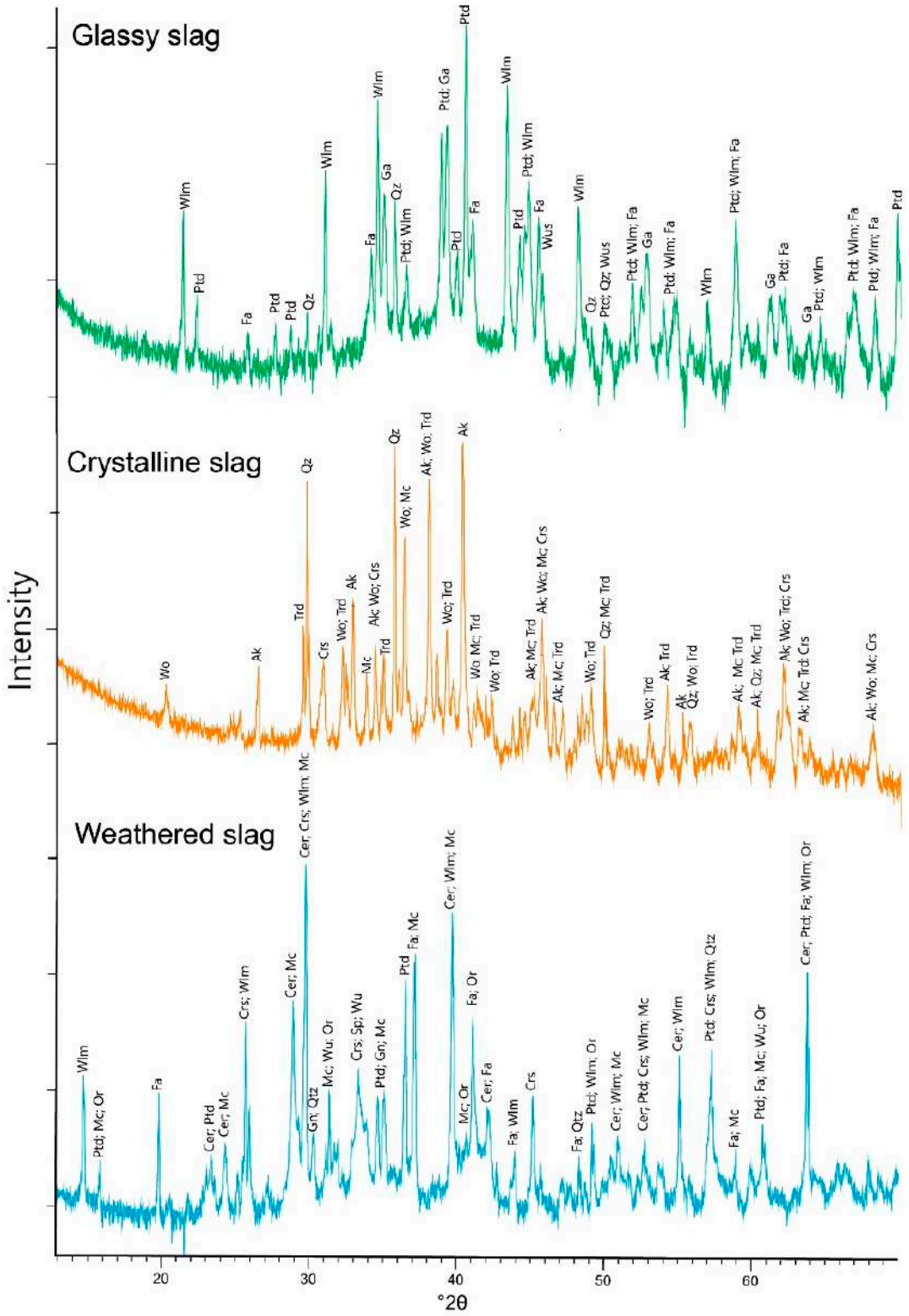

Figure 3. X-ray diffraction patterns of investigated slag samples. Abbreviations: Ak—åkermanite; Cer—cerussite; Crs—cristobalite; Fa—fayalite; Gn—galena; Lct—leucite; Mc—microcline; Or—orthoclase; Ptd—petedunnite; Qz—quartz; Sp—sphalerite; Trd—tridymite; Wlm—willemite; Wo—wollastonite; Wu—wurcite; Wus—wüstite.

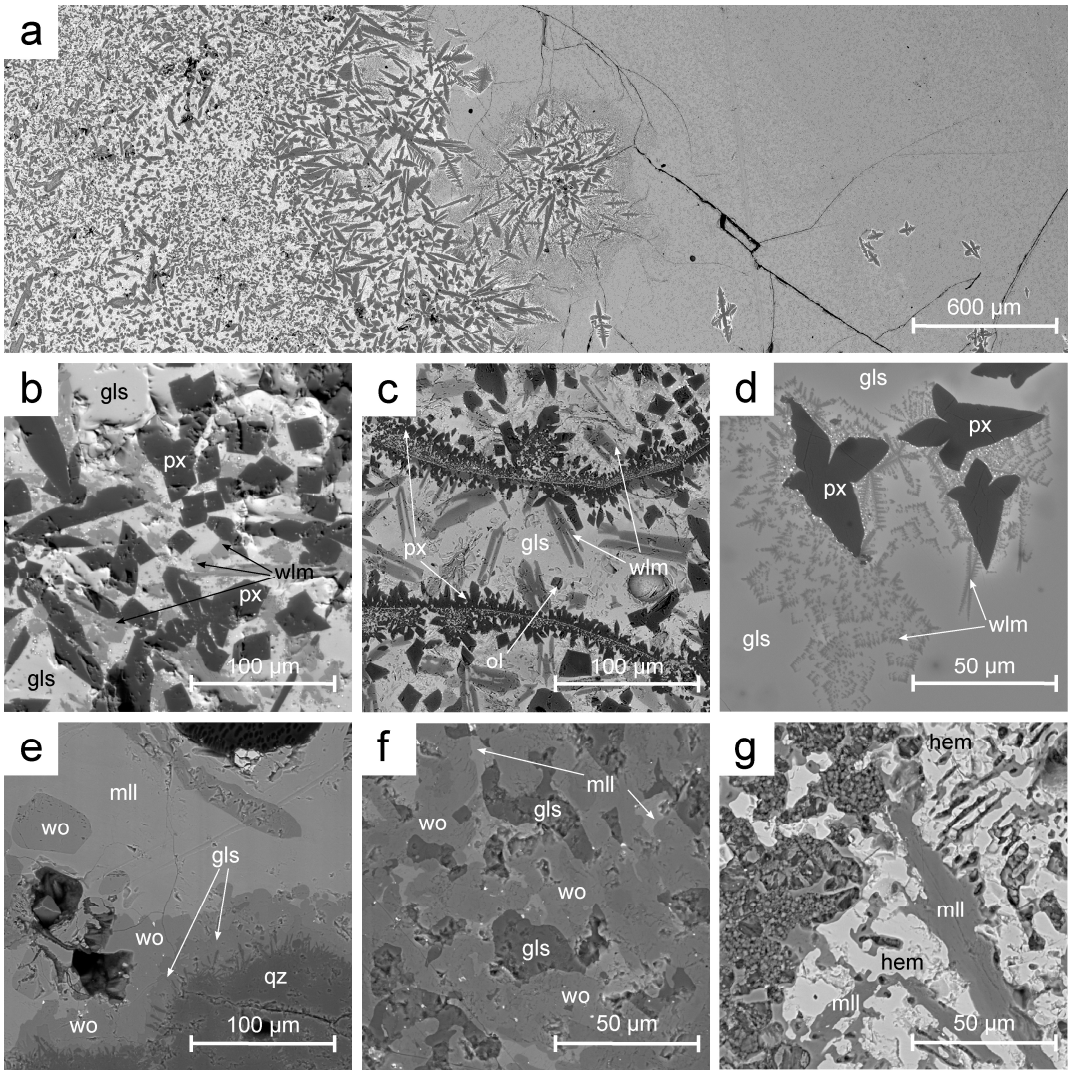

Figure 4. BSE images of slags from Sławków: (**a**) glass slag with the visible front of crystallization; (**b**,**c**) more crystalline part of glassy slag; (**d**) amorphous phase dominated part of glassy slag; (**e**–**g**) different textures and assemblages of crystalline slag. Abbreviations: gls—glass; hem—hematite; mll—melilite; ol—olivine; px—pyroxene; qz—quartz; wlm—willemite; wo—wollastonite.

Table 1. Representative chemical composition of the phases building glassy slags (EPMA; wt.%). Abbreviations: gls_p—primitive glass; gls_r—residual glass; ol—olivine; PbO—litharge or massicot; px—pyroxene; wlm—willemite; bd—below detection limit; na—not analyzed; a.p.f.u. (atoms per formula unit)—recalculation of the composition of the oxides to illustrate the number of particular atoms in the mineral formula.

	Glassy Slag						
	px	**px**	**wlm**	**ol**	**PbO**	**gls_p**	**gls_r**
SiO_2	53.90	45.40	27.34	39.56	0.17	38.55	30.89
TiO_2	bd	0.12	na	bd	bd	0.17	0.11
Al_2O_3	1.24	2.08	bd	bd	bd	2.27	2.71
As_2O_3	bd	bd	bd	bd	bd	bd	0.17
Fe_2O_3	0.00	0.00	0.00	0.00	0.00	21.27	11.46
FeO	7.31	19.28	18.29	15.10	0.37	0.00	0.00
MnO	0.12	0.29	0.23	bd	bd	0.21	0.17

Table 1. *Cont.*

	Glassy Slag						
	px	**px**	**wlm**	**ol**	**PbO**	**gls$_p$**	**gls$_r$**
ZnO	bd	7.34	50.10	bd	0.40	12.61	4.92
PbO	na	0.28	bd	na	98.18	8.88	39.51
BaO	na	na	na	na	na	bd	0.56
MgO	21.00	5.46	2.34	44.48	bd	3.07	0.12
CaO	16.14	17.67	0.12	0.50	bd	11.15	3.19
K_2O	bd	bd	na	bd	bd	1.20	2.53
Na_2O	bd	0.35	na	bd	bd	0.56	0.45
P_2O_5	na	0.57	0.22	na	bd	0.74	0.77
SO_3	na	na	na	na	na	0.43	0.27
Total	99.71	98.84	98.64	99.64	99.12	101.11	97.83
a.p.f.u. (atoms per formula unit)							
Si	1.96	1.88	0.98	1.00			
Ti^{4+}	0.00	0.00	0.00	0.00			
Al	0.05	0.10	0.00	0.00			
As^{3+}	0.00	0.00	0.00	0.00			
Fe^{3+}	0.00	0.00	0.00	0.00			
Fe^{2+}	0.22	0.67	0.55	0.32			
Mn	0.00	0.01	0.01	0.00			
Zn	0.00	0.22	1.33	0.00			
Pb	0.00	0.00	0.00	0.00			
Ba	0.00	0.00	0.00	0.00			
Mg	1.14	0.34	0.13	1.67			
Ca	0.63	0.78	0.00	0.01			
K	0.00	0.00	0.00	0.00			
Na	0.00	0.03	0.00	0.00			
P^{5+}	0.00	0.02	0.01	0.00			
S^{6+}	0.00	0.00	0.00	0.00			
O^{2-}	6.00	6.00	4.00	4.00			

Besides glass concentrates numerous (Al, Mg, K, P, Na, S, Mn, and Ti) of other elements in lower amounts (Table 1). Differences in the glass composition are due to the advancement of the crystallization process. Primitive glass in areas with none or rare crystallites is enriched in Si, Fe, Zn, Mg, and Ca (Table 1). Crystallization of phases containing these elements (pyroxene, olivine, willemite) leads to the enrichment of residual glass in Pb and K which are incompatible with crystallizing phases.

4.2.2. Crystalline Slag

According to the XRD data (Figure 3), the crystalline slag consists of åkermanite (43 vol.%; $Ca_2Mg(Si_2O_7)$), SiO_2 polymorphs (27 vol.% in total; 14 vol.% of quartz; 11 vol.% of tridymite; 2 vol.% of cristobalite), wollastonite (20 vol.%; $CaSiO_3$), and microcline (10 vol.%; $KAlSi_3O_8$). The petrographic image of crystalline slag is largely determined by the occurrence of quartz grains up to a few hundred of μm across. Their surface is locally covered by a thin (few μm) layer of glass (Figure 4e) resulting from quartz melting and recrystallization and exchange of cations with melt. Further from the surface of quartz grains wollastonite layer (up to 30 μm thick) crystallizes followed by anhedral melilite building the slag matrix (Figure 4e). Spaces in slag between quartz grains are filled with overgrown anhedral crystals (up to 60 μm across) of wollastonite and melilite accompanied by feldspars, glass, and occasionally by rankinite ($Ca_3Si_2O_7$, Figure 4f). Rarely segregations rich in anhedral spinel and hematite up to 100 μm occur in this slag type (Figure 4g).

Wollastonite occurs as crystals with an almost pure chemical composition (Table 2) or with numerous substitutions among which Fe (11.17 wt.% of FeO); Zn (2.31 wt.% of ZnO); Mg (1.57 wt.% of MgO) and K (1.02 wt.% of K_2O) (Table 2) are most significant. Analyzed melilites belong to the complex solid solution of åkermanite ($Ca_2Mg(Si_2O_7)$)—gehlenite ($Ca_2Al(AlSiO_7)$)—hardystonite

($Ca_2Zn(Si_2O_7)$)—ferri-gehlenite ($Ca_2Fe^{3+}(AlSiO_7)$) (Table 2). As such, they concentrate wide spectrum of elements: Al (1.36–27.43 wt.% of Al_2O_3), Fe (6.25–9.28 wt.% of Fe_2O_3), Zn (1.15–11.92 wt.% of ZnO), and Mg (0.63–2.42 wt.% of MgO) (Table 2). Rankinite has a composition close to ideal: $Ca_{2.96}Fe_{0.03}Si_2O_7$ (Table 2). Plagioclase is represented by the Ca-rich endmember (An_{93}) enriched in Fe (1.04 wt.% of FeO), Zn (0.45 wt.% of ZnO), and Pb (0.22 wt.% of PbO) (Table 2). K-feldspar contains only minor amounts of Fe (0.62 wt.% of FeO) (Table 2). Due to numerous elements in its structure spinel can be classified as magnetite ($Fe^{2+}Fe^{3+}{}_2O_4$)—gahnite ($ZnAl_2O_4$)—franklinite ($Zn^{2+}Fe^{3+}{}_2O_4$)—hercynite ($Fe^{2+}Al_2O_4$)—chromite ($Fe^{2+}Cr^{3+}{}_2O_4$)—coulsonite ($Fe^{2+}V^{3+}{}_2O_4$) solid solution (Table 2). Hematite (ideally Fe_2O_3) additionally concentrates Ti (0.52–7.93 wt.% of TiO_2), Al (3.28–11.57 wt.% of Al_2O_3), V (0.00–1.92 wt.% of V_2O_3), Mn (0.65–0.77 wt.% of MnO), Zn (0.99–6.60 wt.% of ZnO), Mg (0.00–2.50 wt.% of MgO), and Ca (0.62–1.12 wt.% of CaO) (Table 2). Compared with amorphous phases from glassy slag, here they are enriched in Si (mean 73.17 vs. 34.72 wt.% of SiO_2), Al (mean 10.10 vs. 2.49 wt.% of Al_2O_3), and K (mean 4.06 vs. 1.87 wt.% of K_2O)(Table 2). At the same time they are impoverished in Fe (mean 6.05 vs. 16.37 wt.% of Fe_2O_3), Zn (mean 2.66 vs. 8.76 wt.% of ZnO), Pb (mean 1.20 vs. 24.20 wt.% of PbO), and Ca (mean 1.51 vs. 7.17 wt.% of CaO) (Table 2).

Table 2. Representative chemical composition of the phases building crystalline slags (EPMA; wt.%). Abbreviations: gls—glass; hem—hematite; kfs—K-feldspar; mll—melilite; pl—plagioclase; rnk—rankinite; spl—spinel; wo—wollastonite; bd—below detection limit; na—not analyzed; a.p.f.u. (atoms per formula unit)—recalculation of the composition of the oxides to illustrate the number of particular atoms in the mineral formula.

	Crystalline Slag													
	wo	**wo**	**mll**	**mll**	**mll**	**rnk**	**pl**	**kfs**	**spl**	**hem**	**hem**	**gls**	**gls**	**gls**
SiO_2	53.50	50.85	39.28	37.74	23.14	41.04	43.61	60.31	na	na	na	77.48	67.45	74.59
TiO_2	bd	0.10	bd	bd	bd	bd	bd	bd	7.74	7.93	0.52	0.17	bd	0.11
Al_2O_3	0.83	0.11	1.36	3.16	27.43	bd	33.03	24.09	13.24	3.28	11.57	4.38	24.69	1.22
FeO	11.17	0.43	-	-	-	0.67	1.04	0.62	27.68	-	-	-	-	-
Fe_2O_{3calc}	-	-	9.28	8.33	6.25	-	-	-	24.45	83.96	76.46	6.38	0.62	11.14
Cr_2O_3	bd	bd	bd	bd	bd	bd	bd	bd	10.91	0.10	bd	bd	bd	bd
V_2O_3	bd	bd	bd	bd	bd	bd	bd	bd	2.76	1.92	bd	bd	bd	bd
MnO	0.27	bd	bd	0.17	bd	bd	bd	bd	0.19	0.65	0.77	bd	bd	0.23
ZnO	2.31	bd	11.92	8.90	1.15	0.13	0.45	bd	10.95	0.99	6.60	3.74	0.14	4.10
PbO	0.20	bd	0.60	bd	bd	0.11	0.22	bd	na	na	na	1.55	bd	0.84
MgO	1.57	bd	0.68	2.42	0.63	bd	bd	bd	0.26	bd	2.50	0.20	bd	0.24
CaO	27.72	47.40	35.43	36.98	39.41	56.82	18.14	0.89	1.16	1.12	0.62	1.67	0.24	2.62
K_2O	1.02	bd	0.17	0.23	bd	bd	0.42	13.18	na	na	na	2.80	6.15	3.24
Na_2O	0.10	bd	0.73	0.33	bd	bd	0.43	bd	na	na	na	0.30	0.14	0.31
Total	98.69	98.89	99.45	98.26	98.01	98.77	97.34	99.09	99.34	99.95	99.04	98.67	99.43	98.64
a.p.f.u. (atoms per formula unit)														
Si	3.15	2.99	2.01	1.92	1.11	2.00	2.09	2.79	na	na	na			
Ti^{4+}	0.00	0.00	0.00	0.00	0.00	0.00	0.00	0.00	0.21	0.15	0.01			
Al	0.06	0.01	0.08	0.19	1.55	0.00	1.86	1.31	0.56	0.10	0.35			
Fe^{2+}	0.55	0.02	0.00	0.00	0.00	0.03	0.04	0.02	0.83	0.00	0.00			
Fe^{3+}	0.00	0.00	0.36	0.32	0.22	0.00	0.00	0.00	0.66	1.61	1.47			
Cr^{3+}	0.00	0.00	0.00	0.00	0.00	0.00	0.00	0.00	0.31	0.00	0.00			
V^{3+}	0.00	0.00	0.00	0.00	0.00	0.00	0.00	0.00	0.08	0.04	0.00			
Mn	0.01	0.00	0.00	0.01	0.00	0.00	0.00	0.00	0.01	0.01	0.02			
Zn	0.10	0.00	0.45	0.33	0.04	0.00	0.02	0.00	0.29	0.02	0.12			
Pb	0.00	0.00	0.01	0.00	0.00	0.00	0.00	0.00	na	na	na			
Mg	0.14	0.00	0.05	0.18	0.05	0.00	0.00	0.00	0.01	0.00	0.10			
Ca	1.75	2.98	1.94	2.01	2.03	2.96	0.93	0.04	0.04	0.03	0.02			
K	0.08	0.00	0.01	0.02	0.00	0.00	0.03	0.78	na	na	na			
Na	0.01	0.00	0.07	0.03	0.00	0.00	0.04	0.00	na	na	na			
O^{2-}	9.00	9.00	7.00	7.00	7.00	7.00	8.00	8.00	4.00	3.00	3.00			

4.2.3. Weathered Slags

According to XRD data weathered slags are composed of a mixture of ore minerals, primary slag-building, and secondary phases. Ore minerals are represented by sphalerite and wurtzite (2.5 vol.%), and galena (1 vol.%) (Figure 3). The following primary phases were distinguished: fayalite (25.5 vol.%), K-feldspars (20 vol.%), and petedunnite (15 vol.%), and cristobalite (2 vol.%) (Figure 3). Secondary

phases are represented by the cerussite ($PbCO_3$; 6.5 vol.%). Willemite (27.5 vol.%) (Figure 3) may be the result of both the smelting process and weathering of the slags.

SEM-EDS confirmed the presence of all mineral groups distinguished in XRD (Figure 5). Ore minerals are represented by the sphalerite/wurtzite, which forms partly melted crystals up to 100 µm across, surrounded by the glass with a composition similar to the primary one from glassy slag as it is rich in Si, Ca, Zn, Pb, Fe, K, Al, and Ba (Figure 5a).

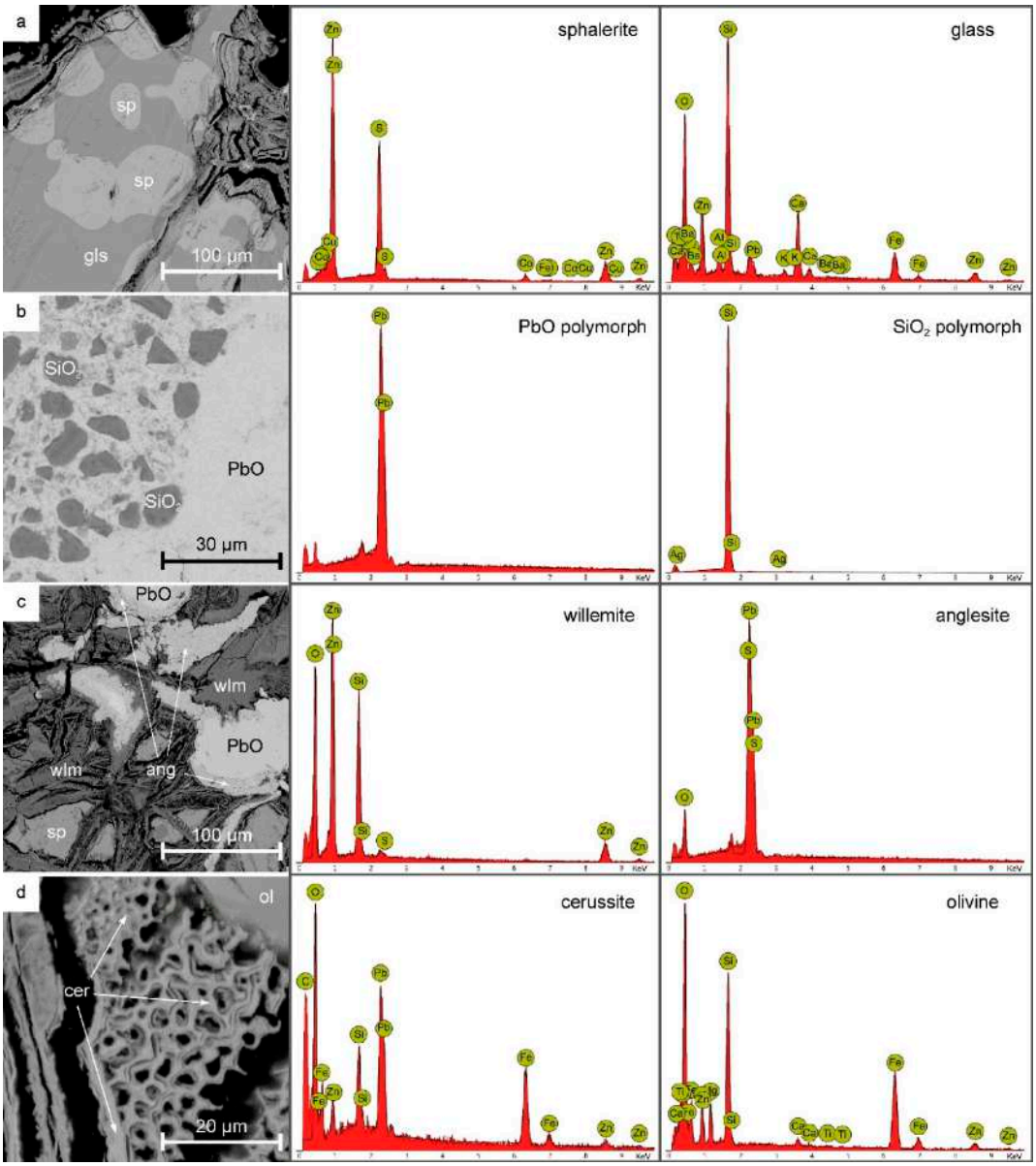

Figure 5. BSE images and EDS spectra of weathered slags. Abbreviations: ang—anglesite; cer—cerussite; gls—glass; ol—olivine; PbO—litharge or massicot; SiO_2—quartz, tridymite or cristobalite; sp—sphalerite; wlm—willemite.

Quartz (or its polymorphs) form small grain (up to 20 µm) dispersed in the PbO phase (Figure 5b). As a result of the weathering of PbO, anglesite ($PbSO_4$) forms as layers around the PbO core (Figure 5c). It co-occurs with secondary willemite forming irregular lath/needle aggregates, which in opposition to the primary willemite, lacks in Fe (Figure 5c). Olivine forms anhedral crystals to a few dozens of µm (Figure 5d). Cerussite is common among secondary minerals, and it forms highly irregular layered

aggregates up to 50 μm (Figure 5d; due to the small width of singular layers cerussite EDS contains elements from neighbor phases).

4.3. Chemical Composition of Slags

Glassy slag is mainly composed of the Si (34.58 wt.% of SiO_2), Fe (21.65 wt.% of Fe_2O_3), Ca (11.19 wt.% of CaO), Mg (3.39 wt.% of MgO), Al (1.81 wt.% of Al_2O_3) and K (1.19 wt.% of K_2O) (Table 3). It also contains extremely high amounts of Pb (above the detection limit of the method which was 10 wt.%) and Zn (13.25 wt.%) (Table 3). Among trace elements five concentrates above 100 ppm: As, Ba, Cu, Sr, and Sb (Table 3). The chemistry of the glassy slag almost perfectly fits the composition of the primary glass occurring within this slag type (Table 1). Crystalline in comparison with glassy slag is enriched in Si (46.50 wt.% of SiO_2), Ca (30.39 wt.% of CaO) and Al (3.50 wt.% of Al_2O_3) (Table 3), but is impoverished in Fe (9.81 wt.% of Fe_2O_3), Mg (0.99 wt.% of MgO), Pb (1.07 wt.%), Zn (2.83 wt.%) (Table 3). Weathered slag has the lowest content of Si (26.18 wt.% of SiO_2), Ca (4.48 wt.% of CaO), Al (1.17 wt.% of Al_2O_3), K (0.28 wt.% of K_2O) (Table 3), but highest of Fe (22.83 wt.% of Fe_2O_3), Mg, (4.31 wt.% of MgO), Zn (21.50 wt.%) (Table 3) and lead, which similarly to glassy slag reached detection limit of the method (10 wt.%) (Table 3).

Table 3. Chemical composition of the slags from Sławków.

		Glassy Slag	Crystalline Slag	Weathered Slag
SiO_2	wt.%	34.58	46.50	26.18
TiO_2	wt.%	0.11	0.15	0.10
Al_2O_3	wt.%	1.81	3.50	1.17
Fe_2O_3	wt.%	21.65	9.81	22.83
MnO	wt.%	0.20	0.18	0.25
MgO	wt.%	3.39	0.99	4.31
CaO	wt.%	11.19	30.39	4.48
K_2O	wt.%	1.19	1.69	0.28
Na_2O	wt.%	0.11	0.11	0.04
P_2O_5	wt.%	0.74	0.22	0.21
TOT/C	wt.%	0.08	0.43	0.30
TOT/S	wt.%	0.62	0.15	0.90
LOI	wt.%	−1.40	2.00	0.00
Ag	ppm	2	6	10
As	ppm	330	83	303
Ba	ppm	1424	273	672
Cr	ppm	48	67	208
Cu	ppm	108	25	87
Pb	ppm	>100,000	10,707	>100,000
Sr	ppm	384	109	120
Sb	ppm	415	6	101
V	ppm	52	137	18
Zn	ppm	132,504	28,276	214,973
Zr	ppm	73	73	151

4.4. Melting Point of Slags

As a consequence of heating, slags have undergone the following changes: (i) after heating in temperatures of up to 1000 °C, the colour of the slag changed to rusty-red, and the morphology of the sample became more oval (Figure 6b); (ii) heating up to 1100 °C caused melting of the sample in the entire volume, but the result is not fully unified; (Figure 6c); (iii) after heating in the temperature of up to 1150 °C, the slag is completely melted and unified (Figure 6d).

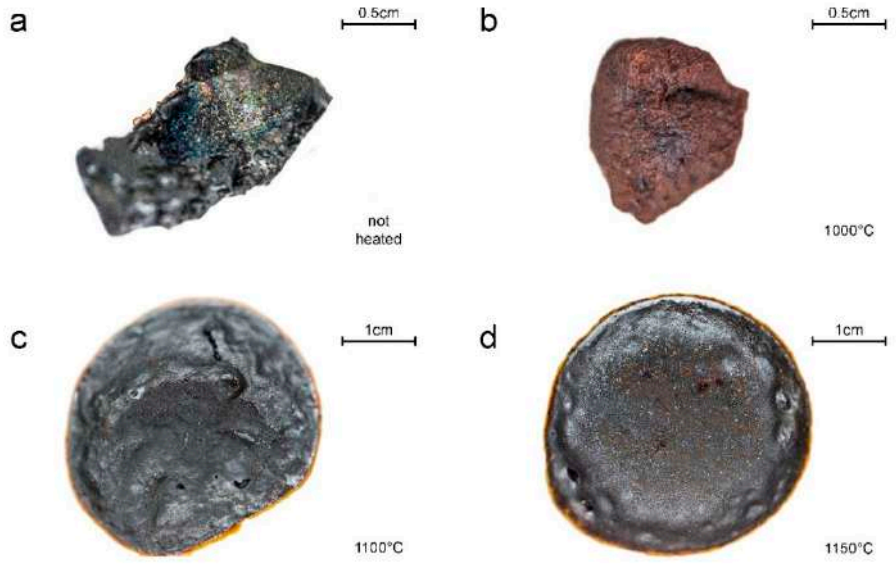

Figure 6. Macro photographs of glassy slag from Sławków after heating experiments in varied temperatures.

5. Discussion

5.1. Furnace Construction

Based on historical sources [22] and archaeological research [43] it is known that lead smelting in Sławków was divided into several stages. The first step in preparing the ore for further processing was enrichment. For this purpose, after the rocks were brought to the surface, they were crushed. Crushed ore was washed. Rinsing led to the separation of heavy minerals (containing lead) in specially prepared troughs [22,43]. During the archaeological research in the vicinity of Olkusz, the presence of this type of installation was found [43]. Lead ore might have been roasted by setting fire to a pile of wood with crushed ore [22]. This activity allowed the workers to get rid of sulfur and other unnecessary ingredients. As a result of roasting, sulfide minerals were oxidized, which in the later stages facilitated the smelting process. Historical data from Sławków [40] describes the existence of roasters in a neighbor of the smelter, thus we can assume that this process was used in Sławków. Smelting was carried out in a brick blast furnace. This was confirmed by the presence of bricks irregularly covered by the glass (Figure 7a) with a composition of glassy slag (Figure 7b,c). From the descriptions contained in the *De Re Metallica* [22], and other data [40] we attempted reconstruction of the smelter construction (Figure 8). Most often lead smelting installations consisted of six furnaces arranged in a sequence [22] while in Sławków there were only two [40] (Figure 8). In the room behind the blast furnaces, there were four bellows (powered by water from the Przemsza River) [40]. The bellows' nozzles were introduced into the furnace through an opening in the rear wall. In turn, the raw materials for production (e.g., ore, charcoal) were stored in rooms located in front of the furnaces. Before melting, the furnace had to be properly prepared. For this purpose, the internal walls and settling tanks were covered with a layer of a mixture of charcoal and clay. After preparation, the furnace was filled with charcoal. Then the ore was added [22]. During heating, lead and slag flowed to the bottom of the furnace. At the bottom, there was a settling tank (internal) in which the liquid lead and slag accumulated. Due to the difference in density, liquid lead accumulated at the bottom of the settler, followed by a layer of slag. After filling the internal settling tank, slag flowed through the drain hole to the settling tank in front of the furnace. The outflowing slag was removed by workers and tossed on the ground which contained sand (Figure 2b) [9]. Lead smelting was often carried out for several days. This was possible because the tapping holes were not closed, and the molten slag and lead could continuously flow out of the furnace [22].

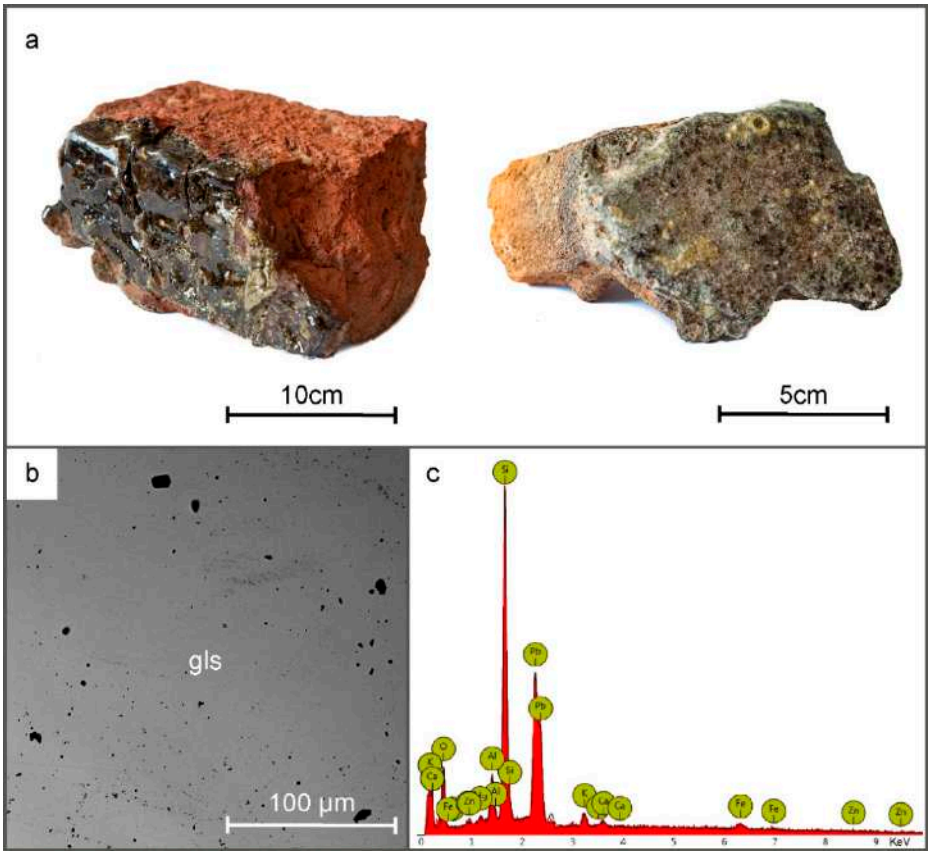

Figure 7. (**a**) macroscopic images of bricks covered with glass, (**b**) BSE image of glass covering the bricks, (**c**) EDS spectra of glass covering the brick. Abbreviation: gls—glass.

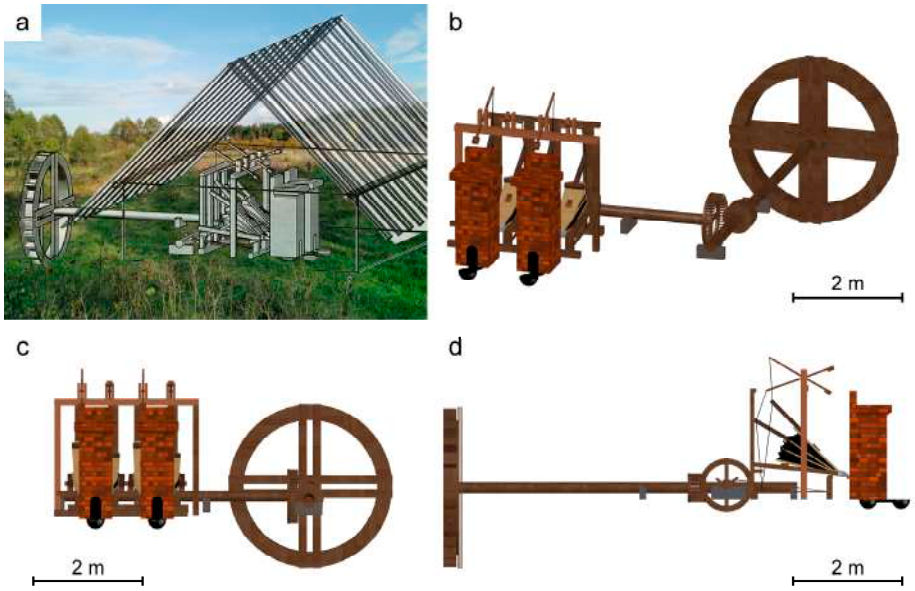

Figure 8. (**a**) reconstruction of the smelter at its original location in Sławków based on [9,22,40] (**b**–**d**) designs of the furnace in Sławków from different angles of view based on [22,40] and data from this study. The full, three-dimensional version of the project is available for download as Supplementary Figure S1.

5.2. Temperature Estimates

We decided to use an experimental approach to estimate the temperature during smelting in Sławków. Bearing in mind the fact that the slag is composed of elements almost entirely in the oxidized form (Table 1), this method should ensure precise estimations of temperature conditions during the historical smelting process, regardless of oxidation that might occur during experiments. Due to the diversified chemical composition, which includes eight main elements (Si, Fe, Zn, Pb, Ca, Al, K; Table 3), the application of popularly used [10,12,21,44] phase diagrams would be burdened with a significant error due to the depreciation of the liquidus by the elements not included. The phase composition (Figure 3) and the non-equilibrium crystallization of the material make it impossible to use geothermometers [21,44]. The conducted experiments indicate that the temperature during the metallurgical process was at least 1150 °C (Figure 6). At this temperature, the slag sample was entirely melted and unified, with the solidus for this material in the range of 900–1000 °C (Figure 6). On the base of experiments, in the 12th century, Ag-Pb furnace from Łosień (Polska) temperatures could be as high as 1450–1550 °C [8]. In 13th–14th century Cu-Pb-Ag slags from Massa Marittima (Italy), the estimated solidification temperatures were 1150–1300 °C [30]. In the case of material from Bohutín (14th century Ag-Pb slags, Czech Republic), the estimated temperature of melting based on phase diagrams was around 800–1200 °C [10]. The temperature during smelting process of Ag in the 14th–15th century in Kutná Hora was estimated at 1150–1300 °C [32]. In high-medieval Ag-Pb slags from Wiesloch (Germany), based on experiments, liquidus was at ca. 1100 °C [12]. The obtained temperature for the metallurgical process in Sławków coincides with the mentioned locations. Moreover, the reduction of furnace temperature over the centuries can be observed. This phenomenon is probably due to advancements in the metallurgical process and deepening knowledge about metal smelting. The later (19th century and later) smelting of MVT ores in Poland was carried out at higher temperatures up to 1350 °C [21], which, however, resulted from a different technological process and, above all, the recovery of Zn and not Pb.

5.3. Ores and Additions

The smelter in Sławków used the MVT deposits occurring in this area. As mentioned ore mineralization consists mainly of sulphides (galena, sphalerite, wurtzite, pyrite, and marcasite) and carbonates/silicates (smithsonite, monheimite, hydrozincite, cerussite, hemimorphite) as calamine, hosted in Middle Triassic dolomites [38,39]. Considering that the shallow deposits of calamine were probably exhausted by the 16th century, the activity of the smelter had to be based on sulphides. Confirmation of this fact is the existence of roasting furnaces [40] at the smelter for the oxidation of sulphide ores. The low content of sulphur (Table 3) in all slag types proves the high efficiency of the process. In crystalline and weathered slag, we found the presence of minor amounts of galena, sphalerite, and wurtzite (Figure 3), which additionally confirms the use of sulphide ores. Considering the phase (Figure 3) and chemical composition (Table 3), and the fact that used ores do not contain large amounts of silicates [38,39], the main addition in the process had to be SiO_2 concentrating phases. Its addition is responsible for separating and binding impurities formed during smelting from the obtained lead. Considering the location of the smelter near the river (Figure 1), river sand was an easily accessible source of this element, which was also indicated by the presence of fused quartz grains in the crystalline slag (Figure 4e). The use of sand in the historical lead recovery process has already been described in Łosień (Poland), Prague, and Kutná Hora (Czech Republic) [8,24,32]. The high iron content (up to 22.83 wt.% Fe_2O_3; Table 3) resulted from its common occurrence in the ore in the form of sulphides, mainly pyrite and marcasite [38,39]. Due to their overgrowth with galena in the deposits, it could not be effectively removed. This fact did not have an impact on the lead yield because Fe was bound in the oxide and silicate phases (Tables 1 and 2) that prevented the contamination of the lead obtained. Crystalline slag has a significantly different chemical composition from the glassy one (Table 3). It contains increased levels of SiO_2 (46.50 vs. 34.58 wt.%), CaO (30.39 vs. 11.19 wt.%), and Al_2O_3 (3.50 vs. 1.81 wt.%), and it is depleted in the elements building ore mineralization, i.e., Pb, Zn,

and Fe (Table 3). The phase composition is also dominated by minerals characteristic of high-calcium rocks, e.g., wollastonite, rankinite, melilite (Figure 3, Table 3). The existence of this type of slag may be associated with errors during smelting: not thorough cleaning of the ore from dolomite (increasing CaO amount, and decreasing the concentration of ore elements (Table 1) and too high sand addition (increasing the SiO_2 content; Table 3). Slags with similar phase composition were described in Na Slupi site, Prague (Czech Republic) [24], but they were considered a product of Ag production using the cupellation process. Existing historic data [40] does not mention Ag production in Sławków smelters thus until new information becomes available, we insist on the thesis of poor charge preparation. Moreover, the rare character of crystalline slag indicates the periodic occurrence of similar episodes during the existence of the smelter.

5.4. Atmosphere

The metallurgical process must have taken place under reducing conditions as they were necessary to obtain the metallic lead. However, the presence of zinc in the silicate and oxide phases indicates a significant variation in the oxygen fugacity within the metallurgical furnace. In reducing conditions and at temperatures above 907 °C [44], zinc vaporizes, and in this form, it migrates to the upper part of the furnace by convection. Under stabile reducing conditions, it would be completely removed from it. The high content of zinc in the slag (up to 13 wt.% In the glass slag; Table 3) indicates its secondary oxidation to ZnO with a boiling point of 2360 °C [44], which is significantly above the values obtainable in a similar process. Oxidation of Zn could have taken place in the upper parts of the furnace where the influence of C and CO is limited, or near the bellows supplying oxygen for the combustion of charcoal. In the oxidized form, zinc could react with the melt and enter the structure of almost all phases forming the studied slags (Tables 1 and 2). Increased Zn contents are typical for slags after Ag and Pb production [17,31,32]. Even higher Zn contents (up to 23 wt.% ZnO) were described in Wiesloch (Germany) [12], where, despite the different structure of the furnace, its concentration was explained based on the same thermodynamic relations. The coexistence of wüstite (Figure 3), hematite, and spinel (Table 2) within the analyzed slags additionally emphasizes large fluctuations in oxygen fugacity (from −12 $\log f\ O_2$ for wüstite-magnetite oxygen buffer to −4.5 $\log f\ O_2$ for magnetite-hematite oxygen buffer at a temperature of 1150 °C, the pressure of 1 bar [45]). The presence of these phases was found and similarly interpreted also in slags from other locations, e.g., Bohutín (Czech Republic) [10], Wiesloch (Germany) [12] and Massa Marittima (Italy) [31].

5.5. Viscosity

The melts viscosities have been widely studied in slag researches. It is due to the impact of melt viscosity on the segregation of components, the speed of crystallization, or the recovery of metals in the metallurgical process. The commonly used [10,46,47] method of calculating the melt viscosity index (v.i.) in archaeological research was developed by Bachmann [48]. The method base on the proportion of polymerizing to depolymerizing components in the silicate melt (values in wt.%):

$$\text{v.i.} = (CaO + MgO + MnO + FeO)/(SiO_2 + Al_2O_3)$$

Lower values of v.i. indicate a higher melt viscosity. In the case of the studied slags, their viscosity index ranges from 0.83 (crystalline slag) to 1.00 (glassy slag). These values are within the range proposed by Bachmann [48], according to which the values of v.i. are within 0.5–1. The glassy slag is characterized by a lower viscosity, which should have resulted in easier separation of the lead from it. This confirms that the smelting process that resulted in the formation of crystalline slag was less efficient. Values of v.i. for other locations often exceed the limits proposed by Bachmann [48]: for Mass Marittima (Italy), it ranges from 0.79 to 3.74 [31], and for Bohutín (Czech Republic) from 0.08 to 1.58 [10]. Due to the high

content of elements not included in the original Bachmann equation, a corrected formula has been proposed [10] that takes into account the high amount of lead and zinc:

$$\text{v.i.} = (CaO + MgO + MnO + FeO + PbO + ZnO)/(SiO_2 + Al_2O_3)$$

In this case, v.i. values of the slags from Sławków are elevated, especially in the case of glassy slag where it reaches 1.75. This indicates the importance of considering the influence of other elements in lowering the melt viscosity. A similar change was observed by Ettler et al. [10]. In the case of the Bohutín slags, where slags v.i. increased to 0.57–2.25.

Another method of calculating the viscosity was proposed by Giordano et al. [49]. This model is based on the chemical composition in mol% and calculates the viscosity values (Pa s) at the indicated temperatures according to the formula:

$$\log_{10}\eta = b_1 + (b_2 \cdot b_3)/(b_3 + SM) + b_4$$

where b_1–b_4 are temperature-dependent parameters derived from the model, and SM is structure modifier calculated as Σ mol% ($Na_2O + K_2O + CaO + MgO + MnO + FeO_{tot}/2$). In our study, we followed the modification proposed by Ettler et al. [10] including PbO and ZnO in the calculations. Details of the model can be found in the original publication by Giordano et al. [49]. For a temperature of 1150 °C and composition of Sławków slags, their viscosity is log η = 1.34 Pa s for glassy slag and 1.48 Pa s for crystalline slag. At the temperature of 630 °C (model [49] has been designed for the temperature range 630–2000 °C) the log η value increases to 11.71 Pa s for glassy slag and 11.88 Pa s for crystalline slag, showing rising viscosity as the melt cools down. The difference between these two types of material is consistent with the previous calculation methods. The viscosity of the slags in Bohutín was significantly higher (average log η = 2.20 Pa s for 1200 °C), which results from the much higher concentration of SiO_2 found in them [10].

6. Conclusions

The conducted research has allowed for the reconstruction of the lead smelting process in Sławków in the 16th–17th centuries. It confirms that the furnaces existing in the smelter had a brick structure, as evidenced by the finding of their glass-covered fragments with a glass composition corresponding to the slag from the location. In conjunction with literature studies, it was determined that the process based on the sulphide ores, which were roasted before the actual smelting. The furnace charge consisted of roasted ore, charcoal, and quartz sand. The addition of SiO_2 served to bind impurities in the form of glassy slag. During the smelting process, reducing conditions enabling to obtain metallic Pb prevailed, however, in the studied slags there were found phases (co-occurrence of wüstite, magnetite, and hematite) and elements indicating differentiated oxygen fugacity in the furnace. It probably resulted from the greater availability of oxygen in the highest part of the furnace and the vicinity of its supply with bellows. The characteristics of the slag show that the employees of the smelter were knowledgeable about the conditions during smelting. Despite the addition of SiO_2, the low melt viscosity was maintained (logη = 1.34 for 1150 °C), which facilitated the separation of metallic lead by density. Moreover, the melting point of the system was as low as 1150 °C. The obtained results in comparison with the data presented for earlier periods (early to late Middle Ages) illustrate the growing knowledge about lead smelting techniques, in particular in terms of the importance of additives on the course of the liquidus of the system and the effectiveness of metal separation from the melt.

Supplementary Materials: The following are available online at http://www.mdpi.com/2075 163X/10/11/1039/s1, Figure S1: three-dimensional design of the furnace in Sławków.

Author Contributions: Conceptualization, R.W. and M.S.; methodology, R.W., M.S. and K.K.; software, R.W., M.S. and K.K.; validation, R.W., M.S. and K.K.; formal analysis, R.W., M.S. and K.K.; investigation, R.W., M.S. and K.K.; resources, R.W., M.S. and K.K.; data curation, R.W., M.S. and K.K.; writing—original draft preparation, R.W., M.S. and K.K.; writing—review and editing, R.W., M.S. and K.K.; visualization, R.W., M.S. and K.K; supervision,

R.W.; project administration, R.W.; funding acquisition, R.W. and K.K. All authors have read and agreed to the published version of the manuscript.

Funding: This study was supported by the National Science Center (NCN) grant no. 2016/21/N/ST10/00838 (awarded to RW), and National Science Center (NCN) grant no. 2019/35/O/ST10/00313 (awarded to KK).

Acknowledgments: We would like to express our deepest gratitude to the Society of Sławków Lovers (Towarzystwo Miłośników Sławkowa) for their help and support during the research.

Conflicts of Interest: The authors declare no conflict of interest.

References

1. Waldron, H.A. Lead poisoning in the ancient world. *Med Hist.* **1973**, *17*, 391–399. [CrossRef] [PubMed]
2. Rozmus, D. *Wczesnośredniowieczne Zagłębie Hutnictwa Srebra i Ołowiu na Obszarach Obecnego Pogranicza Śląska i Małopolski (Druga Połowa XI–XII/XIII Wiek)*; Księgarnia Akademicka: Kraków, Poland, 2014.
3. Yahalom-Mack, N.; Langgut, D.; Dvir, O.; Tirosh, O.; Eliyahu-Behar, A.; Erel, Y.; Langford, B.; Frumkin, A.; Ullman, M.; Davidovich, U. The earliest lead object in the levant. *PLoS ONE* **2015**, *10*, e0142948. [CrossRef] [PubMed]
4. Hansen, S.; Montero-Ruiz, I.; Rovira, S.; Steiniger, D.; Toderaş, M. The earliest lead ore processing in Europe. 5th millennium BC finds from Pietrele on the Lower Danube. *PLoS ONE* **2019**, *14*, e0214218. [CrossRef] [PubMed]
5. Krzywy, I.; Krzywy, E.; Pastuszak-Gabinowska, M.; Brodkiewicz, A. Ołów-Czy jest się czego obawiać. *Rocz. Pomor. Akad. Med. W Szczec.* **2010**, *56*, 118–128.
6. Retief, F.P.; Cilliers, L. Lead poisoning in ancient Rome. *Acta Theol.* **2006**, *26*, 147–164. [CrossRef]
7. Jerome, O.N. *Lead and Lead Poisoning in Antiquity*; Wiley: Amsterdam, The Netherlands, 1983.
8. Cabała, J.; Warchulski, R.; Rozmus, D.; Środek, D.; Szełęg, E. Pb-rich slags, minerals, and pollution resulted from a medieval Ag-Pb smelting and mining operation in the Silesian-Cracovian region (southern Poland). *Minerals* **2020**, *10*, 28. [CrossRef]
9. Mendecki, M.J.; Warchulski, R.; Szczuka, M.; Środek, D.; Pierwoła, J. Geophysical and petrological studies of the former lead smelting waste dump in Sławków, Poland. *J. Appl. Geophys.* **2020**, *179*, 104080. [CrossRef]
10. Ettler, V.; Červinka, R.; Johan, Z. Mineralogy of medieval slags from lead and silver smelting (Bohutín, Příbram district, Czech Republic): Towards estimation of historical smelting conditions. *Archaeometry* **2009**, *51*, 987–1007. [CrossRef]
11. Anguilano, L.; Timberlake, S.; Rehren, T. An early medieval lead-smelting bole from Banc Tynddol, Cwmystwyth, Ceredigion. *Hist. Metall.* **2010**, *19*, 85–103.
12. Ströbele, F.; Wenzel, T.; Kronz, A.; Hildebrandt, L.H.; Markl, G. Mineralogical and geochemical characterization of high-medieval lead-silver smelting slags from Wiesloch near Heidelberg (Germany)—An approach to process reconstruction. *Archaeol. Anthropol. Sci.* **2010**, *2*, 191–215. [CrossRef]
13. Kupczak, K.; Warchulski, R.; Dulski, M.; Środek, D. Chemical and Phase Reactions on the Contact between Refractory Materials and Slags, a Case from the 19th Century Zn-Pb Smelter in Ruda Śląska, Poland. *Minerals* **2020**, *10*, 1006. [CrossRef]
14. Ploquin, A.; Allée, P.; Bailly-Maître, M.-C.; Baron, S.; de Beaulieu, J.-L.; Carignan, J.; Laurent, S.; de Veslud, C.L.C.; Lavoie, M.; Pulido, M. Medieval lead smelting on the Mont Lozère, southern France. In Proceedings of the Archaeometallurgy in Europe: International Conference, Milan, Italy, 24–26 September 2003; pp. 635–644.
15. Warchulski, R.; Mendecki, M.; Gawęda, A.; Sołtysiak, M.; Gadowski, M. Rainwater-induced migration of potentially toxic elements from a Zn-Pb slag dump in Ruda Śląska in light of mineralogical, geochemical and geophysical investigations. *Appl. Geochem.* **2019**, *109*, 104396. [CrossRef]
16. Tyszka, R.; Kierczak, J.; Pietranik, A.; Ettler, V.; Mihaljevič, M. Extensive weathering of zinc smelting slag in a heap in Upper Silesia (Poland): Potential environmental risks posed by mechanical disturbance of slag deposits. *Appl. Geochem.* **2014**, *40*, 70–81. [CrossRef]
17. Ettler, V.; Legendre, O.; Bodénan, F.; Touray, J.-C. Primary phases and natural weathering of old lead–zinc pyrometallurgical slag from Príbram, Czech Republic. *Can. Mineral.* **2001**, *39*, 873–888. [CrossRef]

18. Warchulski, R.; Gawęda, A.; Kupczak, K.; Banasik, K.; Krzykawski, T. Slags from Ruda Śląska, Poland as a large-scale laboratory for the crystallization of rare natural rocks: Melilitolites and paralavas. *Lithos* **2020**, *372–373*, 105666. [CrossRef]
19. Branca, T.A.; Colla, V. *Possible Uses of Steelmaking Slag in Agriculture: An Overview*; Intech Open Access Publisher: London, UK, 2012; pp. 335–356.
20. Geiseler, J. Use of steelworks slag in Europe. *Waste Manag.* **1996**, *16*, 59–63. [CrossRef]
21. Warchulski, R. Zn-Pb slag crystallization: Evaluating temperature conditions on the basis of geothermometry. *Eur. J. Mineral.* **2016**, *28*, 375–384. [CrossRef]
22. Agricola, G. *De Re Metallica*; Muzeum Karkonoskie w Jeleniej Górze: Jelenia Góra, Poland, 2000.
23. Chiarantini, L.; Benvenuti, M.; Costagliola, P.; Fedi, M.E.; Guideri, S.; Romualdi, A. Copper production at Baratti (Populonia, southern Tuscany) in the early Etruscan period (9th–8th centuries BC). *J. Archaeol. Sci.* **2009**, *36*, 1626–1636. [CrossRef]
24. Ettler, V.; Johan, Z.; Zavřel, J.; Wallisová, M.S.; Mihaljevič, M.; Šebek, O. Slag remains from the Na Slupi site (Prague, Czech Republic): Evidence for early medieval non-ferrous metal smelting. *J. Archaeol. Sci.* **2015**, *53*, 72–83. [CrossRef]
25. Chirikure, S. Geochemistry of ancient metallurgy: Examples from Africa and elsewhere. In *Treatise on Geochemistry*, 2nd ed.; Elsevier: Amsterdam, The Netherlands, 2014; pp. 169–189.
26. Warchulski, R.; Juszczuk, P.; Gawęda, A. Geochemistry, petrology and evolutionary computations in the service of archaeology: Restoration of the historical smelting process at the Katowice-Szopienice site. *Archaeol. Anthropol. Sci.* **2018**, *10*, 1023–1035. [CrossRef]
27. Kierczak, J.; Pietranik, A. Mineralogy and composition of historical Cu slags from the Rudawy Janowickie Mountains, southwestern Poland. *Can. Mineral.* **2011**, *49*, 1281–1296. [CrossRef]
28. Tumiati, S.; Casartelli, P.; Mambretti, A.; Martin, S.; Frizzo, P.; Rottoli, M. The ancient mine of Servette (Saint-Marcel, Val d'Aosta, Western Italian Alps): A mineralogical, metallurgical and charcoal analysis of furnace slags. *Archaeometry* **2005**, *47*, 317–340. [CrossRef]
29. Toffolo, L.; Addis, A.; Martin, S.; Nimis, P.; Rottoli, M.; Godard, G. The Misérègne slag deposit (Valle d'Aosta, Western Alps, Italy): Insights into (pre-) Roman copper metallurgy. *J. Archaeol. Sci. Rep.* **2018**, *19*, 248–260. [CrossRef]
30. Kądziołka, K.; Pietranik, A.; Kierczak, J.; Potysz, A.; Stolarczyk, A. Towards better reconstruction of smelting temperatures: Methodological review and the case of historical K-rich Cu-slags from the Old Copper Basin, Poland. *J. Archaeol. Sci.* **2020**, *118*, 105142. [CrossRef]
31. Manasse, A.; Mellini, M. Chemical and textural characterisation of medieval slags from the Massa Marittima smelting sites (Tuscany, Italy). *J. Cult. Herit.* **2002**, *3*, 187–198. [CrossRef]
32. Manasse, A.; Mellini, M. Archaeometallurgic slags from Kutná Hora. *N. Jahrb. Mineral. Mon.* **2002**, *2002*, 369–384. [CrossRef]
33. Benvenuti, M.; Orlando, A.; Borrini, D.; Chiarantini, L.; Costagliola, P.; Mazzotta, C.; Rimondi, V. Experimental smelting of iron ores from Elba Island (Tuscany, Italy): Results and implications for the reconstruction of ancient metallurgical processes and iron provenance. *J. Archaeol. Sci.* **2016**, *70*, 1–14. [CrossRef]
34. Saez, R.; Nocete, F.; Nieto, J.M.; Capitan, M.A.; Rovira, S. The extractive metallurgy of copper from cabezo Jure, huelva, Spain: Chemical and mineralogical study of slags dated to the third millenium B.C. *Can. Mineral.* **2003**, *41*, 627–638. [CrossRef]
35. Tropper, P.; Krismer, M.; Goldenberg, G. Recent and ancient copper production in the lower inn valley. An overview of prehistoric mining and primary copper metallurgy in the brixlegg mining district. *Mitt. Osterr. Mineral. Ges.* **2017**, *163*, 97–115.
36. Morawiec, J. Szlak handlowy Kijów-Kraków-Praga a ziemie nad Przemszą i Brynicą w IX-XI wieku. In *Osadnictwo nad Przemszą i Brynicą w Średniowieczu*; Sperka, J., Witkowski, S., Eds.; Polskie Towarzystwo Historyczne, Oddział w Cieszynie: Cieszyn, Poland, 2005; pp. 89–100.
37. Kownacki, H. *O Starozytnosci Kopalni Kruszcow Wyrabiania Metallow Czyli Robot Gorniczych w Kluczu Sławkowskim, Dobrach Niegdyś do Biskupstwa Krakowskiego Należących; i w Całey Tegoż Klucza Okolicy, w Znacznoy Części Powiatu Krakowskiego, Graniczący z Szląskiem*; Drukarnia Korpusu Kadetów: Warszawa, Poland, 1791.
38. Cabała, J.; Żogała, B.; Dubiel, R. Geochemical and geophysical study of historical Zn-Pb ore processing waste dump areas (southern Poland). *Pol. J. Environ. Stud.* **2008**, *17*, 693–700.

39. Cabała, J. *Development of Oxidation in Zn-Pb Deposits in Olkusz Area. Mineral Deposits at the Beginning of the 21st Century*; Balkema Publ.: Kraków, Poland, 2001; pp. 121–124.
40. Witkowski, S.; Krajniewski, J. *Inwentarz i Lustracje Klucza Sławkowskiego z XVII i XVIII Wieku*; Muzeum Miejskie "Sztygarka": Dąbrowa Górnicza, Poland, 2013.
41. Geoportal. Available online: https://www.geoportal.gov.pl (accessed on 10 October 2020).
42. Openstreetmap. ©OpenStreetMap Contributors under the Open Database License. Available online: https://www.openstreetmap.org (accessed on 10 October 2020).
43. Rozmus, D. Wokół Agricoli, czyli znaleziska archeologiczne średniowiecznych i nowożytnych reliktów górnictwa i hutnictwa kruszców. In *Z Notatnika Agricoli, Czyli u Źródeł Górnictwa Kruszcowego na Złożach Śląsko-Krakowskich*; Rams, A., Ed.; Muzeum Miasta Jaworzna: Jaworzno, Poland, 2016.
44. Pubchem. Available online: https://www.pubchem.ncbi.nlm.nih.gov/ (accessed on 2 October 2020).
45. Zhao, G.; Essene, E.; Zhang, Y. An oxygen barometer for rutile-ilmenite assemblages: Oxidation state of metasomatic agents in the mantle. *Earth Planet. Sci. Lett.* **1999**, *166*, 127–137. [CrossRef]
46. Puziewicz, J.; Zainoun, K.; Bril, H. Primary phases in pyrometallurgical slags from a zinc-smelting waste dump, Świętochłowice, Upper Silesia, Poland. *Can. Mineral.* **2007**, *45*, 1189–1200. [CrossRef]
47. Warchulski, R.; Gawęda, A.; Kądziołka-Gaweł, M.; Szopa, K. Composition and element mobilization in pyrometallurgical slags from the Orzeł Biały smelting plant in the Bytom-Piekary Śląskie area, Poland. *Mineral. Mag.* **2015**, *79*, 459–483. [CrossRef]
48. Bachmann, H.G. *The Identification of Slags from Archaeological Sites*; Institute of Archaeology Occasional Publication: London, UK, 1982.
49. Giordano, D.; Mangiacapra, A.; Potuzak, M.; Russell, J.K.; Romano, C.; Dingwell, D.B.; Di Muro, A. An expanded non-Arrhenian model for silicate melt viscosity: A treatment for metaluminous, peraluminous and peralkaline liquids. *Chem. Geol.* **2006**, *229*, 42–56. [CrossRef]

Received: 21 April 2022 | Accepted: 5 October 2022

DOI: 10.1111/arcm.12837

ORIGINAL ARTICLE

Reconstruction of smelting conditions during 16th- to 18th-century copper ore processing in the Kielce region (Old Polish Industrial District) based on slags from Miedziana Góra, Poland

Krzysztof Kupczak | **Rafał Warchulski** | **Aleksandra Gawęda**

Faculty of Natural Sciences, Institute of Earth Sciences, University of Silesia in Katowice, Sosnowiec, Poland

Correspondence

Krzysztof Kupczak, University of Silesia in Katowice, Faculty of Natural Sciences, Institute of Earth Sciences, Będzińska 60, 41-200 Sosnowiec, Poland.
Email: krzysztof.kupczak@us.edu.pl

Funding information

National Science Center (NCN), Grant/Award Number: 2019/35/O/ST10/00313

Abstract

This study presents the first reconstruction of the smelting conditions in 16th- to 18th-century smelters from Miedziana Góra (Holy Cross Mountains, Poland). Based on geochemical (inductively coupled plasma mass spectrometry/emission spectrometry, X-ray fluorescence) and mineralogical analysis (X-ray diffractometry, scanning electron microscopy, electron probe micro-analysis) of historical slags, their chemical/phase composition and the basic smelting parameters (temperature, melt viscosity, and oxygen fugacity) were determined. Due to the differences in chemical and phase composition, slags from different smelting stages have been distinguished: hypocrystalline slags (MG6) from speiss/matte production and glassy (MG1–MG5) from matte conversion. In glassy slags, pyroxenes, quartz/cristobalite grains, and aggregates composed of metallic Cu and PbO are dispersed in the glass. Hypocrystalline slags are composed of wollastonites, anorthites, and metallic Cu. The temperature range at which the slags were formed was from ~1100°C (solidus temperature) to 1150–1200°C (liquidus temperature). The silicate melt's viscosity was from $\log \eta = 1.19$ to 4.42 Pa s (at 1100–1200°C). The higher viscosity of MG1–MG5 slags indicates that, unlike MG6 slags, they were not formed during gravity separation. Information about the phase composition made it possible to determine the oxygen fugacity in the range of $\log fO_2 = -4$ to -12 atm. High oxygen fugacity indicates the oxidizing nature of the smelting process.

KEYWORDS
copper, oxygen fugacity, process reconstruction, slags, smelting, temperature, viscosity

INTRODUCTION

Copper was one of the first metals used by humanity, with the oldest traces of processing dating back over 10,000 years (Davis, 2001; Kundig & Weed, 2015). Initially, fragments of native copper were transformed by forging (Davis, 2001; US Congress, Office of Technology Assessment, 1988) and later by casting and smelting (Davis, 2001; Roberts et al., 2009). An important step in metallurgy was combining copper with other metals. The production of copper–tin alloys led to the beginning of the Bronze Age. Since then, this metal has become one of the most desirable materials (Davis, 2001; Kundig & Weed, 2015; Roberts et al., 2009; Tylecote, 1992). Today, copper is also an important material. It ranks third, after iron and aluminum, in production volume. Copper owes its position to very good electrical and thermal properties, corrosion resistance, ease of processing, and aesthetic values (Davenport et al., 2002; Davis, 2001).

Due to the thousand-year history of copper smelting, in many places around the world we can observe the remains of various stages of the production processes (Bassiakos & Catapotis, 2006; Bourgarit et al., 2003; Burger et al., 2010; Derkowska et al., 2021; Kapper et al., 2017; Maldonado & Rehren, 2009; Manasse et al., 2001; Rozendaal & Horn, 2013). The most common metallurgical residues are slags—materials formed during pyrometallurgical processing of ores. This process consists of heating the previously prepared material in a metallurgical furnace. After melting, the desired metal is separated from other charge components. Thus, the end product of the process is a pure metal and a solidified silicate melt (slag) containing the remaining components (e.g., Warchulski, Gawęda, et al., 2020). In the past, slags were often stored in landfills and partially used in subsequent melts as fluxes (Agricola, 1556; US Congress, Office of Technology Assessment, 1988; Warchulski, Szczuka, & Kupczak, 2020; Warchulski et al., 2022).

Analyses of old metallurgical residues are carried out to understand the issues related to historical metallurgy. Currently, slag analyses focus on several aspects. The main purpose is to understand the processes during crystallization (Kupczak et al., 2020; Warchulski, Gawęda, et al., 2020) and to reconstruct the smelting processes (e.g., Derkowska et al., 2021; Ströbele et al., 2010; Warchulski, Szczuka, & Kupczak, 2020; Warchulski et al., 2022). As slags were often stored in the vicinity of smelters, they seem to be the best source of information on the character of the metallurgical process carried out. The chemical and phase composition of slags are used to determine the smelting temperature, the viscosity of the melt, the type of oxidation–reduction conditions, and the type of added fluxes (Derkowska et al., 2021; Ettler et al., 2009; Kierczak & Pietranik, 2011; Maldonado & Rehren, 2009; Warchulski, 2016; Warchulski, Szczuka, & Kupczak, 2020; Warchulski et al., 2022). Another reason for their study is the environmental aspect. In historical times, due to the lack of tools enabling ecological protection (e.g., flue gas cleaning systems), the application of technologies using harmful elements (e.g., Hg during amalgamation; Nriagu, 1994), and the storage of waste containing potentially toxic elements (PTEs; Cabała et al., 2020; Kierczak et al., 2013; Warchulski et al., 2019) metallurgy led to the deterioration of the natural environment. Analyses of slags (Kierczak et al., 2013; Potysz et al., 2018), sediments (Aleksander-Kwaterczak & Helios-Rybicka, 2009; Bränvall et al., 2001; Kierczak et al., 2013), and soils (Baron et al., 2006; Ettler, 2016; Kierczak et al., 2013; Sutkowska et al., 2013; Zhou et al., 2020) provide information on the impact of historical smelting activities on the present contamination of the natural environment. These analyses allow determination of how PTEs migrate to the natural environment.

The Holy Cross Mountains area was one of the most important centers of Polish copper metallurgy from the 14th to the 20th century (Paulewicz, 1992), with numerous mines and smelters (Kowalczewski

& Szczecińska, 1977), but traces of most of them are becoming blurred. One of the most important copper deposits in the Holy Cross Mountains was Miedziana Góra (Old Polish Industrial District; Figure 1). This area has been gradually developed, and there is a risk of complete destruction of the traces of historical mining and metallurgy (Król & Urban, 2003). So far, many studies have been prepared on mining works carried out in Miedziana Góra (Kowalczewski, 1972; Król & Urban, 2003, 2007; Miczulski, 1972; Wojciechowski, 2002). Published data mainly concern the mined ores and the production volume (Król & Urban, 2003; Wojciechowski, 2002), and describe macroscopic features and chemical analyses of singular slag samples (Kowalczewski & Szczecińska, 1977). Some studies describe in detail the impact of mining and metallurgical works in the area of the Holy Cross Mountains on the local community (Paulewicz, 1992). Still, there is no detailed information on the phase composition of the slags and the smelting process itself. The primary aim of this research is to fill this gap. To achieve this goal, we have to answer the following questions: (i) What is the phase and chemical composition of slags from Miedziana Góra? (ii) What was the smelting temperature? (iii) What was the viscosity of the metallurgical melt during smelting? (iv) What kind of oxidation–reduction conditions existed during the process? (v) What kind of fluxes were used during smelting? For this purpose, slag samples were collected from the Kapliczna Hill, where metallurgical works were carried out in the 16th to 18th century (Figure 1). The conducted research is also crucial for future research to determine the impact of historical smelting on the natural environment. In order to assess the impact of metallurgy on the environment, the waste must first be analyzed in terms of mineralogy, petrography, and the conditions for its formation.

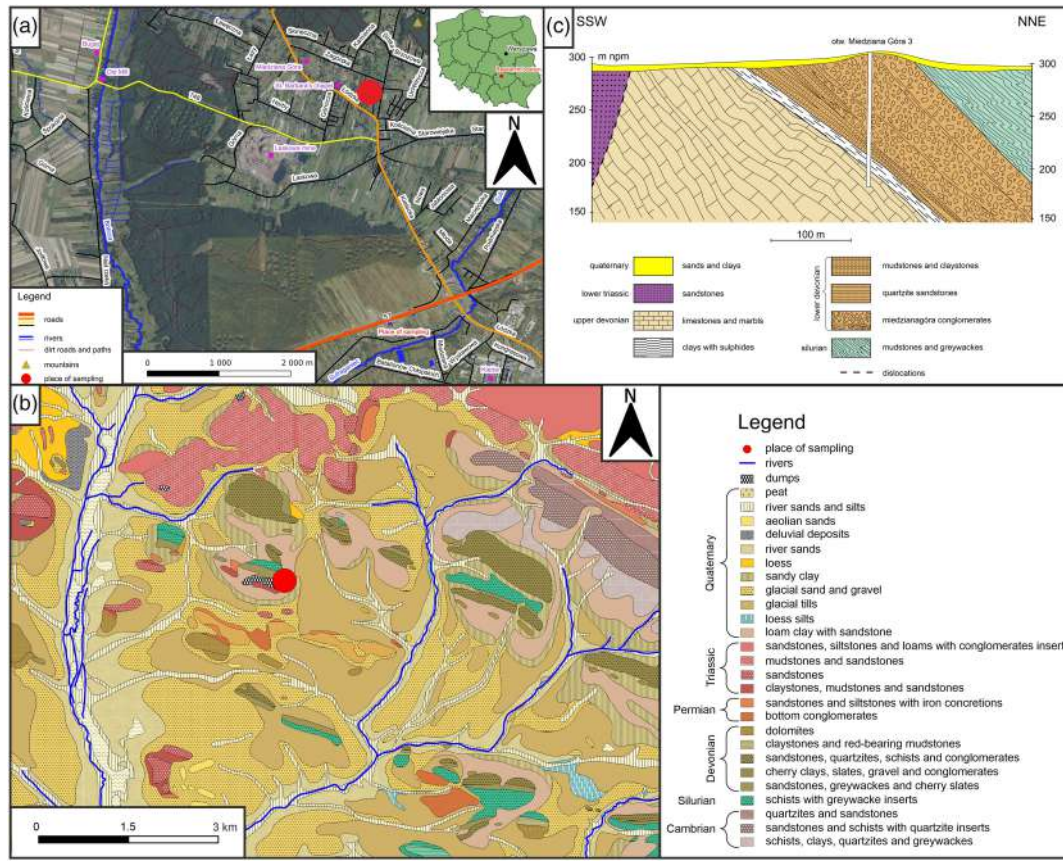

FIGURE 1 Localization (a) and geological (b) geoportal.gov.pl), and a cross-section through the Miedziana Góra ore (c) (modified from Rubinowski, 1970) [Color figure can be viewed at wileyonlinelibrary.com]

LOCATION AND HISTORICAL BACKGROUND

The research area is located in central Poland within the Holy Cross Mountains (Old Polish Industrial District; Figure 1). Miedziana Góra is located in the Świętokrzyskie voivodship, Kielce district. During fieldwork, slag samples were collected from the place where, in historical times, copper ore was mined and processed (Kowalczewski, 1972; Kowalczewski & Szczecińska, 1977; Figure 1).

Historical data show that the beginnings of mining work in Miedziana Góra date back to 1590–1592. At that time, copper ore was most likely discovered during the exploitation of iron ores (Król & Urban, 2007; Miczulski, 1972). Polymetallic ore from Miedziana Góra was used for Cu and PbO production. Exploitation was carried out by vertical shafts, which were then connected with galleries (Król & Urban, 2003). The metallurgical works in Miedziana Góra were carried out intermittently up to the 18th century in a small smelter on the Kapliczna Hill (Wojciechowski, 2002). The copper obtained from these deposits was used to produce raw fittings, sheets, vessels, and alloys with lead and zinc. In addition, at the end of the 18th century, the metals produced were used to make coins in the Polish royal mint and to create weapons (Król & Urban, 2003; Molenda, 1989). One of the most famous products made of copper from Miedziana Góra was the copper sheets used to cover the roof of the Wawel Royal Castle after a fire in the 16th century (Cracow; Król & Urban, 2003). From the end of the 17th century, problems during operation (including the lack of effective drainage of the mines) caused a crisis in the mining and metallurgy in Miedziana Góra. Despite the fact that attempts were made to improve the situation, mainly through subsidies and building drainage adits, the ore was exploited only periodically (Król & Urban, 2003). Along with the region's development, large smelters processing ores from the entire area replaced the small ones next to the mines (Kowalczewski, 1972). At the end of the 18th century, copper mines were reinvested, but metallurgical works were carried out in other localities (Wojciechowski, 2002). Due to the lack of historical data (most of the documents were destroyed during World War II), the production volume in Miedziana Góra is estimated only based on geological data. According to the existing studies, the production volume between the 16th and early 18th centuries is estimated at 4750–6250 tons (Kowalczewski, 1972), or at least 6200 tons (Molenda, 1989). In the later period, only data are available for the years 1785–1788, when 26 tons of copper and 26 tons of PbO were produced (Król & Urban, 2003). Due to the high demand for copper in Poland at that time, the production did not cover the local needs, and copper was imported from abroad during the period of metallurgical activity in the Old Polish Industrial District (Molenda, 1989). Despite production mainly for the Polish market, specialists from other metallurgical centers from Poland (e.g., Olkusz, Tarnowskie Góry) and Europe (e.g., Germany, Italy, Slovakia) were involved in conducting mining and metallurgical work within the Old Polish Industrial District (Kowalczewski, 1972). Craftsmen associated with mining in the Holy Cross Mountains had numerous privileges. However, the privileges were associated with severe penalties for infractions, resulting in separating of a specific social group (Paulewicz, 1992).

Geology

The polymetallic ores in the Kielce region occur in many locations. However, apart from Miedziana Góra and Miedzianka, they form only small concentrations (Kowalczewski, 1972). The Miedziana Góra ore is located in the zone of the Miedziana Góra fold, overlapping the northern part of the Kostomłoty syncline. Lower Devonian sediments (conglomerates, quartzites, silts, schist, and ore-bearing clays) are overlaid from the northeast by Upper Devonian formations (limestones and marbles; Wojciechowski, 2002; Figure 1). Based on complete chemical analyses that were carried out during the documentation of the ore in the 20th century, it consists mainly of SiO_2 (av. 40.93 wt%), Al_2O_3 (av. 20.84 wt%), and Fe (over 10 wt% of Fe + FeS + FeO + Fe_2O_3), with Cu content up to 1.72 wt% (as Cu + CuS + CuO), Pb up to 0.07 wt% and Zn up to 0.85 wt%. However, in historical times

ores with Cu content of up to 12 wt% were processed (Rubinowski, 1970). The Miedziana Góra ore can be divided into an oxidized zone and a sulfide zone (primary zone). In the primary zone, the main ore minerals are pyrite (FeS_2), chalcopyrite ($CuFeS_2$), chalcocite (Cu_2S), bornite (Cu_5FeS_4), tetrahedrite ($[Cu,Fe]_{12}Sb_4S_{13}$), sphalerite (ZnS), and galena (PbS). Sulfide minerals occur as single grains or clusters and radial clusters in clay rocks. The oxidation zone contains malachite ($Cu_2(CO_3)(OH)_2$), azurite ($Cu_3(CO_3)_2(OH)_2$), chrysocolla ($(Cu, Al)_2H_2Si_2O_5(OH)_4 \cdot n(H_2O)$), iron oxides and hydroxides, siderite ($FeCO_3$), smithsonite ($ZnCO_3$), and manganese oxides (Piekarski, 1961).

MATERIALS AND METHODS

Sampling

During fieldwork, in the spring of 2021 slag samples were collected from the area of Kapliczna Hill (in Miedziana Góra; Figure 1), where the smelter was most probably located (Figure 1). During the works, 62 samples of slags were collected, which were then divided into six macroscopically different types (MG1–MG6), described below.

Chemical and phase analyzes

The first stage of the analysis involved macroscopic and microscopic observations to assess the slag's texture. For this purpose, an Olympus BX-51 polarizing microscope was used (Institute of Earth Sciences, University of Silesia). The samples were then analyzed by scanning electron microscopy with energy-dispersive spectrometry (SEM-EDS). Analysis with SEM allowed us to more accurately determine the morphology of phases present in slags and their approximate chemical composition. A Phenom XL microscope (Faculty of Natural Sciences, University of Silesia) was used during this analysis. An electron micro-probe (Cameca SX100, Inter-Institutional Laboratory of Microanalysis of Minerals and Synthetic Materials, University of Warsaw) was used to determine the exact chemical composition of the phases present in the samples. EPM analyses were performed at 15 keV accelerating voltage, a 10–20.1 nA beam current, and a beam diameter of up to 5 μm. The following standards were used during the measurements: Na—albite ($NaAlSi_3O_8$); Mg, Si, Ca—diopside ($[Ca,Mg,Fe]_2SiO_3$); Al, K—orthoclase ($KAlSi_3O_8$); Ba—barite ($BaSO_4$); Ti—rutile (TiO_2); Cr—Cr_2O_3; Pb—crocoite ($PbCrO_4$); Fe—Fe_2O_3, chalcopyrite ($CuFeS_2$); Mn—rhodonite ($CaMn_3Mn[Si_5O_{15}]$); Zn—sphalerite (ZnS); Cl—sodalite ($Na_8[Al_6Si_6O_{24}]Cl_2$); P—YPO_4; As—GaAs; Sr—celestine ($SrSO_4$); Co—CoO; Ni—NiO; V—V_2O_5; Cu—cuprite (Cu_2O); As—GaAs; S—chalcopyrite ($CuFeS_2$), barite ($BaSO_4$); Sb—stibnite (Sb_2S_3).

Samples representing all six types of slags were also analyzed for phase composition and chemistry. The phase composition of the samples was determined using the PANalytical X'PERT PRO-PW 3040/60 and PANalytical X'Pert PW 3710 X-ray diffractometers equipped with $CoK_{\alpha 1}$ (PW 3040/60) and $CuK_{\alpha 1}$ (PW 3710) source radiation, Fe-filter (for Co) and Ni-filter (for Cu) to reduce the K_β radiation. During analyses, the X'celerator detectors were used (Faculty of Natural Sciences, University of Silesia). The analyses were performed in the 5–90° 2θ angular range at 40 kV voltage (40 mA). For quantitative phase composition, a Rietveld analysis was performed. The X'PERT High Score Plus software and the PDF4+ database were used.

To obtain the chemical composition, including major, minor, and trace elements, the combination of X-ray fluorescence (XRF) spectrometry, inductively coupled plasma emission spectrometer (ICP-ES), and inductively coupled plasma mass spectrometry (ICP-MS) was applied. During the ICP analyses, multi-acid digestion was used. XRF and ICP-MS/ES analyses were performed by Bureau Veritas Mineral Laboratories (Canada). Loss of ignition was determined at 1000°C.

High-temperature experiments

Experimental melting in a laboratory furnace was used to determine the solidus and liquidus temperature of slags. Two types of slag were selected for the experiment (MG3 and MG6), representing the two most diverse slags. The MG3 sample is the most common type of slag among glassy samples (23 out of 58 samples), while the MG6 sample is the only hypocrystalline type of slag. The samples were crushed, cut into fragments with a volume of about 1 cm^3, and heated in crucibles with gradually rising temperature until the entire material was melted. Each time after heating, the samples were subjected to rapid cooling. Experiments were performed at the Institute of Earth Sciences of the University of Silesia in a chamber furnace PLF 160/5 with a PC 442/18 controller, SiC heaters, and Thermocouple S with a maximum working temperature of 1550°C.

Software

To determine the liquidus temperatures, the MELTS-Rhyolite v.1.0.2 software package (Ghiorso & Gualda, 2015; Gualda et al., 2012) was used. The liquidus temperature was calculated based on the bulk chemical composition (MG6) and the averaged chemical composition of the glass that forms the slags (MG1–MG4). Due to the presence of zones with increased accumulation of metallic and quartz/cristobalite phases, the MG5 sample was not used for temperature determination. For calculations by MELTS-Rhyolite, chemical composition was normalized to 100 wt%, a pressure of 1 bar, and a Q-Fa-Mt oxygen buffer was used. For graphical data processing, the AUTODESK AutoCAD 2021 and CorelDRAW2021 version 22.1.1.523 (educational licenses) were used.

RESULTS

Petrographic characteristics of slags

Slags from Miedziana Góra were divided into glassy (MG1–MG5) and hypocrystalline (MG6) samples. X-ray diffractometry (XRD) analyses confirmed the presence of an amorphous (glassy) phase in MG1–MG5 samples (Figure 3). Apart from the glass, MG1–MG5 slags contain SiO_2 polymorphs (quartz and cristobalite; 15.7–90.4 vol%), clinopyroxenes (6.4–79.5 vol%), copper (Cu; 0.3–4.7 vol%), and litharge (PbO; up to 0.4 vol%). However, due to the lack of information on the percentage of glass, the presented results only include the relative proportions of the crystalline phases (Figure 3).

The MG1 slag is black and contains quartz/cristobalite grains (up to 2–3 mm, occasionally up to 20 mm in size; 83.9 vol%; Figures 2a and 3). Imprints or fragments of charcoal appear on the surface. SEM (Figure 4a) observations confirmed that the MG1 sample comprises glass with numerous small (a few micrometers across; rarely up to several dozen micrometers; Figure 4a) metallic phases. They are composed of metallic Cu (1.4 vol%; Figure 3) and litharge (0.1 vol%; Figures 3 and 4a).

MG2 slags have a light blue/greenish color with visible dark-blue glassy layers with quartz/cristobalite grains up to 5 mm (83.2 vol%; Figures 2b and 3). This sample also contains metallic phases: Cu (0.3 vol%; Figure 3) and litharge (0.4 vol%; Figure 3) with a diameter up to 30 μm (Figure 4b) and skeletal clinopyroxene crystals (16.0 vol.%).

The MG3 sample is dark blue in color with light-blue and brown layers (Figure 2c). In MG3, quartz/cristobalite (76.4 vol%; Figure 3) grains are up to 1–2 mm, occasionally up to 5 mm in diameter (Figure 2c). In MG3 samples, clinopyroxene crystals were found in the form of dendritic crystals with lengths up to 100 μm (22.5 vol%; Figures 3 and 4c). In MG3 metallic phases were present as metallic copper (1.1 vol%). Cu sulfides (matte) and arsenides (speiss) are also present.

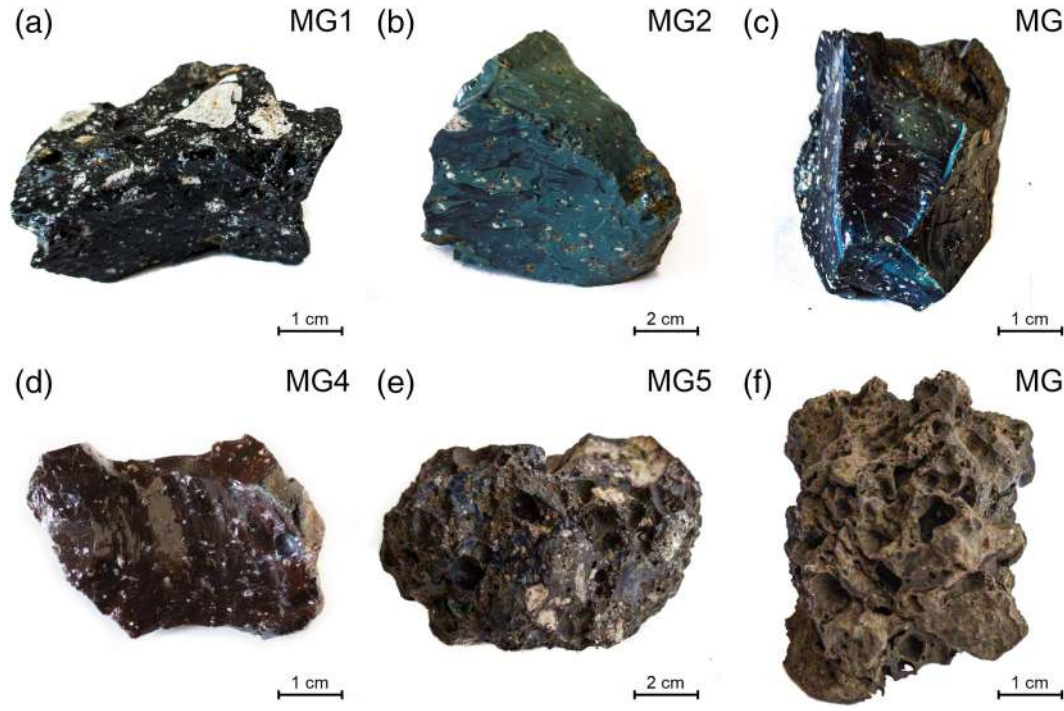

FIGURE 2 Macroscopic images of slags occurring in Miedziana Góra [Color figure can be viewed at wileyonlinelibrary.com]

The MG4 slag is brown in color, with visible interlacing of black slags. Quartz/cristobalite grains are present here in smaller quantities (15.7 vol%; Figure 3) than in the other glassy slag types (Figure 3) and are up to 1 mm in diameter (Figure 2). Clinopyroxenes constitute 79.5 vol% of crystalline phases present in the MG4 sample (Figure 3). In this sample, along with metallic Cu (4.7 vol%; Figure 3), metallic Pb, matte, and speiss occur (Figure 4d).

Unlike the MG1–MG4 samples, the MG5 slags have a porous texture, with pores up to 20 mm in diameter. The MG5 slags are characterized by a variety of colors, but blue and greenish-blue predominate. The MG5 sample consists of SiO_2 polymorphs (90.4 vol%), clinopyroxene (6.4 vol%), metallic Cu (3.1 vol%), and litharge (0.1 vol%; Figure 3). The size of quartz/cristobalite grains reaches up to 20 mm (Figure 2e). Metallic aggregates composed of metallic Cu and litharge are up to 50 μm in diameter (Figure 4e). Occasionally present, azurite ($Cu_3(CO_3)_2(OH)_2$) (Figure 4e) is a secondary phase.

The MG6 slags, unlike the others, are characterized by a hypocrystalline texture and a gray color. That type of slag is porous, with pore size up to 20–30 mm in diameter (Figure 2f). During SEM observations, skeletal crystals up to 400 μm long were commonly observed. These crystals are composed of phases with a structure corresponding to the wollastonite group minerals (54.6 vol% of bustamite and 5.6 vol% of ferrobustamite; Figure 3). Metallic Cu, along with Cu sulfides, are also noted up to a few micrometers in diameter (Figure 4f). The presence of anorthite (34.2 vol%), quartz (3.8 vol%), pyroxenes (1.2 vol%), and metallic phases (0.6 vol% Cu and 0.1 vol% Pb;) was revealed by XRD (Figure 3).

Bulk chemical composition

The glassy samples (MG1–MG5), despite the macroscopic differences, are characterized by similar chemical compositions (Table 1). Their main chemical components are: SiO_2 (54.41–57.14 wt%;

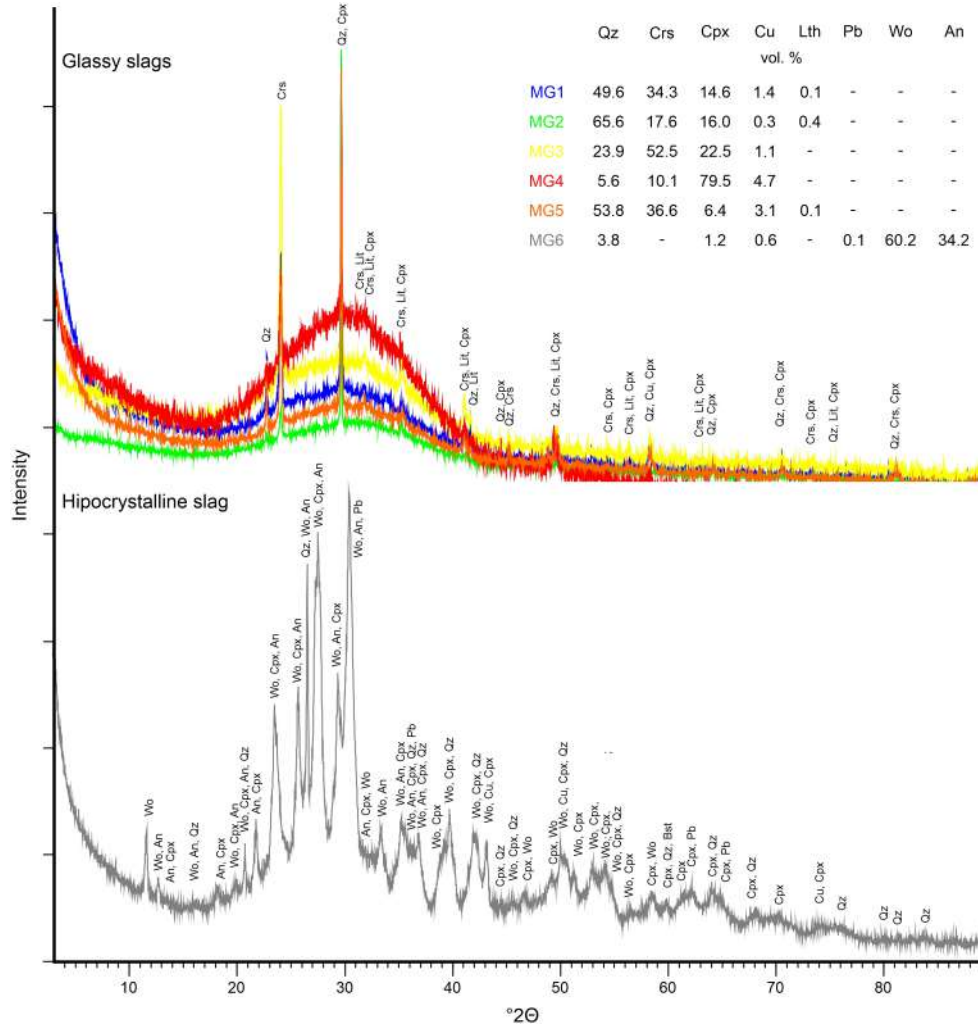

FIGURE 3 Results of X-ray diffraction analyses of slag samples from Miedziana Góra. Abbreviations: An, anorthite; Cpx, clinopyroxene; Cu, copper; Crs, cristobalite; Lth, litharge; Pb, lead; Qz, quartz; Wo, wollastonite group (bustamite + ferrobustamite) [Color figure can be viewed at wileyonlinelibrary.com]

Table 1), CaO (11.25–15.36 wt%), FeO (8.42–11.03 wt%), and Al_2O_3 (7.77–9.14 wt%). Additionally, the presence of K_2O (2.32–2.72 wt%), MgO (1.18–1.74 wt%), and MnO (0.99–1.56 wt%) was found (Table 1). Large differences among glassy slags occur in the content of Pb and Cu. The MG1, MG4, and MG5 slags contain more Pb (4.32–5.91 wt%) than the MG2 and MG3 slags (2.25 and 2.53 wt%, respectively), while samples MG1 and MG5 are characterized by higher Cu contents (0.97 and 1.61 wt%, respectively) than MG2 (0.40 wt%), MG3 (0.56 wt%), and MG4 (0.55 wt%; Table 1). Glassy slags also concentrate Zn (2168–5575 ppm), As (88–374 ppm), and Sb (72–298 ppm; Table 1). The hypocrystalline MG6 slag contains less SiO_2 (49.81 wt%) and Pb (0.50 wt%), with higher amounts of CaO (21.64 wt%) and Cu (4.98 wt%) compared to glassy slags (MG1–MG5; Table 1).

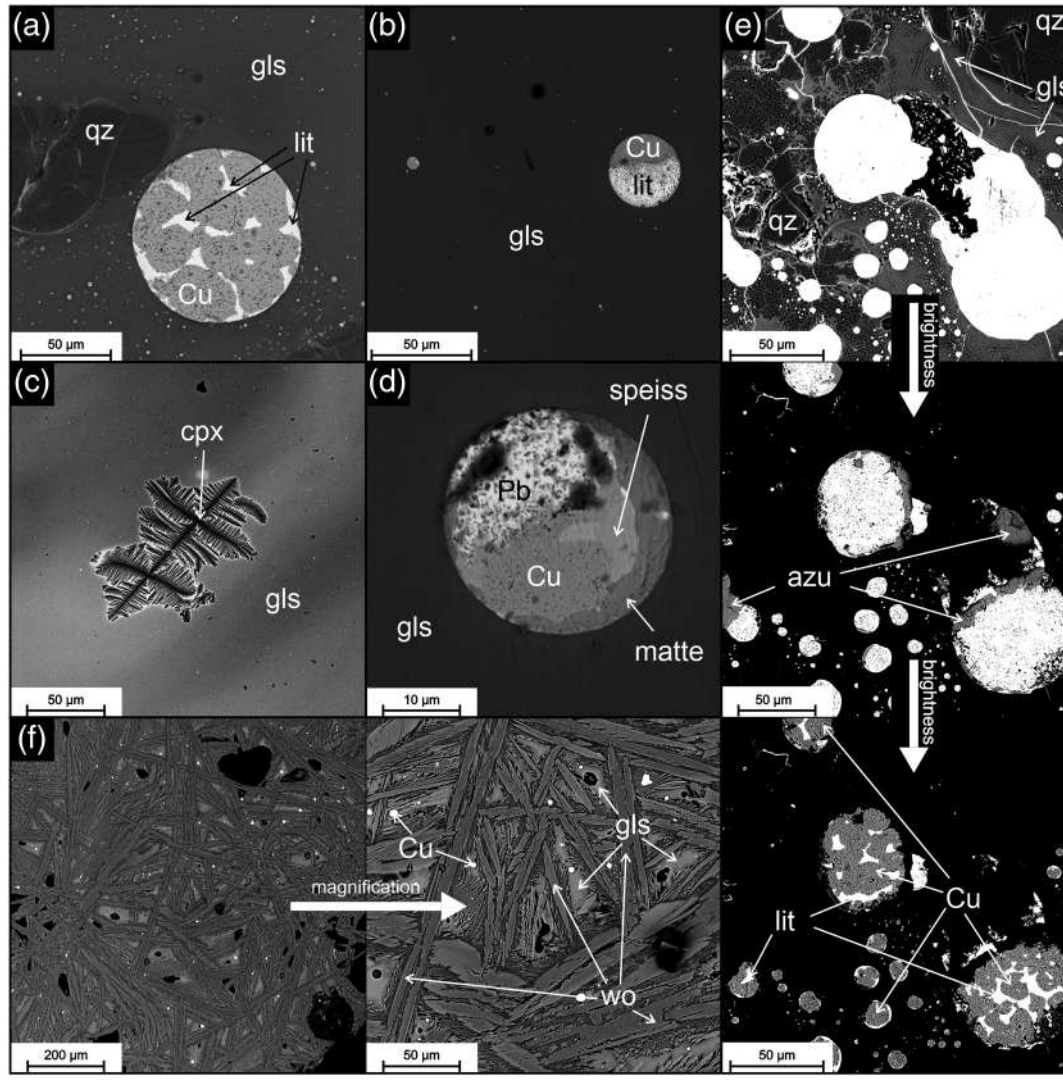

FIGURE 4 Backscattered electron images of phases occurring in slags from Miedziana Góra: (a) MG1 sample; (b) MG2 sample; (c) MG3 sample; (d) MG4 sample; (e) MG5 sample with decreasing brightness; (f) MG6 sample with magnification. Abbreviations: azu, azurite; cpx, clinopyroxene; Cu, metallic copper; gls, Glass; lit, litharge; wo, wollastonite group phases

Phase chemistry

Oxides

The most common oxides in the analyzed slags are the SiO_2 polymorphs. Quartz/cristobalite crystals (up to 99.1 wt% of SiO_2; Table 2) are commonly found in MG1–MG5 slags and, to a lesser extent, in MG6 sample (Figures 3 and 4). Litharge (PbO) was observed in MG1, MG2, and MG5 slags in the form of phases resulting from chemical demixing of the metallic melt (Figure 4). It contains the addition of Cu (up to 1.1 wt% of CuO; Table 2).

TABLE 1 Chemical composition of slags from Miedziana Góra

		MG1	MG2	MG3	MG4	MG5	MG6
P_2O_5	%	0.58	0.43	0.44	0.59	0.61	0.38
SiO_2		55.28	55.61	57.14	54.41	55.61	49.81
TiO_2		0.46	0.39	0.44	0.47	0.42	0.33
Al_2O_3		9.14	7.79	8.80	8.94	7.77	7.54
FeO		8.42	10.61	11.03	10.43	9.78	10.75
MnO		0.99	1.56	1.47	1.16	1.05	1.51
CaO		14.83	15.36	11.25	12.69	11.52	21.64
MgO		1.19	1.74	1.55	1.69	1.18	1.10
Na_2O		0.17	0.15	0.14	0.15	0.15	0.10
K_2O		2.32	2.46	2.64	2.72	2.45	1.67
SO_3		0.06	0.05	0.03	0.09	0.08	0.11
BaO		0.77	0.87	0.83	0.85	1.04	0.27
TOT/C		<0.02	<0.02	0.09	<0.02	0.04	0.10
TOT/S		0.02	<0.02	0.02	0.04	0.03	0.05
LOI		−1.30	−1.40	−1.30	−1.10	−1.30	−1.60
Cu		0.97	0.40	0.56	0.55	1.61	4.98
Pb		4.32	2.25	2.53	4.93	5.91	0.50
Zn	ppm	3784	2168	4524	5063	5575	2403
As		172	88	127	235	374	471
Sb		149	72	86	202	298	101
Ni		65	38	48	68	116	88
Co		208	99	136	141	234	162

Carbonates

Carbonates, represented by azurite, were found only in sample MG5 and occur only in the vicinity of metallic phases (Figure 4e). Chemically, azurite comprises Cu (up to 67.0 wt% of CuO), with Pb substitutions reaching up to 2.9 wt% of PbO (Table 2).

Silicates

Two types of silicate were distinguished in the Miedziana Góra slags. The MG1–MG5 slags contain clinopyroxenes, with a chemical composition corresponding to diopside ($CaMgSi_2O_6$)–hedenbergite ($CaFe^{2+}Si_2O_6$) solid solution, with numerous substitutions: Al (1.71–2.93 wt% of Al_2O_3), Mn (1.41–1.60 wt% of MnO), and minor concentrations of K_2O, TiO_2, and Cr_2O_3 (Table 2). In the MG6 sample, the wollastonite group are the only silicate phases found during EPM analyses, consisting of Si (50.3–50.5 wt% of SiO_2), Ca (36.1–39.3 wt% of CaO), Fe (5.0–6.4 wt% of FeO), and Mn (1.90–1.97 wt% of MnO). The substitution of Al (up to 2.20 wt% of Al_2O_3), Mg (up to 1.24 wt% of MgO), and less than 0.5 wt% of oxide of Ti and K was observed (Table 2). The Fe^{2+} substitutions affect the unit cell size (Yamanaka et al., 1977). For this reason, in these phases, the unit cell is more closely related to the bustamite/ferrobustamite than to the wollastonite (Figure 3). The zoning visible in backscattered electron (BSE) images (Figure 4f) results from enrichment of the crystal rims in FeO with a simultaneous decrease in the CaO content.

TABLE 2 Representative EPMA (Electron Probe Micro-analysis) data of the chemical composition of phases occurring in slags

	qz	wo	wo	cpx	cpx	cpx	azu	lit		bdss	cc	Cu	Cu
SiO2	99.1	50.5	50.3	50.2	50.6	50.4	na	0.64	**S**	25.7	19.7	bdl	bdl
TiO2	bd	0.10	0.11	0.21	bdl	bdl	na	bdl	**Fe**	9.4	0.43	0.15	bdl
Al2O3	0.08	0.35	2.20	1.71	2.93	2.28	na	0.37	**Mn**	0.04	bdl	bdl	bdl
FeO	0.06	5.0	6.4	12.8	13.8	12.9	na	bdl	**Co**	0.01	bdl	bdl	bdl
MnO	bdl	1.90	1.97	1.41	1.48	1.60	na	bdl	**Ni**	bdl	bdl	0.20	bdl
MgO	bdl	1.08	1.24	8.8	7.5	8.1	na	bdl	**Cu**	61.9	77.6	93.6	98.0
CaO	bdl	39.3	36.1	23.5	22.2	22.5	na	0.14	**Zn**	0.12	bdl	0.15	bdl
K2O	bdl	0.10	0.42	bdl	0.32	0.28	na	bdl	**As**	0.06	0.17	2.8	0.15
PbO	na	bdl	bdl	na	na	na	2.90	98.1	**Sb**	bdl	bdl	0.50	bdl
CuO	na	na	na	na	na	na	67.0	1.10	Total	97.23	97.9	97.4	98.15
Cr2O3	bdl	bdl	bdl	0.07	0.05	bdl	na	bdl					
CoO	na	na	na	na	na	na	0.12	na					
Total	99.24	98.33	98.74	98.7	98.88	98.06	70.02	100.35					
a.p.f.u. (atom per formula unit)									**Atomic concentration**				
Si	1	1	0.99	1.96	1.96	1.97	-	0.02	**S**	41.14	33.29	0.03	-
Ti	-	-	-	0.01	0.01	0.01	-	-	**Fe**	8.61	0.42	0.17	-
Al	-	0.01	0.05	0.08	0.13	0.1	-	0.01	**Mn**	0.03	-	-	-
Fe2+	-	0.08	0.11	0.42	0.45	0.42	-	-	**Co**	0.01	-	0	-
Mn	-	0.03	0.03	0.04	0.05	0.05	-	-	**Ni**	-	-	0.23	-
Mg	-	0.03	0.04	0.51	0.43	0.47	-	-	**Cu**	50.07	66.17	96.7	99.87
Ca	-	0.84	0.76	0.98	0.92	0.94	-	0.01	**Zn**	0.09	-	0.15	-
K	-	-	0.01	0	0.02	0.01	-	-	**As**	0.04	0.12	2.44	0.13
Pb	-	-	-	-	-	-	0.04	0.89	**Sb**	-	-	0.27	-
Cu	-	-	-	-	-	-	2.95	0.03	Total	100	100	100	100
Cr	-	-	-	-	-	-	-	-					
Co	-	-	-	-	-	-	-						
o2-	2	3	3	6	6	6	3	2					

Abbreviations: azu, azurite; bdss, bornite–digenite solid solution; cc, chalcocite; cpx, clinopyroxene; Cu, copper; lit, litharge; qz, quartz; wo, wollastonite group; bdl, below detection limit; na, not analyzed.

Sulfides and metallic phases

Sulfides in the Miedziana Góra slags are represented by bornite (Cu_5FeS_4)–digenite (Cu_9S_5) solid solution (bdss) phases and by chalcocite. The bdss phases are mainly composed of Cu (up to 61.9 wt%), S (up to 25.7 wt%), and Fe (up to 9.4 wt%). In addition, they concentrate Zn (up to 0.12 wt%) and less than 0.1 wt% of Mn, Co, and As (Table 2). Chalcocite is composed of Cu (up to 77.6 wt%) and S (up to 19.7 wt%) with Fe (up to 0.43 wt%) and As (up to 0.17 wt%) substitution (Table 2). The metallic copper, apart from Cu (93.6–98.0 wt%), contains As (up to 2.8 wt%), Sb (up to 0.50 wt%), Ni (up to 0.20 wt%), Fe (up to 0.15 wt%), and Zn (up to 0.15 wt%; Table 2).

Glass

All slag samples from Miedziana Góra contain glass. In MG1–MG5 samples, it is the main component. The glass in the MG1–MG4 slags is, on average, rich in SiO_2 (52.1–57.1 wt%), Al_2O_3 (6.5–11.4 wt%), FeO (5.6–11.9 wt%), and CaO (15.3–16.3 wt%; Table 3). Additionally, PbO enrichment (up to 6.3 wt%) was observed. In the MG5 sample, zones with metallic phases and SiO_2 polymorph concentrations are present (Figure 4e and Table 3). In these zones, glass contains more PbO (up to 21.2 wt%) and less CaO (av. 8.9 wt%) than in MG1–MG4 slags (Table 3). When compared to MG1–MG4 slags, a greater variation in SiO_2 content was also observed in MG5 slags (up to 68.8 wt%; Table 3). In the MG6 slag, the average glass is also mostly made of SiO_2 (av. 50.5 wt%), but the glass has a higher CaO (av. 21.9 wt%) and a lower PbO (av. 0.38 wt%) content. The proportion of other elements is similar to those observed in the MG1–MG5 slags (Table 3).

Smelting temperature

Experiment

During the smelting experiment, the first changes in the samples were observed at 1000°C. At this temperature, only the color of the slags was changed from blue to greenish-gray in MG3 and from orange-gray to greenish-gray in MG6 samples, possibly due to the oxidation (Figure 5). At a temperature of 1100°C, sample MG3 was partially melted, leaving parts of the sample and quartz grains unchanged. Clear traces of partial melting also appeared on the surface of the MG6 sample (slag edges were smoothed; Figure 5). These changes indicate that the solidus temperature of both analyzed slags was exceeded. At a temperature of 1150°C, both types of slag were melted but not homogenized (Figure 5). The experiment was completed at a temperature of 1200°C. At this temperature, both samples were almost completely melted and homogenized. Only single quartz grains were visible on the glassy surface (Figure 5). Considering that quartz occurs in slags as grains unmelted during the smelting process, its occurrence at these temperatures could be ignored. Continuation of the experiment until the quartz melted and dissolved would lead to falsely elevated results.

Phase diagrams

The chemical composition of the MG6 slag and the average chemical composition of the glass in the MG1–MG4 slags were plotted on the $CaO–SiO_2–Al_2O_3$ and $CaO–SiO_2–MgO–10\%\ Al_2O_3$ phase diagrams (Muan & Osborn, 1965; Supplementary Material 1). In the case of glassy slags, the averaged glass composition was used because the chemical composition of the entire sample includes unmelted SiO_2 grains (Figures 2 and 4). Due to the chemical composition of glass in the MG5 sample differing from the range for which the diagrams were designed, it was not included in plotting. Based on the $CaO–SiO_2–MgO–10\%\ Al_2O_3$ phase diagram, the liquidus temperature for the MG1–MG4 samples was in the range of 1400–1500°C (Supplementary Material 1; Table 4), while, for MG6, it was slightly below 1300°C (Supplementary Material 1; Table 4). Diagram $CaO–SiO_2–Al_2O_3$ gave values of 1400–1500°C for MG2–MG4 slags and 1300–1400°C for MG1 and MG6 slags (Supplementary Material 1; Table 4).

MELTS-Rhyolite software

The modeling using MELTS-Rhyolite software was another method applied to determine the smelting temperature (Ghiorso & Gualda, 2015; Gualda et al., 2012). During calculations, the average chemical

TABLE 3 Chemical composition of glasses occurring in Miedziana Góra slags

	MG1		MG2		MG3		MG4		MG5		MG6	
	Range	**Av. (*n* = 65)**	**Range**	**Av. (*n* = 39)**	**Range**	**Av. (*n* = 35)**	**Range**	**Av. (*n* = 21)**	**Range**	**Av. (*n* = 8)**	**Range**	**Av. (*n* = 5)**
P_2O_5	0.08–0.71	0.57	0.36–0.56	0.45	0.36–0.56	0.47	0.44–0.70	0.54	0.26–0.67	0.56	0.29–0.37	0.34
SiO_2	54.9–72.4	57.1	52.3–55.3	53.7	51.4–54.0	52.8	49.8–54.0	52.1	50.6–68.8	56.8	50.3–50.9	50.5
TiO_2	0.32–0.65	0.53	0.29–0.45	0.36	0.32–0.45	0.37	0.24–0.43	0.34	0.29–0.85	0.47	0.31–0.37	0.33
Al_2O_3	8.8–12.8	11.4	6.8–7.8	7.2	6.7–7.1	6.9	6.1–7.3	6.5	7.5–15.8	10.2	7.4–7.8	7.6
FeO	2.2–6.7	5.6	9.4–11.8	10.6	10.5–11.8	11.2	11.0–12.9	11.9	2.4–10.0	7.2	10.3–14.2	11.5
MnO	0.22–0.99	0.82	1.5–1.9	1.70	1.7–1.9	1.80	1.5–2.0	1.60	0.28–1.11	0.83	1.2–1.7	1.50
CaO	5.1–17.1	15.5	14.2–16.2	15.3	15.7–17.3	16.3	14.9–17.3	16.3	2.9–13.3	8.9	18.9–23.2	21.9
MgO	0.31–1.20	1.00	1.7–2.0	1.80	1.8–2.0	1.90	0.99–2.0	1.70	0.28–1.47	0.89	1.1–1.2	1.10
Na_2O	0.00–0.19	0.10	0.00–2.23	0.11	0.00–0.20	0.09	0.00–0.17	0.07	0.12–0.31	0.20	0.02–0.09	0.05
K_2O	2.4–5.4	2.80	2.0–2.6	2.30	2.0–2.4	2.20	1.8–2.4	2.10	1.6–5.9	2.90	1.3–1.8	1.50
PbO	0.00–4.0	2.00	1.7–4.3	3.0	2.4–3.6	3.0	2.6–6.3	4.2	2.1–21.2	8.8	0.23–0.61	0.38
CuO	0.00–0.34	0.03	0.00–0.86	0.03	0.00–0.26	0.07	0.00–5.8	0.37	0.20–0.39	0.26	0.15–0.43	0.30
ZnO	0.00–0.54	0.24	0.00–0.47	0.22	0.00–0.59	0.30	0.00–0.62	0.31	0.09–0.72	0.50	0.23–0.37	0.30
BaO	0.48–1.05	0.80	0.65–0.94	0.80	0.58–0.80	0.70	0.57–0.82	0.69	0.26–1.39	0.94	0.22–0.28	0.25

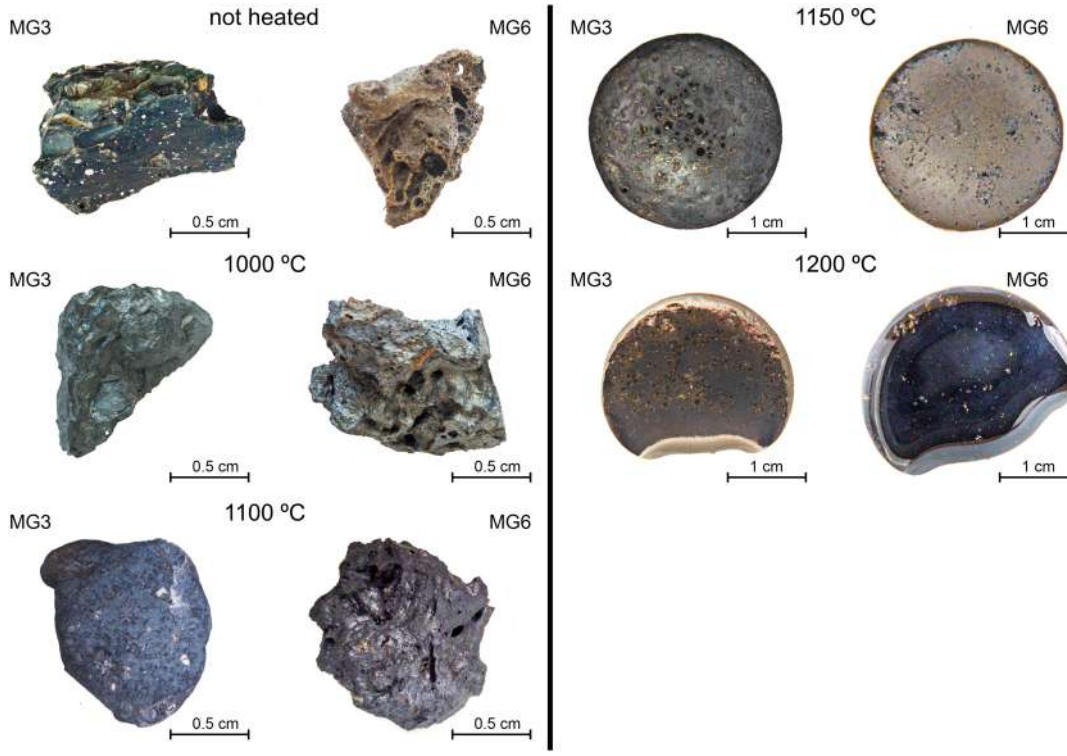

FIGURE 5 Photos of samples after high-temperature experiments [Color figure can be viewed at wileyonlinelibrary.com]

TABLE 4 Liquidus and solidus temperatures of Miedziana Góra slags depending on the method used

	MG1	MG2	MG3	MG4	MG5	MG6
MELTS-rhyolite–liquidus temperature	1118°C	1150°C	1155°C	1150°C	-	1139°C
CaO–SiO_2–MgO–10% Al_2O_3 phase diagram–liquidus temperature	1400–1500°C	1400–1500°C	1400–1500°C	1400–1500°C	-	1200–1300°C
CaO–SiO_2–Al_2O_3 phase diagrams–liquidus temperature	1300–1400°C	1400–1500°C	1400–1500°C	1400–1500°C	-	1300–1400°C
Experiment–liquidus temperature	-	-	1150–1200°C	-	-	1150–1200°C
Experiment–solidus temperature	-	-	1100°C	-	-	1100°C

composition of the glasses (MG1–MG4) and the bulk chemical composition of MG6 slag samples were used. The liquidus temperatures calculated with the MELTS-Rhyolite software were in the range of 1118°C (MG1)–1155°C (MG3; Table 4).

Viscosity

One of the most popular methods of melt viscosity determination in historical slags is the viscosity index (v.i.) proposed by Bachmann (1982) and modified by Ettler et al. (2009). This method is widely used in the analysis of smelting slags (e.g., Derkowska et al., 2021; Kupczak et al., 2020; Warchulski,

Szczuka, & Kupczak, 2020; Warchulski et al., 2022) and takes into account the polymerizing to depolymerizing components ratio:

$$\text{v.i.} = \frac{CaO + MgO + MnO + FeO + PbO + ZnO}{SiO_2 + Al_2O_3}.$$

To omit the unmelted SiO_2 fragments present in the glassy slags for viscosity calculations, the bulk chemical composition of MG6 samples and the average chemical composition of the glass present in the MG1–MG5 samples were used. Considering this, the viscosity index for Miedziana Góra slags is in the range of 0.37–0.62 for glassy (MG1–MG5) and 0.62 for hypocrystalline (MG6) slags.

Viscosity was also determined by using a model that includes both chemical composition and temperature (Giordano et al., 2006). In this method, the melt temperature is included in the calculation, and the resulting values are in SI units (Pa s). This model was proposed for natural rocks, and it has also been successfully applied for slags (Ettler et al., 2009; Warchulski, Szczuka, & Kupczak, 2020; Warchulski et al., 2022). The model is based on the following equation:

$$\log \eta = b1 + \frac{b2 * b3}{b3 + \text{SM}} + b4,$$

where $b1$–$b4$ are temperature-dependent parameters and SM is the structure modifier parameter. More detail on this model can be found in Giordano et al. (2006). In the case of Miedziana Góra slags, the viscosity was calculated for the temperature range of 1100–1200°C (Supplementary Material 2). Due to unmelted SiO_2 fragments in glassy slags, calculations were performed for the averaged chemical composition of the glasses present in the MG1–MG5 samples. Due to the hypocrystalline nature, in the MG6 slags calculations were performed for bulk chemical composition. Viscosity calculated for glassy slags was mostly in the range of log η = 3.52–2.06 Pa s (for MG1–MG4 samples; Supplementary Material 2). Only porous glassy sample (MG5) has a higher viscosity (log η = 4.42–3.47 Pa s; Supplementary Material 2). The MG6 sample is characterized by lower viscosity (log η = 2.52–1.72 Pa s) than glassy slags (Supplementary Material 2).

Due to the significant content of Cu and Pb in the slags from Miedziana Góra (Table 1; Table 3), additional viscosity calculations were applied according to the model proposed by Utigard and Warczok (UW model; 1995). Similar to the Giordano et al. (2006) method, the UW model considers the temperature and chemical composition of the slags. An additional advantage of this method is the fact that it has been proposed for metallurgical slags. Therefore, it takes into account Cu (as Cu_2O) and Pb (as PbO). The calculations were made according to the formula

$$\log \eta \left(\frac{\text{kg}}{\text{ms}}\right) = -0.49 - 5.1\sqrt{\text{VR}} + \frac{-3660 + 12080\sqrt{\text{VR}}}{T(K)},$$

where VR (viscosity ratio) is the ratio of acidic oxides to basic oxides, calculated using the equation:

$$\text{VR} = \frac{(\%SiO_2) + 1.5\,(\%Cr_2O_3) + 1.2\,(\%ZrO_2) + 1.8\,(\%Al_2O_3)}{1.2\,(\%FeO) + 0.5\,(\%Fe_2O_3 + \%PbO) + 0.8\,(\%MgO) + 0.7\,(\%CaO) + 2.3\,(\%Na_2O + \%K_2O) + 0.7\,(\%Cu_2O) + 1.6\,(\%CaF_2)}.$$

In this case, it was also decided to perform calculations for the average composition of the glass from glassy (MG1–MG5) slags and for the bulk chemical composition of the MG6 sample. During these calculations, the entire content of Cu was converted into Cu_2O and Pb into PbO. Considering phase composition, the Fe occurs in slags as FeO rather than Fe_2O_3, and this was used for calculations. Calculations made with this method for glassy samples (MG1–MG5) gave results in the range of log η = 3.20–1.25 Pa s (Supplementary Material 2). The viscosity of the MG6 slag calculated by the UW model was lower (log η = 1.81–1.19 Pa s; Supplementary Material 2), but the difference was not as large as in the case of the Giordano et al. (2006) model.

DISCUSSION

Temperature estimations

The conducted experiment suggests that the solidus temperature of the studied slags was ~1100°C, while the liquidus temperature (in which it was possible to carry out smelting) was in the range of 1150–1200°C (Table 4). The temperatures obtained with MELTS software are slightly lower when compared to those obtained from the experimental method. The results obtained using phase diagrams (Supplementary Material 1) significantly exceed the temperatures determined by the experiment and calculations with the MELTS-Rhyolite software (Table 4). The multicomponent nature of analyzed slags causes limited possibilities of effective application of phase diagrams. Most of the available diagrams take into account three to four components, and not necessarily those present in the analyzed slags in significant amounts. There are also diagrams designed for minerals that take into account more components, but in that case the chemical composition of the analyzed material should correspond to the chemical composition of the phases for which they were designed (e.g., Warchulski et al., 2022). For this reason, it is necessary to use those matching best the chemical composition of analyzed slags. Phase diagrams have been successfully used in the estimation of temperature in Rudawy Janowickie, Poland (Kierczak & Pietranik, 2011) and in Campiglia Marittima, Italy (Manasse et al., 2001), due to the less complex chemistry of the slags.

The smelting temperature in the case of slags from Miedziana Góra is within the range of temperatures determined for slags after copper production in Spain (about 3000 years ago; ~1200°C; Sáez et al., 2003), in Crete in the Bronze Age (1150–1300°C; Bassiakos & Catapotis, 2006), and in Italy in the 13th to 14th century (1150–1300°C; Manasse & Mellini, 2002; Table 3), but slightly lower than in the smelters in the area of Old Copper Basin in Poland (14th to 20th century; 1200–1400°C; Derkowska et al., 2021; Kierczak & Pietranik, 2011; Kądziołka et al., 2020; Table 3).

Viscosity estimations

The melt viscosity during metal production is one of the most critical parameters that can describe the efficiency of the process. In the case of Miedziana Góra slags, the calculated values of v.i. (0.37–0.62) are comparable with the slags from Leszczyna, Kondratów (18th to 20th century; 0.43–0.75; Table 5; Derkowska et al., 2021) and Okiep Copper District, South Africa (19th to 21st century; 0.22–0.69;

TABLE 5 Smelting temperatures and viscosities of Cu slags from selected locations

Location	Time (century)	Temperature (°C)	Viscosity (v.i.)	Viscosity [$\log_{10}\eta$ = (pa s)]**
Miedziana Góra	16–18	1150–1200	0.37–0.62	1.72–4.42 (1200–1100°C)
Kondratów and Leszczyna, Poland(Derkowska et al., 2021)	18–20	1210–1400	0.43–0.75	0.23–2.19 (1400–1200°C)
Rudawy Janowickie, Poland(Kierczak & Pietranik, 2011)	14–16	1200–1300	0.16–1.55	1.37–5.79 (1200–1300°C)
Itziparátzico, Mexico(Maldonado & Rehren, 2009)	14–16	nd	0.48–1.31*	-
Marsiliana, Italy(Manasse & Mellini, 2002)	13–14	1150–1300	0.79–1.86	0.57–2.24 (1300–1150°C)
Okiep Copper District, South Africa(Rozendaal & Horn, 2013)	19–21	nd	0.22–0.69*	-

Notes: nd, no data;

*calculated based on chemical composition of slags;

**calculated according to Giordano et al.'s (2006) model based on chemical composition of slags.

Table 5). Higher v.i. were calculated for slags after copper production in the Rudawy Janowickie, Poland (14th to 16th century; 0.16–1.55, but mainly in the range of 0.55–1.55; Kierczak & Pietranik, 2011), Marsiliana, Italy (0.79–1.86; Table 5; Manasse & Mellini, 2002), and Itziparátzico, Mexico (14th to 16th century; 0.48–1.31; Table 5; Maldonado & Rehren, 2009). The high v.i. testifies to a better separation of copper-containing phases from the slag and thus a more effective metallurgical process.

The viscosity calculated according to Giordano et al. (2006) for the slags from Miedziana Góra ($\log \eta$ = 1.72–4.42 Pa s; Table 5) is within the viscosity range of the slags from the Rudawy Janowickie ($\log \eta$ = 1.37–5.79 Pa s; Table 5). The slags from Leszczyna and Kondratów (Derkowska et al., 2021) and slags from Marsiliana (Manasse & Mellini, 2002) are characterized by lower viscosity than those from Miedziana Góra (Table 5). It can be supposed that the metallurgy in Miedziana Góra was less efficient than the italian one and Leszczyna/Kondratów (Poland) metallurgy. Calculations made with the UW (Utigard & Warczok, 1995) model gave a similar range of results to the Giordano et al. (2006) method (Supplementary Material 2). Due to the lack of consideration of some components (mainly Pb and Cu) in samples with a high content of these metals, the Giordano et al. (2006) method significantly increases the viscosity (e.g., calculations made for glass in the MG5 sample; Supplementary Material 2).

Atmosphere

Redox conditions are one of the most important factors that should be considered in reconstructing metallurgical processes. For this purpose, Fe buffers are most often used, taking into account the temperature and the oxidation states of Fe in the samples (Sáez et al., 2003; Warchulski, Szczuka, & Kupczak, 2020). In the analyzed slags, Fe is present as Fe^{2+} rather than Fe^{3+}. For this reason, the fugacity of oxygen can be described by quartz–fayalite–magnetite and wüstite–magnetite buffers (Zhao et al., 1999). Based on Fe buffers in the temperature range of 1100–1200°C, the fugacity of oxygen in the Miedziana Góra slag falls within the range of $\log fO_2 = -12$ (wüstite–magnetite buffer in 1100°C) to −8 atm. (quartz–fayalite–magnetite buffer at 1200°C; Zhao et al., 1999).

When analyzing the slags after the production of metals from polymetallic deposits, apart from iron, the oxidation state of other metals can also be taken into account. The Ellingham diagram describes the transformations between the oxides and metallic phases most widely (Supplementary Material 3). The analyses show that in the MG6 slags Cu occurs mainly in metallic form (Figures 3 and 4f). For this reason, the fugacity of oxygen should be lower than $\log fO_2 = -5$ atm., while the lack of metallic Fe indicates the fugacity of oxygen greater than $\log fO_2 = -14$ atm. (Supplementary Material 3).

In contrast, in glassy samples, aggregates made of Cu and PbO occur (Figure 4). The Ellingham diagram predicts the coexistence of metallic copper with PbO only in a narrow range of oxygen fugacity ($\log fO_2 = -7$ to −5 atm at 1100–1200°C; Supplementary Material 3). However, considering that the process was carried out in a sulfur-rich atmosphere, the greater affinity of sulfur for Cu than for Pb widens the range of their coexistence (Supplementary Material 3).

The diagrams (Supplementary Material 3) show that the production of Cu through matte also depends on sulfur fugacity (Supplementary Material 3). Unfortunately, no diagrams describing the relationship between the fugacity of oxygen and sulfur in the discussed temperature range (1100–1200°C) have been found.

Despite the higher temperature, the diagrams proposed by Yazawa (1974) can be used to estimate the oxidation–reduction conditions during smelting in Miedziana Góra. As copper is mainly in the metallic form (except the MG5 sample, where it is in the carbonate form and results from slags weathering) during the smelting in Miedziana Góra, the oxygen fugacity can be estimated in the range of $\log fO_2 = -4$ to −12 atm. (Supplementary Material 3). The differentiation of samples in terms of chemical and phase composition makes it possible to estimate the oxidation-reduction conditions at individual stages. During formation of the MG6 sample, oxygen fugacity should be in the range of

approx. log fO_2 = −6 to −12 atm. (Supplementary Material 3) and, during MG1–MG5 slag formation (to oxidize Pb), in the range of approx. log fO_2 = −4 to −5 atm (Supplementary Material 3).

Oxygen fugacity analysis based on Fe buffers in the case of Cu smelting showed a strongly reducing environment. In fact, the extent to which it can be carried out is wider and also depends on the fugacity of S_2 (Supplementary Material 3).

Summary of the metallurgical process

In Miedziana Góra, ore processing was carried out mainly to produce Cu and PbO (Król & Urban, 2003). The presence of metallic copper (Figures 3 and 4) indicates that the analyzed slags most likely come from the Cu production process. According to Agricola (1556), copper from sulfide ores was produced in a two-stage process. The differences in chemistry (mainly in the content of Cu and Pb) and phase composition between glassy (MG1–MG5) and hypocrystalline (MG6) slags suggest they are the result of different smelting process stages. In the first smelting step, ore mixed with fluxes and witch charcoal was added to the shaft furnace and heated. In this production step, the primary goal was to heat the ore to form: (i) silicate slag; (ii) Cu-rich speiss/matte (Davenport et al., 2002); (iii) metallic Cu. The workers controlled the amount of oxygen supplied during heating to oxidize as much Fe as possible (FeO was bonded within the slag). In order not to reduce the efficiency of the process, the workers did not allow Cu to be oxidized (Cu oxides would remain in the slags). As a result, part of Fe also did not oxidize and together with Cu, S, and As formed speiss/matte (Davenport et al., 2002). After the melt separation, the tapping hole was opened to remove and sort the metallic Cu, speiss/matte, and slag. The speiss/matte was further processed (in the second step) to obtain converted copper, while slags were discarded (Agricola, 1556; US Congress, Office of Technology Assessment, 1988).

The lower Pb content in MG6 compared to MG1–MG5 slags may indicate that MG6 slags come from this stage of the process (Table 1). Due to the differences in density between Pb (11.35 g/cm^3), Cu (8.94 g/cm^3), and Fe (7.87 g/cm^3; Atkins, 2001), the Pb should be effectively separated during this stage, where it must have accumulated at the lowest part of the furnace, leading to the formation of slags with low Pb content. The hypocrystalline nature of these slags is due to their lower viscosity (Supplementary Material 2). Under conditions of rapid cooling, low viscosity allows the formation of crystalline phases (Puziewicz et al., 2007). The presence of mainly metallic Cu and Fe^{2+} in wollastonite group phases marks the relatively low oxygen fugacity conditions during the formation of these slags.

During the second step, the speiss/matte was remelted. At this stage, air was blown into the melt's surface to oxidize undesirable elements, and fluxes were added to bind them in the slags. In the case of Miedziana Góra, mainly Fe and Pb were removed during this step. Considering the high content of Pb and lower content of Cu, the glassy (MG1–MG5) slags most likely come from this stage of copper production (speiss/matte conversion). The presence of Pb in the form of PbO confirms the oxidative nature of this process. However, oxygen fugacity was not sufficient to oxidize Cu, which led to the formation of demix structures consisting of PbO and metallic Cu (Figure 4a,e). This was possible because of the higher sulfur affinity for Cu than for Pb and Fe (Supplementary Material 3). It also explains the absence of other sulfides (Pb or Fe) in the analyzed slags. The coexistence of metallic Cu with PbS could occur only in extremely non-equilibrium conditions (Supplementary Material 3). The oxidation of Pb and Fe allowed them to react with fluxes, resulting in the formation of slags floating on the surface. The slag was then successively removed from the furnace. This resulted in a rapid temperature change, which, combined with the high viscosity of these slags, favors the formation of glass. The low diffusion rate and the lack of nucleation seeds could also be the reason for the low number of crystalline phases (Gawęda et al., 2013). The occasional presence of metallic Pb and Cu sulfides/arsenides in glassy slags could also be caused by the low oxygen diffusion. After all Fe and Pb were removed from the furnace, further oxidation cleaned the melt from sulfur (as SO_2) and arsenic

(as As_2O_3), leaving metallic copper in the furnace (Davis, 2001; US Congress, Office of Technology Assessment, 1988).

The shaft furnace used for copper smelting in the 16th to 18th century was similar to those used in lead and gold metallurgy (Agricola, 1556; Warchulski, Szczuka, & Kupczak, 2020; Warchulski et al., 2022; Figure 6). The only difference was in the use of a different type of drive. In most cases, the smelters were located near rivers, the energy of which was used to drive the bellows (e.g., Warchulski, Szczuka, & Kupczak, 2020). In the case of Miedziana Góra, there is no river that could fulfill this function (Figure 1). For this reason, horse mills must have been used (Figure 6).

Ores and additives

The documentation of the Miedziana Góra ore shows that ore minerals are found mainly in clays (Rubinowski, 1970). Chemically, these rocks are composed of SiO_2, Al_2O_3, and Fe at different states of oxidation. The remaining elements are present in smaller amounts (on average, less than 5 wt% of oxide; Rubinowski, 1970). Comparing ore composition with the chemical composition of MG6 slags (resulting from speiss/matte production; Table 1) shows that the slags are characterized by a higher content of CaO and SiO_2, with a lower content of Al_2O_3 (Table 1; Rubinowski, 1970). Higher SiO_2 content (Table 1) may indicate the addition of sandstones occurring in the vicinity of the smelter (Figure 1). The primary aim of SiO_2 addition was to produce two immiscible liquids and bond the FeO

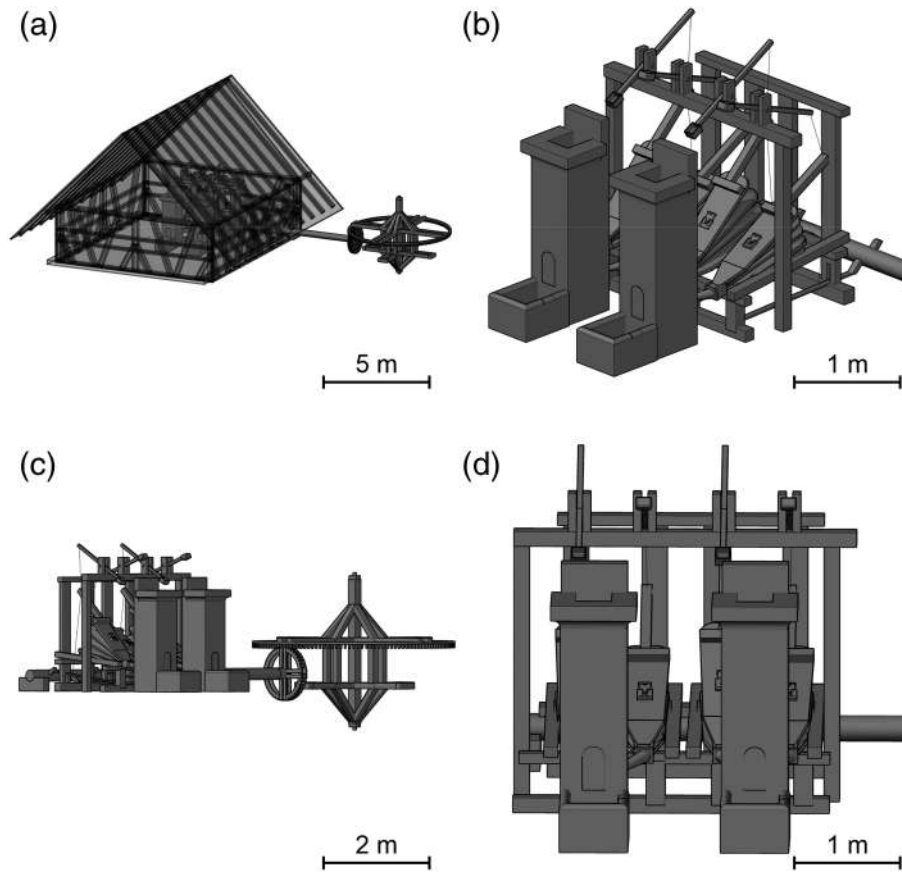

FIGURE 6 Reconstruction of the smelter that operated in Miedziana Góra, based on the description of the smelters operating in a similar period (Agricola, 1556)

(Davenport et al., 2002). However, too much SiO_2 has a negative effect, increasing the viscosity of the melt, which reduces the separation efficiency. For this reason, elements that break the silicate network were often added during the production of copper (Davenport et al., 2002; Potysz et al., 2015). In the case of Miedziana Góra, due to the increased content of CaO, limestones were most probably used for this purpose (Devonian carbonates; Figure 1).

High SiO_2 content (Table 1) and unmelted quartz/cristobalite (Figure 4) grains and the presence of other components (e.g., CaO, Al_2O_3; Table 1) in MG1–MG5 slags suggest that during the speiss/matte conversion process material containing SiO_2, CaO, and Al_2O_3 (e.g., waste resulting from the enrichment of ores combined with sandstones/carbonates from the surface) was used. SiO_2 polymorphs, as the most resistant to high temperature, have not been completely melted down.

CONCLUSIONS

The presence of metal ores positively affected the development of the Old Polish Industrial District. It was possible thanks to the involvement of metallurgists from more experienced industrial centers, where the conditions under which smelting was carried out were similar. Based on the conducted analysis, the basic parameters that prevailed during the pyrometallurgical processing of ores from Miedziana Góra were reconstructed. Geochemical and mineralogical analyses allowed the isolation of slags from the production focused on speiss/matte and those from matte conversion. Both of these were formed under similar temperature conditions (liquidus temperature in the range of 1150–1200°C). The differences are visible in the viscosity of the metallurgical melt. The viscosity of the MG6 ranged between $\log\eta = 1.19$ Pa s (UW model at 1200°C) and 2.52 Pa s (Giordano model at 1100°C). Low viscosity promoted the separation of the desired phases from the silicate melt, increasing melting efficiency. Because the second smelting step did not require low viscosity, slags after matte conversion are characterized by higher viscosity, ranging from $\log_{10}\eta = 1.25$ Pa s (UW model at 1200°C) to 4.42 Pa s (Giordano et al., 2006 model at 1100°C). During this step, the main goal of metallurgists was to oxidize and bind undesirable elements with fluxes. The addition of SiO_2 (a viscosity-enhancing component) enabled the efficient removal of Fe from the furnace through crystallization of the Fe silicates. Differences in viscosity contributed to macroscopic differences between slags. In high-viscosity slags, crystallization processes were hindered, which resulted in their glassy form. Based on the chemical and phase composition, the type of fluxes used during smelting was determined. The higher SiO_2 and CaO content compared to the chemical composition of ores indicate the use of both carbonates and sand/sandstones during speiss/matte production, most probably from the vicinity of the smelter. In turn, during the speiss/matte conversion process, the waste resulting from the enrichment of ores combined with sandstones/carbonates from the surface was used. With the wide range of coexistence of phases found in the slags, oxidation–reduction conditions were also determined. The oxygen fugacity during speiss/matte smelting in Miedziana Góra was in the range of $\log fO_2 = -5$ (Supplementary Material 3) to −12 (wüstite–magnetite buffer at 1100°C; Zhao et al., 1999). Maintaining oxygen fugacity below the value at which copper would oxidize was necessary to limit losses due to the binding of copper oxides to slags during separation. During matte conversion, the oxygen fugacity was from $\log fO_2 = -4$ (Supplementary Material 3) to −7 (Supplementary Material 3). Oxygen fugacity in this range during matte conversion was necessary to purify the final product from Pb (through oxidation and binding to fluxes).

ACKNOWLEDGEMENTS

This study was supported by the National Science Center (NCN) grant no. 2019/35/O/ST10/00313.

DATA CITATION

No dataset from external repositories was used in this study. All existing data used for this publication are cited in reference section.

DATA AVAILABILITY STATEMENT

The data that support the finding of the study are given in the tables and figures within the main text. This study brought together existing data from several different sources, which are cited throughout.

ORCID

Krzysztof Kupczak https://orcid.org/0000-0002-3395-9547
Rafał Warchulski https://orcid.org/0000-0002-0508-347X
Aleksandra Gawęda https://orcid.org/0000-0001-9102-2149

REFERENCES

Agricola, G. (1556). *De Re metallica libri XII* (Ed Muzeum Karkonoskie w Jeleniej Górze, 2000), Jelenia Góra.

Aleksander-Kwaterczak, U., & Helios-Rybicka, E. (2009). Contaminated sediments as a potential source of Zn, Pb, and cd for a river system in the historical metalliferous ore mining and smelting industry area of South Poland. *Journal of Soils and Sediments*, *9*, 13–22. https://doi.org/10.1007/s11368-008-0051-z

Atkins, P. W. (2001). *Chemia fizyczna*. Wydaw.

Bachmann, H. G. (1982). *The identification of slags from archaeological sites*. Institute of Archaeology Occasional Publication.

Baron, S., Carignan, J., & Ploquin, A. (2006). Dispersion of heavy metals (metalloids) in soils from 800-year-old pollution (Mont-Lozere, France). *Environmental Science & Technology*, *40*(17), 5319–5326. https://doi.org/10.1021/es0606430

Bassiakos, Y., & Catapotis, M. (2006). Reconstruction of the copper smelting process based on the analysis of ore and slag samples. *Hesperia Supplements*, *36*, 329–353.

Bourgarit, D., Mille, B., Prange, M., Ambert, P., & Hauptmann, A. (2003). Chalcolithic fahlore smelting at Cabrières: Reconstruction of smelting processes by archaeometallurgical finds. *Archaeometallurgy in Europe*, *1*, 431–440.

Bränvall, M. L., Bindler, R., Emteryd, O., & Renberg, I. (2001). Four thousand years of atmospheric lead pollution in northern Europe: A summary from Swedish lake sediments. *Journal of Paleolimnology*, *25*(4), 421–435. https://doi.org/10.1023/A:1011186100081

Burger, E., Bourgarit, D., Wattiaux, A., & Fialin, M. (2010). The reconstruction of the first copper-smelting processes in Europe during the 4th and the 3rd millennium BC: Where does the oxygen come from? *Applied Physics a*, *100*, 713–724. https://doi.org/10.1007/s00339-010-5651-y

Cabała, J., Warchulski, R., Rozmus, D., Środek, D., & Szełęg, E. (2020). Pb-rich slags, minerals, and pollution resulted from a medieval ag-Pb smelting and mining operation in the Silesian-Cracovian region (southern Poland). *Minerals*, *10*, 28. https://doi.org/10.3390/min10010028

Chirikure, S. (2015). *Metals in past societies: A global perspective on indigenous African metallurgy*. Springer.

Davenport, W. G., King, M. J., Schlesinger, M. E., & Biswas, A. K. (2002). *Extractive metallurgy of copper*. Elsevier.

Davis, J. R. (Ed.) (2001). *Copper and copper alloys*. ASM international. https://doi.org/10.31399/asm.tb.aub.t61170457

Derkowska, K., Świerk, M., & Nowak, K. (2021). Reconstruction of copper smelting technology based on 18–20th-century slag remains from the old Copper Basin, Poland. *Minerals*, *11*(9), 926. https://doi.org/10.3390/min11090926

Ettler, V. (2016). Soil contamination near non-ferrous metal smelters: A review. *Applied Geochemistry*, *64*, 56–74. https://doi.org/10.1016/j.apgeochem.2015.09.020

Ettler, V., Červinka, R., & Johan, Z. (2009). Mineralogy of medieval slags from lead and silver smelting (Bohutín, Příbram district, Czech Republic): Towards estimation of historical smelting conditions. *Archaeometry*, *51*, 987–1007. https://doi.org/10.1111/j.1475-4754.2008.00455.x

Gawęda, A., Janeczek, J., Kierepka, M., Kądziołko-Gaweł, M., & Krzykawski, T. (2013). Indialite-rich paralava from a coalmine waste-dump, Sosnowiec, Poland. *Neues Jahrbuch für Mineralogie-Abhandlungen*, *190*, 237–251. https://doi.org/10.1127/0077-7757/2013/0238

Geoportal. n.d. Available online: https://www.geoportal.gov.pl (accessed on 10 January 2020).

Ghiorso, M. S., & Gualda, G. A. (2015). An H_2O–CO_2 mixed fluid saturation model compatible with rhyolite-MELTS. *Contributions to Mineralogy and Petrology*, *169*(6), 1, 53–30. https://doi.org/10.1007/s00410-015-1141-8

Giordano, D., Mangiacapra, A., Potuzak, M., Russell, J. K., Romano, C., Dingwell, D. B., & Di Muro, A. (2006). An expanded non-Arrhenian model for silicate melt viscosity: A treatment for metaluminous, peraluminous and peralkaline liquids. *Chemical Geology.*, *229*(1–3), 42–56. https://doi.org/10.1016/j.chemgeo.2006.01.007

Gualda, G. A., Ghiorso, M. S., Lemons, R. V., & Carley, T. L. (2012). Rhyolite-MELTS: A modified calibration of MELTS optimized for silica-rich, fluid-bearing magmatic systems. *Journal of Petrology*, *53*(5), 875–890. https://doi.org/10.1093/petrology/egr080

Kądziołka, K., Pietranik, A., Kierczak, J., Potysz, A., & Stolarczyk, T. (2020). Towards better reconstruction of smelting temperatures: Methodological review and the case of historical K-rich cu-slags from the old Copper Basin, Poland. *Journal of Archaeological Science*, *118*, 105142. https://doi.org/10.1016/j.jas.2020.105142

Kapper, L., Turck, R., Goguichaishvili, A., & Morales, J. (2017). Rock – And archeomagnetic investigation of prehistoric copper slag from the Swiss Alps. *Latinmag Letters*, *7*, 1–4.

Kierczak, J., & Pietranik, A. (2011). Mineralogy and composition of historical cu slags from the Rudawy Janowickie Mountains, southwestern Poland. *The Canadian Mineralogist*, *49*(5), 1281–1296. https://doi.org/10.3749/canmin.49.5.1281

Kierczak, J., Potysz, A., Pietranik, A., Tyszka, R., Modelska, M., Néel, C., Ettler, V., & Mihaljevič, M. (2013). Environmental impact of the historical cu smelting in the Rudawy Janowickie Mountains (South-Western Poland). *Journal of Geochemical Exploration*, *124*, 183–194. https://doi.org/10.1016/j.gexplo.2012.09.008

Kowalczewski, Z. (1972). Podstawowe problemy świętokrzyskiego górnictwa kruszcowego w świetle danych geologicznych. In *Materiały do sesji naukowej odbytej z okazji jubileuszu IX wieków Kielc* (pp. 57–78). Wydawnictwa Geologiczne.

Kowalczewski, Z., & Szczecińska, A. (1977). Wyniki badań nad żużlami z kilku stanowisk dawnego hutnictwa metali nieżelaznych w Górach Świętokrzyskich. *Rocz. Świętokrz*, *5*, 151–168.

Król, P., & Urban, J. (2003). *Kopalnie w Miedzianej Górze iw Ławęcznej oraz ochrona ich pozostałości* (p. 29). Rocznik Świętokrzyski. Seria B. Nauki Przyrodnicze.

Król, P., & Urban, J. (2007). *Kopalnie Miedzianogórskie*. Kielce.

Kundig, K. J., & Weed, R. D. (2015). Copper and copper alloys. *Mechanical Engineers' Handbook (3rd Edition): Materials and Mechanical Design*, *1*, 117–228.

Kupczak, K., Warchulski, R., Dulski, M., & Środek, D. (2020). Chemical and phase reactions on the contact between refractory materials and slags, a case from the 19th century Zn-Pb smelter in Ruda Śląska, Poland. *Minerals*, *10*, 1006. https://doi.org/10.3390/min10111006

Maldonado, B., & Rehren, T. (2009). Early copper smelting at Itziparátzico, Mexico. *Journal of Archaeological Science*, *36*(9), 1998–2006. https://doi.org/10.1016/j.jas.2009.05.019

Manasse, A., & Mellini, M. (2002). Archaeometallurgic slags from Kutná Hora. *Neues Jahrbuch Für Mineralogie-Monatshefte*, *369-384*, 369–384. https://doi.org/10.1127/0028-3649/2002/2002-0369

Manasse, A., Mellini, M., & Viti, C. (2001). The copper slags of the Capattoli Valley, Campiglia Marittima, Italy. *European Journal of Mineralogy*, *13*(5), 949–960. https://doi.org/10.1127/0935-1221/2001/0013/0949

Miczulski, S., 1972. Początki rozwoju górnictwa i hutnictwa kruszcowego w rejonie Kielc do końca XVI w., [in:] Kowalczewski Z. (red.) *Dzieje i Technika Świętokrzyskiego Górnictwa i Hutnictwa Kruszcowego. Wydawnictwa geologiczne*, Warszawa, pp. 79–100.

Molenda, D. (1989). Eksploatacja rud miedzi i handel miedzią w Polsce w późnym średniowieczu iw początkach nowożytności (do 1795 r.). *Przegląd Historyczny*, *80*(4), 801-814.

Muan, A., & Osborn, E. F. (1965). *Phase equilibria among oxides in steelmaking*. Addison-Wesley publishing company, INC.

Nriagu, J. O. (1994). Mercury pollution from the past mining of gold and silver in the Americas. *Science of the Total Environment*, *149*, 167–181. https://doi.org/10.1016/0048-9697(94)90177-5

Paulewicz, M. (1992). Chęcińskie górnictwo kruszcowe (IV do poł. XVII wieku). Kieleckie Towarzystwo Naukowe, Kielce.

Piekarski, K. (1961). W sprawie genezy złoża rud miedzi w Miedzianej Górze koło Kielc. *Prace Geologiczne*, *3*, 43–58.

Potysz, A., Kierczak, J., Pietranik, A., & Kądziołka, K. (2018). Mineralogical, geochemical, and leaching study of historical cu-slags issued from processing of the Zechstein formation (old Copper Basin, southwestern Poland). *Applied Geochemistry*, *98*, 22–35. https://doi.org/10.1016/j.apgeochem.2018.08.027

Potysz, A., van Hullebusch, E. D., Kierczak, J., Grybos, M., Lens, P. N., & Guibaud, G. (2015). Copper metallurgical slags–current knowledge and fate: A review. *Critical Reviews in Environmental Science and Technology*, *45*, 2424–2488. https://doi.org/10.1080/10643389.2015.1046769

Puziewicz, J., Zainoun, K., & Bril, H. (2007). Primary phases in pyrometallurgical slags from a zinc-smelting waste dump, Swietochłowice, upper Silesia, Poland. *The Canadian Mineralogist*, *45*(5), 1189–1200. https://doi.org/10.2113/gscanmin.45.5.1189

Roberts, B. W., Thornton, C. P., & Pigott, V. C. (2009). Development of metallurgy in Eurasia. *Antiquity*, *83*(322), 1012–1022. https://doi.org/10.1017/S0003598X00099312

Rozendaal, A., & Horn, R. (2013). Textural, mineralogical and chemical characteristics of copper reverb furnace smelter slag of the Okiep Copper District, South Africa. *Minerals Engineering*, *52*, 184–190. https://doi.org/10.1016/j.mineng.2013.06.020

Rubinowski, Z. (1970). *Wyniki badań rudonośności w rejonie Miedzianej Góry i Ławeczna*. Archiwum Państwego Instytutu Geologicznego.

Sáez, R., Nocete, F., Nieto, J. M., Capitán, M. Á., & Rovira, S. (2003). The extractive metallurgy of copper from Cabezo Juré, Huelva, Spain: Chemical and mineralogical study of slags dated to the third millenium BC. *The Canadian Mineralogist*, *41*(3), 627–638. https://doi.org/10.2113/gscanmin.41.3.627

Ströbele, F., Wenzel, T., Kronz, A., Hildebrandt, L. H., & Markl, G. (2010). Mineralogical and geochemical characterization of high-medieval lead–silver smelting slags from Wiesloch near Heidelberg (Germany)—An approach to process reconstruction. *Archaeological and Anthropological Sciences*, *2*(3), 191–215. https://doi.org/10.1007/s12520-010-0039-7

Sutkowska, K., Czech, T., Teper, L., & Krzykawski, T. (2013). Heavy metals soil contamination induced by historical zinc smelting in Jaworzno. *Ecological Chemistry and Engineering a*, *20*(12), 1441–1450. https://doi.org/10.2428/ecea.2013.20(12)130

Tylecote, R. F. (1992). *A history of metallurgy* (2nd ed.). The Institute of Materials.

US Congress, Office of Technology Assessment. (1988). *Copper production technology*. Government Printing Office.

Utigard, T. A., & Warczok, A. (1995). Density and viscosity of copperhickel sulphide smelting and converting slags. In W. J. Chen, C. Dim, A. Luraschi, & P. J. Mackey (Eds.), *Copper 95-Cobre 95 proceedings of the third international conference, Vol. l V Pyrometallurgy of copper* (pp. 423–437). The Metallurgical Society of CIM.

Warchulski, R. (2016). Zn-Pb slag crystallization: Evaluating temperature conditions on the basis of geothermometry. *European Journal of Mineralogy*, *28*(2), 375–384. https://doi.org/10.1127/ejm/2015/0027-2496

Warchulski, R., Gawęda, A., Kupczak, K., Banasik, K., & Krzykawski, T. (2020). Slags from Ruda Śląska, Poland as a large-scale laboratory for the crystallization of rare natural rocks: Melilitolites and paralavas. *Lithos*, *372–373*, 105666. https://doi.org/10.1016/j.lithos.2020.105666

Warchulski, R., Kupczak, K., Gawęda, A., & Sitko, R. (2022). Complete reconstruction of the process and conditions during gold smelting in the 15-17th century in Złoty Stok based on metallurgical slags. *Archaeometry*, *64*, 916–934. https://doi.org/10.1111/arcm.12752

Warchulski, R., Mendecki, M., Gawęda, A., Sołtysiak, M., & Gadowski, M. (2019). Rainwater-induced migration of potentially toxic elements from a Zn–Pb slag dump in Ruda Śląska in light of mineralogical, geochemical and geophysical investigations. *Applied Geochemistry*, *109*, 104396. https://doi.org/10.1016/j.apgeochem.2019.104396

Warchulski, R., Szczuka, M., & Kupczak, K. (2020). Reconstruction of 16th—17th century Lead smelting processes on the basis of slag properties: A case study from Sławków, Poland. *Minerals*, *10*(11), 1039. https://doi.org/10.3390/min10111039

Wojciechowski, A. (2002). Hałdy dawnego górnictwa świętokrzyskiego jako źródło metali kolorowych i szlachetnych. *Przegląd Geologiczny*, *50*(3), 240–244.

Yamanaka, T., Sadanaga, R., & Takeuchi, Y. (1977). Structural variation in the ferrobustamite solid solution. *American Mineralogist*, *62*(11–12), 1216–1224.

Yazawa, A. (1974). Thermodynamic considerations of copper smelting. *Canadian Metallurgical Quarterly*, *13*(3), 443–453. https://doi.org/10.1179/cmq.1974.13.3.443

Zhao, D., Essene, E. J., & Zhang, Y. (1999). An oxygen barometer for rutile–ilmenite assemblages: Oxidation state of metasomatic agents in the mantle. *Earth and Planetary Science Letters*, *166*(3–4), 127–137. https://doi.org/10.1016/S0012-821X(98)00281-7

Zhou, Y., Wang, L., Xiao, T., Chen, Y., Beiyuan, J., She, J., Zhou, Y., Yin, M., Liu, J., Liu, Y., Wang, Y., & Wang, J. (2020). Legacy of multiple heavy metal (loid)s contamination and ecological risks in farmland soils from a historical artisanal zinc smelting area. *Science of the Total Environment*, *720*, 137541. https://doi.org/10.1016/j.scitotenv.2020.137541

SUPPORTING INFORMATION

Additional supporting information can be found online in the Supporting Information section at the end of this article.

How to cite this article: Kupczak, K., Warchulski, R., & Gawęda, A. (2023). Reconstruction of smelting conditions during 16th- to 18th-century copper ore processing in the Kielce region (Old Polish Industrial District) based on slags from Miedziana Góra, Poland. *Archaeometry*, *65*(3), 547–569. https://doi.org/10.1111/arcm.12837

Received: 16 June 2021 | Accepted: 7 January 2022

DOI: 10.1111/arcm.12752

ORIGINAL ARTICLE

Complete reconstruction of the process and conditions during gold smelting in the 15th–17th centuries in Złoty Stok based on metallurgical slags

Rafał Warchulski[1] | **Krzysztof Kupczak**[1] | **Aleksandra Gawęda**[1] | **Rafał Sitko**[2]

[1]Faculty of Natural Sciences, Institute of Earth Sciences, University of Silesia in Katowice, Sosnowiec, Poland

[2]Institute of Chemistry, Department of Analytical Chemistry, University of Silesia in Katowice Faculty of Science and Technology, Katowice, Poland

Correspondence
Warchulski Rafał, University of Silesia in Katowice, Faculty of Natural Sciences, Institute of Earth Sciences, Będzińska 60, PL-41-200 Sosnowiec, Poland.
Email: rafal.warchulski@us.edu.pl

Funding information
National Science Center (NCN), Grant/Award Numbers: 2016/21/N/ST10/00838, 2019/35/O/ST10/00313

Abstract

This study presents the first complete reconstruction of gold metallurgy in Złoty Stok, Poland. The key parameters of the process (i.e., temperature of smelting and solidification, melt viscosity, oxygen fugacity) are calculated using the remnants of the process: metallurgical slags. The slags consist of silicate phases (i.e., olivine, pyroxene), sulfides and arsenides (i.e., pyrrhotite, Fe_2As), as well as glass. These slags are chemically dominated by SiO_2 (< 56.60 wt%), MgO (< 18.36 wt%), FeO (< 15.36 wt%), and CaO (< 15.19 wt%). The obtained results indicate that the temperature during the metallurgical process was at least 1300–1350°C, and crystallization of the slags took place until they cooled to < 1200°C. The morphology of olivine crystals in the slags indicates large differences in their cooling rate, from 5 to 300°C/h. Strongly reducing conditions during the metallurgical process (−10.5 to −11.5 log fO_2) was confirmed. Low melt viscosity ($\log_\eta = 0.26 – 0.90$ Pa s) facilitated the separation of the sulfide melt rich in gold from the silicate melt being the slag precursor. The obtained results allowed existing descriptions of the smelting process in Złoty Stok to be corrected.

KEYWORDS

gold, oxygen fugacity, process reconstruction, slags, smelting, temperature, viscosity

INTRODUCTION

The mining of gold, like other metals, leaves behind residues in the form of waste from various mining and refining stages. One of the possible remnants of historical metallurgy are slags. They are often the subject of research due to potential adverse impacts on the natural environment (Kierczak et al., 2013; Mendecki et al., 2020; Tyszka et al., 2014; Warchulski et al., 2019). In addition to environmental aspects, slags are often analysed for their possible use in modern industry (Branca & Colla, 2012; Geiseler, 1996). In recent years, slags have also been increasingly used to recreate historic metallurgical processes (Addis et al., 2016; Ströbele et al., 2010; Warchulski et al., 2018). Using their chemical and phase composition, parameters such as the temperature in the blast furnace, melt viscosity, type of added fluxes and type of oxidation–reduction conditions at certain stages of the process are determined. The temperature at which the smelting was carried out can be determined using phase diagrams (Chiarantini et al., 2009; Ettler et al., 2009; Kierczak & Pietranik, 2011), experimental smelt (Cabała et al., 2020; Ströbele et al., 2010; Warchulski et al., 2020), geothermometers (Toffolo et al., 2018; Warchulski, 2016) and melt modelling software (Kądziołka et al., 2020). The melt viscosity, in turn, has a very significant influence on the separation of the metallic phases during the smelting process. The most important aim during the metallurgical process was to obtain the lowest possible melt viscosity, which resulted in improved process efficiency (Ettler et al., 2009; Puziewicz et al., 2007; Warchulski et al., 2015, 2020). The analysis of metallurgical slags also allows the determination of oxygen volatility during smelting (Manasse & Mellini, 2002; Warchulski et al., 2020).

Slags from the pyrometallurgical processing of gold ores are not as common as those from other metals' production because they were mostly reprocessed with new methods of metal recovery. One of the few places where we can observe the remains of pyrometallurgical gold production is in Złoty Stok (see Supplementary Material 1 in the additional supporting information). Metallurgical slag remnants survived in this area due to the redirection of production in the 18th century to arsenic extraction (Dziekoński, 1972).

Information on gold production in blast furnaces in Złoty Stok is scarce and comes mainly from historical sources. These sources mainly focused on the amount of precious metal produced (Dziekoński, 1972) and the design of the smelting devices (Agricola, 1556), without taking into account other factors important during production (e.g., temperature or melt viscosity). For this reason, little is known about the conditions in these blast furnaces. The primary goal of this research is to recreate the historical (15th–17th centuries) gold production process in Złoty Stok. This reconstruction is possible by determining: (1) the temperature during smelting; (2) the viscosity of the metallurgical melt; (3) the oxidation–reduction conditions at individual production stages; and (4) the additives added during smelting. For this purpose, a series of mineralogical, geochemical and petrographic studies were carried out. The implementation of the assumed research will be the first complete description of the gold recovery process with all the critical parameters.

GEOLOGY AND HISTORY OF ORE PROCESSING IN ZŁOTY STOK

The deposits in Złoty Stok are metasomatic in origin, of skarn type (Mikulski & Speczik, 2016). Faults formed during the Alpine orogenic events facilitated the migration of fluids as a source of the ore minerals (Marszałek & Wąsik, 2000). Mineralization occurred in pyroxenites, amphibolites, dolomitic marbles, calc-silicate rocks and serpentinites in the form of veins and nests (Gil et al., 2015; Mikulski & Speczik, 2016) (see Supplementary Material 1 in the additional supporting information). Ore mineralization consists mainly of löllingite ($FeAs_2$) and arsenopyrite (FeAsS). The gold in the mined ores occurs as finely dispersed submicroscopic

inclusions in sulfides/arsenides, or in the form of native gold or electrum (Mikulski, 2011; Mikulski & Speczik, 2016). The mining of gold ores in Lower Silesia is a centuries-old tradition (Mikulski, 2015). The beginnings of mining and metallurgy related to it in Złoty Stok date back to at least the 13th century (Dziekoński, 1972). The period of maximum development was in the 15th–16th centuries. It was related to exploitation of the richest parts of the deposits and the merging of smaller enterprises into larger ones. From the 17th century a slowdown in production was observed. This was mainly associated with various wars and the depletion of available resources. Industrial activity began to revive in 1709 when arsenic production on an industrial scale began in Złoty Stok (Dziekoński, 1972). Since the industry was diverted to arsenic production, smelting of gold was occasional and based on different processes and moved to other locations. The metallurgical sector survived in Złoty Stok until the 1960s when the last arsenic ore-processing plant was closed (Dziekoński, 1972).

MATERIALS AND METHODS

Sampling

A total of 41 slag samples were collected from the slopes surrounding the 'Trująca' ('Poisonous') stream. Based on macroscopic differentiation and the degree of weathering, seven main types of slags were distinguished (Fig. 1, a–g), from which representative fragments were prepared for geochemical and petrological analyses.

Geochemical and petrological analyses

For quantitative and qualitative phase composition of samples, samples were examined using an Olympus BX-51 polarizing microscope, scanning electron microscope (SEM; Phenom XL), equipped with an energy-dispersive spectrometer (EDS) at the Faculty of Natural Sciences, University of Silesia in Katowice, followed by an electron probe micro-analyser (EPMA), a CAMECA SX 100 at the Inter-Institutional Laboratory of Microanalysis of Minerals and Synthetic Materials, University of Warsaw. EPM analyses were performed at 15 keV accelerating voltage, a 10–20.1 nA beam current and a beam diameter of up to 5 μm. Standards included: Na-albite ($NaAlSi_3O_8$); Mg, Si, Ca-diopside ([Ca, Mg, Fe]SiO_3); Al, K-orthoclase ($KAlSi_3O_8$); Fe-Fe_2O_3, chalcopyrite ($CuFeS_2$); Mn-rhodonite ($CaMn_3Mn[Si_5O_{15}]$); Co-CoO; Ni-NiO; Ti-rutile (TiO_2); Cu-cuprite (Cu_2O); Zn-sphalerite (ZnS); As-GaAs; Au-Au-SPI; P-YPO_4; and S-shalcopyrite ($CuFeS_2$). Seven slag samples differing in macroscopic properties were analysed for chemical composition using X-ray fluorescence (XRF) spectrometry, inductively coupled plasma-mass spectrometry (ICP-MS) and energy-dispersive X-ray fluorescence (EDXRF) for a broader spectrum of major, minor and trace elements. Sample preparation consisted of $LiBO_2$ fusion for XRF and lithium tetraborate decomposition and Aqua Regia digestion for ICP-MS. Loss on ignition was determined before XRF at 1000°C. XRF and ICP-MS analyses were performed by the Bureau Veritas Mineral Laboratories (Canada), and EDXRF analyses were performed at the Faculty of Science and Technology, University of Silesia in Katowice, using an Epsilon 3 (Panalytical) spectrometer equipped with Rh target X-ray tube and thermoelectrically cooled silicon drift detector (SDD) with 8 μm Be window and resolution of 135 eV at 5.9 keV. The measurements were performed under the following measurement conditions: 30 kV, 300 μA, 600 s counting time, atmospheric air and 100 μm Ag primary beam filter. The analytical reproducibility for bulk chemical analyses was estimated from replicate analyses of ZS4 and ZS3 slag samples. The uncertainty (2σ) reached up to 0.23% for Fe_2O_3, while the relative standard deviation (RSD) was up to 9.43% for TiO_2. Analytical accuracy was calculated with

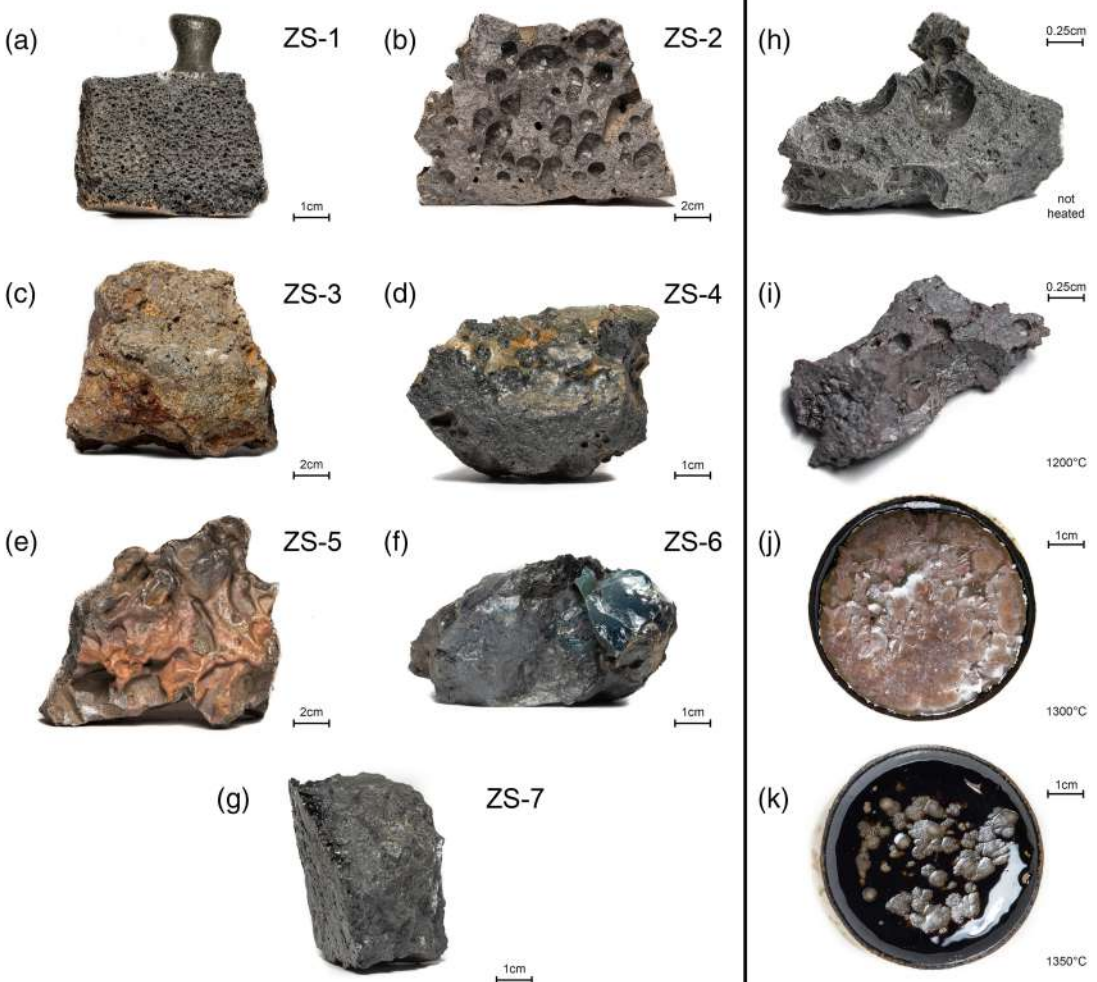

FIGURE 1 Scaled macroscopic images of the: (a–g) slag types from Złoty Stok; and (h–k) slags after the heating experiments [Color figure can be viewed at wileyonlinelibrary.com]

87:1038052227

proper standards. The calculated error reached the maximum for Fe_2O_3 and TOT/S (0.26%), and the relative error was maximal for P_2O_5 (17.65%). For details on quality assurance/quality control (QA/QC), see the Supplementary Material 2 in the additional supporting information.

Furnace experiments

Furnace experiments were performed at the Faculty of Natural Sciences, Institute of Earth Sciences, University of Silesia, in a chamber furnace PLF 160/5 with a PC 442/18 controller, SiC heaters and Thermocouple S with a maximum working temperature of 1550°C. Due to their dominant share, the ZS-2 type slag (Fig. 1, b, h) was selected for high-temperature experiments. Samples were melted in alumina pots. To determine the slag samples' melting temperature, successive experiments were performed with rising temperatures and fast cooling until complete melting of the sample (about 1 cm^3) had occurred.

Geothermometry

The features of the studied slags enable the use of geothermometers to estimate the system's liquidus temperature following the methodology proposed by Warchulski (2016). Also, the presence of glass inclusions inside olivine crystals in sample ZS-2 enabled the use of geothermometers to assess the temperature of the slag crystallization process itself. For this purpose, two geothermometers, olivine-glass/whole-rock composition and clinopyroxene-glass/whole-rock composition, were used.

$$\log_{10}\left[\frac{X_{MgO^{ol}}}{X_{MgO^{liq}}\left(X_{SiO_2^{liq}}\right)^{0.5}}\right]=\frac{4129}{T(K)}-2.082+0.0146\frac{P(bar)-1}{T(K)} \quad (1)$$

$$\frac{10^4}{T(K)}=7.53-0.14\ln\left(\frac{X_{Jd}^{cpx}X_{CaO}^{liq}X_{Fm}^{liq}}{X_{DiHd}^{cpx}X_{Na}^{liq}X_{Al}^{liq}}\right)+0.07\left(H_2O^{liq}\right)-14.9\left(X_{CaO}^{liq}X_{SiO_2}^{liq}\right)-0.08\ln\left(X_{TiO_2}^{liq}\right)$$
$$-3.62\left(X_{NaO_{0.5}}^{liq}+X_{KO0.5}^{liq}\right)-1.1\left(Mg\#^{liq}\right)-0.18\ln\left(X_{EnFs}^{cpx}\right)-0.027\,P\,(kbar) \quad (2)$$

Equation 1 from Sisson and Grove (1993) was selected over newer calculations in the olivine-glass system (Putirka et al., 2007) due to its proven utility in CO_2-bearing systems (Dasgupta et al., 2007), relevant in this case. Equation 2 is relevant to mafic igneous rocks and estimates temperature to ± 10–20 K standard error (Putirka, 2008). All details on temperature estimations using geothermometers are presented in Warchulski (2016). Three samples were not included in temperature estimations: ZS-1 due to the uncertain determination of the crystallization sequence, ZS-3 due to the weathering of the sample and ZS-6 due to the small crystal size.

Software

The MELTS-rhyolite v.1.0.2. software package (Ghiorso & Gualda, 2015; Gualda et al., 2012) was used to estimate the liquidus and solidus temperature of the studied slag samples. For

calculations of liquidus, bulk slag composition was used, while for solidus composition of the glass phases analysed with EPMA. Based on petrographical analyses for calculations atmospheric pressure (1 bar), and iron-wüstite (IW) oxygen buffer was assumed.

RESULTS

Slag types in Złoty Stok

Based on macroscopic properties, we were able to distinguish seven types of slags in Złoty Stok. Samples ZS-1 and ZS-2 are light-grey, highly porous, with crystals visible inside the pores. The difference between them is the size of the vesicles: from a few millimetres in diameter in sample ZS-1 to a few centimetres in diameter in sample ZS-2 (Fig. 1, a–b). According to the SEM-EDS/EPMA data, ZS-1 comprises intergrown, anhedral/skeletal crystals of olivine (up to a few millimetres in length) and pyroxene (up to 500 μm length). The spaces between the crystals are filled with residual glass (Fig. 2, a). The textural relationships indicate the cotectic

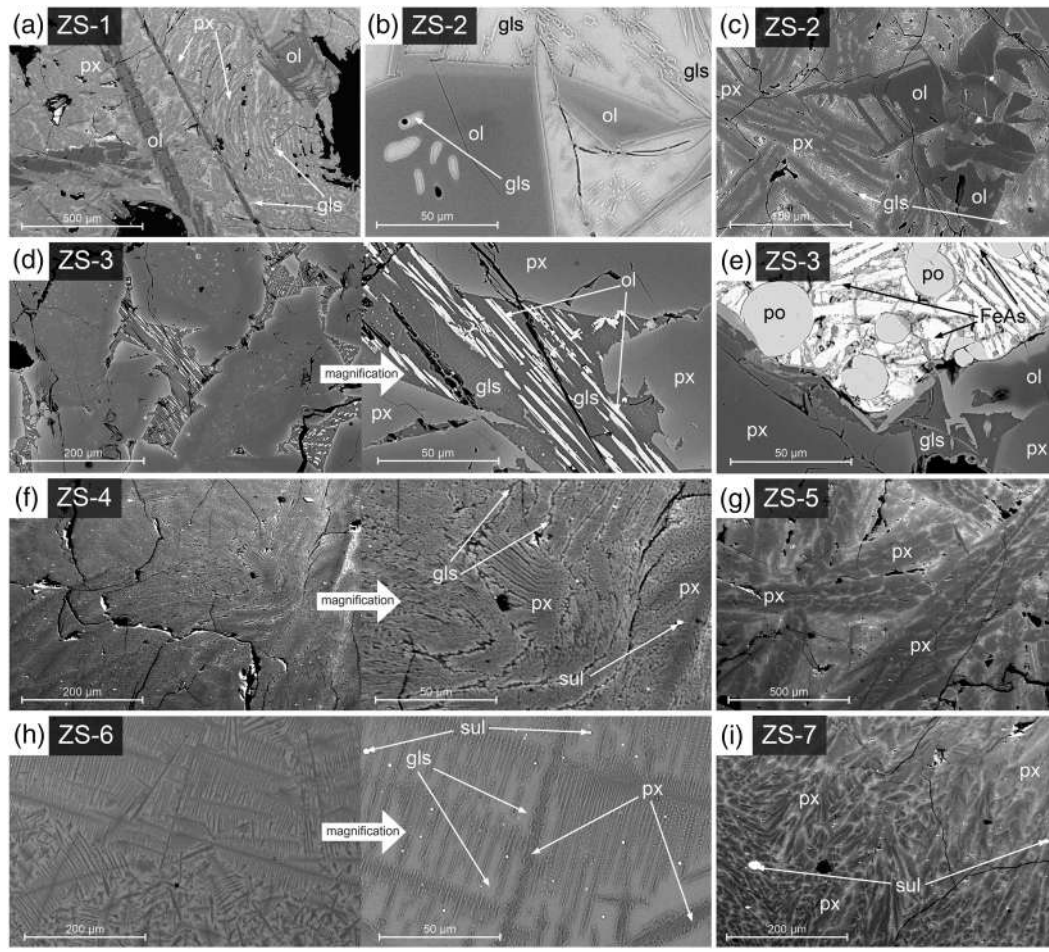

FIGURE 2 Scaled BSE (backscattered electron) images of slag types from Złoty Stok. FeAs, iron arsenide; gls, glass; ol, olivine; po, pyrrhotite; px, pyroxene; and sul, sulfide

crystallization of olivine and pyroxene. In sample ZS-2, zones with varying levels of crystallinity were distinguished (Fig. 2, b–c). In zones with high glass content, only anhedral olivine up to 100 μm occurs (Fig. 2, b). More crystalline zones resemble the ZS-1 sample, but crystals are smaller (< 150 μm) (Fig. 2, c). A characteristic feature of olivine crystals in the ZS-2 sample are inclusions of glass. The presence of zones with different degrees of crystallinity allows reconstruction of the crystallization sequence in this type of material. Olivine crystals were first to crystallize, followed by cotectic crystallization of olivine and pyroxene. It is worth noting that the ZS-2 type of slag is dominant (26 of 41 pieces). The ZS-3 sample is highly porous, with visible weathering signatures: it is covered by a brown-orange coating consisting of secondary mineralization (Fig. 1, c). SEM-EDS/EPMA allows for distinguishing subhedral pyroxene up to 500 μm as the dominant phase, accompanied by skeletal olivine up to 50 μm long occurring within the residual glass filling spaces between pyroxene crystals (Fig. 2, d). Sulfides are subordinate in all samples, and in most cases their crystals do not reach a size allowing for good quality analysis. Only in ZS-3 sample did the segregation of pyrrhotite (< 50 μm across) and Fe-As phase (< 100 μm long) were distinguished (Fig. 2, e). The order of crystallization in case of the ZS-3 slag is opposite to that of the ZS-2 sample. Pyroxene was the first phase, while olivine was separated from the melt in the last stage before solidifying the glass. ZS-4 is massive, grey to black, and locally covered by a thin yellow-green layer (Fig. 1, d). According to SEM-EDS/EPMA, ZS-4 is almost entirely composed of skeletal pyroxene crystals up to a few hundred μm, with only traces of residual glass between them (Fig. 2, f). ZS-5 is a black-grey with a red covering and a visible flowing texture on the sample surface (Fig. 1, e). Phase composition resembles the ZS-4 sample, but skeletal pyroxenes are significantly larger and reach up to a few millimetres in size (Fig. 2, g). ZS-6 and ZS-7 slags are black and grey, massive, containing glassy parts (Fig. 1, f–g). Glass in sample ZS-6 is blue to black, and in ZS-7 is black. According to SEM-EDS/EPMA, the ZS-6 sample is dominated by the glass with a diverse amount of pyroxene crystals (Fig. 2, h). In contrast, the ZS-7 sample comprises intergrown pyroxenes with a minor amount of residual glass resembling the ZS-4 sample. In the case of the ZS-7 slag, the 'glassy' covering is also composed of intergrown pyroxenes of fibrous morphology (Fig. 2, i). Samples from ZS-4 to ZS-7 follow the same straightforward crystallization sequence, starting from pyroxene with glass solidification in the end. In this case, the textural differences result only from the size of the crystals, that is, the time of crystallization of the melt.

Phase composition and chemistry of phases

Olivine

The presence of olivines has been found in three types of material: ZS-1, ZS-2 and ZS-3. In the ZS-1 and ZS-2 samples, their composition corresponds to forsterite ($Fo_{80–90}$) (see Supplementary Material 3 in the additional supporting information). In the ZS-3 sample, where olivine was the last to crystallize, their composition is more diversified ($Fo_{20–85}$) (see Supplementary Material 3 online), with a high proportion of crystals with a composition similar to fayalite. These olivine crystals are also characterized by elevated MnO concentrations (< 0.79 wt%). Regardless of the sample, all examined olivine contain CaO (< 0.78 wt%) and As_2O_3 (< 0.55 wt%) in the structure (see Supplementary Material 3 online).

Pyroxene

Pyroxenes appear in all studied samples. They are also characterized by the greatest chemical diversity between slags and within a single sample (see Supplementary Material 3 in the

additional supporting information). Their chemical compositions range from pigeonite to diopside, with augite being the dominant composition (see Supplementary Material 3 online). The pyroxene crystals are zoned in respect to Mg, Ca and Fe (Fig. 2, d). Moreover, pyroxenes may contain small concentrations of TiO_2 (< 0.40 wt%), MnO (< 0.34 wt%) and As_2O_3 (< 0.17 wt %) (see Supplementary Material 3 online).

Sulfides and arsenides

Sulfides are a common phase in the investigated slags (Fig. 2). However, in most cases due to their size or morphology, it is difficult to obtain a good quality EPM analyses. The only exception is the ZS-3 sample, where pyrrhotite was correctly analysed. The investigated pyrrhotite crystals additionally contain the substitutions As (up to 0.36 wt%), Ni (up to 0.18 wt%) and Cu (up to 0.13 wt%) (see Supplementary Material 3 in the additional supporting information). In the studied slags, As phases characteristic of speiss often occur in direct contact with the sulfide phases (Fig. 2, e). In the case of the material from Złoty Stok, they are characterized by a variable ratio of As to Fe, from 1:1 to 2:1. The composition also includes S (0.16–4.40 wt%), Cu (0.07–1.50 wt%), Ni (0.11–0.55 wt%) and Co (0.00–0.42 wt%) (see Supplementary Material 3 online).

Glass

Glass, like pyroxenes, is present in all analysed slags. Residual glass was found in each sample, terminating crystallization. Additionally, the ZS-6 sample contains primary glass, relatively unchanged by the crystallization process, and the ZS-2 sample contains glass inclusions inside olivine crystals (Fig. 2). The composition of the residual glass in the slag from Złoty Stok is very diverse, resulting from fluctuations in the chemistry of the original melt and the crystallization process's advancement. Regardless of the sample, they concentrate mainly SiO_2 (43.2–61.0 wt%), FeO (4.7–27.0 wt%), CaO (2.9–23.8 wt%), Al_2O_3 (4.5–20.4 wt%) and MgO (0.14–13.1 wt%). They are also composed of K, Na, S, P and Ti (see Supplementary Material 3 in the additional supporting information). Glass from olivine inclusions and the bulk composition of the ZS-2 sample differ slightly. The differences are limited to a decrease in Mg concentration (16.9 versus 10.3 wt% of MgO) (Table 1; and see also Supplementary Material 3 online), included in the olivine structure. A similar phenomenon is observed in the case of the ZS-6 sample, where the primary glass, close to the bulk composition of the sample, contains higher Mg concentrations compared with the residual glass (13.3 versus 4.5 wt% of MgO) (Table 1; and see also Supplementary Material 3 online). In the case of ZS-6, Mg enters the pyroxene structure, which implies its lower content in residual glass.

Chemical composition of slags

Despite the differences in the slags' macroscopic appearance (Fig. 1), their chemical composition is similar. In all cases the main components are SiO_2 (average = 53.47 wt%), MgO (average = 15.12 wt%), CaO (average = 13.27 wt%), FeO (average = 11.25 wt%), Al_2O_3 (average = 4.36 wt%) and K_2O (average = 1.29 wt%) (Table 1). Among the trace elements, the highest concentrations show As (415–1906 ppm); the others rarely exceed 100 ppm. The concentration of Au in the samples did not exceed the method's detection limit (10 ppm). The greatest difference between slag types is the content of MgO (7.43–18.36 wt%), CaO (10.84–15.19 wt%) and FeO

TABLE 1 Bulk chemical compositions of slags from Złoty Stok

Sample no.		*ZS-1*	*ZS-2*	*ZS-3*	*ZS-4*	*ZS-5*	*ZS-6*	*ZS-7*
P_2O_5	wt%	0.10	0.11	0.08	0.11	0.09	0.10	0.10
SiO_2		52.12	52.52	53.01	56.60	53.31	53.87	52.88
TiO_2		0.17	0.19	0.14	0.24	0.20	0.26	0.23
Al_2O_3		3.97	4.30	2.66	3.95	4.03	6.15	5.44
FeO		11.82	13.41	9.56	15.36	9.46	9.08	10.01
MnO		0.13	0.11	0.15	0.24	0.13	0.16	0.15
CaO		11.90	10.84	15.19	14.41	12.66	13.68	14.24
MgO		18.36	16.90	17.87	7.43	16.87	13.49	14.93
Na_2O		0.50	0.46	0.31	0.44	0.52	0.95	0.85
K_2O		1.15	1.32	0.74	1.10	1.18	1.99	1.58
TOT/C		0.10	0.07	0.07	< 0.02	0.03	0.04	0.03
TOT/S		0.11	0.16	0.12	0.15	0.11	0.15	0.13
LOI		−0.70	−1.00	−0.20	−1.50	−0.70	−0.80	−0.60
Au	mg/kg	< 10	< 10	< 10	< 10	< 10	< 10	< 10
Ba		14	12	30	11	11	93	128
Cu		44	62	67	2	15	16	29
Pb		49	15	42	14	8	11	22
Zn		36	21	26	8	8	21	17
Ni		10	4	16	1	2	4	3
Co		11	10	12	1	2	5	3
As		916	566	1906	669	770	415	657
Cr		7	5	4	2	2	14	3

(9.08–15.36 wt%). The negative values of LOI (loss on ignition) of the analysed slags were characteristic (Table 1). They indicate an increase in the mass of the sample due to its roasting, which results from the oxidation of the elements contained in it. The ZS-3 sample achieves the highest LOI values since it is partially weathered, so the oxidation process has largely naturally taken place.

Temperature estimations

Furnace experiments

As a consequence of heating, the slags have undergone the following changes: (1) after heating up to 1200°C, the first slight changes in the morphology of the samples are observed as softening of crystal boundaries, thus at this point we possibly reach the solidus of the system (Fig. 1, i); (2) heating up to 1300°C caused melting of the sample in the entire volume, but the sample was not unified; also, advanced recrystallization is observed, possibly due to the presence of unmelted residues constituting the nuclei for accelerating new crystal growth (Fig. 1, j); and (3) after heating up to 1350°C, the slag is completely molten and homogeneous. At this point, limited recrystallization of the sample is observed (Fig. 1, k).

Geothermometers

The results obtained with the help of geothermometers coincide well with those obtained from experimental studies. In determining the crystallization starting temperature (liquidus temperature of the system), the results are in the range of 1280–1320°C (Table 2), regardless of the geothermometer used. The temperature during crystallization based on glass inclusions in olivine from the ZS-2 sample was determined as about 1200°C (Table 2), indicating the temperature at which the crystallization process continued. However, complete crystallization/solidification must occur in lower temperatures.

Phase diagrams

Due to the chemical composition of slags with many elements considered primary (Table 2), among the commonly used phase diagrams (e.g., Warchulski, 2015; Kądziołka et al., 2020), none of them takes into account all these components simultaneously. However, the chemistry of studied slags approximates the composition of pyroxene. This is evidenced by the fact that the minerals from this group are present in all analysed slags and dominate by volume. For this reason, diagrams concerning this mineral group should provide the best approximation of the temperature of solidus and liquidus (see Supplementary Material 4 in the additional supporting information). On their basis, it can be assessed that the liquidus temperature of the analysed material is in the range of 1200–1400°C (Table 2; and see Supplementary Material 4 online). While the results they present are less precise than those obtained from geothermometers or furnace experiments, they identically match (Table 2). The solidus temperature on their basis is in the range 1100–1225°C (Table 2; and see Supplementary Material 4 online). For all samples except ZS-4, this value is approximately 1200°C, so it is consistent with both the experimental work and the result obtained using a geothermometer (Table 2).

MELTS software

The MELTS software made it possible to determine both the liquidus and the solidus temperatures of the studied slags. In the case of the liquidus temperature, bulk chemical compositions of the slags were used. As residual glass is the phase ending the crystallization process, its melting point should be a good approximation of the solidus temperature of the studied material. Thus, the chemical compositions of the residual glass of individual samples were used to assess the solidus temperature. The values for liquidus obtained using the MELTS software range from 1220 to 1410°C. The highest value occurs for the ZS-1 sample and the lowest for the ZS-4 sample. These results correspond well with the temperatures obtained from the phase diagrams. At the same time, apart from the ZS-4 sample, they are overestimated compared with geothermometers or experimental works. In the case of the solidus, the obtained values are in the range of 1070–1270°C and do not differ significantly from the temperatures obtained with the use of other methods (Table 2).

DISCUSSION

Furnace construction and the smelting process

The pyrometallurgical process of gold production from primary ores required a multi-stage approach. The first necessary activity was to enrich the extracted ore. In the case of Złoty Stok,

TABLE 2 Liquidus and solidus temperatures, and viscosity of slags from Złoty Stok

Sample no.	*ZS-1*	*ZS-2*	*ZS-3*	*ZS-4*	*ZS-5*	*ZS-6*	*ZS-7*
Liquidus temperature based on:							
Geothermometers (°C)	–	1290–1320 (1)	–	1300–1340 (2)	1280–1290 (2)	–	1300–1320 (2)
Furnace experiments (°C)	–	1300–1350	–	–	–	–	–
Phase diagrams (°C)	> 1300 (3)	> 1300 (3)	> 1300 (3)	1200–1250 (3)	> 1300 (3)	> 1300 (3)	> 1300 (3)
	1350–1400 (4)	1350–1400 (4)	1300–1350 (4)	1300–1350 (4)	1300–1350 (4)	1300–1350 (4)	1300–1350 (4)
MELTS software (°C) (5)	1410	1400	1370	1220	1360	1330	1340
Solidus/crystallization ending temperature based on:							
Geothermometer (°C) (1)	–	< 1200	–	–	–	–	–
Furnace experiments (°C)	–	About 1200	–	–	–	–	–
Phase diagram (°C) (6)	1200	1150–1200	1200–1225	1100–1150	1200–1225	1150–1200	1200–1225
MELTS software (°C) (5)	–	1170	1180	1070	–	1220	1270
Viscosity index (7)	0.75	0.73	0.77	0.62	0.68	0.61	0.67
Viscosity 1100–1400°C (log pa s) (8)	0.10–1.84	0.21–1.97	0.06–1.78	0.68–2.51	0.18–1.93	0.31–2.09	0.20–1.96

Sources: (1) olivine—glass geothermometer (Sisson & Grove, 1993); (2) pyroxene—glass geothermometer (Putirka et al., 2008); (3) pyroxene liquidus phase diagram diopside ($[Ca,Mg]SiO_3$)–hedenbergite ($[Ca,Fe]SiO_3$)–enstatite ($MgSiO_3$)–ferrosillite ($FeSiO_3$) (Huebner & Turnock, 1980); (4) pyroxene phase diagram Ca/(Ca + Mg + Fe), where Fe/(Mg + Fe) = 30% (Huebner & Turnock, 1980); (5) Gualda et al. (2012) and Ghiorso and Gualda (2015); (6) pyroxene solidus phase diagram diopside–hedenbergite–enstatite–ferrosillite (Huebner & Turnock, 1980); (7) Bachmann (1982); and (8) Giordano et al. (2006).

the miners only excavated those rock fragments in which mineralization aggregates were visible. Selected ore was transported to the smelter, where it was crushed and sorted.

In the gold smelting industry in Złoty Stok, the first stage was the smelting of the enriched ore in conditions preventing the oxidation of sulfide phases. Until this point, there is an agreement between the literature descriptions of the process (Agricola, 1556; Dziekoński, 1972), and the results obtained in the course of this and other research (Garbacz-Klempka et al., 2014) (Fig. 3, a). According to literature descriptions, the subsequent stages included: (1) the metallurgical process under reductive conditions ('raw melting') with the addition of pyrite, which was aimed at easier separation of gold; (2) roasting the resulting raw stone to remove sulfur and As; (3) next smelting under reducing conditions ('stone melting') with the addition of metallic lead to facilitate the separation of gold; and (4) cupellation to separate gold from lead (Dziekoński, 1972). However, this scheme is contradicted by Garbacz-Klempka et al. (2014) when describing the speiss/matte material. Speiss and matte are a typical by-product of metallurgy from sulfide ores (Chiarantini et al., 2021; Ettler et al., 2009; Rehren et al., 1999; Thornton et al., 2009). Matte is composed of a solid solution of Cu, Fe and Pb sulfides, while the speiss of arsenides and antimonides of Cu and Fe (Ravitz & Fisher, 1936). Usually, speiss and matte separate the metallic phases yielded from the silicate slag. According to Garbacz-Klempka et al. (2014), speiss/matte from Złoty Stok contains sulfides with a composition corresponding to pyrrhotite and arsenide. However, it also contains high concentrations of metallic Pb (up to 6 wt%). According to Dziekoński (1972) (Fig. 3, a), 'raw stone' was calcined before adding lead to it, and any material containing S, As and Pb should not be present. Considering this, an alternative diagram of the gold metallurgy process in Złoty Stok has been proposed (Fig. 3, b). Accordingly, in the first stage, enriched ore with fluxes leads to the formation of slag (described here) and a speiss/matte that concentrates the gold. In the process, slags were either stored at the dumps or partially returned to the furnace to serve as fluxes. This scheme was confirmed by the presence of segregation, rich in sulfides and arsenides (sample ZS-3) (Fig. 2, e). The next stage was speiss/matte smelting under reducing conditions with the addition of Pb. During smelting, as in other locations (Agricola, 1556; Bassiakos & Catapotis, 2006; Mendecki et al., 2020; Warchulski et al., 2020), the molten charge material flowed towards the bottom of the furnace. The speiss/matte above the Pb-Au melt was then removed and sorted according to the Au content (Agricola, 1556). The characteristics of such speiss/matte would perfectly match the material described by Garbacz-Klempka et al. (2014). Depending on the potential gold content, matte/speiss was mixed with an appropriate amount of lead and re-smelted (Agricola, 1556) or added during subsequent smelting to the first stage of melting, explaining proposed by Dziekoński (1972) addition of FeS_2 to the process (Fig. 3).

The proposed technological process's scheme (Fig. 3, b) is consistent with all previous publications on this material. and at the same time explains why two different types of slag were not found (after 'raw melting' and 'stone melting') (Fig. 3, a), and why speiss/matte is so rarely found by researchers (it is a gold carrier and is recyclable) (Fig. 3, b). The Pb-Au alloy formed as a result of this process was placed in a cupola furnace where it was again melted. An airstream was directed at the melt, thereby oxidizing the lead. After liquefaction, the Pb oxide flowed out through the opening in the furnace. When Pb oxides were removed, the metallurgists plugged the drain hole, leaving only gold in the furnace.

Ores and additions

According to the literature, in Złoty Stok three types of rocks containing ore mineralization were used in the smelting process (Mikulski, 2011): (1) calc-silicate rocks; (2) amphibolites and pyroxenites (also referred to as nephrites) (Gil et al., 2015); and (3) serpentinized

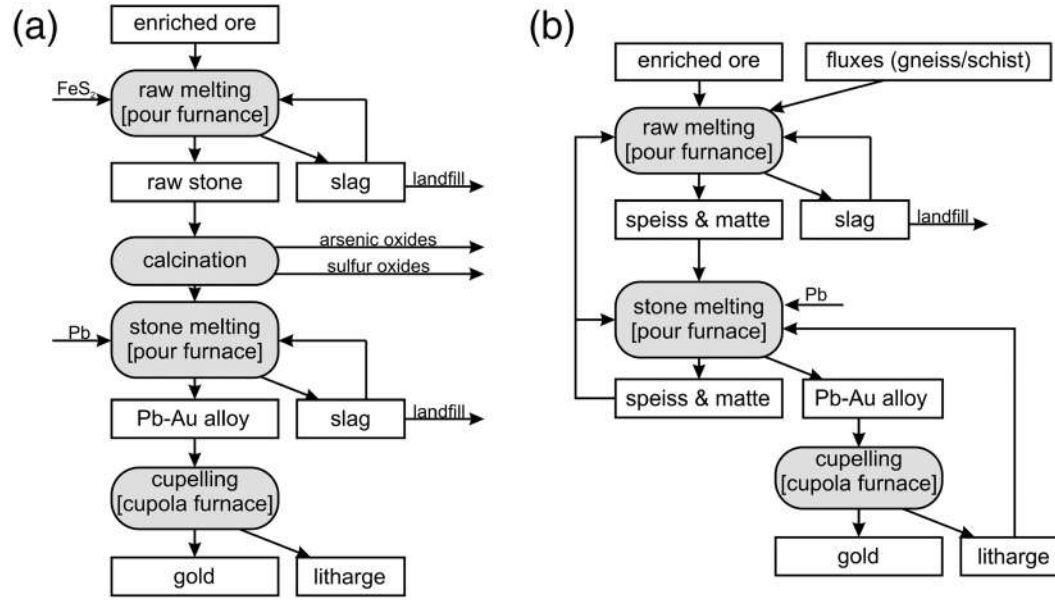

FIGURE 3 Scheme of the gold production process in Złoty Stok: (a) based on literature data (Dziekoński, 1972); and (b) a modified version

dolomitic marbles/serpentinites. By comparing their chemical composition (see Supplementary Material 5 in the additional supporting information) with the composition of the analysed slags (Table 1), it is possible to approximate the composition of additives to the metallurgical process. Regardless of the type of rock used in the metallurgical process, they are all depleted in Al_2O_3 and K_2O in relation to the slag (Péterdi et al., 2014; Mikulski & Speczik, 2008) (Table 1). A depletion in SiO_2 is also visible (except nephrites) (Table 1; see also Supplementary Material 5 online). Silica, SiO_2 is a necessary component to produce the slag melt, which is particularly important when using carbonate rocks in the process (e.g., dolomitic marble). In other locations, the addition of sand was a possible SiO_2 source (Cabała et al., 2020; Ettler et al., 2015; Manasse & Mellini, 2002; Warchulski et al., 2020). In Złoty Stok, SiO_2, Al_2O_3 and K_2O could have been delivered with the rocks occurring in the location: blastomylonitic schist and gneiss. They contain high concentrations of SiO_2, Al_2O_3 and K_2O, and are depleted in FeO, MgO and CaO (Kozłowska-Koch, 1973). Previously mentioned speiss/matte was a good addition to the process, facilitating the separation of gold-containing melt. However, the addition of other fluxes rich in Al_2O_3 and K_2O would cause a lowering of the liquidus temperature, thus making the process more economical and efficient.

Temperature estimates

To assess metallurgical slags' from Złoty Stok crystallization temperature, we decided to use four independent methods: furnace experiments, geothermometers, phase diagrams and MELTS software. The conducted experimental work shows that the investigated slags' composition liquidus is in the temperature range of 1300–1350°C (Fig. 1). The liquidus reflects the minimum temperature needed to melt the slag completely, and therefore the minimum temperature during the smelting process. Based on the experiments, a solidus temperature was

determined at about 1200°C; below this temperature, the last phase, residual glass, solidifies. Although all methods have their merits (Warchulski et al., 2016; Kądziołka et al., 2020), the experimental work still gives the most certain results. On this basis, we can conclude that in the case of slags from Złoty Stok, the best non-experimental method were geothermometers, as results they gave (1280–1340°C for liquidus and < 1200°C for solidus) (Table 2), coincides almost perfectly with the temperatures obtained with experiments. Phase diagrams, with the least precision, still gave accurate results for sample ZS-2, while the MELTS software overestimated liquidus by at least by 50°C, at the same time giving well-fitted results for solidus (Table 2).

The slags from gold smelting from this period have not been investigated from the perspective of the metallurgical process's temperature. For this reason, it is difficult to compare the studied material to other locations. However, when comparing the slags from Złoty Stok with the metallurgical wastes of other metals from a similar period (Table 3), and based on similar technologies (Agricola, 1556), it can be concluded that the temperature conditions described in this study correspond well with them, but are slightly higher (Tables 2 and 3).

The relationship between olivine crystal morphology and cooling rate, and the degree of undercooling can be used to approximate temperature change during slag crystallization (Donaldson, 1976; Faure et al., 2003). Taking into account the morphology of olivine crystals in the analysed slags, the thermal gradient was from about 5°C/h for the ZS-2 sample (subhedral crystals up to 150 μm) (Fig. 2, c) to even 300°C/h for the ZS-1 sample (skeletal crystals up to a few hundred μm) (Fig. 2, a) (Donaldson, 1976). These values, combined with the known liquidus and solidus temperatures, suggest that the slags crystallized in 30 min to several hours. However, the existence of a slag composed almost entirely of glass with a small number of skeletal pyroxenes (Fig. 2, h) and zones with different levels of crystallinity within one sample (Figs 1, d, f–g; and 2, b–c) indicates that this gradient could, in some cases, be much higher. Such a phenomenon indicates varied conditions during the storage of the slag melt.

Atmosphere

During the metallurgical process, the atmosphere had to be reducing to precipitate the formation of gold concentrating speiss and matte. Also, the petrographic image of slag from Złoty Stok is unambiguous in this matter—the presence of olivines and pyroxenes containing Fe^{2+} indicates the limited oxygen (O_2) fugacity during the metallurgical process (Fig. 2; see also Supplementary Material 3 in the additional supporting information). With free access of O_2, sulfides would convert to S oxides, As after oxidation to As_2O_3 would vaporize at temperatures above 457°C (Perry and Chilton, 1973), while Fe would be oxidized to Fe^{3+}, which would prevent its going into the olivine crystal structure. Critical here is the ZS-3 sample, where the olivine terminating the crystallization are dominated by Fe^{2+} (up to 56.50 wt% FeO) (see Supplementary Material 3 online), which indicates that the reducing conditions were also maintained during the melt storage and whole slag crystallization. The coexistence of olivine with Fe sulfides and Fe arsenide phases indicates that the conditions during smelting corresponded to the O_2 buffer quartz–iron–fayalite (QIF), which at atmospheric pressure and temperatures of 1300–1350°C is −10.5 to −11.5 log fO_2. Such a low value underlines the unique nature of the studied material. In the literature, there are no slags from a similar period with close O_2 fugacity values. In most cases, they contain Fe^{3+} concentrating in spinels (Ettler et al., 2001, 2009; Kierczak & Pietranik, 2011; Manasse & Mellini, 2002; Warchulski et al., 2020) or hematite (Ettler et al., 2001, 2009; Warchulski et al., 2020), pointing out the higher O_2 availability during or after the process.

Viscosity

The melt viscosity is crucial for the segregation of components, the speed of crystallization and the recovery of metals in the metallurgical process (Ettler et al., 2009). The lower the viscosity, the more effective the separation of the desired metals, and the higher the yield will be. For this reason, its calculations appear in most studies on the reconstruction of historical metallurgical processes as an indicator of their effectiveness. Mostly (Ettler et al., 2001; Kądziołka et al., 2020; Kierczak & Pietranik, 2011) they are based on Bachmann's (1984) viscosity index calculation method:

$$\text{v.i.} = \frac{\text{CaO} + \text{MgO} + \text{MnO} + \text{FeO}}{\text{SiO}_2 + \text{Al}_2\text{O}_3}$$

Lower values of v.i. indicate a higher melt viscosity. For the studied material, v.i. is from 0.61 to 0.76 (Table 2). The obtained results are similar for the metallurgy of other metals in a similar period (Table 3).

The main disadvantage of the method proposed by Bachmann is the inability to compare the obtained results with a wide range of substances due to the lack of an assigned SI unit and not taking into account the influence of temperature on the melt viscosity. The other method of calculating the viscosity of the melts was also proposed by Giordano et al. (2006). This model was designed for natural rocks and for the temperature range of 630–2000°C; however, the high chemical similarity of the analysed material to, for example, basalt or komatiite and the process temperatures falling within this range allowed its usage for slags. Additionally, Giordano et al.'s (2006) method is based on the chemical composition in mol% and calculates the viscosity values (Pa s) at the indicated temperatures according to the formula:

$$\log 10_\eta = \text{b1} + \frac{\text{b2} * \text{b3}}{\text{b3} + \text{SM}} + \text{b4}$$

TABLE 3 Summary of previous slag studies concerning similar periods and smelting technology

Location	*Smelting activity*	*Metal smelted*	*Method of temperature estimations*	*Liquidus temperature (°C)*	*Viscosity index*	*Viscosity (log pa s) (7)*
Bohutín, Czech Republic (1)	14th century	Ag, Pb	Phase diagrams	1150–1450	0.08–1.58 (6) 0.57–2.25 (1)	0.99–4.46 (1200–800°C)
Kutná Hora, Czech Republic (2)	14th–15th centuries	Ag	Phase diagrams	1150–1300	1.09–1.35 (6)	0.74–2.31 (1300–1150°C)*
Rudawy Janowickie, Poland (3)	14th–16th centuries	Cu	Phase diagrams	1200–1300	0.16–1.55 (6)	1.30–5.36 (1300–1200°C)*
Sławków, Polska (4)	16th–17th centuries	Pb	High-temperature experiments	1000–1150	0.82–1.00 (6) 0.90–1.75 (1)	1.34–1.48 (1150°C)
Kondratów, Poland (5)	18th century	Cu	MELTS software	1210–1240	0.43–0.75 (6)	0.88–2.49 (1240–1210°C)*

Sources: (1) Ettler et al. (2001; (2) Manasse and Mellini (2002); (3) Kierczak and Pietranik (2011); (4) Warchulski et al. (2020); (5) Kądziołka et al. (2020); (6) Bachmann (1982); and (7) Giordano et al. (2006); *results calculated based on the data from the source publication.

where b1 – b4 are temperature-dependent parameters; and SM is a structure modifier calculated as: Σ mol.% $\left(Na_2O + K_2O + CaO + MgO + MnO + \frac{FeO_{tot}}{2}\right)$.

For more details about the model, see Giordano et al. (2006).

In the studied material, calculations were performed for the temperature range corresponding to the extreme values indicated by the applied temperature estimation methods (1100–1400°C) (Table 2). At these temperatures, the viscosity of the studied slags is in the range of $\log_\eta$ = 0.06 – 2.51 Pa s (see Supplementary Material 6 in the additional supporting information). For the most probable liquidus temperature determined by furnace experiments (1350°C), these values are $\log_\eta$ = 0.26 – 0.90 Pa s. The highest values are shown by samples ZS-4 and ZS-6 (Table 2; and see Supplementary Material 6 online) as in the viscosity index. Slags from Złoty Stok, compared with smelters of other metals operating in a similar period, are characterized by significantly lower viscosity values at the temperature of their liquiduses. Such a phenomenon is partly due to the higher temperature of the smelting process in Złoty Stok (Tables 2 and 3). However, even taking this factor into account, in the lower temperature ranges, the viscosity of the melt being the precursor of the studied slags will still be one of the lowest (Table 3; see also Supplementary Material 6 online). This suggests high efficiency of the gold separation process from the melt, which is confirmed by the fact that the gold in the slags from Złoty Stok is present in concentrations below the detection limit (< 10 ppm) (Table 1).

CONCLUSIONS

The research carried out allowed for a complete reconstruction of the gold metallurgy process in the 15th–17th centuries. This determined that the process in Złoty Stok, Poland, was based on sulfide ores. Ambient rocks rich in SiO_2, K_2O and Al_2O_3 were used as fluxes, and speiss/matte from later stages were used to facilitate the separation of Au-rich sulfide melt. The existing scheme of the metallurgical process has been revised. The unnecessary and inconsistent data within the current state of the research roasting process have been removed. This modification explains the lack of two diametrically different types of slags among the samples from Złoty Stok described by various researchers, and the fact that speiss/matte is rare at slag dumps in Złoty Stok. The study of the slags themselves using experimental works, geothermometers, phase diagrams and the MELTS software allowed for an indication of the minimum temperature during the process at the range of 1300–1350°C, and the slag solidification temperature at 1100–1200°C. The process leading to the slag formation was carried out under strongly reducing conditions (−10.5 to −11.5 log fO_2) and at atmospheric pressure. The exceptionally low melt viscosity ($\log_\eta$ = 0.26 – 0.90 Pa s) guaranteed the high efficiency of the process. Such low viscosity resulted from the chemical composition of the charge and the high temperature during melting. The high efficiency of the process is confirmed by the lack of gold in the analysed slag samples from Złoty Stok. The conducted research is the first reconstruction of gold metallurgy based on metallurgical slag and shows considerable potential in using this type of material to recreate all parameters during historical metallurgical processes.

ACKNOWLEDGEMENTS

This study was supported by the National ScienceCenter (NCN) grant no. 2016/21/N/ST10/00838 (awarded to RW), and NationalScience Center (NCN) grant no. 2019/35/O/ST10/00313 (awarded to AG). AshleyGumsley help in final English proof reading is highly appreciated.

DATA AVAILABILITY STATEMENT

The data that support the findings of this study (quality assurance/quality control, geochemical and petrological data) are given in the tables and in additional supporting information. This study brought together existing data from several different sources, which are cited throughout.

ORCID

Rafał Warchulski https://orcid.org/0000-0002-0508-347X
Krzysztof Kupczak https://orcid.org/0000-0002-3395-9547
Aleksandra Gawęda https://orcid.org/0000-0001-9102-2149
Rafał Sitko https://orcid.org/0000-0002-0469-5159

REFERENCES

Addis, A., Angelini, I., Nimis, P., & Artioli, G. (2016). Late bronze age copper smelting slags from Luserna (Trentino, Italy): Interpretation of the metallurgical process. *Archaeometry*, *58*, 96–114. https://doi.org/10.1111/arcm.12160

Agricola, G. (1556). De Re metallica libri XII. Ed Muzeum Karkonoskie w Jeleniej Górze, 2000, Jelenia Góra.

Bachmann, H. G. (1982). *The identification of slags from archaeological sites*. Institute of Archaeology Occasional Publication.

Bassiakos, Y., & Catapotis, M. (2006). Reconstruction of the copper smelting process based on the analysis of ore and slag samples. *Hesperia Supplements*, *36*, 329–353.

Branca, T. A., & Colla, V. (2012). *Possible uses of steelmaking slag in agriculture: An overview* (pp. 335–356). INTECH Open Access Publisher.

Cabała, J., Warchulski, R., Rozmus, D., Środek, D., & Szełęg, E. (2020). Pb-rich slags, minerals, and pollution resulted from a medieval Ag-Pb smelting and mining operation in the Silesian–Cracovian region (southern Poland). *Minerals*, *10*, 28. https://doi.org/10.3390/min10010028

Chiarantini, L., Benvenuti, M., Bianchi, G., Dallai, L., Volpi, V., & Manca, R. (2021). Medieval Pb (Cu-Ag) smelting in the Colline Metallifere District (Tuscany, Italy): Slag heterogeneity as a tracer of ore provenance and technological process. *Minerals*, *11*(2), 97. https://doi.org/10.3390/min11020097

Chiarantini, L., Benvenuti, M., Costagliola, P., Fedi, M. E., Guideri, S., & Romualdi, A. (2009). Copper production at Baratti (Populonia, southern Tuscany) in the early Etruscan period (9th–8th centuries BC). *Journal of Archaeological Science*, *36*, 1626–1636. https://doi.org/10.1016/j.jas.2009.03.026

Cwojdziński, S. (2009). Szczegółowa mapa geologiczna Polski w skali 1:50000, sheet 902—Złoty Stok, PIG-PIB

Dasgupta, R., Hirschmann, M. M., & Smith, N. (2007). Partial melting experiments of peridotite + CO2 at 3 GPa and genesis of alkalic ocean island basalts. *Journal of Petrology*, *48*, 2093–2124. https://doi.org/10.1093/petrology/egm053

Donaldson, C. H. (1976). An experimental investigation of olivine morphology. *Contributions to Mineralogy and Petrology*, *57*, 187–213. https://doi.org/10.1007/BF00405225

Dziekoński, T. (1972). *Wydobywanie rud i metalurgia złota i arsenu w Złotym Stoku* (pp. 133–202). Zakład Narodowy im. Ossolińskich.

Ettler, V., Červinka, R., & Johan, Z. (2009). Mineralogy of medieval slags from lead and silver smelting (Bohutín, Příbram district, Czech Republic): Towards estimation of historical smelting conditions. *Archaeometry*, *51*, 987–1007. https://doi.org/10.1111/j.1475-4754.2008.00455.x

Ettler, V., Johan, Z., Zavřel, J., Wallisová, M. S., Mihaljevič, M., & Šebek, O. (2015). Slag remains from the Na Slupi site (Prague, Czech Republic): Evidence for early medieval non-ferrous metal smelting. *Journal of Archaeological Science*, *53*, 72–83. https://doi.org/10.1016/j.jas.2014.10.007

Ettler, V., Legendre, O., Bodean, F., & Touray, J. C. (2001). Primary phases and natural weathering of old lead–zinc pyrometallurgical slag from Príbram, Czech Republic. *The Canadian Mineralogist*, *39*, 873–888. https://doi.org/10.2113/gscanmin.39.3.873

Faure, F., Trolliard, G., Nicollet, C., & Montel, J.-M. (2003). A developmental model of olivine morphology as a function of the cooling rate and the degree of undercooling. *Contributions to Mineralogy and Petrology*, *145*, 251–263. https://doi.org/10.1007/s00410-003-0449-y

Garbacz-Klempka, A., Wardas-Lasoń, M., & Rzadkosz, S. (2014). Odpady hutnicze z rejonu Złotego Stoku. *Archieves of Foundry Engineering*, *14*, 23–28. https://doi.org/10.7494/mafe.2013.39.2.23

Geiseler, J. (1996). Use of steelworks slag in Europe. *Waste Management*, *16*, 59–63. https://doi.org/10.1016/S0956-053X(96)00070-0

Ghiorso, M. S., & Gualda, G. A. R. (2015). An H_2O-CO_2 mixed fluid saturation model compatible with rhyolite-MELTS. *Contributions to Mineralogy and Petrology*, *169*, 53. https://doi.org/10.1007/s00410-015-1141-8

Gil, G., Barnes, J. D., Boschi, C., Gunia, P., Raczyński, P., Szakmány, G., Bendő, Z., & Péterdi, B. (2015). Nephrite from Złoty Stok (Sudetes, SW Poland): Petrological, geochemical, and isotopic evidence for a dolomite-relate origin. *The Canadian Mineralogist*, *53*, 533–556. https://doi.org/10.3749/canmin.1500018

Giordano, D., Mangiacapra, A., Potuzak, M., Russell, J. K., Romano, C., Dingwell, D. B., & Di Muro, A. (2006). An expanded non-Arrhenian model for silicate melt viscosity: A treatment for metaluminous, peraluminous and peralkaline liquids. *Chemical Geology*, *229*, 42–56. https://doi.org/10.1016/j.chemgeo.2006.01.007

Gualda, G. A. R., Ghiorso, M. S., Lemons, R. V., & Carley, T. L. (2012). Rhyolite-MELTS: A modified calibration of MELTS optimized for silica-rich, fluid-bearing magmatic systems. *Journal of Petrology*, *53*, 875–890. https://doi.org/10.1093/petrology/egr080

Kądziołka, K., Pietranik, A., Kierczak, J., Potysz, A., & Stolarczyk, T. (2020). Towards better reconstruction of smelting temperatures: Methodological review and the case of historical K-rich Cu-slags from the old Copper Basin, Poland. *Journal of Archaeological Science*, *118*, 105142. https://doi.org/10.1016/j.jas.2020.105142

Kierczak, J., & Pietranik, A. (2011). Mineralogy and composition of historical cu slags from the Rudawy Janowickie Mountains, southwestern Poland. *The Canadian Mineralogist*, *49*, 1281–1296. https://doi.org/10.3749/canmin.49.5.1281

Kierczak, J., Potysz, A., Pietranik, A., Tyszka, R., Modelska, M., Néel, C., Ettler, V., & Mihaljevič, M. (2013). Environmental impact of the historical cu smelting in the Rudawy Janowickie Mountains (southwestern Poland). *Journal of Geochemical Exploration*, *124*, 183–194. https://doi.org/10.1016/j.gexplo.2012.09.008

Kozłowska-Koch, M. (1973). Polimetamorfity strefy tektonicznej Złoty Stok-Skrzynka w Sudetach. *Geologia Sudetica*, *8*, 121–158.

Manasse, A., & Mellini, M. (2002). Chemical and textural characterisation of medieval slags from the Massa Marittima smelting sites (Tuscany, Italy). *Journal of Cultural Heritage*, *3*, 187–198. https://doi.org/10.1016/S1296-2074(02)01176-7

Marszałek, H., & Wąsik, M. (2000). Influence of arsenic-bearing gold deposits on water quality in zloty Stok mining area (SW Poland). *Environmental Geology*, *39*, 888–892. https://doi.org/10.1007/s002549900036

Mendecki, M. J., Warchulski, R., Szczuka, M., Środek, D., & Pierwoła, J. (2020). Geophysical and petrological studies of the former lead smelting waste dump in Sławków, Poland. *Journal of Applied Geophysics*, *179*, 104080. https://doi.org/10.1016/j.jappgeo.2020.104080

Mikulski, S. (2011). Gold mineralization of the Kłodzko-Złoty Stok intrusion contact zone, Sudetes, SW Poland. Kozłowski, A. & Mikulski, S., *Gold in Poland*, Warszawa: AM Monograph, 27–43.

Mikulski, S. Z. (2015). Mapy obszarów perspektywicznych wystąpień rud metali w Polsce w skali 1: 200 000—rudy złota typu żyłowego i metasomatycznego towarzyszące mineralizacji siarczkowej na Dolnym i Górnym Śląsku oraz w Małopolsce (południowa Polska). *Przegląd Geologiczny*, *63*, 546–555.

Mikulski, S. Z., & Speczik, S. (2008). Organic and inorganic geochemistry of gold mineralisation at the zloty Stok, Southwest Poland. *Applied Earth Science*, *117*(4), 149–159. https://doi.org/10.1179/174327508X387474

Mikulski, S. Z., & Speczik, S. (2016). The auriferous ore mineralisation and its zonal distribution around the Variscan Kłodzko–Złoty Stok granitoid pluton in the Sudetes (SW Poland)–an overview. *Geological Quarterly*, *60*, 650–674. https://doi.org/10.7306/gq.1284

Perry, R. H., & Chilton, C. H. (1973). *Chemical Engineers' handbook* (5th ed.) (p. 50). McGraw-Hill.

Péterdi, B., Szakmány, G., Judik, K., Dobosi, G., Kasztovszky, Z., Szilágyi, V., Maróti, B., Bendő, Z., & Gil, G. (2014). Petrographic and geochemical investigation of a stone adze made of nephrite from the site Balatonőszöd—Temetői dűlő (Hungary). *Geological Quarterly*, *58*(1), 191–192. https://doi.org/10.7306/gq.1146

Putirka, K. (2008). Thermometers and barometers for volcanic systems. *Reviews in Mineralogy and Geochemistry*, *69*, 61–120. https://doi.org/10.2138/rmg.2008.69.3

Putirka, K., Perfit, M., Ryerson, F. J., & Jackson, M. G. (2007). Ambient and excess mantle temperatures, olivine thermometry, and active versus passive upwelling. *Chemical Geology*, *241*, 177–206. https://doi.org/10.1016/j.chemgeo.2007.01.014

Puziewicz, J., Zainoun, K., & Bril, H. (2007). Primary phases in pyrometallurgical slags from a zinc-smelting waste dump, Swietochłowice, upper Silesia, Poland. *The Canadian Mineralogist*, *45*, 1189–1200. https://doi.org/10.2113/gscanmin.45.5.1189

Ravitz, S. F., & Fisher, K. E. (1936). Equilibrium in lead smelting. *AIME Trans*, *121*, 119–126.

Rehren, T., Schneider, J., & Bartels, C. (1999). Medieval lead-silver smelting in the Siegerland, West Germany. *JHMS*, *33*(2), 73–84.

Sisson, T. W., & Grove, T. L. (1993). Temperatures and H2O contents of low-MgO high-alumina basalts. *Contributions to Mineralogy and Petrology*, *113*, 167–184. https://doi.org/10.1007/BF00283226

Ströbele, F., Wenzel, T., Kronz, A., Hildebrandt, L. H., & Markl, G. (2010). Mineralogical and geochemical characterization of high-medieval lead–silver smelting slags from Wiesloch near Heidelberg (Germany)—An approach to process reconstruction. *Archaeological and Anthropological Sciences*, *2*, 191–215. https://doi.org/10.1007/s12520-010-0039-7

Thornton, C. P., Rehren, T., & Pigott, V. C. (2009). The production of speiss (iron arsenide) during the early bronze age in Iran. *Journal of Archaeological Science*, *36*(2), 308–316. https://doi.org/10.1016/j.jas.2008.09.017

Toffolo, L., Addis, A., Martin, S., Nimis, P., Rottoli, M., & Godard, G. (2018). The Misérègne slag deposit (Valle d'Aosta, Western Alps, Italy): Insights into (pre-) Roman copper metallurgy. *Journal of Archaeological Science: Reports*, *19*, 248–260.

Tyszka, R., Kierczak, J., Pietranik, A., Ettler, V., & Mihaljevič, M. (2014). Extensive weathering of zinc smelting slag in a heap in upper Silesia (Poland): Potential environmental risks posed by mechanical disturbance of slag deposits. *Applied Geochemistry*, *40*, 70–81. https://doi.org/10.1016/j.apgeochem.2013.10.010

Warchulski, R. (2016). Zn-Pb slag crystallization: Evaluating temperature conditions on the basis of geothermometry. *European Journal of Mineralogy*, *28*, 375–384. https://doi.org/10.1127/ejm/2015/0027-2496

Warchulski, R., Gawęda, A., Kądziołka-Gaweł, M., & Szopa, K. (2015). Composition and element mobilization in pyrometallurgical slags from the Orzeł Biały smelting plant in the Bytom–Piekary Śląskie area, Poland. *Mineralogical Magazine*, *79*, 459–483. https://doi.org/10.1180/minmag.2015.079.2.21

Warchulski, R., Juszczuk, P., & Gaw da, A. (2018). Geochemistry, petrology and evolutionary computations in the service of archaeology: Restoration of the historical smelting process at the Katowice-Szopienice site. *Archaeological and Anthropological Sciences*, *10*, 1023–1035. https://doi.org/10.1007/s12520-016-0435-8

Warchulski, R., Mendecki, M., Gawęda, A., Sołtysiak, M., & Gadowski, M. (2019). Rainwater-induced migration of potentially toxic elements from a Zn–Pb slag dump in Ruda Śląska in light of mineralogical, geochemical and geophysical investigations. *Applied Geochemistry*, *109*, 104396. https://doi.org/10.1016/j.apgeochem.2019.104396

Warchulski, R., Szczuka, M., & Kupczak, K. (2020). Reconstruction of 16th—17th century Lead smelting processes on the basis of slag properties: A case study from Sławków, Poland. *Minerals*, *10*, 1039. https://doi.org/10.3390/min10111039

SUPPORTING INFORMATION

Additional supporting information may be found in the online version of the article at the publisher's website.

How to cite this article: Warchulski, R., Kupczak, K., Gawęda, A., & Sitko, R. (2022). Complete reconstruction of the process and conditions during gold smelting in the 15th–17th centuries in Złoty Stok based on metallurgical slags. *Archaeometry*, *64*(4), 916–934. https://doi.org/10.1111/arcm.12752

Heritage Science

RESEARCH Open Access

Bloomery iron production in the Holy Cross Mountains (Poland) area during the Roman period: conditions during the metallurgical process and their uniformity between locations

Krzysztof Kupczak[1*], Rafał Warchulski[1], Aleksandra Gawęda[1] and Jan Janiec[1]

Abstract

The study assessed the uniformity of the metallurgical process carried out during the period of Roman influence in Poland. The age of the investigated material was confirmed based on an analysis of the $^{12}C/^{14}C$ isotope ratio in the charcoal found in slag. The comparison was based on four Holy Cross Mountains (Poland) locations. The evaluation included smelting temperature, viscosity of the metallurgical melt, oxidation–reduction conditions, and slag cooling rate determined based on geochemical (XRF) and mineralogical (XRD, SEM, EPMA) analyses. Despite the distance between individual sampling sites, the conditions in which smelting was carried out were similar for all samples. The liquidus temperature of the analyzed slags was in the range of 1150–1200 °C. Oxidation–reduction conditions were determined through thermodynamic calculations using SLAG software. In the temperature range of 1150–1200 °C, the oxygen fugacity had to be below logP $O_2 = -13.20$ to -12.53 atm to reduce iron oxides to metallic iron. The viscosity of the metallurgical melt was calculated and ranged from 0.15 to 1.02 Pa s, indicating a low viscosity. The slag cooling rate determined based on olivine morphology was in the range of > 5 to 300 °C/h. Smelting parameters were compared with other locations in Poland, and similar results were obtained for slags from Masovia and Tarchlice. In the case of one site (Opole), despite the higher maximum value of liquidus temperature, it was indicated that the process could have taken place in similar conditions, and the differences resulted from contamination of the slag with material from the furnace/pit walls.

Keywords Slags, Iron, Process reconstruction, Smelting, Viscosity, Temperature, Oxygen fugacity

Introduction

Slags are waste materials generated during the smelting of metals using pyrometallurgical methods [1]. As a result of high temperature at a suitably reducing environment in the smelting furnace, a metallic phase (or intermediates) and a waste material (slag) can be formed [2]. In the case of many historical metallurgical centers, documentation describing the technical aspects of the metallurgical process is not available (e.g., [3–5]). Modern analytical methods based on determinations of the chemical and phase composition of metallurgical by-products, together with the use of experimental methods, allow to fill this gap by reconstructing the conditions under which the slags were formed and, thus, the conditions under which the smelting was carried out [6–13]. Since historical metallurgical processes often vary from location to location, there is no single path to follow during such archaeometric research. Thus, each studied material requires an individual approach.

*Correspondence:
Krzysztof Kupczak
krzysztof.kupczak@us.edu.pl
[1] Faculty of Natural Sciences, Institute of Earth Sciences, University of Silesia in Katowice, Będzińska 60, 41-200 Sosnowiec, Poland

Iron, however abundant, is rarely observed in a native state on the Earth's surface. Native iron has so far only been found in a few places, e.g., the volcanic rocks of Disko Island (Greenland), Siberian traps (Russia), and Miocene volcanic rocks in Central Germany (Bühl) [14]. Iron in metallic form can also be observed in iron meteorites, which consist mainly of Fe–Ni alloys [15]. Apart from these exceptions, Fe is overwhelmingly found on the Earth's surface as FeO and Fe_2O_3 to form many minerals [16].

The oldest objects made of iron date back to the 6th to 4th millennium BC and have been found in the Middle East and Egypt. Still, no reduction processes were carried out to form iron objects during this period, but meteorite iron was used for this purpose [17]. The first attempts to smelt iron from ores most likely come from the Anatolian area and are dated to the 2nd millennium BC. From the 16th to the twelfth century BC, the Hittite Empire was the only region where iron production was carried out. Over time, the ability of smelting Fe spread worldwide, reaching present-day Poland in about the second century BC [18]. The oldest Fe mining centers in Poland are related to the period of Roman influence and include, among others, the Holy Cross Mountains, Mazovia, Silesia, and Wołów regions [19]. The period of Roman influence refers to the age covering the 3rd period of the Iron Age in the area of the so-called Barbaricum (including the area of today's Poland). Even though the Roman Empire did not rule over the Barbaricum, its influence was significant and contributed to the development of local communities mainly through trade and knowledge exchange [20].

The Holy Cross Mountains region is the largest and best-known among Polish centers of ancient metallurgy thanks to the long-term research of Mieczyslaw Radwan, Kazimierz Bielenin, Szymon Orzechowski and others (e.g., [21, 22]). During archaeological works, tap slags, iron products, remains of furnace walls, places of ore storage, charcoal production, and items indirectly related to metallurgical production, such as ceramics, ornaments, and coins, were found [19, 21, 23]. Based on archaeological findings, it was possible to date them from 100 BC to 350 AD (mainly based on found ceramics and coins). The antique nature of the finds was confirmed by isotopic analyses, which yielded results in the range of 300 BC–400 AD [21]. Investigations in the area have revealed numerous remnants of former iron production in the form of smelter slags [21]. The region with the largest number of furnaces occupies an area of about 800 to 1000 km^2 [19]. About 8000 sites were discovered, with more than 550,000 furnaces. Slag fragments found in this area weighed up to 120 kg. Based on the amount of slags/pits found, it is estimated that about 11,000 tons of iron were produced in this area during the period of Roman influence [19]. The presence of numerous remains has contributed to the development of research into ancient iron production methods. They focused mainly on the impact of bloomery iron production on society and experimentally reproducing the process (e.g., [19, 21, 23]). Reconstructions have been focused on providing information on the composition of the smelter charge (proportions of ores and charcoal), the amount of charcoal used for smelting, and the efficiency of the process [21]. Still, only during experiments conducted since 2012 has it been possible to obtain materials equivalent to those produced in historical times [24]. Parameters such as melt viscosity or oxygen fugacity have not been analyzed so far [19, 21, 25].

The main goal of the presented work is to determine the uniformity of bloomery iron production based on the analysis of the conditions prevailing during smelting in selected locations. Geochemical, petrographic, and mineralogical methods allowed for the determination of the liquidus temperature of the slags, the viscosity of the silicate melt from which the slags crystallized, the oxidation–reduction conditions prevailing during the smelting, and the cooling rate of the slags. The obtained data made it possible to determine to what extent the conditions differed during bloomery iron production in the Holy Cross Mountains and to indicate the similarities in process conditions between the Holy Cross Mountains and other locations in Poland.

Samples were collected in the vicinity of the Skarżysko-Kamienna, Starachowice, and Iłża (Fig. 1; [26]). These cities are located in the northern part of the area where iron smelting was carried out during the Roman influence period [21]. Slags from this area have not yet been thoroughly analyzed. Sampling from several locations from an area exceeding 20 km in radius was crucial to ensure that the studied slags originate from different local metallurgical centers (Fig. 1).

In the area where the slags were found, oxide and carbonate iron minerals forming concretions are abundant [22, 27]. The best described are the youngest traces of iron ore mining covering the period of the eighteenth-twentieth centuries [28]. Knowledge about the older ones is based only on written historical sources, without the possibility of locating the mining sites [28]. Only one ancient mining site, i.e., the Rudki mine, has been recognized (Fig. 1). Modern (since 1922) mining has revealed traces of ancient exploitation in the upper, weathered part of the Rudki deposit. Archaeological investigations led to the discovery of tools (shovels, spoons, shells of broken pots) in old mining pits [21]. Most probably, a range of smaller deposits were also exploited in this area [21, 23], especially in locations farther from the Rudki

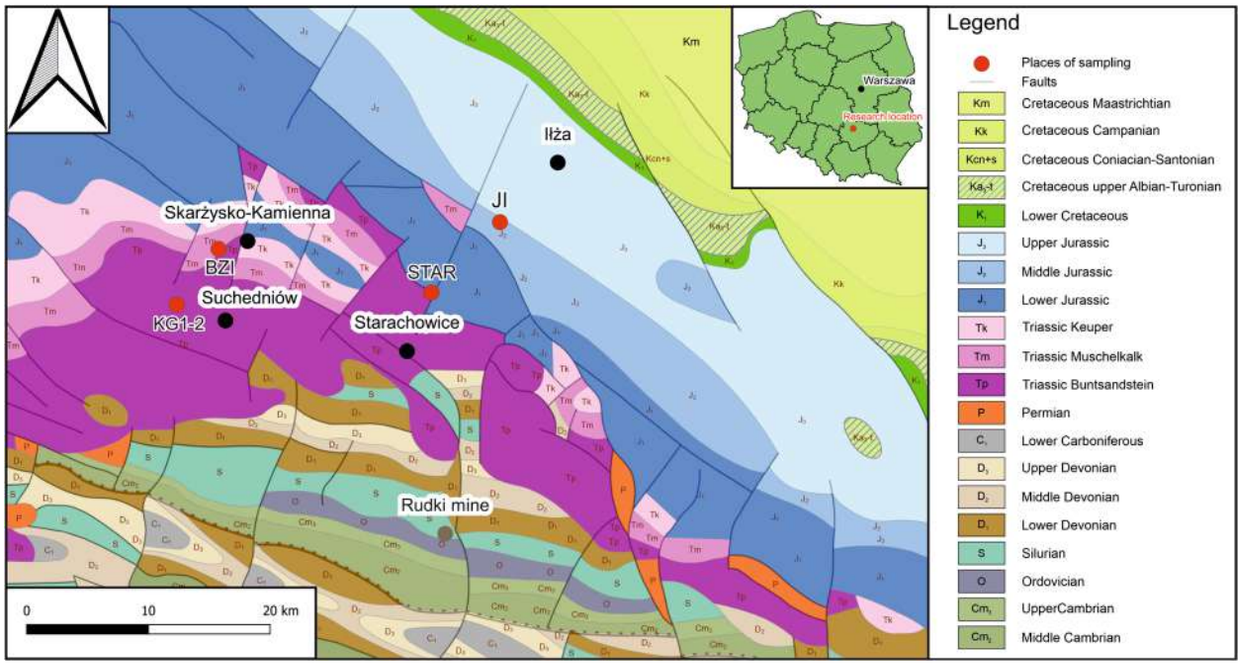

Fig. 1 Geological map showing sampling sites. Prepared based on data available on geoportal.gov.pl [31]

mine [21]. Near Starachowice and Suchedniów, hematite ores occur in Triassic deposits. Triassic and Middle Jurassic clay siderites also occur near Starachowice [21]. Limonite deposits and bog iron also occur in the analyzed area [22].

Materials and methods

Sampling

During the research, slags were collected from the area around the cities located in the Świętokrzyskie Voivodship: Suchedniów (KG1-2), Skarżysko-Kamienna (BZI), Iłża (JI) and one slag sample was obtained from the Museum of Nature and Technology in Starachowice (divided later into two subsamples; STAR1-2; Figs. 1, 2). Samples KG1 and KG2 were collected from two different pits located in close proximity (several dozen meters). The analysis of two samples found close to each other made it possible to check whether there were differences in metallurgical conditions between smelts conducted within one location. Prior to advanced petrological and geochemical analyses, representative samples were chosen from each location based on macro- and microscopic observations (optical microscope and SEM). Nonweathered material from the central part of the slag pieces with typical macro- and microscopical images was selected for further analysis. The samples were crushed, ground, and quartered to obtain the proper amount for chemical and phase composition analyses. Additionally, thin sections were prepared for microscopic observations. After preliminary data was obtained for the STAR sample, it was decided to separately analyze two subsamples (STAR1 and STAR2) differing in terms of chemistry and phase composition.

Chemical and phase analyses

The first step of the analysis was the macroscopic and microscopic observations to assess the slag's texture. An Olympus BX-51 polarizing microscope and a scanning electron microscope (The Phenom XL) equipped with an energy dispersive spectrometer (SEM–EDS) were used for this purpose (Institute of Earth Sciences, University of Silesia). An electron micro-probe (Cameca SX100, Inter-Institutional Laboratory of Microanalysis of Minerals and Synthetic Materials, University of Warsaw) was used to determine the exact chemical composition of the phases. Electron micro-probe analyses were performed at 15 keV accelerating voltage, a 10–20.1 nA beam current, and a beam diameter of up to 5 µm. Approximately 130 analyses of the chemical composition of phases occurring in the analyzed slags were performed, most of which (approx. 90) were performed for olivine crystals. The FeO to Fe_2O_3 ratio in spinel crystals was calculated to balance unit cells ($A^{2+}D^{3+}{}_2O_4$); similar calculations were performed for iscorite crystals. Details on detection limits and measurement parameters are available in Additional files 1, 2.

The phase composition of the samples was determined using the PANalytical X'PERT PRO-PW 3040/60 X-ray

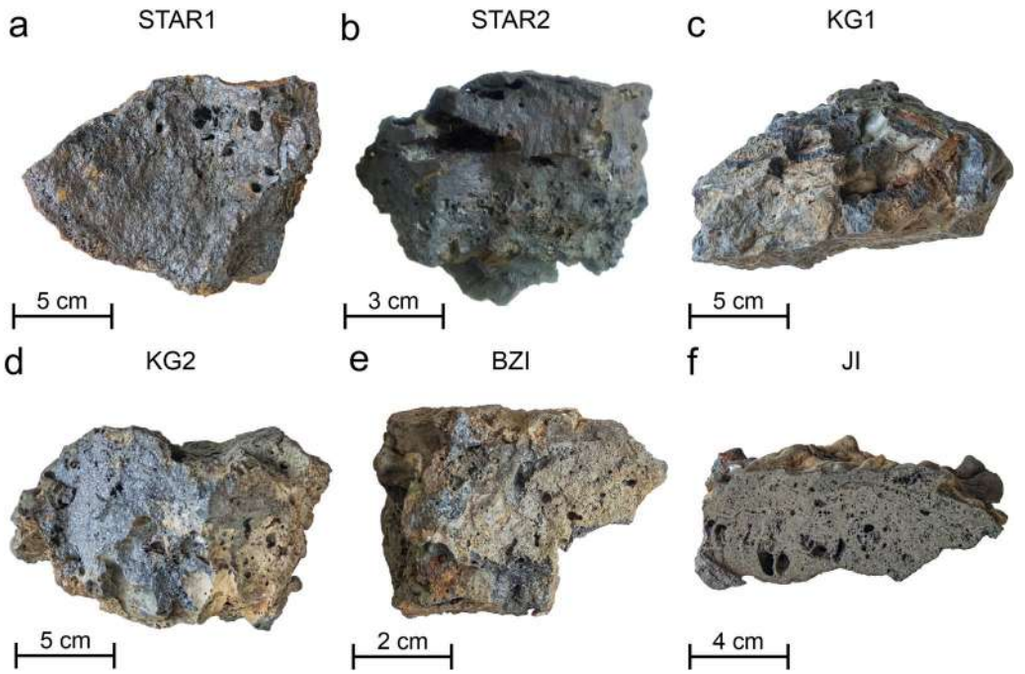

Fig. 2 Macroscopic photos of the analyzed slags

diffractometers (XRD) equipped with $CoK_{\alpha 1}$ source radiation and Fe-filter to reduce the K_{β} radiation. During analyses, the X'celerator detector was used (Faculty of Natural Sciences, University of Silesia). The analyses were performed in the 5–90°2Θ angular range at 40kv voltage (40 mA). For quantitative phase composition, a Rietveld analysis was performed using the X'PERT High Score Plus software with the PDF4 + database [29].

The slags' chemical composition was determined using X-ray fluorescence (XRF) by Bureau Veritas Mineral Laboratories (Canada) on fused discs according to XF702 program. For trace elements, the samples were digested with Aqua Regia and analyzed using ICP ES/MS method by Bureau Veritas Mineral Laboratories. Quality assurance/quality control was calculated based on duplicates and reference materials analyses. Details about quality assurance/quality control (QA/QC) are presented in Additional file 3.

Dating

A radiocarbon dating method was used to estimate the age of the analyzed material. For this purpose, about 1.5 g of charcoal was taken from the STAR1 sample. The charcoal was then processed into graphite and analyzed for $^{14}C/^{12}C$ isotope ratio using an Accelerator Mass Spectrometer (AMS). The CEMIZ Isotope Methods Center in Gliwice carried out AMS analyses. The radiocarbon dates were calibrated using OxCal 4.4 software [30] using the IntCal20 calibration curve [31]. Only the STAR1 sample was used for dating because it was the only one in which charcoal fragments were found.

Software

Graphical spatial (QGIS), raster (Adobe suite), and vector (Corel suite) data processing software were used during this research. SLAG software [32] was also used to determine the thermodynamic equilibrium between metallic Fe and FeO. QGIS and SLAG software were available with an open-source license. Adobe and Corel DRAW software were used with an educational license.

Results

Slag characteristics

Bulk chemistry

Slags reveal consist mainly of FeO (43.97–75.32 wt.%) and SiO_2 (18.04–47.14 wt.%), while minor components are Al_2O_3 (3.67–4.83 wt.%), CaO (0.50–2.47 wt.%), MnO (0.39–3.91 wt.%), P_2O_5 (0.04–1.76 wt.%), and K_2O (0.46–1.39 wt.%; Table 1). Small (less than 1 wt.% of oxide) amounts of TiO_2, MgO, and Na_2O were also detected (Table 1). The negative LOI (Loss on Ignition) values result from iron oxidation at 1000 °C (Table 1). Since the slags are composed mainly of FeO, the LOI values exceeded the limits in most cases (± 5.1 wt.%; Table 1). The concentrations of trace elements (e.g., V, Cr, As, Zn,

Table 1 Chemical composition of slags

		STAR1	STAR2	KG1	KG2	BZI	JI
SiO_2	wt.%	18.04	47.14	28.24	18.53	26.00	22.56
TiO_2		0.16	0.22	0.21	0.17	0.18	0.14
Al_2O_3		3.67	3.83	4.83	4.08	4.33	3.68
FeO		75.32	43.97	56.56	68.25	60.51	68.05
MnO		0.52	0.39	3.38	2.96	3.91	2.16
MgO		0.41	0.32	0.75	0.66	0.64	0.35
CaO		0.50	0.77	2.47	1.86	1.44	0.74
Na_2O		0.05	0.17	0.05	0.03	0.04	0.03
K_2O		0.46	0.94	1.39	0.92	1.00	0.57
P_2O_5		0.04	0.10	1.75	1.54	1.76	0.57
TOT/C		0.03	0.04	0.03	0.03	0.09	0.05
TOT/S		0.05	0.08	< 0.02	< 0.02	< 0.02	< 0.02
Total		99.25	97.97	99.66	99.03	99.9	98.9
LOI		< − 5.1	− 3.4	< − 5.1	< − 5.1	< − 5.1	< − 5.1

LOI: loss on ingnition; TOT/C: total carbon; TOT/S: total sulphur

Pb) in the analyzed slags did not exceed 130 mg kg^{-1} (Additional file 3).

Macro- and microscopic image and phase composition

Macroscopically, the collected slags have a steel-gray color. The surface of all slags shows traces of weathering in the form of a lighter in color or grayish-orange layer reaching a maximum of 1–2 mm deep into the samples (Fig. 2). Numerous pores were observed within slags, rarely exceeding 10–30 mm in diameter (Fig. 2). STAR1 sample was also characterized by the presence of unburned charcoal in the slag. Flow traces were observed on the surface of all samples, but they are best visible in the JI sample (Fig. 2f). Macroscopically, the slags appear entirely crystalline. However, microscopic observations showed the presence of amorphous phases in the samples.

The STAR1 sample consists of olivines ($(Fe, Mg)_2SiO_4$; 60.5 vol.%), wüstite (FeO; 27.0 vol.%), spinels (8.2 vol.%), and leucite ($KAlSi_2O_6$; 4.3 vol.%; Figs. 3; 4). Hypocrystalline and crystalline zones were distinguished in the sample. In zones with a hypocrystalline texture, olivines ($(Fe, Mg)_2SiO_4$) are dispersed within the glass as subhedral, mainly tabular or elongated crystals (Fig. 4b). In contrast, within fully crystalline zones, olivine is the main phase, while oxide phases and leucite are scattered between them (Fig. 4a). Spinel was observed mainly as subhedral crystals, reaching about 100 µm in size (Fig. 4a). Wüstite occurs mainly as small (up to 30 µm) oval grains (Fig. 4a), and leucite as anhedral crystals up to a few tens of µm in size (Fig. 4a).

The STAR2 sample consists of a high content of quartz (46.0 vol.%), cristobalite (1.8 vol.%), and lower (25.8 vol.%) content of fayalite compared to other samples (Fig. 3). This sample also contained leucite (2.1 vol.%), feldspar, and zircon ($Zr(SiO_4)$; Figs. 3, 4c, d). In the STAR2 sample, three distinct zones were observed (Fig. 4c). The first one contained mainly olivine, which filled the vast majority of the sample (Fig. 4c). Spinel, leucite, and wüstite crystals were also observed in this zone. The second zone in the STAR2 sample is the zone composed mainly of SiO_2 phases and glass (Fig. 4c). In this zone, feldspars with a diameter of up to 200 µm and zircon crystals measuring up to 30 µm in length and 10 µm in width also occur sporadically (Fig. 4c, d). Between the zone composed mainly of olivine and the one composed mainly of quartz, there is an area containing olivine crystals dispersed in the glassy phase, up to about 200 µm long and several µm wide (Fig. 4c). Since the STAR2 sample contains both quartz and leucite (Fig. 3), which cannot co-crystallize from the melt, it was concluded that the sample is contaminated by the fragments of the furnace/pit walls. For this reason, it was excluded from further investigations aiming to recreate conditions during the smelting process.

In KG1, olivines account for 74.7 vol.% of the sample (Fig. 3). They were observed as tabular crystals up to 200 µm in length, dispersed in the glass (Fig. 4e). Leucite (6.0 vol.%; Fig. 3) was observed in the form of crystals up to 100 µm in size (Fig. 4e). Sporadically, in KG1 slag iscorite ($Fe^{2+}{}_5Fe^{3+}{}_2SiO_{10}$) occurs in the form of elongated crystals (up to several hundred µm in length; Fig. 4g). The oxide phases in sample KG1 are represented by wüstite (oval crystals up to 30 µm in diameter; 10.5 vol.%; Figs. 3; 4f) and spinel (crystals up to 100 µm in size; 8.2 vol.%; Figs. 3; 4f).

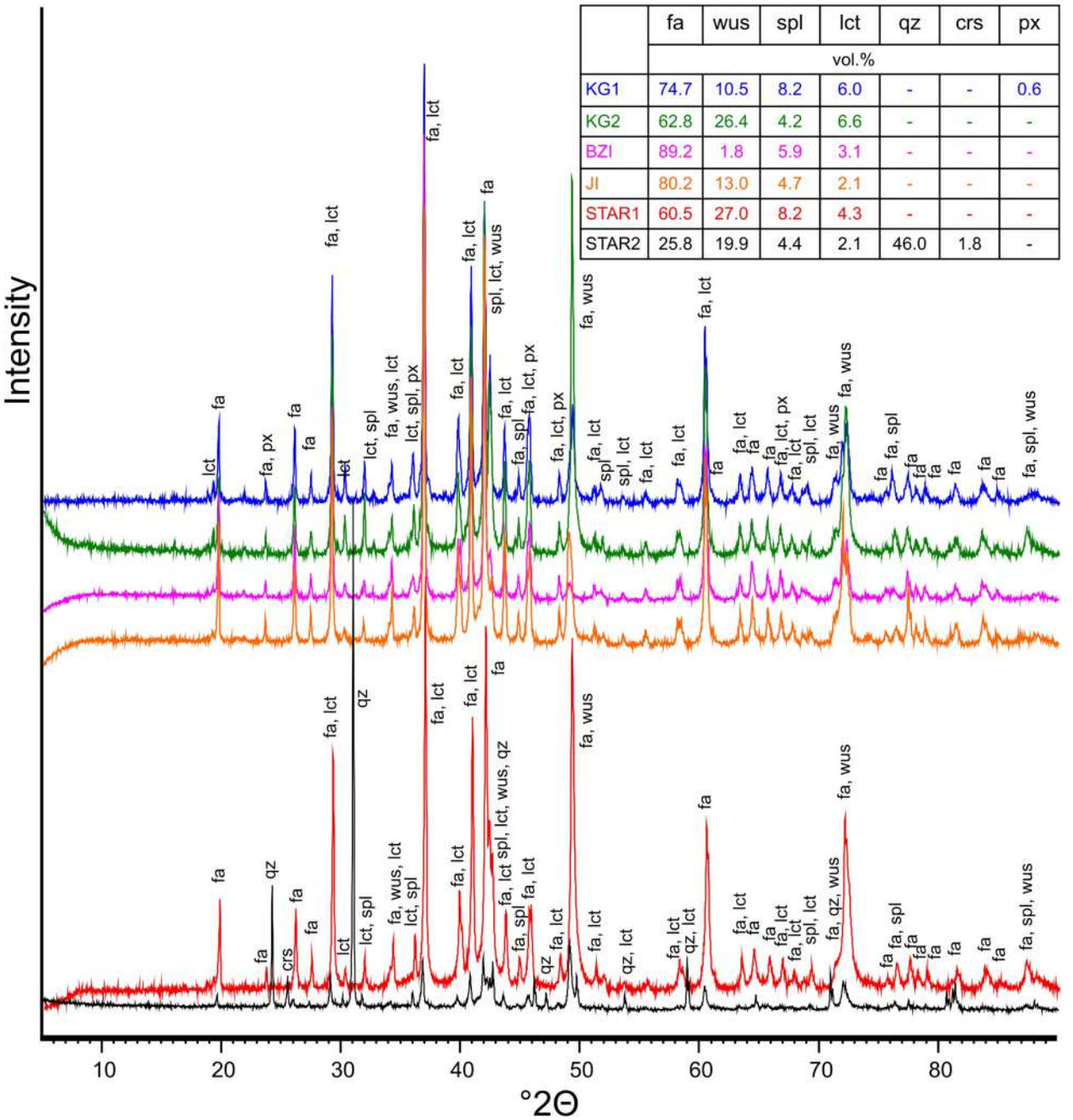

	fa	wus	spl	lct	qz	crs	px
	vol.%						
KG1	74.7	10.5	8.2	6.0	-	-	0.6
KG2	62.8	26.4	4.2	6.6	-	-	-
BZI	89.2	1.8	5.9	3.1	-	-	-
JI	80.2	13.0	4.7	2.1	-	-	-
STAR1	60.5	27.0	8.2	4.3	-	-	-
STAR2	25.8	19.9	4.4	2.1	46.0	1.8	-

Fig. 3 Results of XRD analysis of slags. crs: cristobalite; fa: fayalite; lct: leucite; px: pyroxene; qz: quartz; spl: spinel; wus: wüstite

In sample KG2, olivine (62.8 vol.%; Fig. 3) is present as the main phase, with wüstite (26.4 vol.%; Fig. 3) and spinel (4.2 vol.%; Fig. 3) crystals scattered within the sample (Fig. 4h). Wüstite occurs as oval grains up to 20 µm in diameter (Fig. 4h). Spinel occurs as crystals up to 80 µm in size (Fig. 4h). Sporadically leucite crystals (6.6 vol.%) were also observed (Fig. 3).

In the BZI sample, olivine (89.2 vol.%; Fig. 3) was most commonly observed as elongated, 30–50 µm wide crystals with glass or small (up to a few µm in diameter) spinel crystals between them (5.9 vol.% of the sample; Figs. 3; 4i). Less frequently olivine formed tabular crystals reaching several hundred µm in size (Fig. 4j). Oval wüstite crystals were also observed (1.8 vol.%; Fig. 3) throughout

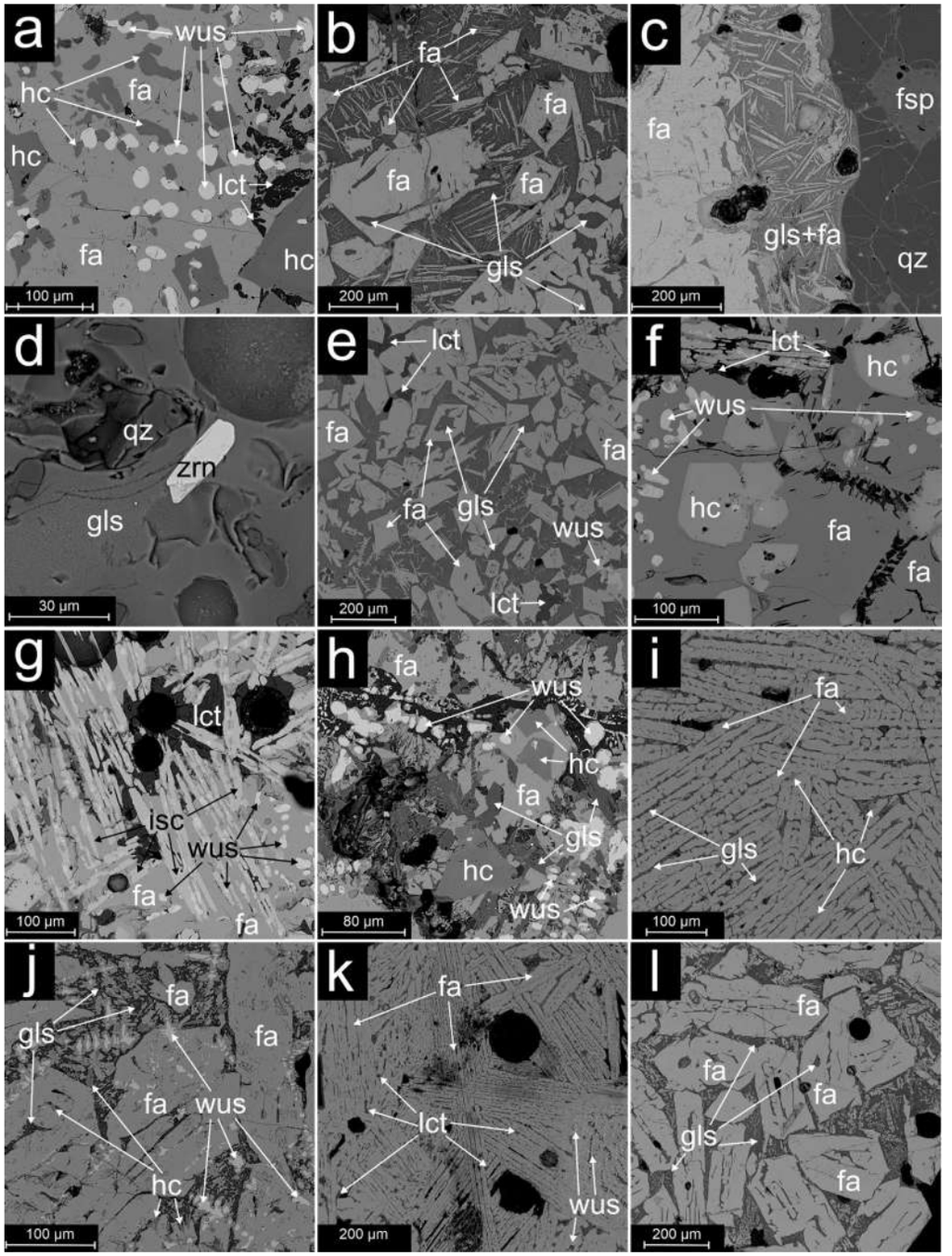

Fig. 4 BSE (back-scattered electrons) images of the slag samples: **a**, **b**—STAR1, **c**, **d**—STAR2 **e**–**g**—KG1; **h**—KG2; **i**, **j**—BZI; **k**, **l**—JI. fa: fayalite; fsp: feldspar; gls: glass; hc: hercynite (spinel); isc: iscorite; lct: leucite; wus: wüstite; zrn: zircon

the sample, with diameters mostly not exceeding 20 µm (Fig. 4j).

In the JI slags, elongated olivine (80.2 vol.%; Fig. 3) reaching several hundred µm in length was observed (Fig. 4k). Less frequently, olivines were observed as tabular crystals up to 200 µm (Fig. 4l). The presence of wüstite (13.0 vol.%) in the form of small (less than 10 µm) oval phases, spinel (4.7 vol.%), and leucite (2.1 vol.%) was found within the sample (Fig. 3).

Phase chemistry

Silicates and aluminosilicates The main silicate phase is olivine with a chemical composition corresponding to fayalite (Fe_2SiO_4; 57.7–67.6 wt.% of FeO; Table 2). Within fayalite, substitutions of Mn (0.76–7.4 wt.% of MnO), Al (0.16–0.31 wt.% of Al_2O_3), and Ca (0.18–1.67 wt.% of CaO) were commonly observed (Table 2). Iscorite crystals were also observed in the analyzed slags. In iscorite substitution of Al (up to 2.8 wt.% of Al_2O_3) and Mn (up to 1.45 wt.% of MnO) was found (Table 2). The only aluminosilicate phase observed in the slags was leucite, with the substitutions of Fe (up to 0.96 wt.% of FeO), Ba (up to 0.22 wt.% of BaO), Na (up to 0.10 wt.% of Na_2O; Table 2).

Oxides Oxide phases in the analyzed slags were observed as wüstite, spinel, and quartz. Spinel occurs as phases with a chemical composition corresponding to the magnetite ($Fe^{2+}Fe^{3+}{}_2O_4$)-hercynite ($Fe^{2+}Al_2O_4$) solid solution with the additions of Ti (0.49–1.08 wt.% of TiO_2), and Mn (0.56–1.28 wt.% of MnO) (Table 2).

Table 2 Representative chemical composition of phases occurring in slags

	ol1 BZI	ol2 JI	ol3 KG1	ol4 KG2	ol5 STAR1	qz KG1	leuc KG1	isc KG1	spl1 KG2	spl2 JI	spl3 BZI	gls (n = 16) KG1	gls (n = 23) BZI
SiO_2	29.6	29.1	30.4	29.4	29.7	98.6	56.4	9.1	0.39	0.78	0.45	44.93 ± 3.79	40.70 ± 2.95
TiO_2	bdl	bdl	bdl	0.07	bdl	bdl	bdl	0.29	0.85	1.08	0.49	0.60 ± 0.14	0.90 ± 0.12
Al_2O_3	0.19	0.25	0.17	0.31	0.16	bdl	23.2	2.8	47.5	10.3	0.4	15.81 ± 1.84	20.65 ± 2.41
Fe_2O_3* -	–	–	–	–	–	–	–	25.9	13.3	54.6	68.7	20.05 ± 3.07	18.94 ± 1.86
FeO	63.2	66.4	59.8	57.7	67.6	bdl	0.96	59.9	35.8	31.4	31.15	–	–
MnO	4.8	2.7	6.6	7.4	0.76	bdl	bdl	1.45	1.28	1.03	0.56	1.40 ± 0.15	0.97 ± 0.25
MgO	1.39	0.79	2.6	1.68	1.26	bdl	bdl	0.4	0.1	0.2	bdl	0.08 ± 0.06	0.09 ± 0.02
CaO	0.18	0.20	0.57	1.67	0.21	bdl	bdl	bdl	bdl	bdl	bdl	8.73 ± 2.73	5.84 ± 1.12
BaO	na	na	na	na	na	bdl	0.22	bdl	na	na	na	0.14 ± 0.10	0.27 ± 0.17
Na_2O	bdl	bdl	bdl	0.05	bdl	bdl	0.10	bdl	bdl	bdl	bdl	0.15 ± 0.12	0.32 ± 0.18
K_2O	bdl	bdl	bdl	bdl	bdl	bdl	20.1	bdl	bdl	bdl	0.05	3.91 ± 1.19	6.53 ± 2.05
P_2O_5	bdl	0.25	bdl	bdl	bdl	bdl	0.09	0.09	na	na	na	4.42 ± 1.30	5.86 ± 2.32
Cr_2O_3	bdl	bdl	bdl	bdl	bdl	bdl	bdl	bdl	0.1	0.05	bdl	bdl	bdl
V_2O_3	bdl	bdl	bdl	bdl	bdl	na	na	bdl	0.12	0.12	bdl	na	na
SO_3	bdl	bdl	bdl	bdl	bdl	bdl	bdl	na	na	na	na	bdl	0.12 ± 0.06
Total	99.36	99.69	100.14	98.28	99.69	98.6	101.07	99.93	99.44	99.56	101.80		
Atomic proportion per formula unit (a.p.f.u.)													
Si	1.00	0.98	1.01	1.00	1.00	1.00	2.02	0.87	0.01	0.03	0.02		
Ti	–	–	–	–	–	–	–	0.02	0.02	0.03	0.01		
Al	0.01	0.01	0.01	0.01	0.01	–	0.98	0.31	1.69	0.44	0.02		
Fe^{3+}	–	–	–	–	–	–	–	1.86	0.30	1.49	1.94		
Fe^{2+}	1.78	1.88	1.66	1.64	1.90	–	0.03	4.78	0.90	0.95	0.98		
Mn	0.13	0.07	0.17	0.20	0.02	–	–	0.11	0.03	0.03	0.02		
Mg	0.07	0.04	0.13	0.80	0.06	–	–	0.06	–	0.01	–		
Ca	0.01	0.01	0.02	0.60	0.01	–	–	–	–	–	–		
Ba	–	–	–	–	–	–	–	–	–	–	–		
Na	–	–	–	–	–	–	0.01	–	–	–	–		
K	–	–	–	–	–	–	0.92	–	–	–	–		
P	–	0.01	–	–	–	–	–	0.01	–	–	–	–	
Cr	–	–	–	–	–	–	–	–	–	–	–		
V	–	–	–	–	–	–	–	–	–	–	–		
S	–	–	–	–	–	–	–	–	–	–	–		
O^{2-}	4.00	4.00	4.00	4.00	4.00	2.00	6.00	10.00	4.00	4.00	4.00		

* - In the glass analyses, all iron was calculated to Fe_2O_3 as the ratio of FeO/Fe_2O_3 was not measured

ol: olivine; gls: glass; spl: spinel; isc: iscorite; lct: leucite; qz: quartz; bdl: below detection limit; na: not analyzed

Glass The glass was observed in all analyzed samples. In most cases, the glass chemistry analysis was impossible due to its small size or nuclei of crystallization within the glassy phase. EPM analyses were possible only in KG1 and BZI slags. The glass in these slags consists mainly of SiO_2 (av. 40.70 and 44.93 wt.%), Fe_2O_3 (av. 18.94 and 20.05 wt.%), and Al_2O_3 (av. 20.65 and 15.81 wt.%) in BZI and KG1 respectively Table 2). Concentrations of CaO (av. 5.84 and 8.73 wt.%), P_2O_5 (av. 5.86 and 4.42 wt.%), and K_2O (av. 6.53 and 3.91 wt.%), MnO (av. 0.97 and 1.40 wt.%) was also observed in BZI and KG1 slags respectively (Table 2).

Age

Based on the $^{12}C/^{14}C$ isotope ratio, the age of the charcoal taken from the STAR1 sample was calculated to be 2090 ± 30 BP. As a result of the calibration of the result using the IntCal20 calibration curve, the calendar age was estimated to be in the range of 196 BC–4AD (95.4% probability). With a 91.4% probability, the age of charcoal is 178–38 BC, with a median age of 102 BC with a (1-sigma) uncertainty of ± 50 BC (Additional file 2).

Smelting conditions

Temperature

Two phase diagrams that best fitted the chemistry of the samples (Table 2) were used for the slags' liquidus temperature estimations: $CaO–SiO_2–FeO$-6 wt.%Al_2O_3 (92.10–97.53 wt.% of elements included) and $FeO–SiO_2–Al_2O_3$ (89.63–97.03 wt.% of elements included). $CaO–SiO_2–FeO$-6 wt.%Al_2O_3 and $FeO–SiO_2–Al_2O_3$ show similar results with liquidus temperatures in the ranges of 1160 to 1250 °C and 1150–1200 °C respectively (Table 3; Fig. 5).

Discussion

Age

The radiocarbon dating uses $^{14}C/^{12}C$ ratios in the analyzed carbonaceous material. In the case of iron metallurgy, isotope ratios may be disturbed due to the addition of C from another source in the production process. By using siderite ores ($FeCO_3$) or fluxes in the form of calcite ($CaCO_3$), carbon with an isotopic age exceeding 10,000 years could be introduced into the metallurgical

Table 3 Summary of the conditions prevailing during the formation of the analyzed slags

	STAR1	KG1	KG2	BZI	JI
$CaO–SiO_2–FeO–6$ wt.%Al_2O_3 diagram [°C] [33]	1200–1250	~ 1160	1200–1250	~ 1160	1160–1180
$FeO–SiO_2–Al_2O_3$ diagram [°C] [35]	1150–1200	1150–1200	1150–1200	1150–1200	1150–1200
Viscosity [Pa s]	0.22–0.15 at 1150–1200 °C	1.02–0.67 at 1150–1200 °C	0.26–0.18 at 1150–1200 °C	0.71–0.32 at 1150–1200 °C	0.41–0.28 at 1150–1200 °C
RII	0.57	1.13	0.62	0.96	0.77
Oxygen fugacity (logP O_2) [atm.]	− 13.20 to − 12.53				

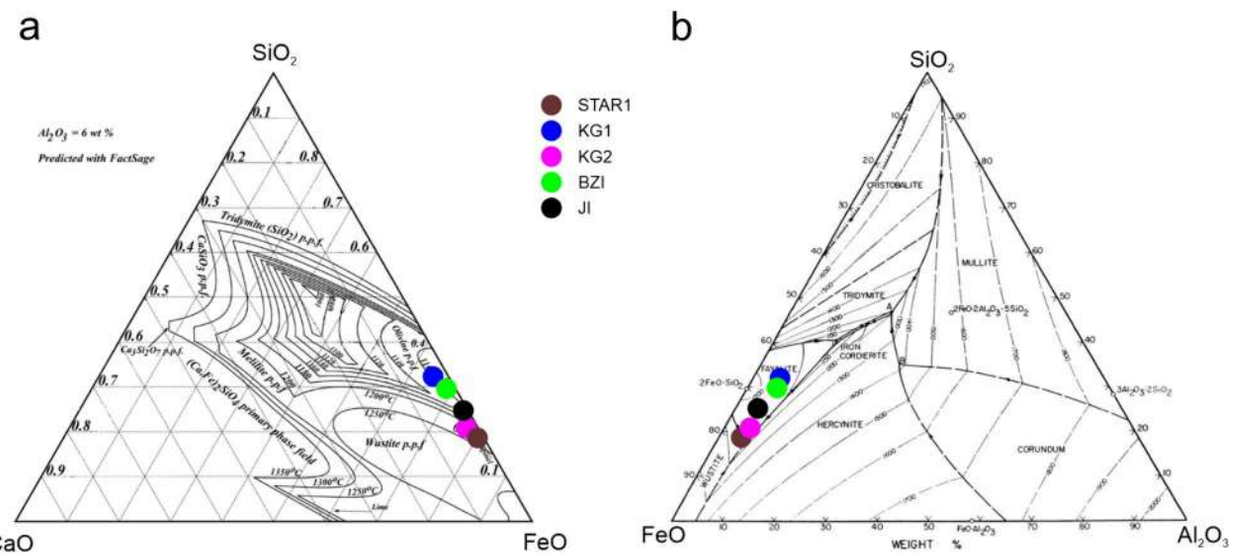

Fig. 5 Phase diagrams with the marked slags' chemical composition (**a**—[33, 34]; **b**—[35])

charge [36, 37]. However, the analyzed slags contain only up to 2.47% CaO, proving that no calcite was added as a flux. Moreover, during smelting, carbonates in the charge decompose at temperatures well below the liquidus temperature of the analyzed slags [38, 39]. Isotope analyses of charcoal are also subject to errors related to the old wood effect [36]. However, considering the large scope and extended period of operation of the Holy Cross Mountains center [21], the metallurgists of that time had to conduct appropriate forest management. In such large centers, trees up to several dozen years old were used for charcoal production, limiting the negative impact on the age determined by ^{14}C analyses [36].

The analysis of charcoal found in the slag gave the date of 196 BC–4 AD, falling within the range of isotope analyses conducted so far, i.e., 300 BC-200 AD [21]. This confirms that the analyzed slags were formed during the Roman influence period, which was characterized by increased metallurgical activity in the areas of present-day Poland [21, 40–42]. Apart from the Holy Cross Mountains, there were many smaller metallurgical centers in Poland. Isotope analyses show that iron smelting in Masovia was carried out in the period covering at least 2450–1890 BP [41], with the greatest development occurring in the first two centuries AD [40]. In Lower Silesia (Poland), the first traces of metallurgical activity date back to the third-first century BC [42]. Dating of iron objects from Nowe Brzesko (Lesser Poland Voivodeship) gave an age in the range of 217–412 AD [37].

Homogeneity of the metallurgical process

Temperature

Temperature is the most critical parameter to be determined when reconstructing historical metallurgical processes. Temperature conditions affect the oxidation–reduction conditions and the melt's viscosity [2, 44]. These three parameters, combined with ore properties, determine the smelting efficiency. The most commonly used method of determining the smelting temperature is estimating the slags' liquidus temperature [45–47]. Considering that the slags were formed from the melt, the minimum temperature at which the process was carried out could not be lower than the liquidus temperature [45]. The liquidus temperature of the analyzed slags was determined based on phase diagrams (Table 3; Fig. 5). All of the analyzed slags consist mainly of FeO and SiO_2, with a small addition of Al_2O_3. Together, these elements account for 90–97 wt.% of the sample (Table 1). In such circumstances, the phase diagram FeO-SiO_2-Al_2O_3 should provide the best temperature estimations with little error due to its excellent fit to the data.

Based on the analyses performed, it can be concluded that in all cases, the temperature during smelting, regardless of location, was similar (1150–1200 °C; Table 3). A similar temperature in the 1130–1260 °C range was determined for most (19 out of 23) of the samples from the Holy Cross Mountains analyzed by Holewinski in the 1950s [21]. The remaining samples are characterized by higher temperatures (1370–1430 °C) due to larger SiO_2 content [21], which could be caused by the contamination of samples with furnace/pit walls material, similar to sample STAR2 described in this study (Table 1; Fig. 3).

Iron production occurred in several metallurgical centers in present-day Poland during a similar period. These include, in addition to the area of the Holy Cross Mountains, centers located in Mazovia (Milanówek/Falęcin) [18], Tarchlice (Lower Silesia) [18, 43], and Opole [18], among others. The liquidus temperature of Mazovia and Tarchlice slags is similar to that of analyzed slags (1150–1200 °C; Table 4). In slags from Opole, the temperature determined for the averaged chemical composition [18] is significantly higher (1050–1400 °C; Table 4) due to the larger content of Al_2O_3 (4.20–18.70 wt.%), and SiO_2 (11.50–34.65 wt.%), which increase the liquidus temperature [35]. Again, possible contamination of slag with furnace material should be considered.

Table 4 Comparison of the properties of slags after bloomery iron production

	Age	Liquidus temperature [°C]	Viscosity [Pa s]**	logP O_2***	RII
This Study	196 BC–4 AD	1150–1200	0.15–1.02	– 13.20 to – 12.53	0.57 to 1.13
Holy Cross Mountains [21]	300BC–400AD	1130–1430	0.08–0.76	– 13.48 to – 10.03	0.67–2.05
Tarchlice[18]	Roman period	1150–1200*	0.48–1.77	– 13.20 to – 12.53	0.98–1.39
Opole [18]	2–5 century AD	1050–1400*	0.13–2.08	– 14.71 to – 10.31	av. 1.01
Mazovia (Milanówek/Falęcin) [18, 43]	Ancient period	1150–1200*	0.07–1.24	– 13.20 to – 12.53	0.72–0.81

* Determined using FeO-SiO_2-Al_2O_3 diagram

** Calculated using BBHLW model,

*** Calculated for liquidus temperatures using SLAG software

Oxidizing-reducing conditions

The oxidation–reduction conditions prevailing during smelting can be determined based on the phase composition of the slags. By observing which phases have been reduced/oxidized, we can determine the minimum and maximum conditions of oxygen fugacity [2, 44, 47, 48]. In the case of slags after bloomery iron production, we cannot rely on the presence of oxidized/metallic phases of various metals because, apart from Fe, other metals that could be reduced do not occur in sufficient quantities in these slags (Table 1; Additional file 3). Regarding phase composition, slags after iron production are similar and consist mainly of olivine with lower amounts of other phases [48–50]. Taking into account the fact that in each case, oxidized Fe (mainly as FeO) in the form of oxides or silicates is observed in the slags, as well as the fact that metallic iron was formed during smelting, the maximum value of oxygen fugacity depends on the state of equilibrium between Fe and FeO. The fugacity of oxygen (logP O_2) at which thermodynamic equilibrium occurs between metallic iron and FeO for temperatures 1150–1200 °C is from − 13.20 to − 12.53 [32]. These are the maximum values at which the reduction of iron oxides to the metallic phase is possible [32]. Since both the Fe-bearing phases (Fig. 3) and liquidus temperature (Table 3) do not differ between analyzed samples, there are no differences in the calculated oxygen fugacity between samples as well (Table 3). Due to the similar liquidus temperature, the maximum oxygen fugacity at which FeO can be reduced to metallic iron is also similar to the values for most of the slags from the Holy Cross Mountains area, Mazovia and Tarchlice (Table 4). In case of Ople location higher range of liquidus temperature of the slags results in the broader oxygen fugacity range: − 14.71 to − 10.31 (Table 4).

The reduction process is also time-dependent. Limited melting time negatively affects reduction efficiency. This dependence forces the creation of a more reducible environment during smelting than required by the thermodynamic equilibrium between the metallic and oxide phases. For this reason, the amount of metal produced depends on how far oxidation–reduction conditions deviate from the equilibrium state and move toward a more reducing environment. The more reducing environment, the amount of Fe remaining in the slag (in oxidized form) is lower. The model proposed by Charlton et al. [51] was used to estimate how strongly reducing the environment prevailed during the studied smelting process:

$$RII = \frac{2.39 * SiO_2}{FeO + MnO}$$

The Reducible Iron Index (RII) is correlated with the oxidation–reduction conditions. The higher the value, the more reductive the environment was during smelting [51]. In all cases, the RII value was 0.57–1.13 in the analyzed slags.

The most reductive conditions occurred during the formation of slag KG1 (1.13) and the least in the case of slag STAR1 (0.57) (Table 3). Comparing the results obtained for other slags from the Holy Cross Mountains [21] shows that the RII index (0.67–1.32) in most cases is similar to the data presented in this study (Table 4). Only two samples are characterized by higher values (ca. 2.0) ([21]; Table 4). The RII value given for the average chemical composition of slags from Opole and Mazovia is within the range marked for slags from the area of the Holy Cross Mountains (0.72–1.01; Table 4). The RII values of slags from Tarchlice (0.98–1.39) seem to be slightly higher; however, they are still within the range of the previously studied slags from the area of the Holy Cross Mountains (Table 4). Similar RII values suggest that similarly reducing conditions prevailed in all locations. However, it should be remembered that the RII value also depends on the metallurgical charge's chemical composition and the melt's possible contamination [51].

Viscosity

Viscosity affects the ability of metallic phases to separate from smelting by-products (e.g. slags) [2, 44, 47]. The presented study determined the melt viscosity using the BBHLW model (named after Browning, Bryant, Hurst, Lucas, and Wall) [52]. This model was designed based on coal ash, smelting, and synthetic slags covering materials with a broad chemical composition (including 18.5–70.0 wt.% of SiO_2, 0–80.0 wt.% of FeO) [53]. Since a high FeO content characterized the analyzed slags, the BBHLW model seems the most appropriate. Viscosity in the range of liquidus temperatures of slags was 0.15–1.02 Pa s (at 1150–1200 °C; Table 3; Fig. 6).

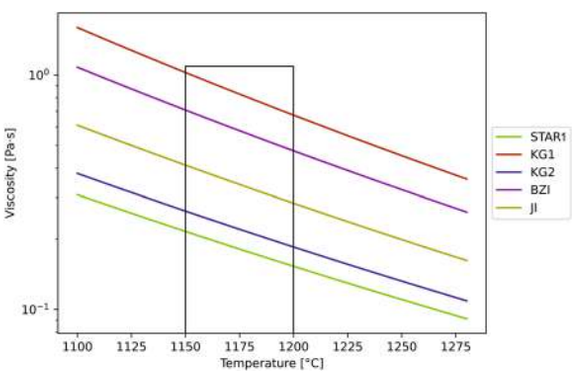

Fig. 6 Viscosity graph obtained from BBHLW model for analyzed slags with liquidus temperature ranges marked

The viscosity of the analyzed slags is similar to the viscosity calculated for the slags from other Holy Cross Mountains locations (0.08–0.76 Pa s) and Mazovia (0.07–1.24 Pa s) (Table 4). Slags from Tarchlice have slightly higher viscosity (0.48–1.77 Pa s; Table 4). Slags from Opole are characterized by a wider viscosity range than others. This is due to the broader temperature range in which the calculations were made (1050–1400 °C). At the lowest temperatures, the viscosity was significantly higher than in the other locations (2.08 Pa s). In addition, a relatively large amount of Al_2O_3 in these slags also affects the viscosity results [18].

Cooling rate

The morphology of olivine crystal can be used to determine the cooling rate of the silicate melt, which is the slag precursor [44, 54]. In the KG1-2, STAR1-2, and JI slags, tabular olivine crystals (Fig. 4d) corresponding to granular olivine described by Donaldson [54] were observed. These are formed at a low 5 °C/h temperature gradient [54]. Elongated olivine crystals were observed in the STAR1-2, JI, and BZI slags (Fig. 4f,h), resembling chain and lattice olivine that crystallize at temperature gradients reaching 80 and 300 °C/h, respectively [54]. The difference in olivine morphologies in STAR1-2 and JI slags indicates the variety of temperature gradients during slag melt cooling. No fiber olivine was distinguished, indicating that the cooling rate never reached 1450 °C/h [54]. Similar variation in olivine crystal habit was described at other locations where bloomery iron production was carried out [55–57].

During the production of iron in the Holy Cross Mountains, the slag flowed down to the bottom of the furnace, from where it was not removed [21]. This procedure allowed for slow cooling of the slag melt, especially considering the volume and mass of the singular slag portions found in the Holy Cross Mountains, reaching up to 120 kg [25]. Still, the slag melt on contact with the pit walls was subjected to faster cooling, hence the varied morphology of olivine crystals (Fig. 4).

Conclusions

The obtained data proves that the conditions under which the smelting process was carried out in varied locations across the Holy Cross Mountains were uniform. Slags were formed at 1150–1200 °C with logP O_2 from − 13.20 to − 12.53. Melt viscosity is comparable in all samples (0.15–1.02 Pa s). The lack of differences between the slags was also noticeable in the cooling rate. The slag crystallized at a rate of 5 to 300 °C/h. The ancient (196 BC—4AD) origin of the slags was confirmed based on the $^{12}C/^{14}C$ isotope ratios of the charcoal found in the STAR1 slag.

Similarities between metallurgy in the Holy Cross Mountains and other ancient bloomery iron production centers in Poland are evident. Liquidus temperature, oxygen fugacity, and viscosity are consistent with data calculated for other Holy Cross Mountains, Mazovia, and Tarchalice locations. One of the ancient metallurgical locations considered in the publication (Opole) could be using slightly different conditions during smelting. Still, considering the high Al_2O_3 content in the slags from Opole, it is likely that the differences in liquidus temperature, oxygen fugacity, and viscosity result from contamination of the slag with the material building the walls of the furnace/pit.

Supplementary Information

The online version contains supplementary material available at https:// doi.org/10.1186/s40494-024-01266-6.

Additional file 1. Detection limits and EPMA measurement conditions.

Additional file 2. Details (standards used) regarding slag chemical composition measurements and EPMA analyses and the result of radioisotope dating.

Additional file 3. Chemical composition of slags including trace elements and quality assurance/quality control (QA/QC).

Acknowledgements

This study was supported by the National Science Center (NCN) Grant No. 2019/35/O/ST10/00313. We would like to thank the Museum of Nature and Technology in Starachowice for providing material for the study.

Data citation

No dataset from external repositories was used in this study. All existing data used for this publication are cited in the reference section.

Author contributions

Conceptualization: K.K., R.W., and A.G.; methodology: K.K., R.W., A.G.; Writing—original draft preparation: K.K.; writing—review and editing: K.K., R.W., and A.G.; resources: K.K., R.W., and J.J.; figures, tables, and additional files: K.K. and R.W. All authors read and approved the manuscript.

Funding

This research was funded by the National Science Center (NCN) Grant No. 2019/35/O/ST10/00313.

Data availability

The data that supports the finding of the study is given in the tables and figures within the main text and in additional files. This study brought together existing data from several different sources, which are cited throughout.

Declarations

Competing interests

The authors declare no competing interests.

Received: 5 January 2024 Accepted: 29 April 2024
Published online: 08 May 2024

References

1. Mikoda B, Kucha H, Potysz A, Kmiecik E. Metallurgical slags from Cu production and Pb recovery in Poland—their environmental stability and

resource potential. Appl Geochem. 2018;98:459–72. https://doi.org/10.1016/j.apgeochem.2018.09.009.
2. Kupczak K, Warchulski R, Gawęda A. Reconstruction of smelting conditions during 16th-to 18th-century copper ore processing in the Kielce region (Old Polish Industrial District) based on slags from Miedziana Góra, Poland. Archaeometry. 2023;65:547–69. https://doi.org/10.1111/arcm.12837.
3. Bebermeier W, Brumlich M, Cordani V, de Vincenzo S, Eilbracht H, Klinger J, et al. The coming of iron in a comparative perspective. J Anc Stud. 2016;6:152–89.
4. Hendrickson M, Leroy S, Hua Q, Kaseka P, Vuthy V. Smelting in the shadow of the iron mountain: preliminary field investigation of the industrial landscape around Phnom Dek, Cambodia (ninth to twentieth centuries AD). Asian Perspect. 2017;56:55–91.
5. Hendrickson M, Leroy S, Castillo C, Hua Q, Vega E, Phon K. Forging empire: angkorian iron smelting, community and ritual practice at Tonle Bak. Antiquity. 2019;93:1586–606.
6. Plaza MT, Garrido F, Larreina-García D. A new piece of the puzzle: slag and ore analysis to reconstruct the prehispanic smelting technology at the Atacama Desert, Chile. Herit Sci. 2023;11:171. https://doi.org/10.1186/s40494- 023- 01017-z.
7. Westner KJ, Klein S, Sergeev D, Müller M. Temperature estimates of historical Pb–Ag smelting slags: a multi-methodological approach. J Archaeol Sci Rep. 2022;46:103654. https://doi.org/10.1016/j.jasrep.2022.103654.
8. Stepanov I, Borodianskiy K, Eliyahu-Behar A. Assessing the quality of iron ores for bloomery smelting: laboratory experiments. Minerals. 2019;10:33.
9. Whiteman J, Okafor EE. Characterization of Nigerian bloomery iron smelting slags. Hist Metall. 2003;37:71–84.
10. Metz O, Bohr R. Theoretical and practical aspects of iron smelting in a bloomery furnace. Mining archaeology: perspectives, conflicts, challenges. In: Proceedings of the 10th International Symposium on Archaeological Mining History Yearbook of the Institute Europa Subterranea Institute Europa Subterranea. 2015. p. 8–21.
11. Li S, Li Y, Zhu R, Wang H. Analysis on ancient bloomery ironmaking technology: the earliest ironmaking evidence in the central plains of China was taken as the research object. Metals. 2022;12:1307.
12. Zou G, Min R, Cui J, Ma R, Zhou X, Yang C. The special iron making in Southwest China around the 10th CE: Scientific evidence from an iron smelting site in Erhai lake area, Yunnan province. J Cult Herit. 2019;37:266–72.
13. Stepanov IS, Sauder L, Keen J, Workman V, Eliyahu-Behar A. By the hand of the smelter: tracing the impact of decision-making in bloomery iron smelting. Archaeol Anthropol Sci. 2022;14:80.
14. Pernet-Fisher JF, Day JMD, Howarth GH, Ryabov VV, Taylor LA. Atmospheric outgassing and native-iron formation during carbonaceous sediment–basalt melt interactions. Earth Planet Sci Lett. 2017;460:201–12. https://doi.org/10.1016/j.epsl.2016.12.022.
15. Goldstein JI, Scott ERD, Chabot NL. Iron meteorites: crystallization, thermal history, parent bodies, and origin. Geochemistry. 2009;69:293–325. https://doi.org/10.1016/j.chemer.2009.01.002.
16. Peacock CL, Lalonde SV, Konhauser KO. Iron minerals as archives of Earth's redox and biogeochemical evolution. In: Ahmed IAM, Hudson-Edwards KA, editors. Redox-reactive minerals: properties, reactions and applications in clean technologies, vol. 17. Strasbourg: European Mineralogical Union; 2017. p. 113–63.
17. Johnson D, Tyldesley J, Lowe T, Withers PJ, Grady MM. Analysis of a prehistoric Egyptian iron bead with implications for the use and perception of meteorite iron in ancient Egypt. Meteorit Planet Sci. 2013;48:997–1006. https://doi.org/10.1111/maps.12120.
18. Thelemann M, Bebermeier W, Hoelzmann P, Lehnhardt E. Bog iron ore as a resource for prehistoric iron production in Central Europe—a case study of the Widawa catchment area in eastern Silesia, Poland. Catena. 2017;149:474–90. https://doi.org/10.1016/j.catena.2016.04.002.
19. Orzechowski S. Socioeconomic determinants of iron production on Polish lands during antiquity: the phenomenon of metallurgical smelting centres of the Przeworsk culture. Archeologické Rozhledy. 2018;70:391–403.
20. Samsonowicz A, Wyczański A, Tazbir J, Staszewski J, Kizwalter T, Nałęcz T, Paczkowski A, Chwalba A. History of Poland. Poland until 1586. Warszawa: Wydawnictwo Naukowe PWN; 2007. p. 623.
21. Bielenin K. Ancient mining and iron smelting in the Holy Cross Mountains. 2nd ed. Kielce: Kieleckie Towarzystwo Naukowe, Towarzystwo Przyjaciół Górnictwa, Hutnictwa i Przemysłu Staropolskiego w Kielcach; 1992. p. 1–267.
22. Janiec J, Kardyś P. Raw material base of ancient metallurgy in the in the Holy Cross Mountains region—an attempt at a different perspective. Świętokrzyskie—Environment, Cultural Heritage, Regional Education. WBP Kielce. 2021;27:173–82.
23. Orzechowski S. Experimental research on the reconstruction of the smoke-making process in the Holy Cross Mountains—scientific and educational significance of the experiment. Skanseny Archeologiczne I Archeologia Eksperymentalna. 2012. p. 307–29.
24. Wrona A. The production of high carbon steel directly in bloomery process: theoretical bases and metallographic analyses of the experiments results. EXARC J. 2013;2:1–16.
25. Orzechowski S. Settlement base and raw material bases of ancient metallurgy in the in the Holy Cross Mountains region. Kieleckie Towarzystwo Naukowe; 2007. p. 1–391
26. Geoportal. https://www.geoportal.gov.pl. Accessed 20 Dec 2023.
27. Heliasz Z, Ostaficzuk S. Historical residues of iron ore mining in environs of the Holy Cross Mountains (the Góry Świętokrzyskie) are recognizable on the Digital Terrain Elevation Model (DEM) derived from the LIDAR data. Gospodarka Surowcami Mineralnymi. 2020;36:161–86. https://doi.org/10.24425/gsm.2020.133946.
28. Samsonowicz J. About the hematite deposit in Rudki near Nowa Słupia. In: Meeting of the Polish Geological Society on November 21; 1922;4:9–10.
29. Fawcett TG, Faber J, Kabbekodu S, McClune F, Rafaja D. 4+, the material identification database. Microstruct Anal Mater Sci. 2005;1–3.
30. Ramsey CB. Bayesian analysis of radiocarbon dates. Radiocarbon. 2009;51:337–60. https://doi.org/10.1017/S0033822200033865.
31. Reimer PJ, Austin WE, Bard E, Bayliss A, Blackwell PG, Ramsey CB, et al. The IntCal20 Northern Hemisphere radiocarbon age calibration curve (0–55 cal kBP). Radiocarbon. 2020;62:725–57. https://doi.org/10.1017/RDC.2020.41.
32. Kupczak K, Warchulski R. SLAG—software for reconstruction of historical smelting processes based on slag properties. Archaeometry. 2024. https://doi.org/10.1111/arcm.12940.
33. Jak E, Hayes P, Pelton A, Decterov S. Thermodynamic modelling of the Al_2O_3–CaO–FeO–Fe_2O_3–PbO–SiO_2–ZnO system with addition of K and Na with metallurgical applications. In Proc VIII Int'l Conf on Molten Slags, Fluxes and Salts; Santiago, Chile. 2009. p. 473–90.
34. Gheribi AE, Audet C, Le Digabel S, Bélisle E, Bale CW, Pelton AD. Calculating optimal conditions for alloy and process design using thermodynamic and property databases, the FactSage software and the Mesh Adaptive Direct Search algorithm. Calphad. 2012;36:135–43.
35. Li Y, Zhang M, Li S, Yang F. Evidence of early iron smelting on the Tibetan plateau. Archaeol Anthropol Sci. 2022;14:52. https://doi.org/10.1007/s12520- 022- 01528-z.
36. Craddock PT, Wayman ML, Jull AJT. The radiocarbon dating and authentication of iron artifacts. Radiocarbon. 2002;44:717–32. https://doi.org/10.1017/ S0033 82220 00321 73.
37. Hüls CM, Bulas J, Kasiński M, Okońska-Bulas M. First results of metallographic analysis and absolute dating of iron finds from Nowe Brzesko, site 26, Proszowice District. Archaeometry. 2023;65:587–602. https://doi.org/10.1111/arcm.12858.
38. El-Bellihi AA. Kinetics of thermal decomposition of iron carbonate. Egypt J Chem. 2010;53:871–84. https://doi.org/10.21608/EJCHEM.2010.1268.
39. Karunadasa KS, Manoratne CH, Pitawala H, Rajapakse RMG. Thermal decomposition of calcium carbonate (calcite polymorph) as examined by in-situ high-temperature X-ray powder diffraction. J Phys Chem Solids. 2019;134:21–8. https://doi.org/10.1016/j.jpcs.2019.05.023.
40. Woyda S. The Błońska Plain at the end of ancient times. Metallurgical center. Problems of the past of Mazovia and Podlasie. 2004. p. 129–66.
41. Janiszewski R. Before or after? Stratigraphic relations of Iron Age slag-pit furnaces in the Mazovian Centre of Metallurgy. Archeologické Rozhledy. 2018;70:381–90.
42. Wrona P, Różański Z, Pach G, Niewiadomski AP, Veiga JP. Historical outline of iron mining and production in the area of present-day Poland. Minerals. 2021;11:1136. https://doi.org/10.3390/min11101136.

43. Woźniak M. Milanówek/Falęcin–a settlement of iron-smelters from the Late Antiquity. Archeologické Rozhledy. 2018;70:363–80.
44. Warchulski R, Szczuka M, Kupczak K. Reconstruction of 16th—17th century lead smelting processes on the basis of slag properties: a case study from Sławków, Poland. Minerals. 2020;10:1039. https://doi.org/10.3390/min10 111039.
45. Kądziołka K, Pietranik A, Kierczak J, Potysz A, Stolarczyk T. Towards better reconstruction of smelting temperatures: methodological review and the case of historical K-rich Cu-slags from the Old Copper Basin, Poland. J Archaeol Sci. 2020;118:105142. https://doi.org/10.1016/j.jas.2020.105142.
46. Derkowska K, Świerk M, Nowak K. Reconstruction of copper smelting technology based on 18–20th-century slag remains from the Old Copper Basin, Poland. Minerals. 2021;11:926. https://doi.org/10.3390/min11090926.
47. Warchulski R, Kupczak K, Gawęda A, Sitko R. Complete reconstruction of the process and conditions during gold smelting in the 15–17th century in Złoty Stok based on metallurgical slags. Archaeometry. 2022;64:916–634. https://doi.org/10.1111/arcm.12752.
48. Crabb S. How did the iron industry in Southern Britain change from the Iron Age to the Roman period? [PhD Thesis]. University of Oxford; 2018. p. 1–376.
49. Kramar S, Lux J, Pristacz H, Mirtič B, Rogan-Šmuc N. Mineralogical and geochemical characterization of Roman slag from the archaeological site near Mosnje (Slovenia). Mater Technol. 2015;49:343–8. https://doi.org/10.17222/mit.2013.299.
50. Nakanishi A. Mössbauer study of ancient iron smelting slag in Japan. Hyperfine Interact. 2008;186:135–9. https://doi.org/10.1007/s10751- 008- 9843-1.
51. Charlton MF, Crew P, Rehren T, Shennan SJ. Explaining the evolution of ironmaking recipes—an example from northwest Wales. J Anthropol Archaeol. 2010;29:352–67. https://doi.org/10.1016/j.jaa.2010.05.001.
52. Browning GJ, Bryant GW, Hurst HJ, Lucas JA, Wall TF. An empirical method for the prediction of coal ash slag viscosity. Energy Fuels. 2003;17:731–7. https://doi.org/10.1021/ef020165o.
53. Bronsch A. Viscosity of slags [PhD Thesis]. Dissertation, Freiberg, Technische Universität Bergakademie Freiberg, 2017. p. 1–238.
54. Donaldson CH. An experimental investigation of olivine morphology. Contrib Mineral Petrol. 1976;57:187–213. https://doi.org/10.1007/BF00405225.
55. Portillo-Blanco H, Zuluaga MC, Ortega LA, Alonso-Olazabal A, Cepeda-Ocampo JJ, Martínez SA. Mineralogical characterization of slags from the Oiola Site (Biscay, Spain) to assess the development in bloomery iron smelting technology from the Roman Period to the Middle Ages. Minerals. 2020;10:321. https://doi.org/10.3390/min10040321.
56. Larreina-Garcia D, Li Y, Liu Y, Martinon-Torres M. Bloomery iron smelting in the Daye County (Hubei): technological traditions in Qing China. Archaeol Res Asia. 2018;16:148–65. https://doi.org/10.1016/j.ara.2018.10.001.
57. Portillo H, Zuluaga MC, Ortega LA, Alonso-Olazabal A, Murelaga X, Martinez-Salcedo A. XRD, SEM/EDX and micro-Raman spectroscopy for mineralogical and chemical characterization of iron slags from the Roman archaeological site of Forua (Biscay, North Spain). Microchem J. 2018;138:246–54. https://doi.org/10.1016/j.microc.2018.01.020.

Publisher's Note

Heritage Science

RESEARCH

Open Access

The use of predominance area diagrams (PAD) to determine the oxygen and sulfur fugacities prevailing during historical metallurgical processes: the case of fifteenth to seventeenth century copper slags from Polichno (Old Polish industrial district)

Krzysztof Kupczak[1*], Rafał Warchulski[1], Aleksandra Gawęda[1], Marta Ślęzak[2] and Piotr Migas[2]

Abstract

The study presents the first use of predominance area diagrams (PADs) to determine oxidation–reduction conditions during reconstructing historical copper smelting processes. The smelting temperature and oxygen and sulfur fugacities during smelting were determined based on experiments and the geochemical (ICP-MS/ES, XRF) and mineralogical (SEM, EPMA) analyses of the fifteenth to seventeenth century slags from Polichno (Holy Cross Mountains, Poland). Results obtained during high-temperature experiments allowed to determine the slags' solidus and liquidus temperatures. The liquidus temperature was in the range of 1100–1200 °C, and the solidus temperature was in the range of 800–1100 °C. Data on temperature conditions were used in thermodynamic calculations to construct predominance area diagrams and then to determine the ranges of oxygen and sulfur fugacities in which the formation of slags was possible. Slags from Polichno were formed with the oxygen fugacity in the range of $\log P_{O_2} = -4.30$ (POL1, POL4 at 1200 °C) to − 14.08 atm. (POL3 at 1090 °C). In turn, the sulfur fugacity during slag formation ranged from $\log P_{S_2} = -2.50$ (POL5 at 1200 °C) to − 6.92 (POL4 at 1060 °C) atm. The relatively high sulfur availability confirms using sulfide ores without prior roasting. The wide range of sulfur and oxygen fugacity indicates the process's heterogeneity.

Keywords Slags, Predominance area diagrams, Process reconstruction, Smelting, Temperature

Introduction

Smelting slags are materials from which a lot of information can be obtained about historical metal production processes. Based on the chemical and phase compositions, it is possible to determine the slags' liquidus (complete melting of the material) and solidus (the beginning of the melting process) temperatures, the viscosity of the metallurgical melt, the batch composition, the oxidation–reduction conditions under which the smelting took place, and to decipher the reactions occurring during the process [1–10]. Temperature is the crucial factor

*Correspondence:
Krzysztof Kupczak
krzysztof.kupczak@us.edu.pl
[1] Institute of Earth Sciences, Faculty of Natural Sciences, University of Silesia in Katowice, Będzińska 60, 41-200 Sosnowiec, Poland
[2] Department of Metal Forming and Metallurgical Engineering, Faculty of Metals Engineering and Industrial Computer Science, AGH University of Krakow, Mickiewicza 30, 30-059 Cracow, Poland

enabling smelting, and so far, the best-described methods are those dedicated to temperature condition reconstructions. Phase diagrams, computer software, geothermometers, and high-temperature experiments allow determining both the liquidus and solidus temperatures of slags [5, 9, 11]. As both viscosity and oxidation–reduction conditions are temperature dependent, they cannot be accurately determined without the smelting temperature estimation [1, 4, 9, 10, 12].

Oxygen fugacity is one of the factors that should be considered in the reconstruction of metallurgical processes [1, 3, 10, 13, 14]. Knowledge about the fugacity of oxygen and sulfur allows to obtain a broad spectrum of information about the technological process and, indirectly, the society conducting it. The high fugacity of sulfur indicates the use of sulfide ores in the process or their addition, with the simultaneous lack of initial ore roasting. On the contrary, the low fugacity of sulfur indicates the use of oxide ores or preliminary roasting of sulfide ores. Combined with geological data from the area, this allows to drawn conclusions about the type of the ores used in the process and even the advancement of mining in the area. Commonly, in the case of sulfide ores, primary mineralization occurs deeper; thus, their exploitation may require an advanced process of excavation drainage, while oxide ores formed as a result of weathering of primary mineralization are closer to the surface [15]. The latter can often be exploited using the most straightforward techniques [16]. Naturally, the high fugacity of oxygen recorded in the slag indicates oxidizing conditions during the process, and low fugacity indicates reducing conditions. A significant variation in the fugacity of oxygen and sulfur within one sample may indicate a low homogeneity of the metallurgical process and its primitiveness [3, 10, 17, 18]. On the other hand, a considerable variation of oxygen and sulfur between different samples from the same location indicates a multistage metallurgical process [9, 19, 20].

Oxygen fugacity prevailing during historical metallurgical processes is most often determined by Fe buffers, which various authors have proposed [21, 22]. However, these methods have some limitations because they only consider the degree of iron oxidation in the analyzed slags [3, 9, 10, 17]. Although the redox conditions estimated with only the Fe buffers are generally correct, the oxygen fugacity prevailing during smelting can be determined more precisely by combining a few other elements occurring in slags. The widest possibilities in this field are provided by slags formed during the processing of nonferrous metal ores, especially polymetallic ores.

This study aims to present a new method for determining the fugacity of oxygen and sulfur during historical metallurgical processes based on predominance area diagrams (PAD). This method allowed determining the fugacity of oxygen and sulfur with much greater precision by considering the O_2 and S_2 fugacity-dependent phase reactions of many elements occurring in the slags. The additional goal was to combine obtained data with a wide range of experimental, geochemical, mineralogical, and petrographic methods to recreate the smelting conditions in the fifteenth to seventeenth century metallurgical processes in Polichno (Old Polish Industrial District, Holy Cross Mountains).

Location and historical/geological background

Polichno (Fig. 1) is a small village (less than 1000 inhabitants) located in the commune of Chęciny in the Świętokrzyskie voivodeship [23]. In Polichno, smelting activities processed the local copper ores since the fifteenth century [24]. The end of metallurgical production most likely came with the crisis of the Chęciny mining industry in the seventeenth century. From the eighteenth century, the resumption of metallurgical activities occurred in other locations in the Kielce region (e.g., Kielce, Wola Murowana) [24]. Historical sources do not contain data on smelting conditions. For this reason, provided information concerning the practical aspects of smelting is based on historical sources from that period [16]. In the vicinity of the analyzed area, copper (e.g., Miedzianka) and lead (e.g., Ołowianka; Fig. 1) deposits occur, and for this reason, the production in Polichno may have involved both metals [24]. Despite the type of metal produced, the first stage of the production process involved the crushing and enrichment of ores. The presence of a river near the smelter made it possible to use water power for this purpose. The ores were then sorted and smelted [16, 24]. At that time, during the lead production processes, the ores were roasted (oxidizing conditions) and then smelted with the addition of charcoal and fluxes (reducing conditions). During smelting, the lead flowed into the settler, from which it was then collected [10, 16, 24]. The production of copper from sulfide ores was carried out in two steps. In the first stage, speiss/matte was produced by heating the ore with charcoal with the addition of fluxes (reducing conditions). The speiss/matte was heated again (matte converting) with air blowing (oxidizing conditions). Additives (usually SiO_2) were added in this step to bond iron and other impurities within the slag melt, which was successively removed from the furnace. In this way, the semi-finished product was cleaned of Fe. The process was sustained until the sulfur/arsenic remaining in the furnace was oxidized and removed in gaseous form, leaving only the metallic copper [12, 25].

Considering that the Miedzianka deposit (Fig. 1) is the largest one exploited in the Polichno area, the

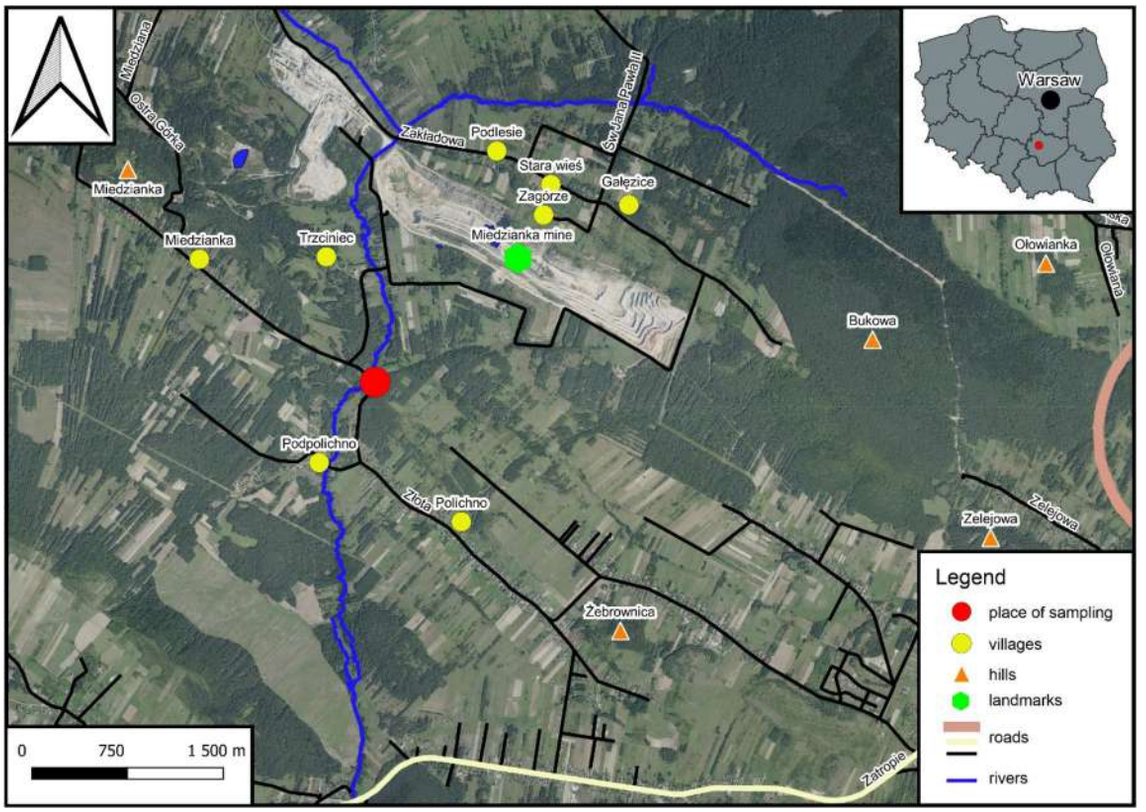

Fig. 1 Location map of the sampling site (made based on data from geoportal.gov.pl [26])

production was likely mainly based on it. Its exploitation since the fifteenth century is confirmed by mentions in a chronicle written by Jan Długosz in 1455–1480 [27]. The ore mineralization within the Miedzianka deposit is located in the southwestern part of the Holy Cross Mountains. Copper occurs both in the form of primary (sulfides, sulfosalts) and secondary mineralization (e.g., sulfides and carbonates) [28, 29]. Primary mineralization is associated with hydrothermal veins within carbonate rocks. The ore minerals mainly include tennantite ($(Cu,Fe)_{12}As_4S_{13}$), chalcopyrite ($CuFeS_2$), gersdorffite (NiAsS), bornite (Cu_5FeS_4), galena (PbS), and sphalerite (ZnS) [29]. The progressive weathering of carbonate rocks that host the primary minerals has resulted in forming zones enriched in secondary mineralization that mainly include chalcocite (Cu_2S), digenite (Cu_9S_5), covellite (CuS), bornite, malachite ($Cu_2(CO_3)(OH)_2$), azurite ($Cu_3(CO_3)_2(OH)_2$), chrysocolla ($((Cu,Al)_2H_2Si_2O_5(OH)_4{\cdot}n(H_2O))$ [29]. Secondary mineralization occurs mainly within clays filling cracks in karsts [29]. In addition to copper and lead minerals, the presence of barite ($BaSO_4$) and hematite (Fe_2O_3) was observed in the Miedzianka [30].

Materials and methods

Sampling

Samples for analysis were collected in the Polichno village, on the road leading from Polichno to Miedzianka (Fig. 1). The slag dump was located in historical times. However, it was destroyed during the construction of the road [31], and now slags can only be found in scattered form in the soil profile. During the fieldwork, 48 slag samples ranging in size from 1 to 10 cm were collected from the soil profile 20 to 150 cm below the ground surface. Slag samples collected were divided into five main slag types (POL1–POL5; Fig. 2). The main criteria for the division were the macroscopic differences between the slags (color, crystallinity/glassiness of the samples). The slags were also divided according to the degree of weathering processes occurring on the samples and the homogeneity/heterogeneity of the slags. Representative material from each type of slag was taken for further analysis.

Chemical and phase analyzes

The collected slags were first subjected to microscopic observations. Several samples were made from each type

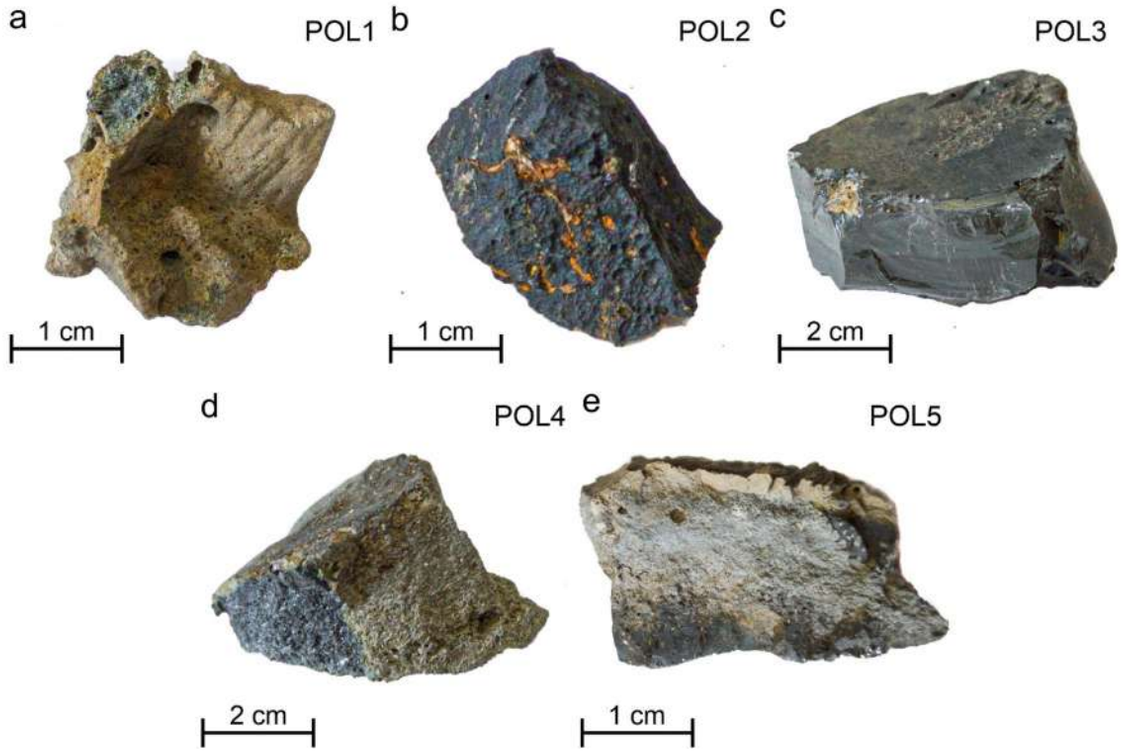

Fig. 2 Macroscopic photos of slags collected during fieldwork in Polichno

of slag for microscopic examination. An Olympus BX-51 polarizing microscope and a scanning electron microscope equipped with an energy dispersive spectrometer (SEM–EDS; Phenom XL) were used for this purpose (Institute of Earth Sciences, University of Silesia). Based on these observations, the slag texture was determined. EPMA (electron micro-probe microanalyzer) was used to determine the exact chemical composition of the phases present in the slags. A CAMECA SX100 electron microprobe (Inter-Institutional Laboratory of Microanalysis of Minerals and Synthetic Materials, University of Warsaw) was used for this purpose. The following standards were used during the EPM analyzes: Na—albite ($NaAlSi_3O_8$); Mg, Si, Ca—diopside ($[Ca,Mg,Fe]_2SiO_3$); Al, K—orthoclase ($KAlSi_3O_8$); Ba—barite ($BaSO_4$); Ti—rutile (TiO_2); Pb—crocoite ($PbCrO_4$); Fe—Fe_2O_3, chalcopyrite ($CuFeS_2$); Mn—rhodonite ($CaMn_3Mn[Si_5O_{15}]$); Zn—sphalerite (ZnS); P—YPO_4, $LaPO_4$; As—GaAs; Co—CoO; Ni—NiO; Cu—cuprite (Cu_2O); S—chalcopyrite ($CuFeS_2$), barite ($BaSO_4$); Sb—stibnite (Sb_2S_3). The slags were also analyzed for chemical composition using the combination of X-ray fluorescence (XRF) on fused discs and inductively coupled plasma emission/mass spectrometry (ICP-ES/ICP-MS). Samples representative of each type of slag were selected for bulk chemical composition analyses. The concentrations of P_2O_5, SiO_2 TiO_2, Al_2O_3, Fe_2O_3, MnO, CaO, MgO, Na_2O, K2O, SO_3, Ba, and LOI were determined by XRF. Concentrations of Cu, Pb, Zn, Ni, As, Sr, and Sb by ICP methods. During the ICP analyzes, multi-acid digestion was used. XRF and ICP-MS/ES analyses were performed by Bureau Veritas Mineral Laboratories (Canada). Loss of ignition was determined at 1000 °C.

High-temperature experiments

Slag samples were subjected to two high-temperature experiments to determine the slags' liquidus and solidus temperatures. In the first one, slag samples were grounded, formed into a cone with a diameter and height of 3 mm, and placed on a corundum plate. Then the plate was placed in the tube furnace and heated until the slag was completely liquefied with a temperature gradient of 70 °C/min to 900 °C, then 30 °C/min to 1100 °C/min, and 10 °C/min to 1350 °C. During heating, samples were observed using a high-temperature microscope (Leitz; Hesse Instruments; Faculty of Metals Engineering and Industrial Computer Science, Department of Metal Forming and Metallurgical Engineering, AGH University of Krakow; Cracow). During the observations, attention was paid to the first changes on the surface of the samples, indicating the start of melting (solidus temperature). Subsequently, the sphere, hemisphere, and flow

temperatures were distinguished. From the point of view of the conducted research, the most important is the flow temperature, which corresponds to the liquidus temperature. Flow temperature was determined when the height of the sample equaled 1/3 of the height of the sample at the hemisphere temperature [32].

Experimental smelting in a laboratory furnace was used as a second experimental method of slags' solidus and liquidus determinations. Two types of slags were selected for the experiment (POL2 and POL4), representing the two most diverse slags. The POL2 sample is the most common glassy type, and POL4 is the most commonly observed hypocrystalline slag. Slag fragments were then divided into several subsamples by crushing and cutting into fragments (about 1 cm^3). During the experiment, the samples were heated in crucibles for 3 h to a certain temperature (800 °C, 1000 °C, 1100 °C, 1150 °C, and 1200 °C). After reaching a certain temperature, the samples were kept at this temperature for 2 h. After this time, the samples were cooled with the temperature gradient of the furnace to ambient temperature. Each time after the experiment, the samples were removed from the furnace for examination, and a new subsample was taken for the next experiment. Experiments were performed at the high-temperature experiments laboratory at the Institute of Earth Sciences of the University of Silesia in the chamber furnace PLF 160/5 with a PC 442/18 controller, SiC heaters, and Thermocouple S with a maximum working temperature of 1550 °C.

Thermodynamic calculations

To determine the oxygen and sulfur fugacities, thermodynamic data [33] were used to construct predominance area diagrams (PADs) that accounted for the phase transitions between the most common phases observed in slags (metallic, oxides, and sulfides). The diagrams were created based on the method described by Barin [33] for the liquidus and solidus temperatures of the analyzed slags.

Results

Slags overview

In the samples from Polichno, hypocrystalline (POL1, POL4-5) and glassy slags (POL2-3) were distinguished (Fig. 2). Hypocrystalline samples had a gray color with pores up to 10 mm in diameter. The hypocrystalline slags' surface was characterized by a lighter color (layer up to 2 mm thick) compared to a darker color inside the slags (Fig. 2a, d). A lighter color was also observed around the pores. The color change suggests the progressive weathering of the slags. Glassy slags were most commonly black (POL2; Fig. 2b) or greenish (POL3; Fig. 2c) in color with small (about 1 mm) orange-colored layers (in POL2). This type of slag had a glassy luster in the cross-section and a dull luster on the surface (Fig. 2b, c), which resulted from the weathering process. Scattered quartz/cristobalite (SiO_2) crystals were observed within them during macroscopic observations. SiO_2 crystals were mainly in the form of small (less than 1 mm in diameter) crystals.

In POL1 slags, surface changes due to weathering are more evident than in other hypocrystalline samples (Fig. 2). Secondary crystallization in the form of a green surface (most likely malachite) is often observed on the surface of the samples. In the unaltered by weathering part of the slags, crystallization is visible in the form of very fine, barely visible phases. Microscopic observations of POL1 slags revealed the presence of phases from the wollastonite group ($CaSiO_3$; Fig. 3a; Table 1). Occasionally, calcite ($CaCO_3$) and single quartz/cristobalite crystals were also observed (Table 1). The presence of sulfides (mainly in the form of chalcocite), arsenides, and metallic Cu was also found (Table 1). Arsenides (domeykite (Cu_3As) and CuFeAs) were slightly less common than sulfides. Sulfide and arsenide phases most often co-occur as oval phases (up to 30 μm). Still, larger aggregations were also observed (Fig. 3a). Metallic copper was found only in areas with higher Cu sulfide/arsenide concentrations (Fig. 3a; Table 1).

During microscopic observations, it was confirmed that POL2 slags were mainly composed of glassy phases. PbO-enriched glasses were observed among other glassy phases as bright (in BSE imaging) domains (Fig. 3b). Crystals of quartz/cristobalite, pyroxene (usually up to several μm in length), and oval phases (up to 50 μm in diameter) containing mainly litharge and sometimes galena (up to 20 μm in diameter) were scattered within the glass (Fig. 3b; Table 1). Occasionally the oval metallic phases composed of metallic Cu and Pb (up to 15 μm in diameter) were observed (Table 1). Barite and cerussite ($PbCO_3$) were also found within these slags (Table 1), mainly in the form of aggregates up to 100 μm in length.

In POL3 slags, only dispersed metallic phases and pyroxene were observed within the glass. Metallic phases were mainly composed of metallic Cu and Fe (Fig. 3c; Table 1). Sometimes, metallic Cu coexisted with copper sulfides and arsenides. The diameter of metallic phases reached up to 600 μm (Fig. 3c). While metallic Cu was commonly found within POL3 slags, metallic Fe was observed only sporadically.

POL4 slags were hypocrystalline (Fig. 2d; Fig. 3d), and the changes resulting from weathering are not as advanced as in POL1 slags. On the surface of these samples, secondary crystallization was not observed as far-reaching as in POL1 slags. The slag's inner part is dark gray with clearly visible crystalline phases

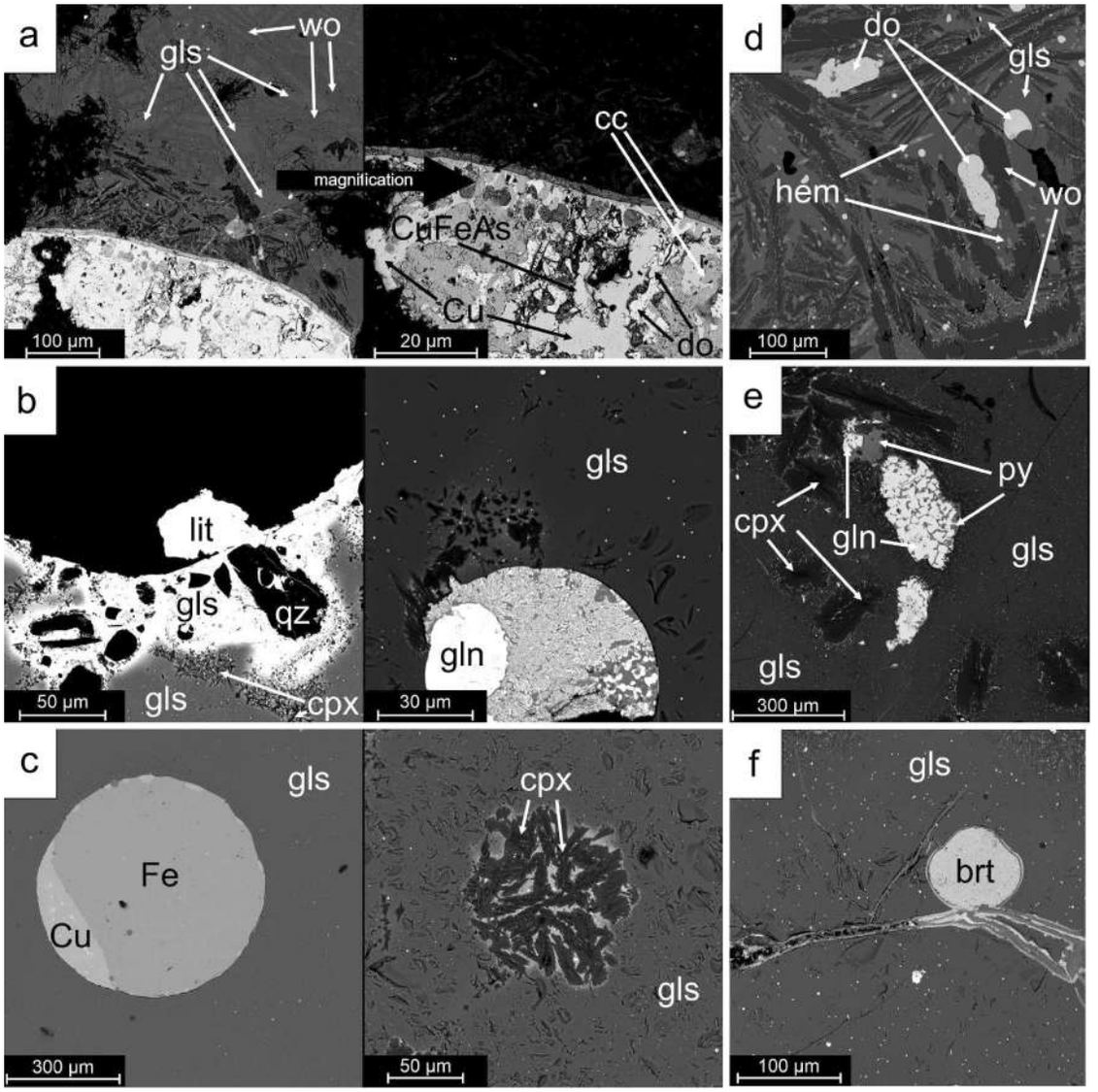

Fig. 3 Representative BSE images of the analyzed slags: **a** POL1; **b** POL2; **c** POL3; **d** POL4; **e**, **f** POL5. brt—barite; cc—chalcocite; Cu—metallic copper; cpx—clinopyroxene; do—domeykite; Fe—metallic iron; gln—galena; gls—glass; hem—hematite; lit—litharge; py—pyrrhotite; wo—wollastonite; qz—quartz

Table 1 Phases occurring in slags from Polichno

	POL1	POL2	POL3	POL4	POL5
Silicates	Wollastonite	Pyroxene	Pyroxene	Wollastonite	Pyroxene
Oxides	SiO_2 phases	SiO_2 phases, Litharge	SiO_2 phases	Hematite	SiO_2 phases, Litharge
Metallic phases	Cu	Cu, Pb	Cu, Fe	Cu	–
Sulfides	Chalcocite	Galena	Chalcocite	Chalcocite	Galena, Pyrrhotite
Arsenides	Domeykite, CuFeAs	–	Domeykite	Domeykite	–
Sulfates	–	Barite	–	–	Barite
carbonates	–	Cerussite	–	Calcite	–

that reach up to 2 mm in length. During microscopic observations, it was found that the main phase present in the slags was skeletal wollastonite. The wollastonite crystals are up to several hundred μm in length and were dispersed within the glassy material (Fig. 3d; Table 1). Hematite crystals up to a dozen μm long (Fig. 3d), calcite, and oval phases containing copper were also scattered in the glass (Fig. 3d; Table 1). These phases had a diameter of up to 100 μm and were mainly composed of arsenides, sulfides, and metallic Cu (Fig. 3d; Table 1).

POL5 slags are the least homogeneous of all slag types. The inner part of the slags is light gray (Fig. 2). The crystalline phases are mostly very small and barely visible. However, larger crystals can occasionally be seen, reaching several mm in length. Within the POL5 slags, zones of darker color can also be seen (Fig. 2). During microscopic observations, quartz/cristobalite (up to 150 μm in length), skeletal pyroxene up to 200 μm long, and oval clusters containing litharge (PbO), galena (PbS), and pyrrhotite ($Fe_{1-x}S$) were observed (Fig. 3e; Table 1). In the POL5 slags, oval barite crystals up to 90 μm in diameter were also observed (Fig. 3f; Table 1).

Slags composition and chemistry of phases

The POL1–POL5 slags were mainly composed of SiO_2 (34.88–49.69 wt.%), FeO (12.62–17.71 wt.%), CaO (12.57–29.95 wt.%), and to a lesser extent of Al_2O_3 (up to 4.32 wt.%), P_2O_5 (up to 2.95 wt.%), and MgO (up to 1.01 wt.%; Table 2). The presence of Cu (up to 27,746 ppm) and Pb (up to 39,941 ppm) was also found in Polichno slags (Table 2). In one of the samples (POL2), increased content of BaO (24.48 wt.%) and Sr (up to 3748 ppm) was distinguished. Compared to POL1 and POL4-5 in POL2-3 slags, higher content of SiO_2 (up to 49.69 wt.%), Pb (18,954–39,941 ppm) with a reduced CaO content (up to 19.20 wt.%; Table 2) was observed. In POL1, POL4-5 slags, an increased concentration of Cu (16,918–27,746 ppm), As (up to 9166 ppm), and Sb (up to 1391 ppm) was observed (Table 2).

Silicates

In Polichno slags, silicates occurred as wollastonite in POL1 and POL4 samples and as clinopyroxene in POL2-3 and POL5 samples (Fig. 3). Wollastonite crystals were characterized by the substitution of Fe (0.15–2.3 wt.% of FeO), and less than 0.50 wt.% of oxide of Ti, Al, Mg, Mn, and Zn. Clinopyroxene crystals had a chemical composition corresponding to a diopside-hedenbergite

Table 2 Bulk chemical composition of slags from Polichno

		POL1	POL2	POL3	POL4	POL5
P_2O_5	wt.%	2.95	2.14	2.13	2.90	2.66
SiO_2		36.64	38.02	49.69	34.88	37.77
TiO_2		0.26	0.18	0.23	0.20	0.21
Al_2O_3		4.32	2.82	3.80	3.42	3.64
FeO		17.71	12.62	17.61	15.90	17.64
MnO		0.63	0.63	0.41	0.43	0.72
CaO		25.49	12.57	19.20	29.95	27.50
MgO		0.52	1.01	0.64	0.44	0.56
BaO		0.69	24.48	0.77	0.90	1.61
Na_2O		0.23	0.05	0.23	0.23	0.19
K_2O		0.97	0.72	1.19	0.81	0.87
SO_3		0.06	0.90	0.35	0.03	0.19
TOT/C		0.30	0.02	0.02	0.09	0.15
TOT/S		0.02	0.48	0.15	< 0.02	0.10
LOI		− 0.9	− 2.0	− 2.2	− 1.4	− 0.8
Cu	ppm	27,746	415	11,054	22,853	16,918
Pb		7104	39,941	18,954	7773	11,496
Zn		20,427	22,225	6921	31,970	15,464
Ni		150	11	164	368	121
As		6248	220	814	9166	5963
Sb		1142	38	387	1391	719
Sr		282	3748	407	298	508

TOT/C—total carbon; TOT/S—total sulfur; LOI—Loss on ignition

Table 3 Representative EPMA analyses of silicates, oxides, carbonates, and average composition of glassy phases occurring in Polichno slags

	wo POL4	wo POL4	cpx POL5	qz POL2	hem POL4	hem POL4	cal POL4	cer POL2	gls1 (n = 4) POL1	gls2 (n = 6) POL2	gls3 (n = 4) POL3	gls4 (n = 5) POL4	gls5 (n = 4) POL5
P_2O_5	na	na	na	bdl	na	na	0.50	0.19	4.4	1.85	2.1	3.7	3.0
SiO_2	50.2	51.7	48.3	99.4	0.49	0.63	bdl	bdl	47.9	41.3	51.7	34.4	40.0
TiO_2	0.08	bdl	bdl	bdl	0.41	0.45	na	bdl	0.36	0.25	0.21	0.14	0.28
Al_2O_3	0.29	bdl	0.27	bdl	2.3	2.1	bdl	bdl	6.0	3.8	4.1	4.0	3.5
FeO^{calc}	2.3	0.15	20.4	bdl	–	–	bdl	bdl	8.5	22.8	16.5	11.9	24.7
$Fe_2O_3^{calc}$	–	–	–	–	88.8	89.6	–	–	–	–	–	–	–
MnO	0.30	bdl	2.1	bdl	0.45	0.51	bdl	bdl	0.36	1.10	0.36	0.45	1.15
CaO	45.6	48.8	25.7	bdl	0.69	0.68	53.3	bdl	27.7	11.5	19.6	31.0	14.88
MgO	0.21	bdl	1.79	bdl	0.37	0.33	bdl	bdl	0.61	0.75	0.65	0.65	0.74
ZnO	0.34	bdl	0.31	bdl	6.2	5.2	bdl	bdl	0.32	0.50	0.59	7.1	0.99
CuO	bdl	bdl	bdl	bdl	na	na	na	bdl	0.24	0.00	0.15	0.21	0.00
PbO	bdl	bdl	bdl	bdl	na	na	bdl	83.4	0.03	6.4	0.67	0.75	3.75
Na_2O	bdl	bdl	bdl	bdl	0.17	bdl	bdl	bdl	0.21	0.14	0.18	0.51	0.30
K_2O	bdl	bdl	bdl	bdl	bdl	bdl	bdl	bdl	1.37	0.87	1.35	0.97	0.86
NiO	bdl	bdl	bdl	na	0.58	0.51	na	bdl	na	na	na	na	na
BaO	na	na	na	bdl	na	na	na	0.32	0.77	7.1	0.41	0.90	5.33
As_2O_3	bdl	bdl	bdl	bdl	na	na	na	bdl	0.07	0.00	0.00	1.81	0.00
SO_3^{calc}	na	na	na	bdl	na	na	na	bdl	0.00	0.28	0.00	0.00	0.59
SO_2^{calc}	na	na	–	na	na	na	0.21	–	–	–	–	–	–
CO_2^{calc}	na	na	–	–	–	–	46.0	16.28	–	–	–	–	–
Total	99.32	100.65	98.87	99.40	100.46	100.01	100.01	100.19	98.84	98.64	98.57	98.49	100.07
	a.p.f.u												
P	–	–	–	–	–	–	0.01	–					
Si	0.99	1.00	1.98	1.00	0.01	0.02	–	–					
Ti	–	–	0.00	0.00	0.01	0.01	–	–					
Al	0.01	–	0.01	0.00	0.07	0.07	–	–					
Fe^{2+}	0.04	–	0.70	0.00	0.00	0.00	–	–					
Fe^{3+}	–	–	–	–	1.78	1.80	–	–					
Mn	–	–	0.07	–	0.01	0.01	–	–					
Ca	0.96	1.01	1.13	–	0.02	0.02	0.93	–					
Mg	0.01	–	0.11	–	0.01	0.01	–	–					
Zn	–	–	0.01	–	0.12	0.10	–	–					
Cu	–	-	–	–	–	–	–	–					
Pb	–	–	–	–	–	–	–	1.03					
Na	–	–	–	–	0.01	–	–	–					
K	–	–	–	–	–	–	–	–					
Ni	–	–	–	–	0.01	0.01	–	–					
Ba	–	–	–	–	–	–	–	–					
As^{3+}	–	–	–	–	–	–	–	–					
S^{6+}	–	–	–	–	–	–	–	–					
S^{4+}	–	–	–	–	–	–	0.01	–					
C	–	–	–	–	–	–	1.02	0.99					
Total	2.00	2.00	4.01	1.00	2.06	2.04	0.94	2.01					
O^{2-}	3.00	3.00	6.00	2.00	3.00	3.00	3.00	3.00					

cal—calcite; cer—cerussite; cpx—clinopyroxene; gls—glass; hem—hematite; lit—litharge; wo—wollastonite; qz—quartz

solid solution and were composed of Si (up to 48.3 wt.% of SiO_2), Fe (up to 20.4 wt.% of FeO), Ca (up to 25.7 wt.% of CaO), and Mg (up to 1.79 wt.% of MgO), with Mn (up to 2.1 wt.% of MnO), Zn (up to 0.31 wt.% of ZnO), and Al (up to 0.27 wt.% of Al_2O_3) substitutions (Table 3).

Oxides

Oxides in the slags from Polichno occur in the form of hematite. Hematite crystals (88.8–89.6 wt.% of Fe_2O_3) were frequently observed in POL4 slags (Fig. 3d). In hematite, the substitution of Zn (5.2–6.2 wt.% of ZnO), Al (2.1–2.3 wt.% of Al_2O_3), and in a smaller amount (less than 1.00 wt.% of oxide) of Ti, Si, Mn, Ca, Mg, Ni, and Na were commonly observed (Table 3).

Glass

The glass was present in all types of slags, differing in chemical composition. In POL1–POL5 glass mainly consists of SiO_2 (34.4–51.7 wt.%), CaO (11.5–31.0 wt.%), and FeO (8.5–24.7 wt.%), with smaller content of ZnO (0.32–7.1 wt.%), P_2O_5 (1.85–4.4 wt.%), Al_2O_3 (3.5–6.0 wt.%), As_2O_3 (up to 1.81 wt.%), BaO (up to 7.1 wt.%), and K_2O (up to 1.37 wt.%; Table 3). The remaining elements were in amounts less than 1 wt.% of oxide (Table 3).

Carbonates

Carbonates were represented by cerussite (Table 3). In cerussite, the substitutions of Ba (up to 0.32 wt.% of BaO) and P (up to 0.19 wt.% of P_2O_5) were observed (Table 3). Cerussite was most likely formed during the weathering of slags.

Sulfides, arsenides, and metallic phases

Sulfides in the analyzed slags occurred as chalcocite, pyrrhotite, and galena. In chalcocite, substitutions of Fe (up to 0.60 wt.%), As (up to 0.43 wt.%), Pb (up to 0.42 wt.%), and less than 0.2 wt.% of Al, P, Si, Ca were observed (Table 4). In galena, less than 0.30 wt.% of Fe and Cu were

Table 4 Representative EPMA analyses of sulfides, arsenides, and metallic phases occurring in Polichno slags

	gln	pyh	cc	do	do	CuFeAs	Metallic phases				
	POL5	POL5	POL3	POL4	POL3	POL1	POL3	POL3	POL3	POL4	POL3
S	13.4	36.2	19.7	0.15	0.10	0.11	0.11	bdl	0.06	bdl	bdl
Fe	0.23	62.4	0.60	0.27	0.38	36.1	82.3	90.9	bdl	0.18	1.04
Co	bdl	bdl	bdl	bdl	bdl	0.65	0.82	0.91	bdl	bdl	bdl
Ni	bdl	bdl	bdl	0.36	1.55	1.07	0.63	0.35	1.21	0.37	bdl
Cu	0.29	0.86	77.8	70.0	66.7	23.2	1.69	2.3	76.4	81.9	94.0
As	bdl	bdl	0.43	28.1	23.0	37.5	2.9	2.5	18.0	17.4	1.17
Al	bdl	bdl	0.12	bdl	bdl	bdl	bdl	bdl	bdl	bdl	0.18
Sb	bdl	bdl	bdl	0.78	9.0	bdl	0.13	bdl	5.6	0.94	1.91
Pb	86.9	bdl	0.42	bdl	bdl	bdl	bdl	bdl	bdl	0.15	bdl
P	bdl	bdl	0.07	bdl	0.09	0.35	11.0	2.1	0.10	bdl	0.41
Si	bdl	bdl	0.09	bdl	bdl	bdl	bdl	bdl	bdl	bdl	0.10
Ca	bdl	bdl	0.09	bdl	bdl	bdl	bdl	bdl	bdl	bdl	bdl
Total	100.82	99.46	99.32	99.66	100.82	98.98	99.58	99.06	101.37	100.94	98.81
	a.p.f.u						Atomic concentration				
S	1.00	1.00	1.00	0.01	0.01	0.01	–	–	0.12	–	–
Fe	–	0.99	0.02	0.01	0.02	1.29	1.87	91.17	0.00	0.21	1.62
Co	–	–	–	–	–	0.02	–	0.87	–	–	–
Ni	–	–	–	0.02	0.07	0.04	–	0.33	1.36	0.41	–
Cu	–	0.01	2.00	2.94	2.86	0.73	93.76	2.00	79.39	83.74	96.31
As	–	–	0.01	1.00	0.84	1.00	4.03	1.84	15.87	15.09	0.87
Al	–	–	0.01	–	–	–	0.23	–	–	–	0.25
Sb	–	–	–	0.02	0.20	–	0.12	–	3.03	0.50	0.76
Pb	0.98	–	–	–	–	–	–	–	–	0.05	0.05
P	–	–	–	0.00	0.01	0.02	–	3.80	0.22	–	–
Si	–	–	–	–	–	–	–	–	–	–	0.15
Ca	–	–	–	–	–	–	–	–	–	–	–
Total	1.98	2.00	3.03	4.00	4.00	3.11	100.00	100.00	100.00	100.00	100.00

cc—chalcocite; do—domeykite; gln—galena; py—pyrrhotite

observed (Table 4). In pyrrhotite Cu (up to 0.86 wt.%; Table 4) substitution was found. Arsenide phases were represented by domeykite and CuFeAs. In domeykite, the substitutions of Sb (0.78–9.0 wt.%), Ni (0.36–1.55 wt.%), and less than 0.5 wt.% of Fe, S, and P were found (Table 4). Due to the amphoteric character of Sb, part of it (in domeykites) was calculated as a cation and part as an anion to balance the unit cell. In CuFeAs phases, substitutions of Ni (up to 1.07 wt.%) and less than 1 wt. % of Co, P, and S were observed (Table 4). Two types of metallic phases were observed in the analyzed slags. The most common metallic Cu was composed of 76.4–94.0 wt.% Cu, 1.17–18.0 wt.% As, 0.94–5.6 wt.% Sb, up to 1.21 wt.% Ni, up to 1.04 wt.% Fe, and smaller amounts (< 1 wt.%) of S, Al, Pb, P, Si (Table 4). The second type was metallic Fe. It was mainly composed of Fe (82.3–90.9 wt.%), P (2.1–11.0 wt.%), As (2.5–2.9 wt.%), Cu (1.69–2.3 wt.%), Co (0.82–0.91 wt.%), Ni (0.35–0.63 wt.%), S (up to 0.11 wt.%), and Sb (up to 0.13 wt.%; Table 4).

Restitic phases

Restitic phases in the analyzed slags are observed in the form of quartz, calcite, and barite. They are most likely residues from additives added during smelting and were not melted/decomposed during smelting. Quartz crystals consist only of SiO_2 (99.4 wt.%; Table 3). No substitutions have been found in their crystal structure (Table 3). In calcite, substitutions of P (up to 0.50 wt.% of P_2O_5) and S (up to 0.21 wt.% of SO_2) were observed (Table 3).

Temperature

Phase diagrams were one of the methods used to determine the slags' liquidus temperature. Calculations were based on the slags' total chemical composition and the glasses' averaged chemical composition. Considering that slags consist mainly of SiO_2, CaO, and FeO (63.21–86.50 wt.%) SiO_2-CaO-FeO diagram [34] is the best fit, although taking into account the presence of Al_2O_3 (2.82–4.32 wt.%) SiO_2-CaO-FeO-6% Al_2O_3 diagram was also used [35] (Fig. 4). The temperature of slags determined with SiO_2-CaO-FeO diagram was in the range of 1200–1600 °C (Fig. 4; Table 5). Based on the SiO_2-CaO-FeO-6% Al_2O_3 diagram, the liquidus temperature ranged from 1060 to 1350 °C (Fig. 4; Table 5).

The second method used during temperature determinations was the high-temperature microscope observations. The first deformations during the heating of the samples appeared at temperatures in the range of 821 °C (POL2)-1100 °C (POL1) (Additional file 1). The edges of the cone became rounded, indicating that the slag's solidus temperature was exceeded. The liquefaction of the slags was observed at the temperature range of 1126 °C (POL2) to 1263 °C (POL1). At this point, the samples reached flow temperature (Table 5; Additional file 1).

The next method of temperature determination was the high-temperature experiments. The first changes on the surface of the sample in the form of rounding the edges of POL2 slags appeared at 800 °C (Fig. 5; Table 5). In the case of sample POL4, the changes were evident when the sample was heated to 1100 °C (Fig. 5). The rounding of the edges indicates that the solidus temperature has been exceeded. Further changes during the experiments appeared when sample POL2 was heated to 1100 °C and sample POL4 to 1200 °C (Fig. 5). At these temperatures, sample POL4 melted completely, while sample POL2 melted almost entirely, but the quartz grains remained

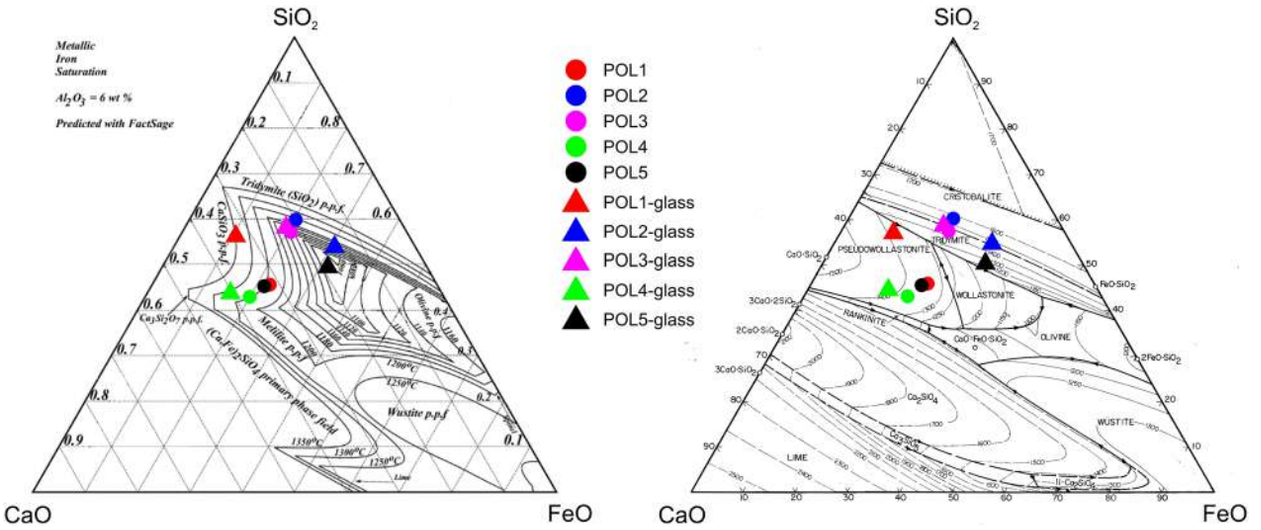

Fig. 4 Phase diagrams with the marked chemical composition of slags from Polichno [34, 35]

Table 5 Summary of temperatures determined during the analysis of slags with various methods

	Temperature in °C	POL1	POL2	POL3	POL4	POL5
Experiment	Liquidus	–	1100 (for glass) 1200 (including SiO_2 grains)	–	1200	–
	Solidus		800		1100	
Microscope observations	Liquidus	1263	1126	1154	1138	1246
	Solidus	1100	821	1090	1060	1058
CaO-SiO_2-FeO diagram	Bulk composition	1300–1400	1500–1600	1400–1500	1300–1400	1300–1400
	Glass	1300–1400	1400–1500	1400–1500	1400–1500	1200–1300
CaO-SiO_2.FeO-6% Al_2O_3 diagram	Bulk composition	1200–1250	1250–1300	1120–1160	~1250	~1250
	Glass	1300–1350	1140–1180	1160–1180	1250–1300	1060–1080

Fig. 5 Macroscopic photos of slags after the high-temperature experiments

unmelted (Fig. 5). Melting of the entire volume (including quartz grains) was observed when the sample POL2 was heated to 1200 °C (Fig. 5). Considering that the unmelted SiO_2 crystals occur in samples of glassy slag, the POL2 slag must result from smelting at a temperature close to 1100 °C and definitely below 1200 °C (Fig. 5; Table 5). Taking into account the similarity in the chemical composition of POL1, POL4-5 slags, the temperatures obtained from the experiment for sample POL4 are also reliable for samples POL1 and POL5.

The volatile properties during smelting

Analyses of the oxygen and sulfur fugacities during the smelting process in the Polichno were based on the thermodynamic data available in the literature [33]. As these data are available only for the temperature interval of 100 K, logK and temperature were plotted on the graph (Additional file 2). Then, the value of the logK for the desired temperature (liquidus and solidus of slags) was read from the graph (Additional file 3). The values were used to calculate the oxygen and sulfur fugacities under which the coexistence of sulfides (MeS), oxides (MeO), and metallic phases (Me) is possible (Additional file 3).

Calculating equilibrium constants (Additional file 3) made it possible to create the predominance area diagrams (Fig. 6). Then, based on the slags' phase composition, the oxygen and sulfur fugacities during the formation of individual types of slags were determined. The line showing the equilibrium constant between the metallic and oxide/sulfide phases shows the conditions under which the coexistence of metallic and sulfide/oxide phases is possible. It also provides information on the minimum sulfur/oxygen fugacity in which the formation of sulfides/oxides is possible.

Considering that in the POL1 slags, Cu occurs mainly in the metallic form or as the sulfides/arsenides, the $\log P_{O_2}$ during their formation had to be below −5.16 at the solidus temperature (1100 °C) and below −4.30 atm. at the liquidus temperature (1200 °C; Fig. 6; Table 1; Additional file 3). The coexistence of metallic Cu and Cu sulfides in slags is possible at the sulfur fugacity ($\log P_{S_2}$) in the range of −6.59 (in 1100 °C) and −5.84 atm. at 1200 °C (Fig. 6; Additional file 3).

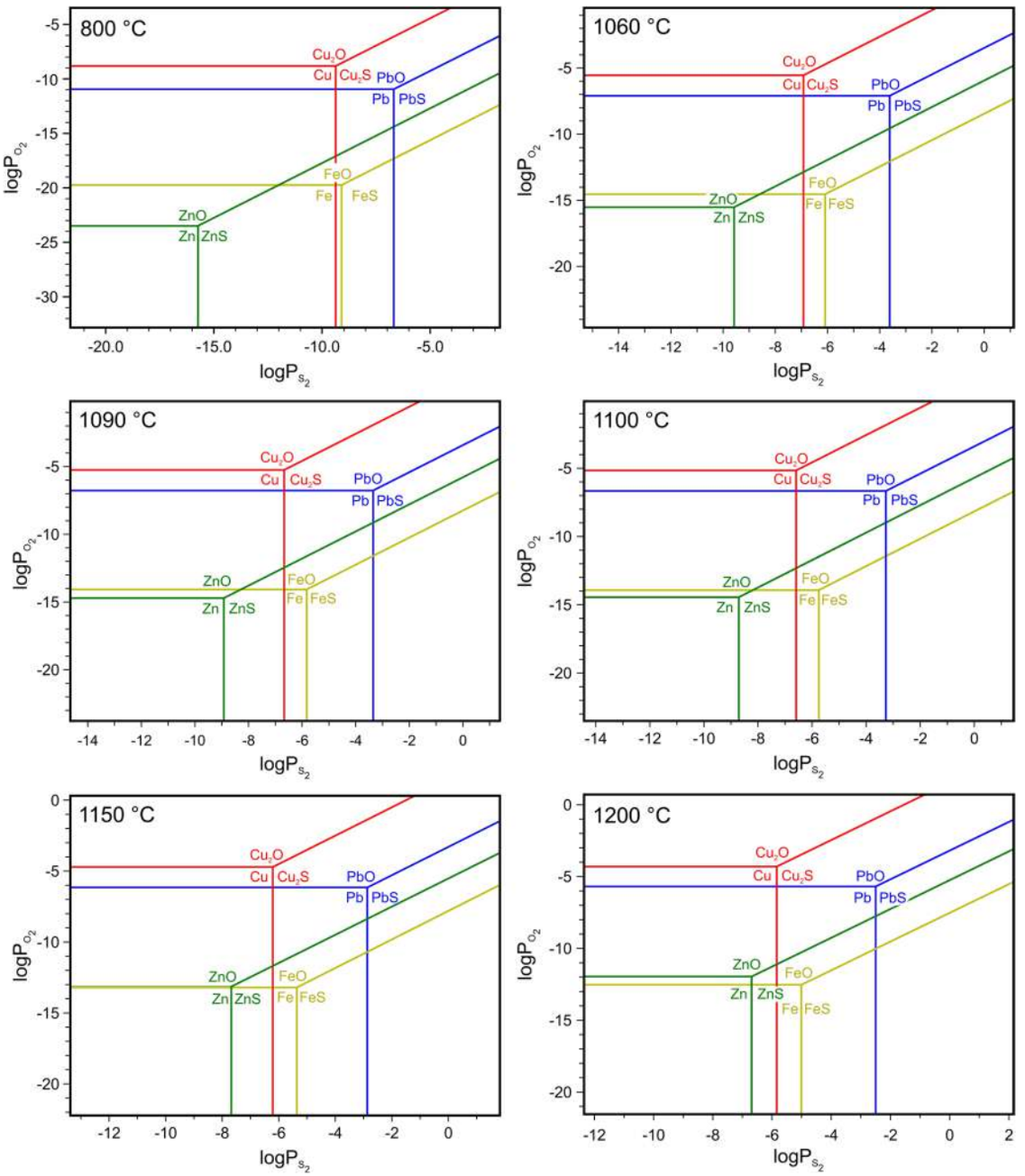

Fig. 6 Predominance area diagrams considering the most important metals present in slags after copper production

In POL2 slags, lead occurs mainly in glassy phases (as PbO) and as litharge. The oxygen fugacity under which Pb was oxidized for liquidus and solidus temperatures should be higher than $\log P_{O_2} = -10.95$ (at 800 °C) and −6.66 (at 1100 °C; Fig. 6; Additional file 3). Under conditions close to thermodynamic equilibrium between PbO and metallic Pb, it was also possible for metallic Pb to occur, which was occasionally observed in POL2 slags (Table 1). Occasionally observed metallic Cu indicates the $\log P_{O_2}$ lower than −8.81 at 800 °C and −5.16 at 1100 °C. The presence of sulfide phases only in the form of PbS indicates the sulfur fugacity above $\log P_{S_2} = -6.68$ at 800 °C and above −3.28 atm. at 1100 °C (Fig. 6; Additional file 3).

Due to the lack of copper oxides in POL3 slags, the oxygen fugacity during their formation had to be lower

than $logP_{O_2} = -5.25$ (at 1090 °C) and −5.16 atm. (at 1100 °C; Fig. 6; Additional file 3). In POL3 slags, metallic Fe was found (Fig. 3c), but its presence is an exception in the scale of the analyzed material. At the same time, metallic Fe occurs surrounded by a glass containing oxidized Fe (Fig. 3c; Table 3). Considering the presence of Fe in the metallic and oxide form, the oxygen fugacity in these zones ranges from $logP_{O_2} = -14.08$ (1090 °C) to −13.93 atm. (1100 °C; Fig. 6; Additional file 3). The coexistence of metallic Cu with Cu sulfides indicates the local thermodynamic equilibrium between Cu_2S and metallic Cu (Fig. 3a). It is possible in the range of sulfur fugacity between $logP_{S_2} = -6.67$ at 1090 °C and −6.59 atm. at 1100 °C (Fig. 6; Additional file 3). The absence of Fe sulfides confirms sulfur fugacity below $logP_{S_2} = -5.83$ (at 1090 °C) and −5.75 atm. (at 1100 °C; Fig. 6; Additional file 3).

In POL4 slags, no copper oxides were found, which proves the $logP_{O_2}$ was below −5.55 at the solidus temperature (1060 °C) and below −4.30 atm. at the liquidus temperature (1200 °C; Fig. 6; Additional file 3). Occasionally observed Cu sulfides and the absence of Fe sulfides indicate sulfur fugacity in the range of $logP_{S_2} = -6.92$ to −6.09 atm. (at 1060 °C) and −5.84 to −5.01 atm. (at 1200 °C; Fig. 6; Additional file 3).

The presence of Pb in the oxidized form in POL5 slags was possible with the minimum oxygen fugacity of $logP_{O_2} = -7.10$ (at 1060 °C) and −5.69 atm. (at 1200 °C; Fig. 6; Additional file 3). Iron sulfides' presence indicates the minimum sulfur fugacity of $logP_{S_2} = -6.09$ at 1060 °C and −5.01 atm. at 1200 °C (Fig. 6). The presence of Pb sulfides proves greater sulfur availability (at least $logP_{S_2} = -3.62$ at 1060 °C and −2.50 atm. at 1200 °C; Fig. 6; Additional file 3).

Discussion

Recreation of the copper smelting process at Polichno

The temperature range at which copper smelting was carried out is crucial to determine the oxygen and sulfur fugacities during the metallurgical process. In this study, we decided to use three independent methods of smelting temperature determination. High-temperature experiments and observations using a high-temperature microscope made it possible to determine the liquidus (1100–1200 °C) and solidus (800–1100 °C) temperatures of the analyzed slags. Temperatures determined by high-temperature microscope observations differ from those determined by experimental smelting.

In the case of glassy slags (POL2), the temperatures determined by microscope observations are higher than those obtained from experiment in a laboratory furnace. The differences are only 21–26 °C for solidus and liquidus temperatures, respectively (Table 5). These differences are most likely due to the rate at which the samples were heated. Regardless of the target temperature, the sample was heated for 3 h during heating in the laboratory furnace. Then, a high temperature was maintained for 2 h. In contrast, during microscopic observations, the temperature gradient ranged from 10 °C (0–900 °C) to 70 °C (1100–1350 °C) per minute. With a rapid temperature change, changes on the surface of the samples could be observed with a delay.

In the POL4 sample, the temperatures determined with the microscope were lower than that determined during experimental smelting. The sample was heated from ambient temperature until complete liquefaction during microscopic observations. For practical reasons, experimental smelting is carried out with only a temperature interval of 50–100 °C, limiting the possibility to observe changes in temperature between this range. A lower liquidus temperature determined during microscopic observations is because the liquidus temperature was considered the one at which the sample liquefied enough to reach the flow temperature (1138 °C; Table 5). As the experiments in the laboratory furnace showed the POL4 sample at 1150 °C was liquid enough to spread to the bottom of the crucible (Fig. 5). However, the sample did not homogenize, which indicates the presence of solid phases within the sample.

Considering the above it was decided to base further considerations on the liquidus temperature determined by high-temperature experiments in a laboratory furnace. In the case of solidus temperature, the first signs of melting are essential. For this reason, the lowest temperature obtained during the experiments should be considered the solidus temperature.

The use of experimental smelting and the presence of unmelted phases in glassy slags made it possible to determine the maximum smelting temperature for glassy (POL2) slags at 1200 °C. At this temperature, all previously unmelted fragments were melted (Additional file 3). It was impossible to determine the maximum smelting temperature for hypocrystalline slags due to the lack of unmelted phases in the slags. The high-temperature experiments allowed the verification of temperature estimations obtained from the phase diagrams. The best diagram was the SiO_2-CaO-FeO-6% Al_2O_3 phase diagram due to the broadest spectrum of the elements included. Its accuracy of the determined temperature is also positively affected by the diagram design with a marked temperature interval of 20 °C (Fig. 4; Table 5).

The smelting temperature of the Polichno slags is slightly lower than observed in other locations where copper smelting was carried out in historical times, e.g., in Marsiliana (1150–1300 °C) [18], Rudawy Janowickie (1200–1300 °C) [6], and in Kondratów and Leszczyna

(1210–1400 °C) [3]. It is also worth noting that glassy slags' first signs of melting appear as early as 800 °C (Fig. 5; Table 5). Such low temperatures are rare and have so far only been described in a few places [4, 36]. Of the slags analyzed, only POL2 had such a low solidus temperature. This type of slag is distinguished from the others by its high content of Pb, Zn, and BaO (Table 2). Taking into account that POL2 are glassy slags (Figs. 2, 3), these elements are mainly included in the amorphous phases (in oxide form; Table 3) generating low solidus temperatures (Table 5). Moreover, due to the presence of unmelted SiO_2 grains within slags, it was possible to determine the maximum temperature at which glassy slags formed. During experiments, the complete meltdown of SiO_2 grains indicated that the smelting temperature must have been lower than 1200 °C. So far, only the minimum smelting temperature has been determined in the reconstruction of historical metallurgical processes [3–5, 9, 10, 18].

Accurate determination of temperature conditions made it possible to determine the fugacity of gases during smelting. The fugacity of O_2 and S_2 was determined with the PADs constructed based on thermodynamic calculations. The conducted research showed a relatively large range ($logP_{O_2}$ from −4.30 at 1200 °C to −19.93 at 1100 °C) of oxygen fugacity in which the production process in Polichno could have been carried out. In the studies conducted so far, oxygen fugacity was often determined in a narrower range [1, 14, 17]. However, the greater accuracy comes from determining oxygen fugacity in these cases for only one temperature [1, 14] or a narrower temperature range [17]. The broad range of values presented in this study is due to various slag types and a wide range of considered smelting temperatures. When determining the redox conditions for particular slag types, oxygen fugacity was often determined over a much narrower range. The type of metal produced is also not insignificant. In the case of slags after Fe production [14, 17], it was necessary to maintain a more reductive environment during smelting. Because of this, the range of oxygen fugacity in which production could have been carried out was narrower and had to be close to the value at which Fe is reduced to metallic form. In the case of Cu production, it was not necessary to maintain a highly reducing environment. Still, values close to the equilibrium line between FeO and Fe were obtained during the process in Polichno in some zones, by which metallic Fe is observed in the slags (Fig. 3c).

The range of oxygen fugacity in which smelting was carried out in Polichno is slightly lower compared to the conditions prevailing in smelters operating during a similar period in Marsiliana, Kondratów, and Leszczyna (Table 6). The difference is mainly due to the lower temperatures prevailing during smelting in Polichno. For the oxide/sulfide phases to be reduced at lower temperatures, it is necessary to maintain a more reducing environment (Fig. 6). In one of the oldest copper smelters (3rd millennium BC in Cabrières and Bronze Age in Crete), the range of oxygen fugacity in which smelting was carried out is comparable to that prevailing during smelting at Polichno (Table 6). Whenever $logP_{O_2}$ values are lower, it indicates a more reductive environment, which may have been achieved by using more reductant (charcoal) during smelting.

Because there is no information on the addition of sulfur during the copper production process in historical times, the fugacity of sulfur depends on the amount of sulfide minerals occurring in the ore. Comparing the fugacity of sulfur in smelters operating during a similar period, the range over which smelting was carried out

Table 6 Liquidus temperatures and oxygen and sulfur fugacities at which slag formation was possible at selected locations

Location	Time	Smelting/liquidus temperature [°C]	Temperature determination method	$logP_{O_2}$ provided by the authors	Oxygen fugacity [$logP_{O_2}$] Based on PADs*	Sulfur fugacity [$logP_{S_2}$]
Polichno	Fifteenth to seventeenth century	1100–1200			−4.30 to −13.93	−2.50 to −6.59
Kondratów and Leszczyna, Poland [3]	Eighteenth to twentieth century	1210–1400	MELTS-Rhyolite software combined with geothermometers and petrological observations	QMF buffer no values given	−3.00 to −12.40	−3.87 to −5.77
Marsiliana, Italy [18]	Thirteenth to fourteenth century	1150–1300	Phase composition	no values given	−3.58 to −13.20	−1.87 to −7.68
Cabrières, France [2]	3rd millennium BC	1000–1200	Phase composition	at least -6	−4.30 to −15.57	−5.01 to −7.43
Crete [1]	Bronze Age	1150–1300	Phase diagrams	−7 to −9.5 (1300 °C)	−3.58 to −13.20	−4.81 to −6.21

*Fugacity has been calculated for the given liquidus temperatures

in Polichno is narrower than that in Marsiliana smelting and broader than the work carried out in Kondratów and Leszczyna (Table 6). The decreasing range of sulfur fugacity during the process may be due to the improvements in the production process between the thirteenth and twentieth centuries. The narrower range may result in better control of the ongoing process and, thus, better efficiency. The range of $\log P_{S_2}$ during smelting in Cabrières and Crete is narrower than in Polichno. At the same time, these locations are characterized by relatively low sulfur fugacity (Table 6). In the case of Crete, this is due to the use of mainly oxidized copper minerals during smelting [1]. In Cabrières, the smelting process was based on sulfide ore, and lower $\log P_{S_2}$ may suggest a less efficient ore enrichment process. The other explanation is the partial roasting of the ore, which may have been used at Cabrières before the actual smelting [2].

Importance of PADs in the O_2 and S_2 fugacity determinations

Based on the PAD, it is possible to determine several critical factors related to smelting. PADs directly give information on the fugacity of oxygen, sulfur, or other relevant components (e.g., arsenic) affecting the smelting process. With PADs, it is also possible to determine whether the smelting process was conducted under thermodynamic equilibrium conditions or measure how deeply non-equilibrium conditions existed. The occurrence of phases in the samples whose fields of occurrence in the diagram do not overlap indicates a thermodynamic non-equilibrium during smelting. The greater the distance between these fields, the more non-equilibrium conditions were. The best example is sample POL5, where PbO and FeS were found. Theoretically, these phases should not co-occur (Fig. 6). In such cases, the temperature and volatile composition most likely changed during crystallization.

Because oxygen fugacity is one of the most critical factors for metal production [3, 9, 17], it should be determined as accurately as possible. PADs make it possible to obtain more precise results compared to commonly used Fe buffers. This is because Fe buffers were designed for natural rocks and only consider the degree of Fe oxidation [21, 22]. Basing studies only on the degree of iron oxidation is understandable when analyzing crystallization processes in natural rocks but may be insufficient when for metallurgical slags. The feasibility of using Fe buffers requires information on the degree of iron oxidation in the samples. This information can be provided through analyses of the chemical composition of iron-containing phases or additional analyses using tools such as, e.g., Mössbauer spectroscopy [11, 14]. Historical metallurgical slags very often consist mainly of glassy phases, and crystalline phases occur only sporadically dispersed in the glass [1, 3, 25], which limits the possibility of determining the degree of Fe oxidation based on the phase composition of slags. Advanced petrological and chemical tools (like mentioned Mössbauer spectroscopy) are not commonly used for archaeological studies due to the limited availability of equipment. Due to the limitations in the use of Fe buffers, the use of PADs appears to be preferable because it is possible to consider all the phases that were observed in the samples (e.g., Cu, Pb, Zn, Fe) when creating the diagram, rather than being limited to Fe only.

Another advantage of PADs over Fe buffers is the ability to determine the fugacity of other furnace gases. Unlike Pb or Fe smelting, where the only relevant gaseous components are O_2, CO, and CO_2, the fugacity of sulfur (and/or arsenic) was equally important during copper production. Copper production in historical times was performed by producing a matte (sulfide melt), which was then processed to produce metallic copper. Matte production could only occur if the sulfur fugacity was sufficient to form sulfides. For this reason, when reconstructing historical processes, it is necessary to determine the P_{S2}, especially in copper smelting. It is impossible to determine it using Fe buffers. During copper production, it was crucial to maintain the right amount of sulfur in the system so that the matte contained as much Cu and as little Fe as possible. At the same time, care was taken to avoid oxidation of Cu, which would pass into the slag in the form of Cu_2O [12]. Former smelters were thus able to manipulate the efficiency of the process by the O_2 and S_2 fugacities during smelting. In addition to knowledge of conditions during smelting, analyzing the sulfur/oxygen fugacity allows us to answer the question of how much-developed technology was used by past metallurgists.

Ellingham diagrams can also determine the gas composition in historical processes [25]. Diagrams that consider the fugacity of oxygen during the oxidation of metallic phases are widely available in the literature [37]. We can also find diagrams from which we can read the fugacity of sulfur with the transition between metallic and sulfide phases [38]. The disadvantage of using Ellingham diagrams is that no single diagram simultaneously considers the fugacity of oxygen and sulfur. In addition, Ellingham diagrams most often consider too many phases in a single diagram, and their readability is limited. An additional advantage of PADs is that the thermodynamic equilibrium conditions directly between the sulfide and oxide phases can also be read from them (Fig. 6). Such transitions are not included in any of the available Ellingham diagrams.

Conclusions

Study proves that the PADs can be effectively applied during the reconstruction of the oxygen and sulfur fugacities during historical metallurgical processes. The diagrams made it possible to determine the oxygen and sulfur fugacities during copper smelting in Polichno. This was possible due to the determination of the slags' liquidus and solidus temperatures, which were then used for thermodynamic calculations. Combining the experimental smelting and high-temperature microscopic observations allowed for more precise solidus temperature determinations. Considering that sulfide ores were processed through the production of speiss/matte, both the oxygen and sulfur fugacity during smelting were determined. The oxygen fugacity during ores processing in Polichno ranges from $\log P_{O_2} = -4.30$ (POL1, POL4 at 1200 °C) to −14.08 atm. (POL3 at 1090 °C). The sulfur fugacity ($\log P_{S_2}$) ranged from −2.50 atm. (POL5 at 1200 °C) to −6.92 (POL4 at 1060 °C). The relatively high sulfur availability during smelting indicates using sulfide ores without roasting in Polichno. The wide range of sulfur and oxygen fugacity, in turn, indicates the heterogeneity of the process. Most often, oxidation–reduction conditions are determined by Fe buffers in reconstructions of historical metallurgical processes. Such treatment has restricted the possible calculation to Fe-containing phases only. It is better to consider the other elements occurring in the slags because determining the iron oxidation degree in slag samples can be problematic, especially for entirely glassy slags. PADs make it possible to consider those metals whose occurrence was confirmed during EPMA studies. An additional advantage of the presented method is the possibility of presenting the fugacity of sulfur and oxygen using a single diagram.

Supplementary Information

The online version contains supplementary material available at https:// doi.org/10.1186/s40494-024-01171-y.

Additional file 1. Results of liquidus and solidus temperature determinations of slags from Polichno using high-temperature microscope observations

Additional file 2. Graphs showing the dependence of the equilibrium constant (logK) on temperature a) for oxides, b) for sulfides (made based on data from barin [31]).

Additional file 3. logK values used in thermodynamic calculations, and a summary of results on the equilibrium constant between the metallic and oxide-sulfide phases.

Acknowledgements
This study was supported by the National Science Center (NCN) Grant No. 2019/35/O/ST10/00313.

Author contributions
Conceptualization: KK, RW, and AG; Methodology: KK, RW, AG, PM, and MŚ; Writing—original draft preparation: KK; Writing—review and editing: KK, RW, and AG; Resources: KK and RW; Figures, tables, and Additional files: KK and RW. All authors read and approved the manuscript.

Funding
This research was funded by the National Science Center (NCN) Grant No. 2019/35/O/ST10/00313.

Data availability
The data that supports the finding of the study is given in the tables and figures within the main text and in Additional files. This study brought together existing data from several different sources, which are cited throughout. No dataset from external repositories was used in this study. All existing data used for this publication are cited in the reference section.

Code availability
Not applicable.

Declarations

Ethics approval and consent to participate
Not applicable.

Consent for publication
Not applicable.

Competing interests
The authors declare no competing interests.

Received: 15 December 2023 Accepted: 5 February 2024
Published online: 12 February 2024

References

1. Bassiakos Y, Catapotis M. Reconstruction of the copper smelting process based on the analysis of ore and slag samples. Hesperia Supplements. 2006;36:329–53.
2. Bourgarit D, Mille B, Prange M, Ambert P, Hauptmann A. Chalcolithic fahlore smelting at Cabrières: reconstruction of smelting processes by archaeometallurgical finds. Archaeometall Eur. 2003;1:431–40.
3. Derkowska K, Świerk M, Nowak K. Reconstruction of copper smelting technology based on 18–20th-century slag remains from the old copper basin, Poland. Minerals. 2021;11:926.
4. Ettler V, Červinka R, Johan Z. Mineralogy of medieval slags from lead and silver smelting (Bohutín, Příbram district, Czech Republic): towards estimation of historical smelting conditions. Archaeometry. 2009;51:987–1007.
5. Kądziołka K, Pietranik A, Kierczak J, Potysz A, Stolarczyk T. Towards better reconstruction of smelting temperatures: methodological review and the case of historical K-rich Cu-slags from the Old Copper Basin, Poland. J Archaeol Sci. 2020;118: 105142.
6. Kierczak J, Pietranik A. Mineralogy and composition of historical Cu slags from the Rudawy Janowickie Mountains, southwestern Poland. Can Mineral. 2011;49:1281–96.
7. Kupczak K, Warchulski R, Dulski M, Środek D. Chemical and phase reactions on the contact between refractory materials and slags, a case from the 19th Century Zn-Pb Smelter in Ruda Śląska, Poland. Minerals. 2020;10:1006.
8. Maldonado B, Rehren T. Early copper smelting at Itziparátzico, Mexico. J Archaeol Sci. 2009;36:1998–2006.
9. Warchulski R, Kupczak K, Gawęda A, Sitko R. Complete reconstruction of the process and conditions during gold smelting in the 15–17th century in Złoty Stok based on metallurgical slags. Archaeometry. 2022;64:916–34.

10. Warchulski R, Szczuka M, Kupczak K. Reconstruction of 16th–17th century lead smelting processes on the basis of slag properties: a case study from Sławków, Poland. Minerals. 2020;10:1039.
11. Warchulski R. Zn-Pb slag crystallization: evaluating temperature conditions on the basis of geothermometry. Eur J Mineral. 2016;28:375–84.
12. Davenport WG, King M, Schlesinger M, Biswas AK. Extractive Metallurgy of Copper. 2002:1–460.
13. Hauptmann A, Rehren T, Schmitt-Strecker S. Early Bronze Age copper metallurgy at Shahr-i Sokhta (Iran) reconsidered. Bochum: Deutsches Bergbau-Museum; 2003. p. 197–213.
14. Nakanishi A. Mössbauer study of ancient iron smelting slag in Japan. Hyperfine Interact. 2008;186:135–9.
15. Cabała J. (in Polish) Heavy metals in the soil environment of the Olkusz Zn-Pb ore mining district. Katowice: Wydawnictwo Uniwersytetu Śląskiego; 2009. p. 1–132.
16 Agricola G. (in Polish) On the nature of metals (De Re Metallica. Jelenia Góra: Muzeum Karkonoskie w Jeleniej Górze; 2000. p. 1–531.
17. Giacometti F, Rebay G, Riccardi MP, Tarantino SC, Cucini TC, Tizzoni M. Iron Age silicate slags from Val Malenco (Italy): the role of textural and compositional studies in the reconstruction of smelting conditions. Periodico di Mineralogia. 2014;83:329–44.
18. Manasse A, Mellini M. Chemical and textural characterisation of medieval slags from the Massa Marittima smelting sites (Tuscany, Italy). J Cult Herit. 2002;3:187–98.
19. Nezafati N, Pernicka E. Early silver Production in Iran. Iranian Archaeology. 2012:10.
20. Ströbele F, Wenzel T, Kronz A, Hildebrandt LH, Markl G. Mineralogical and geochemical characterization of high-medieval lead–silver smelting slags from Wiesloch near Heidelberg (Germany)—an approach to process reconstruction. Archaeol Anthropol Sci. 2010;2:191–215.
21. Lindsley DH. Oxide minerals: petrologic and magnetic significance. Berlin: Walter de Gruyter GmbH & Co KG; 2018. p. 1–10.
22. Zhao D, Essene EJ, Zhang Y. An oxygen barometer for rutile–ilmenite assemblages: oxidation state of metasomatic agents in the mantle. Earth Planet Sci Lett. 1999;166:127–37.
23. Report on the state of the Chęciny commune for 2021. 2022:1–90
24 Paulewicz M. (in Polish) Chęciny ore mining (14th to mid–17th century. Kielce: Kieleckie towarzystwo naukowe; 1992. p. 1–155.
25. Kupczak K, Warchulski R, Gawęda A. Reconstruction of smelting conditions during 16th-to 18th-century copper ore processing in the Kielce region (Old Polish Industrial District) based on slags from Miedziana Góra, Poland. Archaeometry. 2023;65:547–69.
26. Geoportal.n.d. **https:// www .geopo rtal .gov .pl.** Accessed 3 Jan 2023.
27. Długosz J, (in Polish) Annals or chronicles of the famous Kingdom of Poland. Book 1. 1455–1480:169
28. Gałuszka A, Migaszewski ZM, Dołęgowska S, Michalik A, Duczmal-Czernikiewicz A. Geochemical background of potentially toxic trace elements in soils of the historic copper mining area: a case study from Miedzianka Mt., Holy Cross Mountains, south-central Poland. Environ Earth Sci. 2015;74:4589–605.
29. Siuda R, Domańska-Siuda J. STOP 1: Miedzianka deposit—one of the oldest mining centres in Poland. Proceedings of the XXVIth Meeting of the Petrology Group of the Mineralogical Society of Poland. 2019;99–103.
30. Ciurej A, Struska M, Wolska A, Chudzik W. The Miedzianka Mountain Ore Deposit (Świętokrzyskie Mountains, Poland) as a site of historical mining and geological heritage: a case study of the Teresa Adit. Minerals. 2021;11:1177.
31. Kowalczewski Z, Szczecińska A. (in Polish) Results of research on slags from several sites of former non-ferrous metallurgy in the Holy Cross Mountains. Rocznik Świętokrzyski. 1977;5:151–68.
32. Pang CH, Hewakandamby B, Wu T, Lester E. An automated ash fusion test for characterisation of the behaviour of ashes from biomass and coal at elevated temperatures. Fuel. 2013;103:454–66.
33. Barin I. Thermochemical data of pure substances. VCH. 1993;2:1523
34. Muan A, Osborn EF. Phase equilibria among oxides in steelmaking. Massachusetts: Addison-Wesley publishing company, INC; 1965. p. 113.
35. Jak E, Hayes P, Pelton A, Decterov S. Thermodynamic modelling of the A12O3-CaO-FeO-Fe2O3-PbO-SiO2-ZnO system with addition of K and Na with metallurgical applications. In Proc VIII Int'l Conf on Molten Slags, Fluxes and Salts; Santiago, Chile. 2009:473–90
36. Westner KJ, Klein S, Sergeev D, Müller M. Temperature estimates of historical Pb-Ag smelting slags: a multi-methodological approach. J Archaeol Sci Rep. 2022;46: 103654.
37 Hasegawa M. Ellingham diagram. Treatise on process metallurgy. Amsterdam: Elsevier; 2014. p. 507–16.
38. Shatynski SR. The thermochemistry of transition metal sulfides. Oxid Met. 1977;11:307–20.

Publisher's Note

minerals

MDPI

Article

Chemical and Phase Reactions on the Contact between Refractory Materials and Slags, a Case from the 19th Century Zn-Pb Smelter in Ruda Śląska, Poland

Krzysztof Kupczak [1], Rafał Warchulski [1,*], Mateusz Dulski [2] and Dorota Środek [1]

[1] Institute of Earth Sciences, Faculty of Natural Sciences, University of Silesia, Będzińska 60, 41-200 Sosnowiec, Poland; krzysztof.kupczak@us.edu.pl (K.K.); dorota.srodek@us.edu.pl (D.Ś.)

[2] Institute of Materials Engineering, and Silesian Center for Education and Interdisciplinary Research, University of Silesia in Katowice, 75 Pulku Piechoty 1A, 41-500 Chorzow, Poland; mateusz.dulski@smcebi.edu.pl

* Correspondence: rafal.warchulski@us.edu.pl

Received: 6 October 2020; Accepted: 10 November 2020; Published: 12 November 2020

Abstract: Slags from the historic metallurgy of Zn-Pb ores are known for unique chemical and phase compositions. The oxides, silicates, aluminosilicates, and amorphous phases present therein often contain in the structure elements that are rare in natural conditions, such as Zn, Pb, As. The study focuses on processes occurring on the contact of the melted batch and the refractory materials that build the furnace, which lead to the formation of these phases. To describe them, chemical (X-ray fluorescence (XRF), inductively coupled plasma mass spectrometry (ICP-MS)) and petrological ((X-ray diffraction (XRD), electron probe micro-analyses (EPMA), Raman spectroscopy) analyses were performed on refractory material, slag, and contact of both. Two main types of reactions have been distinguished: gas/fluid- refractories and liquid- refractories. The first of them enrich the refractories with elements that migrate with the gas (Pb, K, Na, As, Zn) and transport the components building it (Fe, Mg, Ca) inward. Reactions between melted batch and refractory materials through gravitational differentiation and the melting of refractories lead to the formation of an aluminosilicate liquid with a high content of heavy elements. Cooling of this melt causes crystallization of minerals characteristic for slag, but with a modified composition, such as Fe-rich pyroxenes, Pb-rich K-feldspar, or PbO-As_2O_3-SiO_2 glass.

Keywords: slags; refractory material; zinc; lead; smelting; metallurgy

1. Introduction

One of the characteristic features of the Upper Silesia landscape is the presence of metallurgical waste dumps. These landfills are associated with a centuries-old history of smelting silver, lead, and zinc. The exploitation and processing of the ores in Silesia-Cracow region were carried out from the Mississippi Valley (MTV) type deposits [1]. Metallurgical activity in this region dates back to at least the 12th century, however, it can be assumed that primitive mining and related metallurgy had occurred much earlier [1]. In the past, waste generated during metal production was mostly transported and left in landfills. Due to the high content of heavy metals and other harmful elements, slag research mainly focuses on their impact on the environment [2–14]. Such studies are especially important due to the fact that currently, to reduce the amount of deposited slag, they are increasingly used by local enterprises [2,13]. Slag is most often used in the construction of local roads and the production of cement, concrete [3–5,9,15–18], and hydrotechnical constructions [19]. Metallurgical

waste landfills may also be used to recover metals contained therein. Live organisms (such as fungi, bacteria) can be used for this purpose [20–22]. Recently, slags have been used as the tool for recreating historic metal smelting methods [23–28]. Both in Poland and in the world, smelting temperature, type of oxidation-reduction conditions used in the metallurgical process, composition and amount of additives affecting production efficiency, and silicate melt properties (e.g., viscosity) were determined based on slags [24,25,28–34]. Slags phase composition and chemistry are also studied due to the unusual crystallization environment [3,17,34,35]. The uniqueness of this environment lies mainly in the crystallization of phases at undercooling conditions [24,30,35] and the presence of unique elements in the silicates, oxides, and glass phases [3]. The degree of undercooling has a significant e ect on the order, differentiation [24], and the habit of crystallizing slag phases [24,35]. Little is known about the ion diffusion between the melt and refractory materials and the formation of interaction zones between the melt and refractories. Existing studies [36] focus on the di erent types of refractory materials (made of $MgAl_2O_4$) and metal smelted (copper). Numerous studies [12,33,37,38] mention the occurrence of unique phases, mostly concentrating Potentially Toxic Elements (PTEs), within Zn-Pb slags, but none of them describes the reaction leading to their creation. In this study, we aim to describe such reactions related to the 19th century smelting process of zinc. Results shown in this study give new insight into the already recreated smelting process [27], explain the reactions leading to the formation of unique phases within slags, e.g., SiO_2-PbO-As_2O_3 glass, and suggest the environmental significance of the occurrence of slags with elements of refractory materials.

2. Location and Historical Smelting Process

Studied slag samples were collected at the metallurgical waste landfill located in Ruda Śląska, Silesian Voivodeship, Poland (Figure 1A). The investigated landfill is related to the activities of the "Hugo" zinc smelter, which operated in the years 1812–1932 [39]. The landfill is located less than 100 m from inhabited areas.

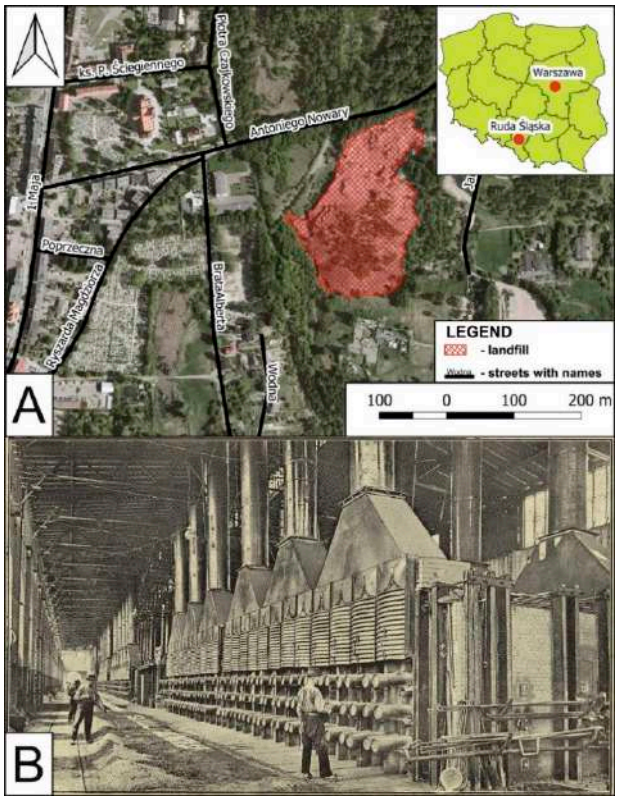

Figure 1. (**A**) Location map of the landfill in Ruda Śląska (based on data from geoportal.gov.pl [40]); (**B**) image showing a Silesian method smelting furnace from the Upper Silesia region [41].

In the case of 19th century zinc smelters in Upper Silesia, the so-called Silesian method of zinc smelting was widely used. It was a method developed by J.C. Ruberg around 1800 in the glassworks in Wesoła village located near Mysłowice city. Detailed documentation describing this process did not remain. However, it is known that calamine and sulfide ores were used and the production process was divided into several stages [27,41–43]: the ore enrichment, roasting, mixing with additives, smelting, and further processing (casting, rolling, etc.). For sulfide ores, the roasting process was crucial due to the necessity to oxidize the ore minerals and remove sulfur [27,43]. Then, the ores prepared in this way were mixed with coal (in later periods with coke) [41], fluxes, and placed with the help of shovels in horizontally arranged muffles (retorts) made of refractory clay (Figure 1B) [43,44]. Muffles lay flat within the continuously heated furnace. A zinc vapor condenser was tightly attached to each retort. The use of this type of furnace enabled the continuous operation of the smelter without cooling the entire system [43]. According to modern research, smelting temperatures at the Ruda Śląska site were within 1063–1261 °C [34]. The addition of coal to the batch resulted in reducing conditions.

3. Materials and Methods

3.1. Sampling

Slags containing elements of refractories occurred in the landfill when the worn muffles and furnace linings were replaced, or when these were damaged in the smelting process. The layers that are rich in refractive materials alternate with the typical glassy slag characteristic for this location [12,35]. To recreate the reactions on the contact between the refractories and slag melt, it was crucial to collect the material containing these elements, and the material should not show signs of weathering. The weathering process could lead to the leaching of some elements from both refractories and slags, influencing performed analyses. After careful investigations, five samples without signs of weathering or secondary mineralization (Figure 2) were selected from previous studies [12,35]. This was possible due to the collection of samples from the fresh exposure of the landfill wall after part of the dump was exploited for commercial purposes.

3.2. Phase Composition and Chemistry of Phases

3.2.1. Microscopic Observations, SEM-EDS and EPMA

Thin sections of samples were examined using an Olympus BX-51 optical microscope and scanning electron microscope (SEM; Thermo Scientific Phenom XL Desktop), equipped with an energy-dispersive spectrometer (EDS) at the Faculty of Natural Sciences, University of Silesia. Electron probe micro-analyses (EPMA) were performed using a CAMECA SX 100 electron microprobe (Inter-Institutional Laboratory of Microanalysis of Minerals and Synthetic Materials, University of Warsaw). Analyses were performed at 15 keV accelerating voltage, a 10–20.1 nA beam current, and a beam diameter of up to 5 μm. Standards used during EPMA analyses are shown in Table 1.

Table 1. Standards used during EPMA calibration.

Element	Standard	Element	Standard	Element	Standard
Na	$NaAlSi_3O_8$	Al	$KAlSi_3O_8$	Mn	$MnSiO_3$
As	GaAs	K	$KAlSi_3O_8$	S	$BaSO_4$
Si	$CaMgSi_2O_6$	Fe	Fe_2O_3	Ti	TiO_2
Mg	$CaMgSi_2O_6$	Zn	ZnS	Pb	$PbCrO_4$
Ca	$CaMgSi_2O_6$	Ni	NiO	P	YPO_4
Cr	Cr_2O_3	Cl	$Na_4BeAlSi_4O_{12}Cl$	Ba	$BaSO_4$
Co	CoO	Sr	$SrSO_4$	V	V_2O_5

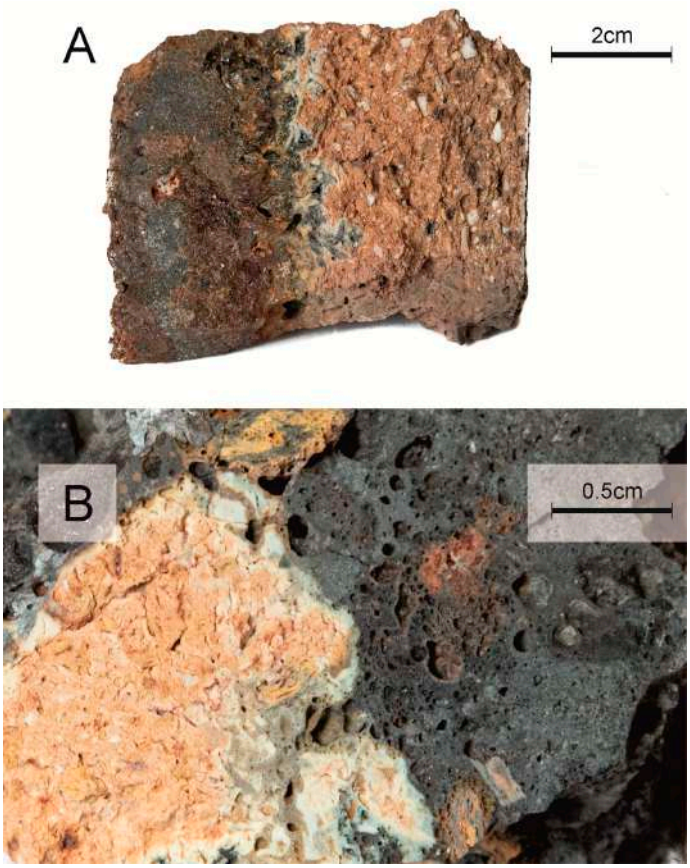

Figure 2. Macroscopic images of (**A**) representative slag sample and (**B**) its cross-section containing contact between slag (dark parts) and refractory materials (light parts).

3.2.2. Raman Spectroscopy

Raman measurements were carried out using a WITec alpha 300 R system equipped with a solid-state laser (λ = 488 nm) and a high sensitivity back-illuminated CCD camera at the Faculty of Natural Sciences, University of Silesia. The excitation laser radiation was coupled into a microscope through a single-mode optical fiber with a 50 μm diameter. An air Olympus MPlan (100×/0.90 na) objective was used during the experiment. Raman-scattered light was focused on multi-mode fiber (100 μm diameter). A grating with a 600 line/mm was applied. Spectra were collected in the 200–1800 cm^{-1} range, wherein each accumulated by 20 scans, the integration time of 10 s, and a resolution of 3 cm^{-1}. The low-frequency range below 200 cm^{-1} was luminescence-affected and it was not taken into account during further interpretation. The spectrometers' monochromator was calibrated using the Raman scattering line of a silicon plate (520.7 cm^{-1}). All data were manipulated in the post-processing approach by performing a baseline correction, cosmic ray removal, and peak fitting analysis in GRAMS 9.2 Software Package.

3.2.3. X-ray Diffraction

Two samples, best representing the uncontaminated refractory material, and slag were selected for chemical analysis and XRD. X-ray powder diffraction data were obtained using a PANalytical X'PERT PRO-PW 3040/60 diffractometer ($CoK_{\alpha 1}$ source radiation, Fe-filter to reduce the K_{β} radiation, and X'Celerator detector), at the Faculty of Natural Sciences, University of Silesia. The analysis was performed in the angular range of 5–90° 2θ with a shift step of 0.02° 2θ, the lamp current voltage was 40 kv at 40 mA. Quantitative data processing was performed using the X'PERT High Score Plus software using the PDF4+ database, and applying the Rietveld method. The Rietveld method uses

least squares approach to match the theoretical profile line with measured peak intensity of a powder sample, thus minimizing the residual function, and refining the crystal structure of the compound.

3.3. Bulk Chemical Composition

The bulk chemical compositions of the primary slags were analysed at Bureau Veritas Mineral Laboratories by a combination of X-ray fluorescence (XRF) spectrometry and inductively coupled plasma mass spectrometry (ICP-MS) for a broader spectrum of major, minor, and trace elements. Sample preparation consisted of $LiBO_2$ fusion for XRF and lithium tetraborate decomposition and Aqua Regia digestion for ICP-MS. Loss-on-Ignition was determined prior to XRF at 1000 °C. The analytical reproducibility for bulk chemical analyses was estimated from a replicate analysis of slag sample. The uncertainty (2σ) ranges from 0.00% to 0.23% for Fe_2O_3, relative standard deviation (RSD) ranges from 0% to 47.14% for Cr_2O_3. Analytical accuracy was calculated with standards OREAS184, SY-3(D), OREAS45E, OREAS25A-4A. Error is within range of 0.0–0.2% for SiO_2, while relative error ranges from 0.0% to 7.22% for Sr.

4. Results

4.1. Chemistry

The refractory material consists of SiO_2 (65.70 wt.%), Al_2O_3 (29.08 wt.%), Fe_2O_3 (2.38 wt.%), TiO_2 (0.73 wt.%), K_2O (0.59 wt.%), CaO (0.41 wt.%), and MgO (0.30 wt.%) (Table 2). Among the trace elements, the following are distinguished above 100 ppm: Zn (223 ppm), Pb (145 ppm), Zr (113 ppm) (Table 2).

Slags are mainly composed of SiO_2 (38.17 wt.%), Fe_2O_3 (22.71 wt.%), Al_2O_3 (15.81 wt.%), CaO (10.56 wt.%), MgO (5.73 wt.%), K_2O (1.58 wt.%), and MnO (0.41 wt.%) (Table 2). Additionally, the presence of Zn (>1%), Pb (3775 ppm), As (2155 ppm), Sr (590 ppm), Zr (156 ppm), V (141 ppm), Ni (141 ppm) is observed (Table 2).

Table 2. Chemical composition of slag and refractory material.

Oxide/Element	Concentration	Slag	Refractory Material
SiO_2	%	38.17	65.70
TiO_2	%	0.69	0.73
Al_2O_3	%	15.81	29.08
Fe_2O_3	%	22.71	2.38
Cr_2O_3	%	0.02	0.03
MnO	%	0.41	0.02
BaO	%	0.71	0.02
MgO	%	5.73	0.30
CaO	%	10.56	0.41
K_2O	%	1.58	0.59
Na_2O	%	0.27	0.06
P_2O_5	%	0.25	0.08
TOT/C	%	0.05	0.02
TOT/S	%	0.13	0.03
LOI	%	−0.3	0.0
V	PPM	141	97
Ni	PPM	141	135
Zn	PPM	>10,000	223
As	PPM	2155	23
Sr	PPM	590	64
Zr	PPM	156	113
Pb	PPM	3775	145

4.2. Phase Composition

Based on the X-ray diffraction data, the refractory materials consist of mullite ($3Al_2O_3 \cdot 2SiO_2$) (57.6 vol.%) and SiO_2 polymorphs (42.4 vol.%), in the form of quartz (15.9 vol.%), cristobalite (14.2 vol.%), and tridymite (12.3 vol.%) (Figure 3). Slag phase composition is dominated by feldspars with a total content of 48.3 vol.% (Figure 3). Among feldspars, anorthite ($CaAl_2Si_2O_8$) is the most abundant (34.4 vol.%) (Figure 3). As well as feldspar, pyroxenes (32.8 vol.%) are also distinguished with a cell corresponding to a diopside ($CaMg(Si_2O_6)$) (19.6 vol.%) and hedenbergite ($CaFe(Si_2O_6)$) (13.2 vol.%). The slag also contains quartz (8.3 vol.%), melilite (3.0 vol.%), and oxide phases (about 7.6 vol.%) (Figure 3). Among oxides, spinels (6.9 vol.%) are most common: magnetite (5.6 vol.%; $Fe^{2+}Fe^{3+}{}_2O_4$), and franklinite (1.3 vol.%; $ZnFe_2O_4$). Zincite (ZnO) occurs in the amount of 0.7 vol.% (Figure 3).

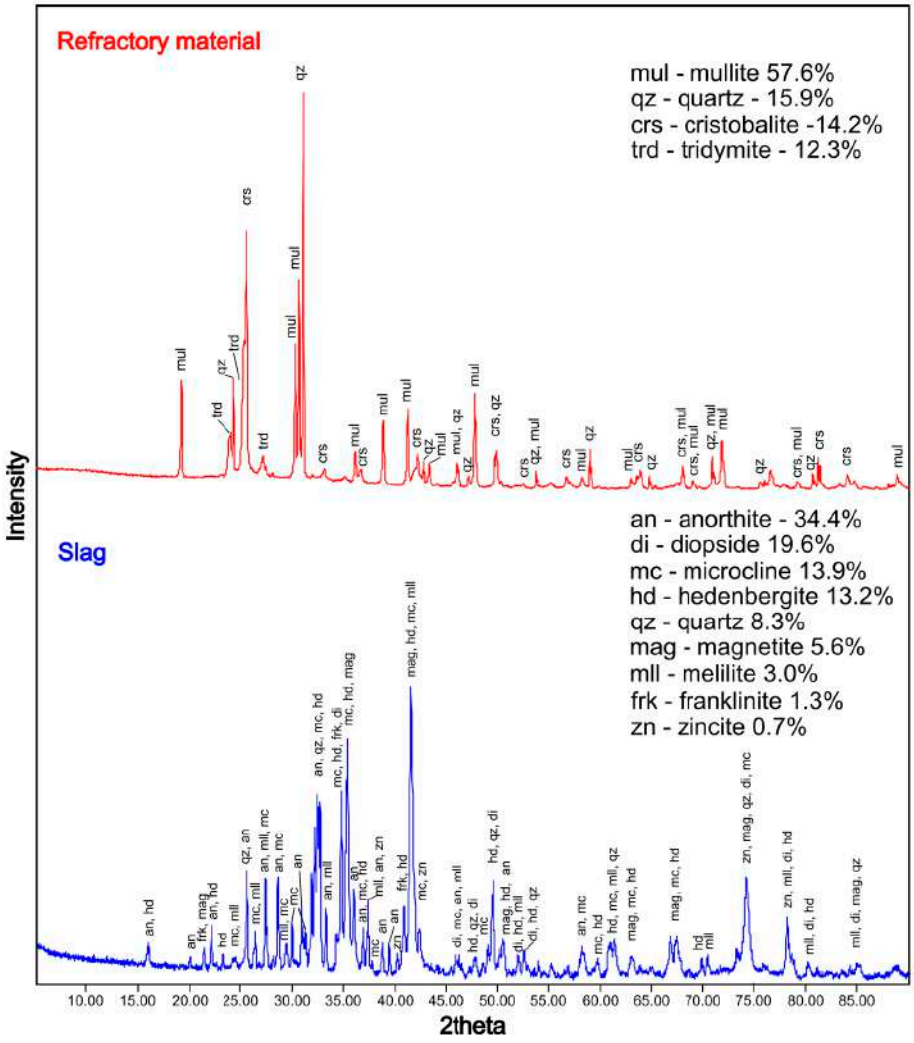

Figure 3. Diffraction pattern of slags and refractory material from Ruda Śląska.

According to SEM-EDS and EPMA, refractories are dominated by oxides and silicates (Figure 4A). Oxide phases are represented by quartz and its polymorphs, which occur in the analysed sample in the form of crystals with diameters from several dozen to about 200 μm (Figure 4A). Cracks were often observed in SiO_2 crystals (Figure 4A). Silicates occur as mullite. Its crystals are elongated without visible cracks, but with a visible zonal structure. The crystal length reaches up to 100 μm. Mullite also occurs in the form of a fine-grained binder (Figure 4A). Corundum (Al_2O_3; Table 3), occurs sporadically as small (up to 100 μm long) crystals with an euhedral structure. The lack of peaks corresponding to corundum on the diffractogram (Figure 3) is caused by its low content in the sample.

According to SEM-EDS and EPMA, slags are composed mostly of silicates and oxides. Feldspars, pyroxenes, melilites, and spinels were observed during SEM observations. Feldspars occur in the form of crystals with a diameter from several up to 60 μm (Figure 4B). Pyroxenes and melilites are mainly anhedral, and their size reaches several dozen μm (Figure 4B). Spinels form euhedral crystals with a diameter of up to 15 μm (Figure 4B).

During microscopic observations, the area of impact of the metallurgical melt on the refractory material was visible (Figure 4D). The zone consists of phases characteristic for both of the aforementioned zones, but with different chemical compositions. New phases, which do not occur in unchanged slag or refractories were also found. In the contact zone, the most common phases are pyroxenes, potassium feldspars, SiO_2 polymorphs, and glass. Pyroxenes are in the form of crystals up to several hundred μm in length. In the area of melt interaction, feldspars are formed in the form of plates. The size of feldspars ranges from several dozen to several hundred μm. During the EPMA and SEM-EDS analyses, it was found that the feldspars crystallizing from the melt near the refractories are often overgrown with fine anhedral quartz crystals (Figure 4C). The size of SiO_2 crystals ranges from a few to a dozen or so μm (Figure 4C). Due to the lack of X-ray structural data in the micro area, it cannot be determined which polymorphs of SiO_2 and in what proportions are occurring in this zone. However, taking into account the temperature during smelting, they are most likely high-temperature varieties such as tridymite or cristobalite. Glasses occurring in the studied slags fill the space in between other phases (Figure 4C). Mullite, corundum, and alumohematite ($(Fe,Al)_2O_3$) are also present in the contact zone. Mullite forms the small crystals with a diameter up to several μm with a homogeneous structure. Corundum occurs as euhedral crystals up to 100 μm in length. Alumiohematite crystals reach up to 20 μm.

Table 3. Representative EPMA data of the oxides.

Oxide	Refractory Material		Slag	Contact Zone	
	qz	crn	spl	qz	alhem
SiO_2	98.71	0.02	0.42	97.72	bd
TiO_2	bd	bd	0.69	bd	0.28
Al_2O_3	0.81	99.68	43.98	0.19	85.63
FeO_{calc}	-	-	13.74	0.28	na
Fe_2O_{3calc}	0.77	-	-	na	13.07
MnO	na	na	0.18	bd	bd
ZnO	na	na	36.79	0.22	na
MgO	na	na	2.94	bd	bd
CaO	0.29	na	bd	bd	0.11
K_2O	0.11	na	na	na	bd
Total	100.69	99.7	98.74	98.41	99.09
Element	**Atoms per formula unit**				
	qz	crn	spl	qz	alhem
Si	0.99	-	0.01	0.99	-
Ti^{4+}	-	-	0.02	-	-
Al	0.01	2	1.69	-	1.81
Fe^{2+}	-	-	0.37	-	-
Fe^{3+}	0.01	-	-	-	0.18
Mn	-	-	-	-	-
Zn	-	-	0.88	-	-
Mg	-	-	0.14	-	-
Ca	-	-	-	-	-
K	-	-	-	-	-
O^{2-}	2.00	3.00	4.00	2.00	3.00

Abbreviations: bd—below detection limit, na—no data, alhem—alumohematite, crn—corundum, spl—spinel, qz—quartz.

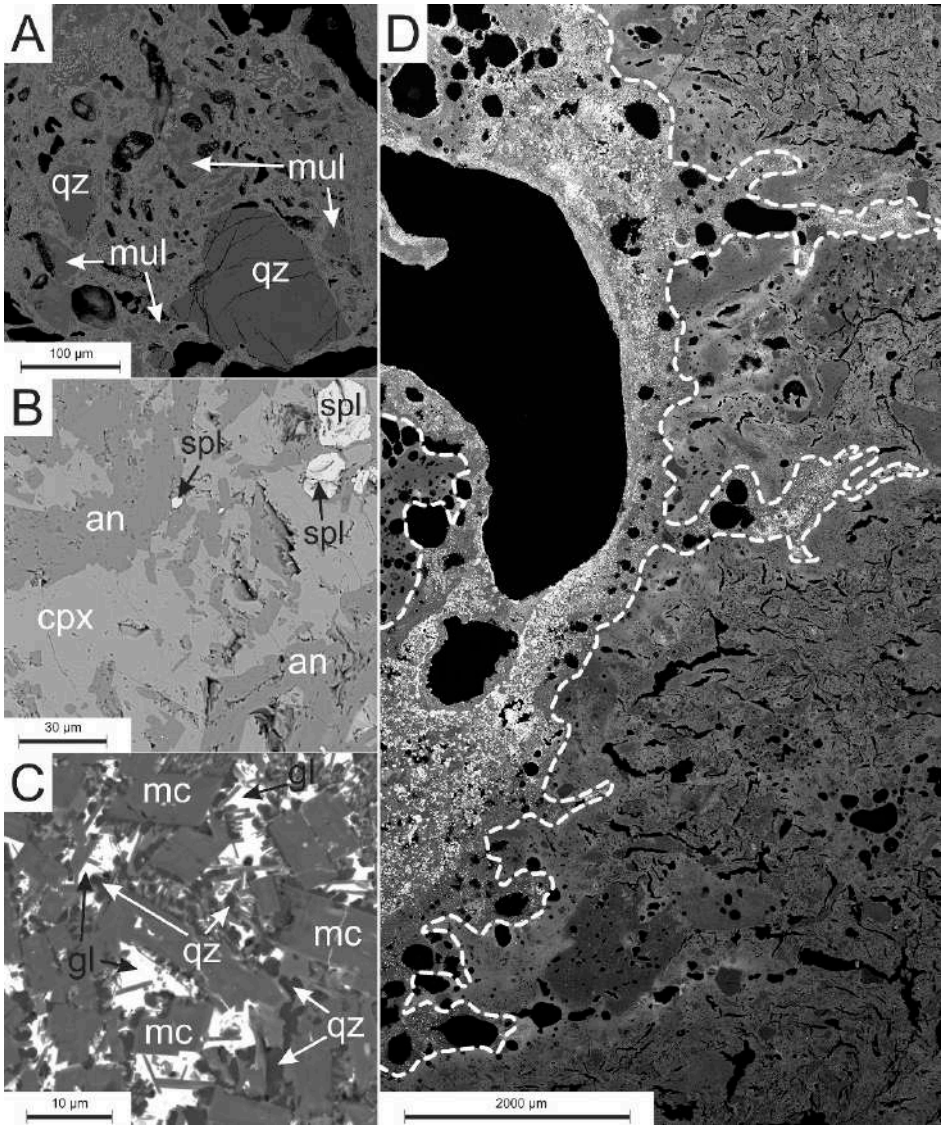

Figure 4. BSE (Backscattered Electrons) image of: (**A**) refractory material, (**B**) slag, (**C**) the contact zone of the slag with the refractories, (**D**) the intrusion of slag melt (left side of the dotted line) within refractory material (right side). Abbreviations: an—anorthite, cpx—clinopyroxene, gl—glass, mc—microcline, mul—mullite, spl—spinel, qz—quartz.

4.3. Chemistry of Phases

4.3.1. Oxides

Oxides in the analysed refractory material occur in the form of SiO_2 polymorphs and corundum crystals. In SiO_2 crystals, small amounts (<1 wt.% of oxide) of Al, Fe, Ca, and K were observed (Table 3). Corundum is almost pure (over 99.5 wt.% of Al_2O_3; Table 3).

In slags, oxides are represented by the spinel supergroup. Magnetite (Fe_3O_4)-gahnite ($ZnAl_2O_4$)-franklinite ($ZnFe_2O_4$) solid solution is the most common (Table 3). Spinels also concentrate Ti (up to 0.69 wt.% of TiO_2) and Mn (up to 0.18 wt.% of MnO) (Table 3).

At the contact zone of slag with refractory materials, the most common oxides are SiO_2 polymorphs. Silicon dioxide phases have a composition close to ideal with only minor amounts of Al (up to 0.19 wt.% of Al_2O_3), Fe (up to 0.28 wt.% of FeO), and Zn (up to 0.22 wt.% of ZnO) (Table 3). The occurrence of

alumohematite was sporadically observed within which small amounts of Ti (up to 0.28 wt.% of TiO) and Ca (up to 0.11 wt.% of CaO) were determined (Table 3).

4.3.2. Silicates and Aluminosilicates

Mullite is common in refractory materials. In the studied sample, despite SiO_2 and Al_2O_3, it concentrates Fe (up to 7.03 wt.% of Fe_2O_3) and Ti (less than 1 wt.% of TiO) (Table 4). Mullite crystals are characterized by chemical zonation. The zones are associated with differences in Fe and Al content, where the rim is relatively enriched in Fe (up to 7.10 wt.% of Fe_2O_3) (Table 4), replacing the Al_2O_3 (Table 4).

Table 4. Representative EPMA data for silicates occurring in the analysed samples.

Oxide	Refractory Material		Slag					Contact Zone				
	mul_{core}	mul_{rim}	cpx 1	cpx 2	mll	mc 1	an 1	cpx 3	mc 3	mc 4	an2	mul
SiO_2	25.55	26.23	44.23	48.74	37.91	62.31	44.94	48.96	60.29	42.40	45.97	25.89
TiO_2	0.90	0.74	0.22	0.72	bd	1.02	bd	0.15	0.36	0.11	bd	0.36
Al_2O_3	72.52	64.84	8.44	3.73	5.75	18.56	33.77	1.44	20.12	19.39	33.42	72.81
FeO^{calc}	-	-	8.96	5.83	5.86	-	-	24.12	-	0.76	-	na
$Fe_2O_3{}^{calc}$	0.87	7.03	-	-	-	0.66	1.62	-	0.41		1.45	0.40
MnO	na	na	0.60	0.48	0.87	bd	bd	1.23	bd	bd	bd	bd
ZnO	na	na	0.34	5.16	2.13	bd	0.29	5.67	bd	1.93	0.59	na
BaO	na	na	na	na	na	4.67	0.11	bd	4.83	0.43	0.19	na
MgO	na	na	10.60	12.55	8.05	bd	bd	9.61	bd	0.10	0.13	na
CaO	bd	bd	25.52	21.69	36.36	0.36	19.70	6.88	0.31	1.39	18.98	na
Na_2O	na	na	bd	0.21	0.67	0.79	0.51	0.12	0.86	0.27	0.17	na
K_2O	bd	bd	bd	bd	0.20	11.65	0.32	na	13.26	4.80	0.38	na
V_2O_3	na	na	bd	0.12	bd	na	na	na	na	na	na	na
Cr_2O_3	na	na	0.19	bd	0.20	na	na	na	na	na	na	na
PbO	na	na	na	na	na	bd	bd	bd	0.14	29.48	bd	na
Total	99.84	98.84	99.10	99.23	98.00	100.02	101.26	98.18	100.58	101.06	101.28	99.46
Element	Atoms per Formula Unit											
	mul_{core}	mul_{rim}	cpx 1	cpx 2	mll 10	mc 1	an 1	cpx 3	mc 3	mc 4	an 2	mul
Si	1.83	1.94	1.71	1.87	1.83	2.93	2.07	1.99	2.87	2.52	2.11	1.85
Ti^{4+}	0.05	0.04	0.01	0.02	-	0.04	-	-	-	-	-	0.02
Al	6.12	5.64	0.38	0.17	0.33	1.03	1.84	0.07	1.13	1.36	1.81	6.15
$Fe^{2+}{}_{calc}$	-	-	0.29	0.19	0.24	-	-	0.82	-	0.04	-	-
$Fe^{3+}{}_{calc}$	0.05	0.39	-	-	-	0.02	0.06	-	-	-	0.05	0.02
Mn	-	-	0.02	0.01	0.03	-	-	0.04	0.02	-	-	-
Zn	-	-	0.01	0.15	0.08	-	0.01	0.17	-	0.08	0.02	-
Ba	-	-	-	-	-	0.09	-	-	0.09	0.01	-	-
Mg	-	-	0.61	0.72	0.58	-	-	0.58	-	0.01	0.01	-
Ca	-	-	1.06	0.89	1.88	0.02	0.97	0.30	0.02	0.09	0.93	-
Na	-	-	-	0.02	0.06	0.07	0.05	0.01	0.08	0.03	0.02	-
K	-	-	-	-	0.01	0.70	0.02	-	0.80	0.36	0.02	-
V^{3+}	-	-	-	-	-	-	-	-	-	-	-	-
Cr^{3+}	-	-	0.01	-	0.01	-	-	-	-	-	-	-
Pb	-	-	-	-	-	-	-	-	-	0.47	-	-
O^{2-}	13.00	13.00	6.00	6.00	7.00	8.00	8.00	6.00	8.00	8.00	8.00	13.00

Abbreviations: bd—below the detection limit, na—no data, an—anortite, cpx—clinopyroxene, mc—microcline, mll—melilite, mul—mullite.

Mullite at the contact zone is chemically similar to this from refractories. It consists of Al (up to 72.81 wt.% of Al_2O_3), Si (up to 25.89 wt.% of SiO_2) and small amounts of Fe (up to 0.40 wt.% of Fe_2O_3), and Ti (up to 0.36 wt.% TiO) (Table 4). Apart from a small addition of Ti and Fe (Table 4), no significant substitutions were observed within the mullite crystals. Mullite does not occur in slags uncontaminated by refractories.

Feldspars are absent in refractory materials. In the slags, they are common and occur as both plagioclase and K-feldspar. Plagioclase forms a calcium member of the $NaAlSi_3O_8$-$CaAl_2Si_2O_8$ series (An_{93}). Additionally, Fe (up to 1.62 wt.% of Fe_2O_3), Zn, and Ba (less than 1% by weight oxide) substitutions were observed (Table 4). Potassium feldspars are represented by microcline ($KAlSi_3O_8$)

(Figure 3), with numerous substitutions, such as: Ba (up to 4.67 wt.% of BaO), Ti (up to 1.02 wt.% of TiO), and Na, Fe, Ca (less than 1 wt.% by oxide) (Table 4).

Feldspars occur often in the zone at the contact of slag with the refractory material. Plagioclases here are dominated by anorthite endmember (An_{96}) (Table 4). Additionally, Fe (up to 1.45 wt.% of Fe_2O_3) and, to a lesser extent Zn, K, Ba, and Mg were observed in the anorthites (Table 4). Potassium feldspars are more common in the contact area than in slags. Potassium feldspars from this zone are characterized by the significant Pb content in the range of 0.14–29.48 wt.% of PbO (Table 4). In addition to Pb, substitutions of Ba (up to 4.83 wt.% of BaO), Ca (up to 1.39 wt.% of CaO), Na (less than 1 wt.% of Na_2O), Fe (less than 1 wt.% of oxide), Ti (less than 1 wt.% of TiO_2), Mg (less than 1 wt.% of MgO), and sporadically Zn (up to 1.93 wt.% of ZnO) were observed (Table 4).

Pyroxenes are absent in refractory materials. In the slags, they have a composition corresponding to the diopside ($CaMgSi_2O_6$) (Table 4, Figure 5). In the tetrahedral positions that build Si_2O_6 chains, Si is replaced by Al (from 3.73 to 8.44 wt.% of Al_2O_3) (Table 4). The analysed pyroxenes also contain Zn (0.34–5.16 wt.% of ZnO) and small amounts of Ti, Na, Cr, and V (less than 1 wt.% of the oxide) in their structure (Table 4).

At the contact zone of the slags with the refractories, clinopyroxenes are common. Pyroxenes in the contact zone have a composition of the augite ($(Ca,Mg,Fe)(Mg,Fe)Si_2O_6$) (Table 4, Figure 5). In contrast to the pyroxenes from slags, here they are characterized by a low Ca content (up to 6.88 wt.% of CaO) (Table 4). The Si content in pyroxenes is up to 48.96 wt.% of SiO_2, Zn up to 5.67 wt.% of ZnO, Al up to 1.44 wt.% of Al_2O_3, Mn up to 1.23 wt.% of MnO, and small amounts of Ti and Na (less than 1 wt.% of oxide) were observed (Table 4).

Melilite group minerals were also distinguished within the slags. The EPMA analysis results allowed them to be classified as alumoåkermanite—$(Ca,Na)_2(Mg,Al,Fe^{2+})Si_2O_7$ (Table 4). Also, small substitutions of Zn (up to 2.13 wt.% of ZnO), Mn (up to 0.87 wt.% of MnO), Na (up to 0.67 wt.% of Na_2O), Cr (up to 0.20 wt.% of Cr_2O_3), and K (up to 0.20 wt.% of K_2O) occur in the melilite structure (Table 4).

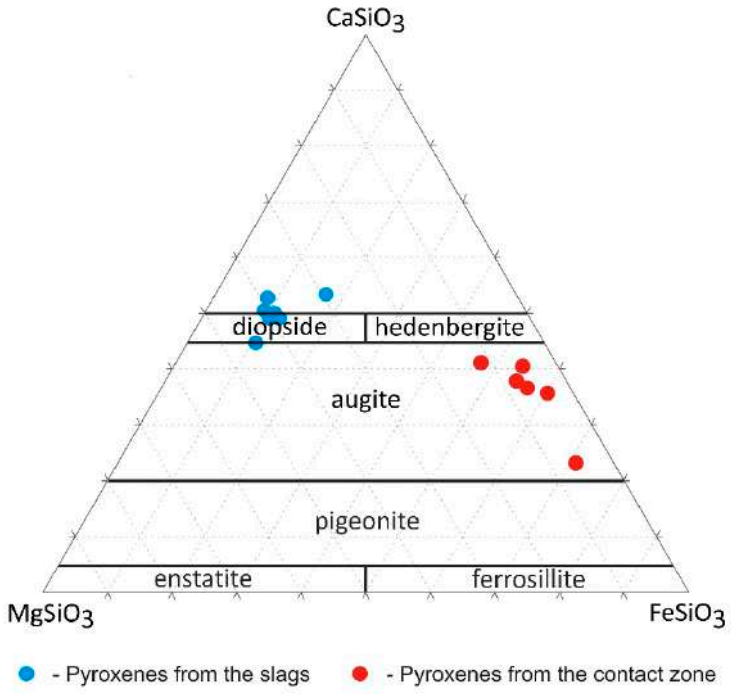

Figure 5. Ternary classification diagram of pyroxenes from the slags and the contact zone (based on Morimoto, 1988 [45]).

4.3.3. Glass

The largest accumulations of glass are present at the neighborhood of the pores and the direct contact with refractory material. These phases consist mainly of different proportions of SiO_2, PbO, and As_2O_3 (Table 5).

Table 5. Representative EPMA data of glass occurring at the contact zone of slag and refractory materials.

Oxide	gl 1	gl 2	gl 3	gl 4 *	gl 5 *
SiO_2	65.92	75.12	44.02	1.64	36.05
TiO_2	1.02	1.27	1.43	0.11	0.70
Al_2O_3	15.98	11.94	16.99	0.24	4.09
$Fe_2O_3^{calc}$	1.51	0.39	14.34	3.25	5.92
MnO	bd	bd	bd	0.22	0.56
ZnO	bd	1.23	na	2.68	6.60
BaO	2.22	0.23	13.43	bd	bd
MgO	0.16	bd	0.21	bd	bd
CaO	1.60	0.78	1.24	1.50	2.80
Na_2O	0.89	0.54	0.12	0.16	0.13
K_2O	9.41	5.92	6.27	0.42	0.21
PbO	bd	3.18	0.53	69.40	28.39
Sb_2O_5	bd	na	na	bd	bd
As_2O_3	bd	na	na	15.52	15.37
SO_3	bd	bd	0.26	1.98	bd
P_2O_5	na	0.14	na	na	na
Cl	bd	na	na	1.58	bd
Total	98.71	100.74	98.84	98.70	100.82

Abbreviations: gl—glass; bd—below detection limit; na—not analyzed; * data from [12].

Two main types of glass can be distinguished: SiO_2-dominated and PbO+As_2O_3-dominated. In silica-dominated glass, besides SiO_2 (44.02–75.12 wt.%; Table 5), the following elements concentrate: Al (11.94–16.99 wt.% of Al_2O_3); Fe (0.39–14.34 wt.% of Fe_2O_3); Ba (0.23–13.43 wt.% of BaO); K (5.92–9.41wt.% of K_2O); Ca (0.78–1.60 wt.% of CaO), Ti (1.02–1.43 wt.% of TiO_2), Pb (0.00–3.18 wt.% of PbO), and Zn (0.00–1.23 wt.% of ZnO) (Table 5).

Lead-arsenic glasses are impoverished in Si (1.64–36.05 wt.% of SiO_2), Al (0.24–4.09 wt.% of Al_2O_3) and K (0.21–0.42 wt.% of K_2O) and enriched in Zn (2.68–6.60 wt.% of ZnO); As (15.37–15.52 wt.% of As_2O_3), and Pb (28.39–69.40 wt.% of PbO) (Table 5).

To confirm the amorphous nature of the phases, a Raman analysis of the phase containing Si, As, and Pb was performed (Figure 6).

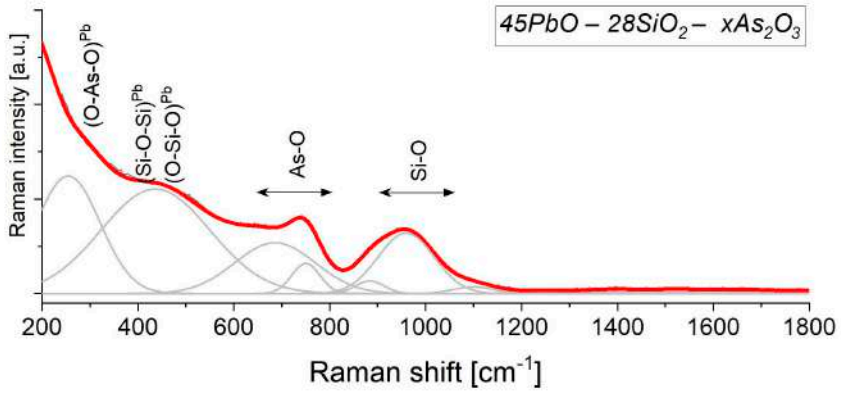

Figure 6. Raman spectrum of 45PbO-28SiO_2-xAs_2O_3 glass measured from Ruda Śląska slags. A peak-fitting analysis was done using Voigt function with preservation of the minimum number of components.

The high values of full-width at half-maximum observed related to the PbO-SiO_2-As_2O_3-Al_2O_3 material may suggest a more or less ordered network. Considering previous studies [46–50], the character of bands in similar materials ascribed to the glassy character of the material. More precisely, isomorphic substitution of arsenic and aluminum ions in a silica glass network leads to the formation of As-O-Si and Al-O-Si linkages and AsO_4^{3-} or AlO_6^{4-} structural units, respectively, due to the bands centered at 257, 437, 690, 750 cm^{-1}. The position of those bands is slightly low considering what other papers reported in the literature [51]. The character and position of both bands is related to the elevated arsenic content and affected by the presence of lead ions occupied by the interstitial positions in the internal system. Three components at 879, 962, 1105 cm^{-1} may correspond to (1) orthosilicate or pyrosilicate units, (2) Si-OH stretching modes, (3) Q^2 units with two non-bridging oxygens, as well as (4) Si-O-Si asymmetric stretching in disilicate units.

5. Discussion

In the analysed slags, we can distinguish two types of reactions: gas-refractory materials and melt-refractory materials. The result of the first type of reaction is mainly the enrichment of refractory materials with elements characteristic for Zn-Pb slags. To a lesser extent, such reactions led to the formation of new (mainly amorphous) phases (Figure 7). The reaction of melt with refractory materials leads mainly to the crystallization of new phases, or modification of the chemistry of existing ones.

5.1. Reactions of the Gas Phase with Refractory Materials

As already mentioned, the smelting of zinc was carried out by converting it to a gaseous form, followed by condensation in condensers. As well as zinc, other components of the charge were also vaporized during the metallurgical process (Table 6). Together with rising pressure within the muffle due to the vaporization of solid phases, it resulted in the formation of fluid that penetrated the cracks and crevices present in the refractories. In high-temperature conditions and due to a change in local chemical equilibrium conditions, the chemistry of the phases building the refractory material changes, and the formation of new phases may occur (Figure 7).

The first type of transformation that took place between the fluid and the refractory material was the enrichment of the latter in PbO, K, As, Zn, and Na_2O. These elements migrate within refractories through the micropores and/or by diffusion. In the 19th-century metallurgical furnaces in Ruda Śląska, the temperature ranged approx. from 1000 to 1300 °C [34]. The PbO was present as a vapor after reaching a sufficiently high temperature, which for pure PbO is 1470 °C (Table 6). A suitable gas mixture composition could cause a reduction in the PbO boiling point (e.g., in the presence of As_2O_3, it can drop down to ca. 1000 °C [52]). The possibility of PbO evaporation (at temperatures of 1220–1320 °C) was also confirmed during research on the reduction of lead slags [53]. Potassium,

sodium, arsenic, and zinc also migrated in gaseous form due to the low boiling points (Figure 7, Table 6). The fluid enriched in PbO, K, As, Zn, and Na_2O reacted with the silicate phases occurring in refractories, causing them to release components through melting and/or diffusion. These components formed melt, which was pushed into the refractories (Figure 7). It was possible thanks to the lowering of the liquidus temperature of refractory materials to the conditions present during the smelting. Previous studies show that the liquidus temperature, with appropriate proportions for the SiO_2-PbO system, can start from 700 °C [54]. The presence of other ingredients further reduced the liquidus temperature [52]. Aluminum-bearing phases in refractories did not melt due to too high melting points, even considering the influence of slag-related elements on their liquidus (Figure 7). The liquid which originated from the melting/diffusion of elements from the refractory phases was composed of FeO/Fe_2O_3, CaO, and MgO with possible minor amounts of SiO_2 (Figure 7). It migrated inwards to the refractories until the point when temperature drop caused its recrystallization as submicroscopic phases (Figure 7). Its presence also limited further fluid migration (Figure 7).

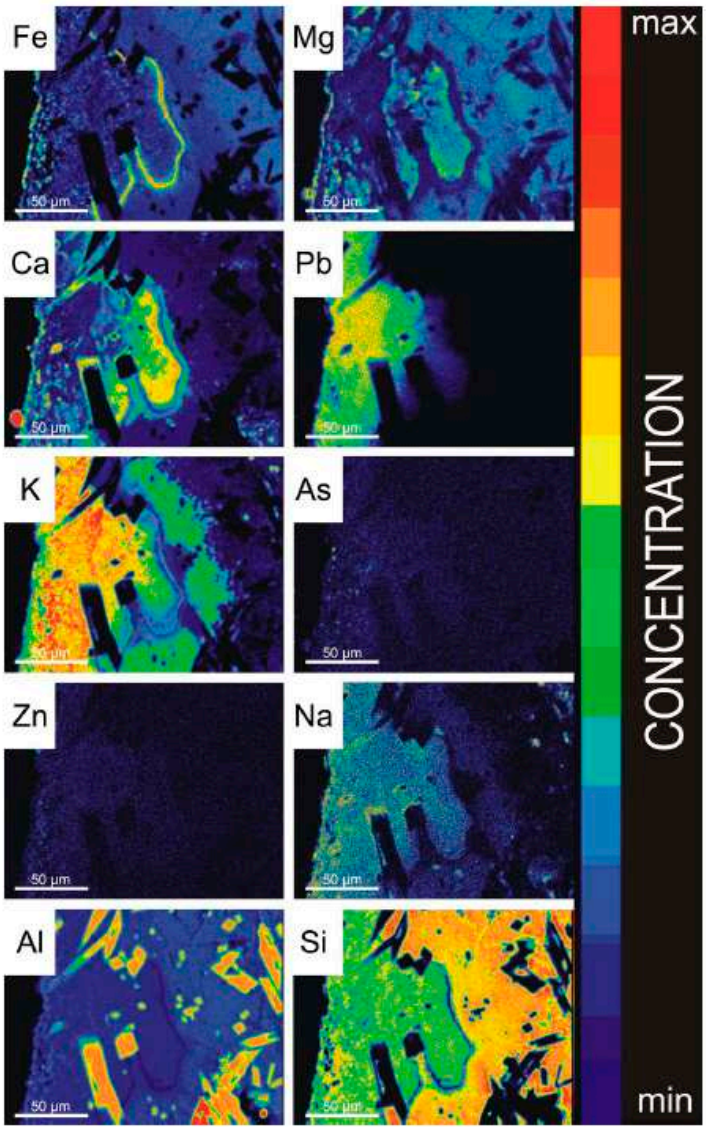

Figure 7. EPMA mapping showing concentrations of selected elements near the crack in the refractory materials.

5.2. Chemical and Phase Reactions on the Contact between Melt and Refractory Elements

In the melt from which slags crystallize, similar processes can be observed, which occur in the natural igneous intrusion. Therefore, the refractory components may be an equivalent to the rocks surrounding the igneous body.

Gravitational differentiation is one such process. In natural magmatic chambers, it occurs as fractional crystallization or as molecular differentiation [55]. Due to the long-term maintenance of high temperatures in the furnace, followed by the rapid cooling of the metallurgical melt, the phenomenon of selective phase crystallization and its sinking to the bottom is limited. For this reason, it can be assumed that after complete liquefaction of the metallurgical charge, the movement of molecules within the melt played a greater role. Compounds and elements with higher density, e.g., Fe or Pb (Table 6), during heating in the furnace, moved to the bottom of the retort and accumulated on the border with the solid (refractory material).

The enrichment of the phases in contact with the refractories in the Pb observed during the analysis may be due to gravitational differentiation during heating (before all the material was melted). Due to the low melting point (290 °C) (Table 6), the plattnerite (PbO_2) present in the feed material liquefied before effective reduction began. The liquid form combined with high density (Table 6) enabled migration towards the bottom of the muffle already at the initial stages of the metallurgical process when other components were present in solid form. Then, during further heating, PbO_2 disintegrated into PbO + O_2 (Table 6). In this way, at the bottom of the muffle, zones of high density and increased oxygen content (from the breakdown of PbO_2) were created, which weakened their reduction by C or CO. In this way, it was possible at a later stage to develop Pb-enriched mineral phases.

A similar situation occurred in the case of As_2O_3, whose melting point is just over 300 °C (Table 6). At a time when the furnace was at a relatively low temperature (~300 °C), As, along with the Pb migrated as a liquid, formed PbO_2-As_2O_3 melt, and at a later stage, PbO-As_2O_3 melt.

Due to the high melting point (Table 6), in contrast to Pb and As, iron oxides did not melt and migrate in the early stages of smelting. Iron oxides melted together with other charge components after obtaining the liquidus temperature of the entire system. For this reason, its migration was possible only through the molecular differentiation of the metallurgical melt. The high density favored the separation (Table 6), thanks to which the contact zone was enriched with phases with a high iron content (Tables 3–5, Figure 5).

Considering that the metallurgical process was not perfect, some of the Zn did not evaporate or was not reduced to the metallic phase and also moved to the lower parts of the retort. In the resulting zones enriched in heavy metals, phases were formed, of which Pb, Fe, and Zn were one of the main components. After reaching the liquidus point of the system, Si and other components (e.g., Ca, K) were added into the PbO-As_2O_3 melt.

Another phenomenon observed in the samples was further contamination of the melt with the elements building refractory materials (mainly Si and Al; Table 2). The assimilation of cover rocks by a hot melt is a common phenomenon in nature and was the reason for the emergence of separate rock types in many parts of the world [55]. For slag, the melt partially dissolved the outermost parts of the refractories. This process in Zn metallurgy is common and was described as corrosion of refractory materials by a melt [43]. The migration of components that build refractories to the slag melt was also reported in an experiment conducted by De Wilde et al. [36].

As a result of the cooling of this complex PbO_2-As_2O_3-rich melt, we observe crystallization of phases characteristic for a contact zone: alumohematite (Table 3), pyroxenes enriched in Fe and depleted in Ca (Table 4), and K-feldspar concentrating lead (up to 29.48 wt.% of PbO; Table 4). Similar type substitutions were described in slags after Zn production from other locations [9,33,34].

Table 6. Density and melting and boiling points of the most common melt/slag components [56] (*-data from [57]).

Component	Density [g/cm^3]	Melting Point [°C]	Boiling Point [°C]
Pb	11.34	327.4	1740
Fe	7.87	1538	2861
Zn	7.13	419	907
As	5.78	817 [1]	614
Mg	1.74	649	1100
Ca	1.54	842	1484
Na	0.97	97.82	881.4
K	0.86	63.5	758.8
PbO	9.5	888	1470
PbO_2	9.38	290	[2]
FeO	5.7	1360	3414
Fe_2O_3	5.24	1565	[3]
ZnO	5.6	1975	2 360
As_2O_3	3.74	312.8 *	457.2 *
As_2O_5	4.3	315	[4]
MgO	3.58	2800	3600
CaO	3.34	2570	2850
Na_2O	2.27	1275	1275 [5]
K_2O	2.3	[6]	
Al_2O_3	3.97	2054	3000
SiO_2	2.6	1713	2230

[1] Arsenic melts only under high pressure. The given temperature applies to approx. 28 atm. [2] At a temperature of 330–570 °C, it decomposes to PbO [58]. [3] It decomposes to FeO at 1199.85 °C [59]. [4] At a temperature above 500 °C, it decomposes to As_2O_3 [60]. [5] Sublimes at melting point [56]. [6] It decomposes at 350 °C [56].

Due to the low melting temperatures (Table 6), Pb and As combined with residual (mainly SiO_2) and incompatible (mainly K_2O) components in the last stages of melt solidification formed an amorphous phase. These glasses were formed during the charge change, transport to the landfill, or at the landfill, because a rapid temperature drop was necessary for their creation. The occurrence of similar phases has been described in previous publications on the Zn metallurgy [9,12,33,34].

6. Conclusions

The study has proven that during the smelting of zinc in the 19th century metallurgical furnaces, reactions between the melt and the refractory materials took place. These include reactions of the batch components in the form of gas/fluid and liquid with refractories. Influence of gas/fluid manifested in the enrichment of parts of refractory materials in PbO, K, Na_2O, and, to a lesser extent, As and Zn, with simultaneous displacement and transport of FeO/Fe_2O_3, MgO, and CaO into the refractories. As a result of temperature drops deeper in refractories, these elements accumulated to form a layer of submicroscopic phases. The reaction between the melt and the refractive materials is related to several processes. The first is gravitational differentiation leading to the formation of the liquid composed of high-density compounds characterized by low melting points, mainly PbO and As_2O_3. After reaching higher temperatures, the liquid phase was additionally enriched with other components of the charge (Fe, and to a lesser extent Zn, K, Mg, Ca, and Si). These elements (except FeO) only partly influence the composition of high-PbO and As_2O_3 melt due to low concentrations or lower densities. Changing the local liquidus course triggers the second process, which is the corrosion of refractory materials building the muffles. Melting of the refractory phases (mainly mullite and SiO_2 polymorphs) enriches the PbO-As_2O_3 liquid in SiO_2 and Al_2O_3. The third process is the crystallization of two melts: PbO-As_2O_3-FeO-SiO_2-Al2O_3 at the contact with refractory materials and K_2O-MgO-CaO-SiO_2 filling the rest of the muffle. Crystallization of these melts leads to the formation of different assemblages: quartz + alumohematite + pyroxene + feldspars + mullite + glass building the contact zone and spinel

+ pyroxene + melilite + feldspar building the slag. Additional differences are visible in the chemistry of phases, where at the contact zone, they are enriched in PTEs (mainly Pb and As). As was proven in previous studies, slags containing such phases pose a high environmental threat.

Author Contributions: Conceptualization, K.K. and R.W.; data curation, K.K. and R.W.; formal analysis, K.K., R.W., M.D. and D.Ś.; funding acquisition, R.W. and M.D.; investigation, K.K., R.W., M.D. and D.Ś.; methodology, R.W.; project administration, R.W.; resources, K.K. and R.W.; supervision, R.W.; validation, K.K. and R.W.; visualization, K.K., R.W. and M.D.; writing—original draft, K.K.; writing—review and editing, R.W. and D.Ś. All authors have read and agreed to the published version of the manuscript.

Funding: This study was supported by the National Science Center (NCN) grant no. 2016/21/N/ST10/00838 (awarded to RW), National Science Center (NCN) grant no. 2017/26/D/ST8/01117 (awarded to MD) and National Science Center (NCN) grant no. 2019/35/O/ST10/00313 (awarded to KK).

Conflicts of Interest: The authors declare no conflict of interest.

References

1. Godzik, B.; Woch, M.W. History of mining in the Olkusz region. In *Natural and Historical Values of the Olkusz Ore-Bearing Region*; Polish Academy of Sciences: Krakow, Poland, 2015; pp. 29–37.
2. De Windt, L.; Chaurand, P.; Rose, J. Kinetics of steel slag leaching: Batch tests and modeling. *Waste Manag.* **2011**, *31*, 225–235. [CrossRef]
3. Ettler, V.; Legendre, O.; Bodean, F.; Touray, J.C. Primary phases and natural weathering of old lead-zinc pyrometallurgical slag from Príbram, Czech Republic. *Can. Miner.* **2001**, *39*, 873–888. [CrossRef]
4. Ettler, V.; Mihaliewic, M.; Touray, J.C.; Piantone, P. Leaching of polished sections: An integrated approach for studying the liberation of heavy metals from lead-zinc metallurgical slags. *Bull. Société Géologique Fr.* **2002**, *173*, 161–169. [CrossRef]
5. Kucha, H.; Martens, A.; Ottenburgs, R.; De Vos, W.; Viaene, W. Primary minerals of Zn-Pb mining and metallurgical dumps and their environmental behavior at Plombières, Belgium. *Environ. Geol.* **1996**, *27*, 1–15. [CrossRef]
6. Liu, T.; Li, F.; Jin, Z.; Yang, Y. Acidic leaching of potentially toxic metals cadmium, cobalt, chromium, copper, nickel, lead, and zinc from two Zn smelting slag materials incubated in an acidic soil. *Environ. Pollut.* **2018**, *238*, 359–368. [CrossRef] [PubMed]
7. Ming, X.; Faheem, M.; Linghao, Z.; Shan, L.; Xiao, H.; Binquan, J.; YanChyuan, S.; Dongwei, L. Solidification/stabilization of lead-zinc smelting slag in composite based geopolymer. *J. Clean. Prod.* **2019**, *209*, 1206–1215.
8. Mouni, L.; Belkhiri, L.; Bouzaza, A.; Bollinger, J.C. Chemical associations and sorption capacity of Pb and Zn: Column experiments on a polluted soil from the Amizour mining district (Algeria). *Environ. Earth Sci.* **2016**, *75*, 96. [CrossRef]
9. Piatak, N.M.; Seal, R., II. Mineralogy and the release of trace elements from slag from the Hegeler Zinc smelter, Illinois (USA). *Appl. Geochem.* **2010**, *25*, 302–320. [CrossRef]
10. Piatak, N.M.; Parsons, M.B.; Seal, R.R., II. Characteristics and environmental aspects of slag: A review. *Appl. Geochem.* **2015**, *57*, 236–266. [CrossRef]
11. Tyszka, R.; Kierczak, J.; Pietranik, A.; Ettler, V.; Mihaljevic, M. Extensive weathering of zinc smelting slag in a heap in Upper Silesia (Poland): Potential environmental risks posed by mechanical disturbance of slag deposits. *Appl. Geochem.* **2014**, *40*, 70–81. [CrossRef]
12. Warchulski, R.; Mendecki, M.; Gawęda, A.; Sołtysiak, M.; Gadowski, M. Rainwater-induced migration of potentially toxic elements from a Zn–Pb slag dump in Ruda Śląska in light of mineralogical, geochemical and geophysical investigations. *Appl. Geochem.* **2019**, *109*, 104396. [CrossRef]
13. Ettler, V.; Mihaljevič, M.; Jarošíková, A.; Culka, A.; Kříbek, B.; Majer, V.; Vaněk, A.; Penížek, V.; Sracek, O.; Mapani, B.; et al. Vanadium-rich slags from the historical processing of Zn–Pb–V ores at Berg Aukas (Namibia): Mineralogy and environmental stability. *Appl. Geochem.* **2020**, *114*, 1935–2016. [CrossRef]
14. Mendecki, M.; Warchulski, R.; Szczuka, M.; Środek, D.; Pierwoła, J. Geophysical and petrological studies of the former lead smelting waste dump in Sławków, Poland. *J. Appl. Geophys.* **2020**, *179*, 104080. [CrossRef]
15. Geseler, J. Use of stellworks slag in Europe. *Waste Manag.* **1996**, *16*, 59–63. [CrossRef]

16. Alwaeli, M. Application of granulated lead–zinc slag in concrete as an opportunity to save natural resources. *Radiat. Phys. Chem.* **2013**, *83*, 54–60. [CrossRef]
17. Warchulski, R.; Gawęda, A.; Janeczek, J.; Kądziołka-Gaweł, M. Mineralogy and origin of coarse-grained segregations in the pyrometallurgical Zn-Pb slags from Katowice-Wełnowiec (Poland). *Mineral. Petrol.* **2016**, *110*, 681–692. [CrossRef]
18. Zieliński, K.; Rzeszowski, M. Wykorzystanie odpadów hutniczych w przemyśle cementowym. *Hut. Wiadomości. Hut.* **2007**, *74*, 610–615.
19. Motz, H.; Geiseler, J. Products of steel slags an opportunity to save natural resources. *Waste Manag.* **2001**, *21*, 285–293. [CrossRef]
20. Bosecker, K. Bioleaching: Metal solubilization by microorganisms. *FEMS Microbiol. Rev.* **1997**, *20*, 591–604. [CrossRef]
21. Fečko, P.; Zechner, V.; Guziurek, M.; Lyčková, B.; Pertile, E. Zastosowanie ługowania bakteryjnego do odpadów ze starych składowisk ekologicznych usytuowanych w regionie Karlove Vary. *Inżynieria Miner.* **2012**, *13*, 55–64.
22. Hołda, A.; Kisielowska, E. Biological removal of Cr(VI) ions from aqueous solutions by Trichoderma viride. *Physicochem. Probl. Miner. Process.* **2013**, *49*, 47–60.
23. Chiarantini, L.; Benvenuti, M.; Costagliola, P.; Fedi, M.E.; Guideri, S.; Romualdi, A. Copper production at Baratti (Populonia, southern Tuscany) in the early Etruscan period (9th–8th centuries BC). *J. Archaeol. Sci.* **2009**, *36*, 1626–1636. [CrossRef]
24. Ettler, V.; Cervinka, R.; Johan, Z. Mineralogy of medieval slags from lead and silver smelting (Bohutín, Příbram district, Czech Republic): Towards estimation of historical smelting conditions. *Archaeometry* **2009**, *51*, 987–1007. [CrossRef]
25. Ettler, V.; Johan, Z.; Zavřel, J.; Wallisová, M.S.; Mihaljevič, M.; Šebek, O. Slag remains from the Na Slupi site (Prague, Czech Republic): Evidence for early medieval non-ferrous metal smelting. *J. Archaeol. Sci.* **2015**, *53*, 72–83. [CrossRef]
26. Toffolo, L.; Addis, A.; Martin, S.; Nimis, P.; Rottoli, M.; Godard, G. The Misérègne slag deposit (Valle d'Aosta, Western Alps, Italy): Insights into (pre-)Roman copper metallurgy. *J. Archaeol. Sci. Rep.* **2018**, *19*, 248–260. [CrossRef]
27. Warchulski, R.; Juszczuk, P.; Gawęda, A. Geochemistry, petrology and evolutionary computations in the service of archaeology: Restoration of the historical smelting process at the Katowice–Szopienice site. *Archaeol. Anthropol. Sci.* **2018**, *10*, 1023–1035. [CrossRef]
28. Cabała, J.; Warchulski, R.; Rozmus, D.; Środek, D.; Szełęg, E. Pb-Rich slags, minerals, and pollution resulted from a medieval Ag-Pb smelting and mining operation in the Silesian-Cracovian region (Southern Poland). *Minerals* **2020**, *10*, 28. [CrossRef]
29. Burger, E.; Bourgarit, D.; Wattiaux, A.; Fialin, M. The reconstruction of the first copper-smeltingprocesses in Europe during the 4th and the 3rd millennium BC: Where does the oxygen come from? *Appl. Phys. A* **2010**, *100*, 713–724. [CrossRef]
30. Kierczak, J.; Pietranik, A. Mineralogy and composition of historical Cu slags from the Rudawy Janowickie mountains, southwestern Poland. *Can. Mineral.* **2011**, *49*, 1281–1296. [CrossRef]
31. Piatak, N.; Seal, R., II. Mineralogy and environmental geochemistry of historical iron slag, Hopewell Furnace National Historic Site, Pennsylvania, USA. *Appl. Geochem.* **2012**, *27*, 623–643. [CrossRef]
32. Ströbele, F.; Wenzel, T.; Kronz, A.; Hildebrandt, L.H.; Markl, G. Mineralogical and geochemical characterization of high-medieval lead–silver smelting slags from Wiesloch near Heidelberg (Germany)—An approach to process reconstruction. *Archaeol. Anthropol. Sci.* **2010**, *2*, 191–215. [CrossRef]
33. Warchulski, R.; Gawęda, A.; Kądziołka-Gaweł, M.; Szopa, K. Composition and element mobilization in pyrometallurgical slags from the Orzeł Biały smelting plant in the Bytom–Piekary Śląskie area, Poland. *Mineral. Mag.* **2015**, *79*, 459–483. [CrossRef]
34. Warchulski, R. Zn-Pb slag crystallization: Evaluating temperature conditions on the basis of geothermometry. *Eur. J. Mineral.* **2016**, *28*, 375–384. [CrossRef]
35. Warchulski, R.; Gawęda, A.; Kupczak, K.; Banasik, K.; Krzykawski, T. Slags from Ruda Śląska, Poland as a large-scale laboratory for the crystallization of rare natural rocks: Melilitolites and paralavas. *Lithos* **2020**, *372–373*, 105666. [CrossRef]

36. De Wilde, E.; Bellemans, I.; Campforts, M.; Guo, M.; Blanpain, B.; Moelans, N.; Verbeken, K. Investigation of high-temperature slag/copper/spinel interactions. *Metall. Mater. Trans. B* **2016**, *47*, 3421–3434. [CrossRef]
37. Puziewicz, J.; Zainoun, K.; Bril, H. Primary phases in pyrometallurgical slags from a zinc-smelting waste dump, Świętochłowice, Upper Silesia, Poland. *Can. Mineral.* **2007**, *45*, 1189–1200. [CrossRef]
38. Tyszka, R.; Pietranik, A.; Kierczak, J.; Zieliński, G.; Darling, J. Cadmium distribution in Pb-Zn slags from Upper Silesia, Poland: Implications for cadmium mobility from slag phases to the environment. *J. Geochem. Explor.* **2018**, *186*, 215–224. [CrossRef]
39. Jonczy, I.; Gawor, Ł. Coal mining and post-metallurgic dumping grounds and their connections with exploitation of raw materials in the region of Ruda Śląska. *Arch. Min. Sci.* **2017**, *62*, 301–311. [CrossRef]
40. Geoportal. Available online: geoportal.gov.pl (accessed on 10 July 2020).
41. Dębicki, J. *Przemysł Cynkowy. Szkic Historyczno-Gospodarczy*; Skład główny; Gebethner i Wolff: Warszawa, Poland, 1927.
42. Dobis, N. *Przemysł Cynku i Ołowiu w Polsce*; Chrześcijańska Drukarnia "Nakładowa": Będzin, Poland, 1938.
43. Domański, W.; Krupkowski, A. *Metalurgia Cynku i Kadmu*; Państwowe Wydawnictwo Naukowe: Warszawa, Poland, 1954.
44. Piernikarczyk, J. *Historia Górnictwa i Hutnictwa na Górnym Śląsku. Cz. 2*; Śląski Związek Akademicki: Katowice, Poland, 1936.
45. Morimoto, N. Nomenclature of Pyroxenes. *Mineral. Petrol.* **1988**, *39*, 55–76. [CrossRef]
46. Brawer, S.A.; White, W.B. Raman spectroscopic investigation of the structure of silicate glasses (II). Soda-alkaline earth-alumina ternary and quaternary glasses. *J. Non Cryst. Solids* **1977**, *23*, 261–278. [CrossRef]
47. McMillan, P. Structural studies of silicate glasses and melts—Applications and limitations of Raman spectroscopy. *Am. Mineral.* **1984**, *69*, 622–644.
48. Mysen, B.O.; Finger, L.W.; Virgo, D.; Seifert, F.A. Curve-fitting of Raman spectra of silicate glasses. *Am. Mineral.* **1982**, *67*, 686–695.
49. Neuville, D.R.; De Ligny, D.; Henderson, G.S. Advances in Raman spectroscopy applied to earth and material sciences. *Rev. Mineral. Geochem.* **2014**, *78*, 509–541. [CrossRef]
50. Seifert, F.A.; Mysen, B.O.; Virgo, D. Three-dimensional network structure of quenched melts (glass) in the systems SiO_2–$NaAlO_2$, SiO_2–$CaAl_2O_4$ and SiO_2–$MgAl_2O_4$. *Am. Mineral.* **1982**, *67*, 696–717.
51. Konijnendijk, W.L.; Buster, J.H.J.M. Raman-scattering measurements of silicate glasses containing sulphate. *J. Non-Cryst. Solids* **1977**, *23*, 401–418. [CrossRef]
52. Bale, C.W.; Bélisle, E.; Chartrand, P.; Decterov, S.A.; Eriksson, G.; Gheribi, A.E.; Hack, K.; Jung, I.H.; Kang, Y.B.; Melançon, J.; et al. FactSage thermochemical software and databases, 2010–2016. *Calphad* **2016**, *54*, 35–53. [CrossRef]
53. Jahanshahi, S.; Wright, S. Kinetics of reduction of CaO-FeOx-MgO-PbO-SiO_2 slags by CO-CO_2 gas mixtures. *Metall. Mater. Trans. B* **2017**, *48*, 2057–2066. [CrossRef]
54. Shevchenko, M.; Jak, E. Experimental phase equilibria studies of the PbO–SiO_2 system. *J. Am. Ceram. Soc.* **2018**, *101*, 458–471. [CrossRef]
55. Cullers, R.L. Magmatic processes. In *Geochemistry. Encyclopedia of Earth Science*; Springer: Dordrecht, The Netherlands, 1998; pp. 373–414.
56. Pubchem. Available online: https://pubchem.ncbi.nlm.nih.gov/ (accessed on 2 September 2020).
57. Perry, R.H.; Chilton, C.H. *Chemical Engineers' Handbook*, 5th ed.; McGraw-Hill: New York, NY, USA, 1973; p. 50.
58. Gavrichev, K.; Bolshakov, A.; Kondakov, D.; Khoroshilov, A.; Denisov, S. Thermal transformations of lead oxides. *J. Therm. Anal. Calorim.* **2008**, *92*, 857–863. [CrossRef]
59. Qu, Y.; Yang, Y.; Zou, Z.; Zeilstra, C.; Meijer, K.; Boom, R. Thermal decomposition behaviour of fine iron ore particles. *ISIJ Int.* **2014**, *54*, 2196–2205. [CrossRef]
60. Helsen, L.; Van den Bulck, E.; Van Bael, M.K.; Vanhoyland, G.; Mullens, J. Thermal behaviour of arsenic oxides (As_2O_5 and As_2O_3) and the influence of reducing agents (glucose and activated carbon). *Thermochim. Acta* **2004**, *414*, 145–153. [CrossRef]

Received: 1 April 2023 | Accepted: 22 November 2023

DOI: 10.1111/arcm.12940

ORIGINAL ARTICLE

SLAG—software for reconstruction of historical smelting processes based on slag properties

Krzysztof Kupczak | **Rafał Warchulski**

Faculty of Natural Sciences, Institute of Earth Sciences, University of Silesia in Katowice, Sosnowiec, Poland

Correspondence
Kupczak Krzysztof, Faculty of Natural Sciences, Institute of Earth Sciences, University of Silesia in Katowice, Będzińska 60, 41-200 Sosnowiec, Poland.
Email: krzysztof.kupczak@us.edu.pl

Funding information
Narodowe Centrum Nauki, Grant/Award Number: 2019/35/O/ST10/00313

Abstract

The publication presents the functions of the SLAG software created to recreate historical metallurgical processes. SLAG allows for determining the smelting temperature, the viscosity of the metallurgical melt, and the oxygen and sulfur fugacities during smelting. With software, both liquidus temperature and melt viscosity can be calculated using different models, covering the range of chemical compositions of historical slags as wide as possible. Based on thermodynamic calculations, SLAG allows the performance of O_2 and S_2 fugacity calculations in the temperature range of 1000–2000 K (727–1727°C). The range of applicability of other properties (viscosity and liquidus temperature) depends only on the limitations of individual models. Using SLAG, it is also possible to create predominance area diagrams (PADs) and diagrams that consider the viscosity's dependence on temperature for slag of a given chemical composition. Based on glass transition temperature (Tg) and melt fragility, it is also possible to reconstruct the conditions that prevailed during the various stages of historical glass manufacturing processes.

KEYWORDS

historical slags, liquidus temperature, predominance area diagrams, smelting, viscosity

INTRODUCTION

The potential to cast any shape made the ability to produce metals one of the essential factors in civilization's development (Milisauskas, 2011). Humanity began smelting activity using metals found in their native state (Patterson, 1971; Roberts et al., 2009). Over time, the increasing need for metallic products led to the development of metallurgy, which aimed to create

metal from ore (Patterson, 1971; Roberts et al., 2009). Depending on its properties, the smelted metal was then used to make necessary items, including agricultural tools, weapons, and jewelry (Milisauskas, 2011). The metallurgical process was usually carried out by heating the enriched ore with additives. An energy carrier was essential to the ore in the metallurgical process, often also acting as a reducer. Initially, wood was used for this purpose (Tylecote, 1987), and with technological progress, it was replaced with more efficient energy carriers—charcoal, coal, and coke (Kupczak et al., 2020; Tylecote, 1987). In some cases, the liquidus temperature of the enriched ores was low enough for smelting to be possible without any other additions (Craddock, 1995). Still, in most cases, it was necessary to add fluxes to lower the liquidus temperature (Milisauskas, 2011). Silicon dioxide (SiO_2) and calcium carbonate ($CaCO_3$) were most often used for this purpose (Potysz et al., 2015; Warchulski et al., 2020). Besides lowering the liquidus temperature, they led to slag formation during the metallurgical process. When the metallurgical charge was heated, a melt was formed, which gravitationally separated into desirable metallic layer and varied layers being the waste products: slag (silicate melt with the lowest density), matte (sulfide melt with medium density), and speiss (arsenide and antimonide melt with highest density) (Khatibi, 2008; Rehren et al., 2012). Depending on the specific metal extraction and particular technological process, some of the products might not occur. Also, pure metal could have been extracted in the independent technological stage, for example, from speiss/matte (Davenport, 2002; Kupczak et al., 2023). The possibility and efficiency of smelting depend on the type of metal, the nature of the ores, and the conditions prevailing during smelting, such as temperature, melt viscosity, and oxidation–reduction conditions (Crabb, 2018; Pater, 2014). Because metal was sold and used for its final purpose, wastes from the process are commonly the only remnants after it (e.g., Bielenin, 1992). As such, smelting wastes are an important record of these factors and can be used to retrieve information about historical smelting technology and civilization's advancement (Addis et al., 2016; Cadet et al., 2021; Derkowska et al., 2021; Kądziołka et al., 2020; Kupczak et al., 2023; Warchulski et al., 2022). Slags are the most common and stable waste from metallurgical processes, and as such, they are the most common object of research aimed at recreating historical metallurgical processes (e.g., Addis et al., 2016; Bassiakos & Catapotis, 2006; Derkowska et al., 2021; Ettler et al., 2009; Kupczak et al., 2023; Warchulski et al., 2020). Temperature is the most thoroughly described parameter that can be obtained from the study of slags. Based on phase diagrams, geothermometers, high-temperature experiments, and computer software, it is possible to determine slags' liquidus and solidus temperatures (Kądziołka et al., 2020; Warchulski, 2016; Westner et al., 2022). Knowledge of temperature conditions allows for determining the other smelting parameters. The viscosity of the metallurgical melt can be determined from the chemical composition combined with temperature conditions (Addis et al., 2016; Ettler et al., 2009). Knowing the phase composition of slags, we can determine the limits of oxygen fugacity and other gaseous components in the smelting furnace (Bassiakos & Catapotis, 2006; Kupczak et al., 2023).

Currently, wastes after smelting processes, especially slags, are considered valuable material for retrieving elements with more advanced smelting techniques (Potysz & Kierczak, 2019; Seyrankaya & Canbazoğlu, 2021; Wang et al., 2015) or are used for construction purposes (Song et al., 2021; Wang, 2016). For this reason, it is crucial to develop efficient tools for the slag-based studies of the historical smelting processes.

The main goal of the presented work was to develop computer software (SLAG; Data S1; Data S2) that will make it possible to efficiently and precisely determine the conditions prevailing during the crystallization of metallurgical slags (liquidus temperature, slag viscosity, oxidation–reduction conditions) using various approaches. SLAG software allows for temperature estimations using mathematical models. Viscosity is calculated for a given temperature and chemical composition of slags according to various models. The viscosity models have been chosen to cover the broad range of slag compositions. The SLAG software facilitates the

determination of oxidation–reduction conditions by generating predominance area diagrams (PADs) from which it is possible to read oxygen and sulfur fugacities, knowing the phase composition of slags. The reducible iron index (RII) is also calculated, which is used to determine how strongly the reductive environment prevailed during iron smelting.

METHODS

The SLAG software presented is available as open source. The 1.0 version can be downloaded from https://github.com/slagKupczak/SLAG.git (2023). The publication describes the functionality of the first version of the program—SLAG 1.0. The software was written in Python (version 3.10.4) using built-in (cmath, re, math), matplotlib (version 3.5.2), numpy (version 1.22.3), cProfile, and setuptools (version 58.1.0) libraries. To create a window application (Figure 1), tkinter (version 8.6) and ttkbootstrap (version 1.10.1) libraries were also used. The software is divided into four parts (tabs; Figure 1). The first tab (About) contains only information about the SLAG and references used (Figure 1a). The second tab ("Liquidus temperature") can be used to calculate the liquidus temperature of slags (Figure 1b). Within the next tab ("Viscosity"), it is possible to determine the viscosity of the metallurgical melt based on the given chemical composition and temperature (Figure 1c). In the last tab ("Predominance Area Diagrams"), the oxygen and sulfur fugacities at the thermodynamic equilibrium among metallic phases, oxides, and sulfides can be calculated for selected elements and a user-specified temperature (in °C; Figure 1d). It is also possible for SLAG software to draw a PAD for the given temperature and considering the selected phases.

To present the functionality of the software, smelting parameters were calculated for slags after Pb (Warchulski et al., 2020) and Cu (Addis et al., 2016; Kądziołka et al., 2020) production, as these are among the most frequently smelted metals in historical times. Studies of Warchulski et al. (2020) and Addis et al. (2016) present results for such parameters as smelting temperature, viscosity of the metallurgical melt, and oxidation–reduction conditions, and thus are perfect fit for the purpose of comparison of original results with the ones obtained with SLAG software. Results from Kądziołka et al. (2020) study were additionally used to present the liquidus temperature estimation function when the data are a good match to the models used in the software.

Liquidus temperature

The liquidus temperature (T_{liq}) is determined based on methods proposed by Dong et al. (2019), Mills et al. (2005), and Mills (2011).

Dong et al. (2019) model

$$\begin{aligned} T_{liq} = {} & a_1 X_{SiO_2} + a_2 X_{Al_2O_3} + a_3 X_{CaO} + a_4 X_{MgO} + a_{12} X_{SiO_2} X_{Al_2O_3} + a_{13} X_{SiO_2} X_{CaO} \\ & + a_{14} X_{SiO_2} X_{MgO} + a_{23} X_{Al_2O_3} X_{CaO} + a_{24} X_{Al_2O_3} X_{MgO} + a_{34} X_{CaO} X_{MgO} \\ & + a_{123} X_{SiO_2} X_{Al_2O_3} X_{CaO} + a_{124} X_{SiO_2} X_{Al_2O_3} X_{MgO} + a_{134} X_{SiO_2} X_{CaO} X_{MgO} \\ & + a_{234} X_{Al_2O_3} X_{CaO} X_{MgO} \end{aligned}$$

Temperature is in °C, X_i is the molar fraction of component i, and a_i are constants: $a_1 = 7842$; $a_2 = 40{,}231$; $a_3 = 7716$; $a_4 = 3888$; $a_{12} = -112{,}543$; $a_{13} = -27{,}435$; $a_{14} = -21{,}433$; $a_{23} = -90{,}112$; $a_{24} = 17{,}168$; $a_{34} = -10{,}365$; $a_{123} = 247{,}223$; $a_{124} = 33{,}451$; $a_{134} = 43{,}694$; $a_{234} = -119{,}393$.

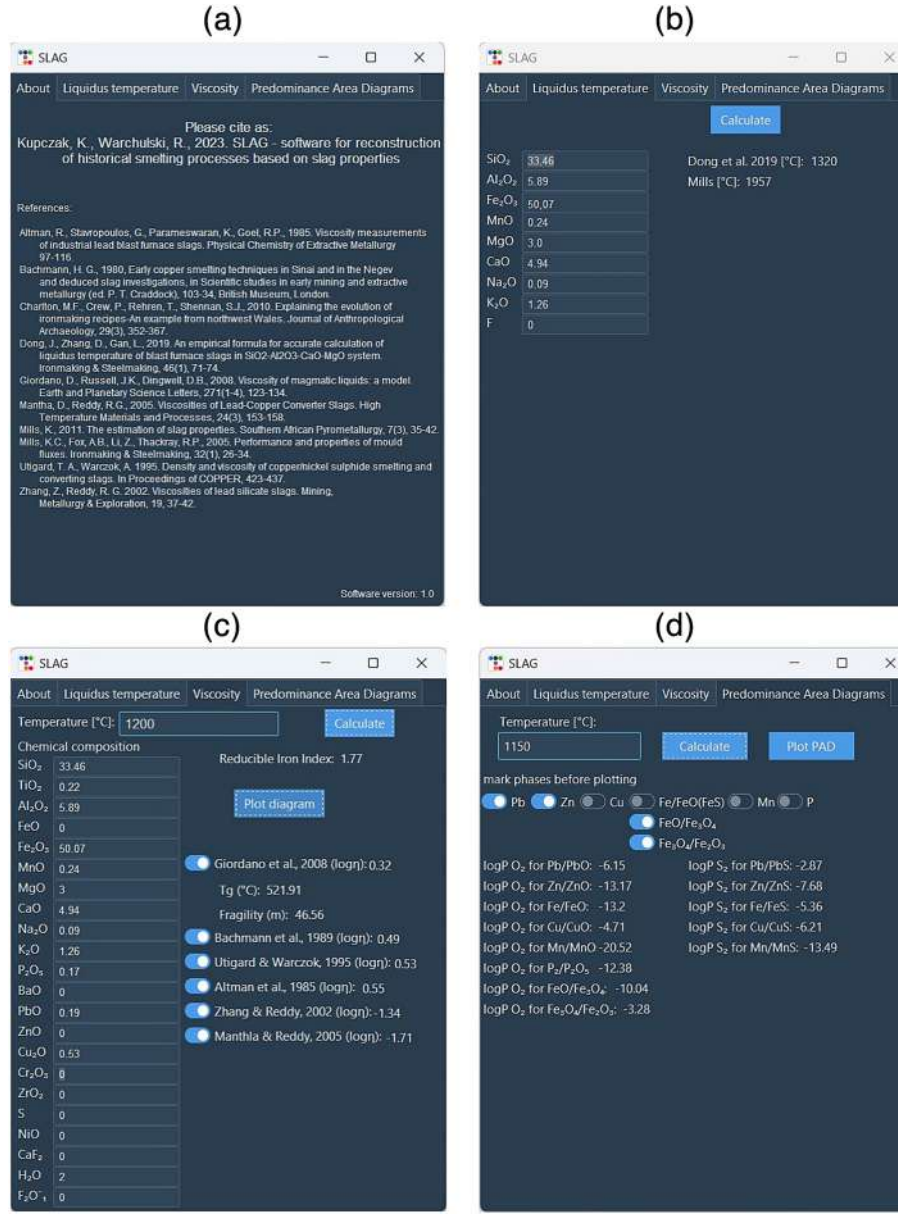

FIGURE 1 View of the running SLAG software: (a) first tab containing information about the software and references; (b) tab for calculating the liquidus temperature; (c) tab for calculating viscosity; (d) tab for determining oxygen and sulfur fugacity.

Mills model (Mills, 2011; Mills et al., 2005)

$$T_{liq} = 1191 + 11.4\%SiO_2 - 11\%CaO + 4.2\%Al_2O_3 + 5.7\%MgO - 10.1\%Na_2O - 15.8\%K_2O + 1.9\%F + 8.3\%Fe_2O_3 + 11.6\%MnO$$

The temperature calculated by this model is in °C, and % is the weight % of components.

Viscosity

Melt viscosity is determined based on models proposed for natural melts (Giordano et al., 2008) and slags (Bachmann et al., 1989; Mantha & Reddy, 2005; Utigard & Warczok, 1995). Depending on the model, viscosity is calculated as follows.

Giordano et al. (2008) model

$$\log\eta = A + \frac{B}{T(\mathrm{K})} - C$$

where $A = -4.55$ and B, C are calculated based on % mol as follows:

$$\begin{aligned} B = {} & (159.6 * (SiO_2 + TiO_2)) + (-173.3 * Al_2O_3) + (72.1 * (FeO + MnO + P_2O_5)) + (75.7 * MgO) \\ & + (-39.0 * CaO) + (-84.1 * (Na_2O + H_2O + F_2O_{-1})) \\ & + (141.5 * (F_2O_{-1} + H_2O + ln(1 + H_2O))) + (-2.43 * (SiO_2 + TiO_2)) \\ & * (FeO + MnO + MgO) + (-0.91 * (SiO_2 + TiO_2 + Al_2O_3 + P_2O_5) * (Na_2O + K_2O + H_2O)) \\ & + (17.6 * (Al_2O_3) * (Na_2O + K_2O)) \end{aligned}$$

$$\begin{aligned} C = {} & (2.75 * SiO_2) + (15.7 * (Al_2O_3 + TiO_2)) + (8.3 * (FeO + MnO + MgO)) + (10.2 * CaO) \\ & + (-12.3 * (Na_2O + K_2O)) + (-99.5 * \ln(1 + H_2O + F_2O_{-1})) \\ & + (0.3 * (Al_2O_3 + FeO + MnO + MgO + CaO - P_2O_5) * (Na_2O + K_2O) + H_2O + F_2O_{-1}) \end{aligned}$$

Bachmann et al. (1989) model (after Addis et al., 2016)

$$\log\eta_{(poise)} = -26.46 - 23.67 * \left(T_{(^\circ C)} * 0.001\right) - 3.12K + 3.84\left(T_{(^\circ \mathrm{C})} * 0.001\right)^3 + 0.59K^2$$

where the ratio of depolymerizing to polymerizing components (K) is calculated based on wt.% of components according to Addis et al. (2016):

$$K = \frac{CaO + MgO + FeO + MnO + TiO_2 + Na_2O + K_2O}{SiO_2 + Al_2O_3}$$

Utigard and Warczok (1995) model (UW model)

$$log\eta\left(\frac{kg}{m \cdot s}\right) = -0.49 - 5.1\sqrt{VR} + \frac{-3660 + 12080\sqrt{VR}}{T(\mathrm{K})}$$

The VR parameter is calculated as follows (components are in wt.%):

$$VR = \frac{(SiO_2) + 1.5(Cr_2O_3) + 1.2(ZrO_2) + 1.8(Al_2O_3)}{1.2(FeO) + 0.5(Fe_2O_3 + PbO) + 0.8(MgO) + 0.7(CaO) + 2.3(Na_2O + K_2O) + 0.7(Cu_2O) + 1.6(CaF_2)}$$

Altman et al. (1985) model

$$\log\eta = 1.06 * \log(CR) + \frac{6801.2}{T(\mathrm{K})} - 3.9881$$

where concentration ratio (CR) is calculated as follows (components are in wt.%):

$$CR = \frac{SiO_2 + Al_2O_3 + MgO}{CaO + FeO + ZnO + S}$$

Zhang and Reddy (2002) model

$$\ln\eta = \left(A_0 + \sum A_i X_{A(i)}\right) + \frac{\left(B_0 + \sum B_i X_{B(i)}\right) * 10^3}{T}$$

where T is the temperature in K, $X_{A(i)}$ and $X_{B(i)}$ are the wt.% of network-forming and depolymerizing oxides, respectively. The constants associated with the individual network-forming components ($X_{A(i)}$) are −31.981886 (A_0); 0.543124 (SiO_2); 0.548868 (Al_2O_3). The constants associated with the depolymerizing components ($X_{B(i)}$) are −26.840100 (B_0), 0.742236 (MgO), 0.683681 (CaO), 0.676625 (ZnO), 0.673338 (FeO), 0.717893 (PbO), 0.785696 (CuO), 0.677901 (NiO), 0.588837 (S), and 0.737147 (other). K_2O, Na_2O, TiO_2, and MnO were included among the other components.

Mantha and Reddy (2005) model

The model considers the temperature (T) in K, and the result is obtained in mPa·s. The calculations are based on the formula:

$$\log\eta = C1 * \log(BI) + \frac{C2}{R * T} + C3$$

where *C1* (1.637), *C2* (49859.112), and *C3* (−2.99) are the regression constants. R is the gas constant, and *BI* is the Basicity Index calculated as follows (Mantha & Reddy, 2005; concentrations of components are in wt.%):

$$BI = \frac{CaO + FeO + MgO + ZnO + BaO}{SiO_2 + Al_2O_3 + Cr_2O_3}$$

The results depending on the models are given in different units. In each case, they are converted to be in logη form in Pa·s. The SLAG software allows the user to enter both FeO and Fe_2O_3. In all cases where the model assumes only the presence of Fe^{2+}, the values entered by the user in the Fe_2O_3 field are converted to Fe^{2+} and added to the FeO.

The RII is also calculated in the Viscosity tab. The calculation is performed according to the formula (Charlton et al., 2010):

$$RII = \frac{2.39 * SiO_2}{FeO * MnO}$$

The formula takes into account the amount of components in the form of wt.% (Charlton et al., 2010).

PADs

Diagrams (PAD) are constructed based on the method and thermodynamic data described by Barin (1993) and based on the following reactions:

$$Me+\frac{1}{2}O_2=MeO;\ Me+\frac{1}{2}S_2=MeS;\ MeO+\frac{1}{2}S_2=MeS+\frac{1}{2}O_2 \text{ — for Pb, Zn, Fe, and Mn;}$$

$$2Cu+\frac{1}{2}O_2=Cu_2O;\ 2Cu+\frac{1}{2}S_2=Cu_2S;\ Cu_2O+\frac{1}{2}S_2=Cu_2S+\frac{1}{2}O_2 \text{ — for Cu;}$$

$$P_2+\frac{5}{2}O_2=P_2O_5 \text{ — for P.}$$

Determination of the reactions leading to the formation of sulfide and oxide phases made it possible to calculate the sulfur and oxygen fugacities using the equilibrium constant (K) based on the equations:

$\log K_1=\log K(MeO/Me_2O)$ — for the equilibrium constant between metallic and oxide phases

$\log K_2=\log K\,(MeS/Me_2S)$ — for the equilibrium constant between metallic and sulfide phases

$\log K_3=\log K_2-\log K_1$ — for the equilibrium constant between oxide and sulfide phases

Using log$K$, logP O_2 and logP S_2 were determined as follows:

$$\log P\,O_2=-2\,logK_1-2logP_{(metal)}$$

$$\log P\,S_2=-2\,logK_2-2logP_{(metal)}$$

$$\log P\,O_2=-2\,logK_3+2logP\,S_2$$

As the thermodynamic data are only available for a temperature interval of 100 K (Barin, 1993), graphs of the relationship between log$K$ and temperature were made. Then, by determining the formula of the function describing the relationship between log$K$ and temperature, the value of log$K$ is calculated for the given temperature. In the case of the reaction $P_2 + 5/2O_2 = P_2O_5$ the log$K$ value is calculated using the equation:

$$\log K=-\Delta G/(RT\ln 10)$$

(ΔG—Gibbs free energy, R—gas constant, T—temperature in K; Barin, 1993). The Gibbs free energy of P_2O_5 formation is calculated using the equation proposed by Turkdogan (2000):

$$\Delta G_T^{\circ}=-1\,655\,480+571.0T(\mathrm{K})$$

The equilibrium among FeO, Fe_3O_4, and Fe_3O_3 was determined from mineral buffers. Wüstite-magnetite (WM) and magnetite–hematite (MH) buffers are calculated using the reactions (Lindsley, 2018):

$$2x/(4x-3)Fe_3O_4 = 6/(4x-3)Fe_xO + O_2 \text{ — for WM buffer;}$$

$$6Fe_2O_3 = 4Fe_3O_4 + O_2 \text{ — for MH buffer.}$$

where $\log P\ O_2 = A/T(K) + B + C(P-1)/T(K)$. The values of A, B, and C are for the WM buffer −32,807, 13.012, 0.083, and for the MH buffer −25,700.6, 14.558, 0.019, respectively (Lindsley, 2018).

For temperatures above 1200°C, the oxygen fugacity is calculated using the equation proposed by Myers and Eugster (1983):

$$\log P\ O_2 = -36,951.3/T(K) + 16.092 \text{ — for MW buffer;}$$

$$\log P\ O_2 = -23,847.6/T(K) + 13.480 \text{ — for MH buffer.}$$

APPLICATION AND LIMITATIONS

Liquidus temperature

Determining the temperature conditions at which smelting was conducted is crucial because both melt viscosity and oxidation–reduction conditions are temperature dependent (Barin, 1993; Warchulski et al., 2020). There are many methods to determine the smelting temperature of historical smelting slags. The liquidus temperature can be determined using phase diagrams, high-temperature experiments, geothermometers, and computer software (Kądziołka et al., 2020; Warchulski, 2016; Warchulski et al., 2022). Several types of software are currently available that can be used to determine crystallization conditions, including liquidus temperature (de Capitani & Petrakakis, 2010; Ghiorso & Gualda, 2015; Gualda et al., 2012). Unfortunately, some of them, like FactStage and Thermo-calc, are not commonly used to reconstruct metallurgical processes due to high licensing costs. There are also open-source software designed for natural rocks like MELTS-Rhyolite and THERIAK-DOMINO software. Previous studies have successfully used MELTS-Rhyolite to determine the liquidus temperature of historical slags (e.g., Kądziołka et al., 2020). However, in some cases, the results differed significantly from the actual liquidus temperature (Kupczak et al., 2023; Warchulski et al., 2022). Simple mathematical models are also available based on which it is possible to determine the liquidus temperature of slags (Dong et al., 2019; Mills, 2011; Mills et al., 2005). Due to the variety of slags in terms of chemical composition, there is no single model appropriate for all types of slags. The SLAG software uses mathematical models proposed for modern slags. They can only be used for material with a chemical composition similar to the material based on which they were designed. In other cases, the differences in calculated temperature might be significant. The model proposed by Dong et al. (2019) was designed for blast furnace slags with chemical compositions in the range of SiO_2 (25–50 wt.%), Al_2O_3 (5–30 wt.%), CaO (25–50 wt.%), MgO (5–20 wt.%) with CaO/SiO_2 in the range of 0.6–1.6. The average error of temperature calculated using the Dong et al. (2019) model is 17.1°C (Dong et al., 2019). Mills model was proposed for mold fluxes, which usually consist of about 70 wt.% ($CaO + SiO_2$), up to 6 wt.% of MgO, 2–6 wt.% of Al_2O_3, 2–10 wt.% of $Na_2O(+K_2O)$, up to 10 wt.% of F with the addition of TiO_2, ZrO_2, B_2O_3, Li_2O, MnO, and C. The temperature is calculated with an accuracy of ±35°C (Mills et al., 2005).

Using the SLAG software to determine the liquidus temperature of slags after 16th–17th centuries Pb smelting (Sławków, Poland; Warchulski et al., 2020), results ranging from 1223 to 1903°C (Table 1) were obtained. The result calculated using the Dong et al. (2019) model exceeded the temperature determined by the authors for glassy slags (1150°C; Warchulski et al., 2020) by 73°C (1223°C; Table 1). A more significant error was for glassy slags and amounted to 753°C (1903°C; Table 1). In both cases, the errors result from the fact that the Dong et al. (2019) model was designed for materials with a different chemical composition. For crystalline slags, compliance in terms of chemical composition was visible for components such as SiO_2, CaO, and the CaO/SiO_2 ratio (Tables 1–2; Warchulski et al., 2020). For glassy slags, only SiO_2 content (Tables 1–2; Warchulski et al., 2020) corresponded to the materials for which the model was proposed. The temperature obtained using the Mills model (Mills, 2011; Mills et al., 2005) was also overestimated (1463–1651°C). In this case, incorrect results are also related to the lack of compliance of the chemical composition of the slags with the materials based on which the model was designed (Tables 1–2).

The liquidus temperature for slags after Cu production (Luserna, Trentino, Italy; Addis et al., 2016) calculated with SLAG software based on the Dong et al. (2019) model ranged from 1186 to 2783°C. The chemical composition of massive and flat slags met the model requirements only regarding SiO_2 content and Al_2O_3, and coarse slags only in Al_2O_3 content (Tables 1–2). The remaining requirements were not met, which resulted in incorrect results. Although in the case of coarse slags, there is no doubt that the result obtained is incorrect, for the remaining slags, the results are similar (1186°C for massive slags; Table 1) or are within the range given by the authors (1320°C for flat slags; Table 1). The Mills model (Mills, 2011; Mills et al., 2005) gave results in the range of 1957–2065°C. In this case, the incorrect temperatures result from the model not being designed for materials with this chemical composition.

Considering that the composition of the slags analyzed by Warchulski et al. (2020) and Addis et al. (2016) differs significantly from the scope for which the Mills model can be used, it was decided to compare results from an additional location after Cu smelting, the B1 site analysed by Kądziołka et al. (2020) (averaged chemical composition of slags from B1 location was used). Due to the high content of CaO and low Fe_2O_3, these slags have a chemical composition very similar to the materials for which the Mills model was designed. The temperature calculated by the Mills model using the SLAG software for these slags is 1414°C. This value is within the temperature range (1366–1445°C; Table 1) obtained by thermodynamic modeling using MELTS-Rhyolite software by Kądziołka et al. (2020). Because the research of Kądziołka et al. (2020) focused on determining temperature and no information on melt viscosity or oxidation–reduction conditions was given, these parameters were not determined using the SLAG software.

A comparison of the results regarding the liquidus temperature indicates that the Mills model can only be used to determine the temperature for materials with chemical compositions very similar to mold fluxes (1B slags; Table 1; Kądziołka et al., 2020). Mills model is susceptible to any deviations in terms of chemical composition. Even minor deviations from the range for which it was proposed give inflated results. In turn, despite some deviations from the chemical composition of the slags for which the Dong et al. (2019) model was proposed, it is possible to obtain results within the temperature range determined by other methods (Table 1).

Viscosity

In all models used in SLAG, the ratio of polymerizing to depolymerizing components of the crystal structure is considered. In some, the importance of all components is equal (Altman et al., 1985; Mantha & Reddy, 2005), and in others, each component has a factor by which it is multiplied (Giordano et al., 2008; Utigard & Warczok, 1995; Zhang & Reddy, 2002).

TABLE 1 Comparison of conditions during historical Pb (Warchulski et al., 2020) and Cu (Addis et al., 2016; Kądziołka et al., 2020) smelting provided by the authors with data obtained from the SLAG software.

		Slags after Pb smelting (Warchulski et al., 2020)		**Slags after Cu smelting (Addis et al., 2016)**			**Slags after Cu smelting (Kądziołka et al., 2020)**
Slag type		Glassy slag	Crystalline slag	Coarse slags	Massive slags	Flat slags	1B
SiO_2	wt.%	34.58	46.50	54.75	28.68	33.46	42.69
TiO_2	wt.%	0.11	0.15	0.20	0.20	0.22	0.72
Al_2O_3	wt.%	1.81	3.50	5.75	5.44	5.89	16.20
Fe_2O_3	wt.%	21.65	9.81	31.65	55.40	50.07	3.80
MnO	wt.%	0.20	0.18	0.14	0.22	0.24	0.26
MgO	wt.%	3.39	0.99	2.00	2.87	3.00	2.93
CaO	wt.%	11.19	30.39	2.94	4.30	4.94	26.64
Na_2O	wt.%	0.11	0.11	0.11	0.08	0.09	0.14
K_2O	wt.%	1.19	1.69	1.08	0.95	1.26	5.59
P_2O_5	wt.%	0.74	0.22	0.15	0.15	0.17	0.19
BaO	wt.%	0.16	0.03	nd	nd	nd	0.04
PbO	wt.%	>10.77	1.15	0.18	0.20	0.19	nd
ZnO	wt.%	16.50	3.52	nd	nd	nd	nd
Cu_2O	wt.%	0.01	bdl	1.18	1.70	0.53	0.42
CaO/SiO_2[a]		0.32	0.65	0.05	0.15	0.15	0.62
Liquidus temperature determined by authors		1150°C		1200–1330°C	1200–1330°C	1200–1350°C	1366–1445°C[b]
Liquidus temperature calculated by SLAG	Mills model	1651°C	1463°C	2065°C	1956°C	1957°C	1414°C
	Dong et al. (2019) model	1903°C	1223°C	2783°C	1183°C	1320°C	1175°C

TABLE 1 (Continued)

		Slags after Pb smelting (Warchulski et al., 2020)		Slags after Cu smelting (Addis et al., 2016)			Slags after Cu smelting (Kądziołka et al., 2020)
Viscosity (logη) determined by authors	Giordano et al. (2006) model	1.34 at 1150°C	1.48 at 1150°C	-	-	-	-
	Bachmann et al. (1989) model	-	-	From 1.26 (at 1400°C) to 2.09 (at 1200°C)	From −0.70 (at 1400°C) to 0.08 (at 1200°C)	From −0.30 (at 1400°C) to 0.49 (at 1200°C)	-
Viscosity (logη) determined by SLAG	Giordano et al. (2008) model	0.84 at 1150°C	2.40 at 1150°C	From 1.22 (at 1400°C) to 2.42 (at 1200°C)	From −0.53 (at 1400°C) to 0.47 (at 1200°C)	From −0.42 (at 1400°C) to 0.58 (at 1200°C)	-
	Bachmann et al. (1989) model	1.59 at 1150°C	1.86 at 1150°C	From 1.25 (at 1400°C) to 2.09 (at 1200°C)	From −0.76 (at 1400°C) to 0.08 (at 1200°C)	From −0.34 (at 1400°C) to 0.49 (at 1200°C)	-
	Utigard and Warczok (1995) model	0.76 at 1150°C	1.31 at 1150°C	From 0.88 (at 1400°C) to 2.23 (at 1200°C)	From −0.51 (at 1400°C) to 0.20 (at 1200°C)	From −0.28 (at 1400°C) to 0.53 (at 1200°C)	-
	Altman et al. (1985) model	0.71 at 1150°C	0.87 at 1150°C	From 0.39 (at 1400°C) to 0.95 (at 1200°C)	From −0.10 (at 1400°C) to 0.45 (at 1200°C)	From 0.00 (at 1400°C) to 0.55 (at 1200°C)	-
	Zhang and Reddy (2002) model	−0.25 at 1150°C	−0.44 at 1150°C	From −0.09 (at 1400°C) to −0.16 (at 1200°C)	From −2.06 (at 1400°C) to −1.55 (at 1200°C)	From −1.73 (at 1400°C) to −1.34 (at 1200°C)	-
	Mantha and Reddy (2005) model	−1.54 at 1150°C	−1.87 at 1150°C	From −2.83 (at 1400°C) to −2.34 (at 1200°C)	From −2.04 (at 1400°C) to −1.55 (at 1200°C)	From −2.19 (at 1400°C) to −1.71 (at 1200°C)	-
logP O_2 determined by authors		From −12.0 to −4.5		From −3.8 to −9.0			-
logP O_2 determined based on SLAG		From −10.04 to −3.28		From −3.00 to −9.26			-

Abbreviations: bdl, below detection limit; nd, no data available.
[a]Calculated.
[b]Temperatures obtained using MELTS modeling based on bulk chemical composition.

The Giordano et al. (2008) model was designed for natural rocks with a wide range of chemical compositions (Table 2). The model has been tested over a temperature range of 245–1705°C. The model also allows the determination of such melt properties as glass transition temperature (Tg) and melt fragility (m) (Giordano et al., 2008). Although the model was proposed for natural rocks, it can also be used for historical smelter slags under favorable circumstances. If the chemical composition of the slags falls within the range given by Giordano et al. (2008), the results obtained using it should be reliable, as was proven by the successful application of the earlier model proposed by Giordano et al. (2006) to reconstruct historical metallurgical processes (Ettler et al., 2009; Kupczak et al., 2023; Warchulski et al., 2022).

Because the chemical composition of slags can differ from that of natural rocks, especially in terms of metal content, the other models implemented within the SLAG software were created based on modern or historical slags. The model proposed by Bachmann et al. (1989) is one of the most widely used models when determining the viscosity of historical metallurgical slags (e.g., Addis et al., 2016; Berger et al., 2022). This model is based on viscosity measurements on modern copper slags. In this model, all chemical components are considered equally important (Bachmann et al., 1989). The UW model (Utigard & Warczok, 1995) was also proposed for slags formed during copper production. In this case, each component has a different weight. UW model is one of the few that consider the FeO and Fe_2O_3 independently (Utigard & Warczok, 1995). It is important because the degree of Fe oxidation affects the viscosity of the melt (Chevrel et al., 2013). The Altman model is one of the first to be proposed for slags after lead production. However, the model does not account for components such as PbO, CuO, Na_2O, or K_2O, which are often observed in slags and affect their viscosity (Altman et al., 1985; Schriner, 2018). High contents of PbO, CuO, and ZnO are often observed in slags after metal production from polymetallic ores. For this type of material, the best solution seems to be using a Zhang and Reddy (2002) model designed for temperatures of 1050–1433°C. The model is suitable for slags with low to very high contents of PbO (0.13–40.23 wt.%), CuO (up to 23.18 wt.%), and ZnO (0.54–24.0 wt.%; Table 2). The last model implemented within the SLAG software is the Mantha and Reddy (2005) model, which was also designed for lead slags. The model was tested for temperatures 927–1300°C. The model error is estimated at ± 32 mPa·s (Mantha & Reddy, 2005), although high accuracy is possible only within a very narrow range of chemical composition. The samples analyzed in the Mantha and Reddy (2005) model did not differ significantly in chemical composition (Table 2). For this reason, this model will work best for slags of similar chemical composition and in a similar temperature range. In other cases, deviations may be significant.

SLAG has the function of creating graphs of viscosity versus temperature for the analyzed chemical composition (Figure 2). The charts can be created over a temperature range of 1000–1400°C, which should be sufficient for most historical metallurgical processes (e.g., Cadet et al., 2021; Charlton & Humphris, 2019; Derkowska et al., 2021; Kupczak et al., 2023). The chart makes it possible to compare the viscosity variation as a function of temperature and the model used. The graphs are only created for models that have been previously selected by clicking on the check buttons (Figure 1c). This option allows the chart to be created only for models whose use is reasonable in terms of their range of applicability.

The viscosity (logη) determined by the authors for slags after historical Pb production in Sławków was from 1.34 to 1.48 Pa·s and was calculated based on the model of Giordano et al. (2006) (Warchulski et al., 2020). The Sławków slags contained high Pb, Zn contents (4.67–>27.27 wt.% of PbO + ZnO). For this reason, the authors used Giordano et al. (2006) model modified by Ettler et al. (2009), which included PbO and ZnO as depolymerizing components. Because the slags from Sławków were created as a result of Pb production (Warchulski et al., 2020), based on calculations made with the models of Altman et al. (1985) and Zhang and Reddy (2002), it can be assumed that the melt viscosity was even lower (from −0.44 to 0.87 Pa·s). However, in the case of the Zhang and Reddy (2002) model, the chemical

TABLE 2 Summary of viscosity models and the melt properties for which they were designed.

Model	Temperature range [°C]	Viscosity range [Pa·s]	Range of chemistry
Giordano et al. (2008)	245–1705	10^{-1}–$10^{13.8}$	SiO_2—41.0–79.0 wt.% TiO_2—0.0–3.0 wt.% Al_2O_3—0.0–23.0 wt.% FeO—0.0–12.0 wt.% MnO—0.0–0.3 wt.% MgO—0.0–32.0 wt.% CaO—0.0–26.0 wt.% Na_2O—0.0–11.0 wt.% K_2O—0.3–9.0 wt.% P_2O_5—0.0–1.2 wt.% H_2O—0.0–8.0 wt.% F—0.0–4.0 wt.%
Bachmann et al. (1989)	nd	nd	Modern copper slags
Utigard and Warczok (1995)	nd	nd	Modern copper slags
Altman et al. (1985)	1126–1298	nd	Lead slags containing SiO_2, Al_2O_3, CaO, FeO, ZnO, MgO, S
Zhang and Reddy (2002)	1050–1433	0.053–9.35	SiO_2—12.03–36.8 wt.% Al_2O_3—2.11–11.5 wt.% MgO—0.2–9.5 wt.% CaO—3.3–21.7 wt.% ZnO—0.54–24.00 wt.% FeO—9.37–34.7 wt.% PbO—0.13–40.23 wt.% CuO—0.00–23.18 wt.% NiO—up to 7.47 wt.% S—up to 6.8 wt.%
Mantha and Reddy (2005)	927–1200	nd	SiO_2—26.69–29.34 wt.% Al_2O_3—3.13–5.69 wt.% MgO—1.44–1.89 wt.% CaO—16.39–20.10 wt.% ZnO—7.11–7.84 wt.% FeO—29.91–32.52 wt.% PbO—0.87–2.70 wt.% CuO—0.43–0.69 wt.% NiO—up to 7.47 wt.% Cr_2O_3—0.10–0.63 wt.% BaO—0.39–0.74

Abbreviation: nd, no data available.

composition of the slags from Sławków does not correspond to the range for which it was designed (Tables 1–2; Warchulski et al., 2020). The best model for this type of slag seems to be the model of Altman et al. (1985), which indicates that the melt viscosity could be in the range of 0.71–0.87 Pa·s.

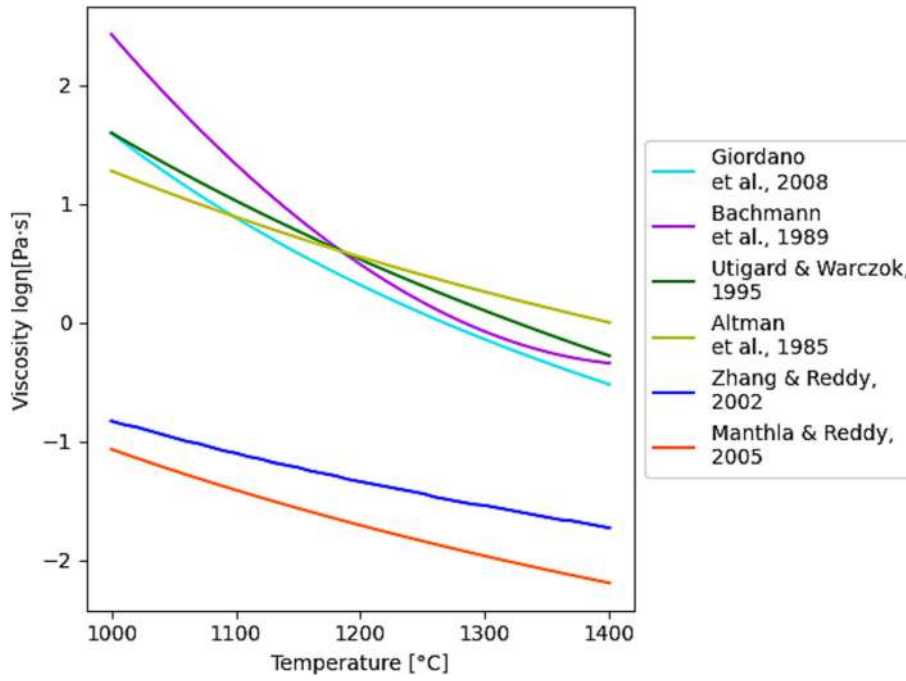

FIGURE 2 Viscosity chart generated by SLAG software based on the mean chemical composition of flat slags from Luserna (Addis et al., 2016).

For slags after Cu production from Luserna (Addis et al., 2016), the results obtained using the SLAG software according to the model of Bachmann et al. (1989) (logη from −0.34 to 2.09) are very close to those reported by the authors (from −0.30 to 2.09; Table 1; Addis et al., 2016). The differences in the calculations are caused by the fact that the authors normalized the chemical composition to 100 wt.%, most probably omitting PbO and CuO. Based on the second model designed for copper production slags (Utigard & Warczok, 1995), the viscosity range calculated with the SLAG software is similar to the results obtained with the model of Bachmann et al. (1989) (Table 1). Mantha and Reddy (2005) model gave significantly underestimated results because the chemical composition of slags (Table 1) differs significantly from the chemical composition range for this model (Table 2). The underestimated results using the Zhang and Reddy (2002) model are caused by too high SiO_2 content in coarse slags and FeO in massive and flat slags (Tables 1–2; Addis et al., 2016). The model of Altman et al. (1985) was designed for Pb slags. Still, for slags after Cu production from Lusern (Addis et al., 2016), the results are close to the values obtained based on Bachmann et al. (1989), Utigard and Warczok (1995), and Giordano et al. (2008) models (Figure 2).

PADs

In slags from processing the polymetallic ore, we often observe the co-occurrence of metallic, sulfide, and oxide phases of various metals (Bassiakos & Catapotis, 2006; Cadet et al., 2021; Derkowska et al., 2021; Warchulski et al., 2020). Iron buffers used in reconstructions of metallurgical processes allow oxygen fugacity to be determined only by the degree of oxidation of this element, omitting the other metals (Derkowska et al., 2021; Giacometti et al., 2014; Warchulski et al., 2022). Using the Ellingham diagram, it is possible to point out the oxygen and sulfur

fugacity in which co-occurrence of selected metallic, sulfide, and oxide phases is possible, assuming the local equilibrium or close-to-equilibrium conditions (Hasegawa, 2014; Shatynski, 1977). Still, Ellingham diagrams have some disadvantages. The diagrams available in the literature (e.g., Hasegawa, 2014; Shatynski, 1977) consider multiple metals on a single chart, which limits their readability. These diagrams also only consider the fugacity of oxygen or sulfur. None of Ellingham's diagrams simultaneously provide oxygen and sulfur fugacity data. The best solution to this problem seems to be using PADs, where we can mark the transitions among metallic, oxide, and sulfide phases.

Because thermodynamic data are available only for the temperature interval of 100 K (Barin, 1993), equilibrium constants for the other temperatures are determined using a graph that considers logK and temperature. The correctness of the calculations was verified by comparing the values obtained from SLAG software with those obtained directly from data contained in the Barin (1993) (Table 3). The differences in oxygen and sulfur fugacity calculated by the SLAG are less than 0.13. The vast majority are below 0.10 (Table 3). Similarly, compared to the diagrams presented by Xie et al. (2016), the values of $\log O_2$ and $\log S_2$ are consistent. In all cases, the differences (max. 0.13) are due to deviations in the thermodynamic (logK) data used in the calculations (Barin, 1993; Xie et al., 2016). Because the program is intended to determine smelting conditions in historical times, such minor differences may be considered acceptable. The possible inaccuracy of reading data directly from Ellingham diagrams or Fe buffers is more considerable.

SLAG software allows the determination of oxygen/sulfur fugacity for any temperature. Still, thermodynamic data are only suitable for a given temperature range. For most phases (Fe/FeO(FeS), Pb, Cu, Mn, Zn), the optimal range is 727–1727°C. In the thermodynamic equilibrium between FeO/Fe_3O_4, and Fe_3O_4/Fe_2O_3, the program allows for obtaining reliable results in the range 565–1300°C and 682–1270°C for WM and MH buffers, respectively (Lindsley, 2018; Myers & Eugster, 1983).

When determining the oxidation–reduction conditions during Pb smelting in Sławków, wüstite-magnetite ($\log P\ O_2 = -12$ atm) and magnetite–hematite ($\log P\ O_2 = -4.5$ atm) oxygen buffers at the temperature of 1150°C were used (Warchulski et al., 2020) from the diagram presented by Zhao et al. (1999). Based on the same buffers, oxygen fugacity ($\log P\ O_2$) was calculated in the range of −10.04 atm (wüstite-magnetite) to −3.28 atm (magnetite–hematite) using the SLAG software (Figure 3; Table 1). The narrower range of $\log P\ O_2$ in the case of SLAG software results from performing calculations for a specific temperature, which positively impacts the accuracy of the results compared to reading values from diagrams. In the case of the slags from Sławków, knowing that metallic Pb was produced during smelting and the fact that PbO was found in the slags, oxygen fugacity can be refined using the Pb/PbO thermodynamic equilibrium. The oxygen fugacity in which Pb and PbO occur in thermodynamic equilibrium at 1150°C is −6.15 atm (Figure 3). On this basis, it can be concluded that lead smelting was carried out in oxygen fugacity oscillating around −6.15 atm. The constructed PAD also explains the high Zn content in slags from Sławków (Warchulski et al., 2020). Conditions during smelting were not reducing enough to produce metallic Zn (Figure 3), which, at temperatures of the smelting process, would instantly vaporize and escape from the furnace. Instead, it concentrates in slags as ZnO, whose boiling point exceeds the temperature possible to obtain in such a furnace (2360°C).

For slags after copper production (Addis et al., 2016), based on the phase composition of the slags and the Ellingham diagram, the authors determined the oxidation–reduction conditions ($\log P\ O_2$) at temperatures 1200–1400°C in a narrower range (−3.8 to −9.0 atm) than was possible based on SLAG software (−3.00 to −9.00 atm). These values in both cases are the conditions under which the co-occurrence of metallic Cu and magnetite is possible. The differences are likely due to the different thermodynamic data used to construct the diagrams. The authors further used the lack of delafossite ($CuFeO_2$) and cuprite (Cu_2O) in the slags to conclude that

TABLE 3 Comparison of oxygen and sulfur fugacity calculated using the SLAG program with the fugacity for the (logK) values given in Barin (1993).

	Oxygen fugacity [logP O_2]									
	Fe/FeO		Pb/PbO		Zn/ZnO		Cu/Cu_2O		Mn/MnO	
T [K]	SLAG	Barin (1993)	SLAG	Barin (1993)	SLAG	Barin (1993)	SLAG	Barin (1993)	SLAG	Barin (1993)
1000	−21.6	−21.62	−12.4	−12.46	−25.92	−25.92	−9.98	−9.98	−32.52	−32.58
1100	−19.1	−19.06	−10.46	−10.4	−22.6	−22.55	−8.41	−8.39	−28.98	−28.91
1200	−16.94	−16.92	−8.84	−8.77	−19.42	−19.55	−7.05	−7.07	−25.92	−25.85
1300	−15.1	−15.11	−7.49	−7.5	−16.45	−16.41	−5.89	−5.96	−23.27	−23.27
1400	−13.53	−13.56	−6.38	−6.43	−13.75	−13.72	−4.91	−4.95	−21	−21.05
1500	−12.19	−12.22	−5.46	−5.51	−11.34	−11.41	−4.09	−4	−19.03	−19.1
1600	−11.04	−11.05	−4.7	−4.71	−9.38	−9.38	−3.41	−3.41	−17.32	−17.36
1700	−10.06	−10.07	−4.05	−4.02	−7.61	−7.61	−2.86	−2.94	−15.81	−15.81
1800	−9.19	−9.24	−3.47	−3.4	−6.03	−6.03	−2.41	−2.52	−14.45	−14.42
1900	−8.4	−8.46	−2.92	−2.86	−4.63	−4.63	−2.04	−2.15	−13.19	−13.19
2000	−7.66	−7.76	−2.36	−2.37	−3.37	−3.37	−1.74	−1.83	−11.97	−12.07
	Sulfur fugacity [logP S_2]									
	Fe/FeS		Pb/PbS		Zn/ZnS		Cu/Cu_2S		Mn/MnS	
T [K]	SLAG	Barin (1993)	SLAG	Barin (1993)	SLAG	Barin (1993)	SLAG	Barin (1993)	SLAG	Barin (1993)
1000	−10.22	−10.2	−7.84	−7.84	−17.49	−17.49	−10.15	−10.25	−22.17	−22.22
1100	−8.71	−8.72	−6.28	−6.29	−15.08	−15.02	−9.08	−9.03	−19.63	−19.57
1200	−7.44	−7.47	−4.99	−5.01	−12.65	−12.78	−8.1	−8.02	−17.42	−17.36
1300	−6.4	−6.42	−3.93	−3.93	−10.31	−10.27	−7.2	−7.16	−15.5	−15.49
1400	−5.54	−5.52	−3.05	−3.02	−8.15	−8.13	−6.38	−6.36	−13.84	−13.89
1500	−4.83	−4.81	−2.32	−2.33	−6.19	−6.29	−5.65	−5.66	−12.41	−12.48
1600	−4.24	−4.28	−1.72	−1.73	−4.68	−4.68	−5.01	−5.04	−11.16	−11.2
1700	−3.75	−3.81	−1.21	−1.21	−3.27	−3.27	−4.45	−4.5	−10.07	−10.06
1800	−3.32	−3.39	−0.77	−0.75	−2.02	−2.02	−3.98	−4.02	−9.1	−9.04
1900	−2.91	−2.98	−0.38	−0.35	−0.91	−0.91	−3.6	−3.6	−8.23	−8.21
2000	−2.51	−2.61	−0.03	0.01	0.08	0.09	−3.3	−3.22	−7.41	−7.47

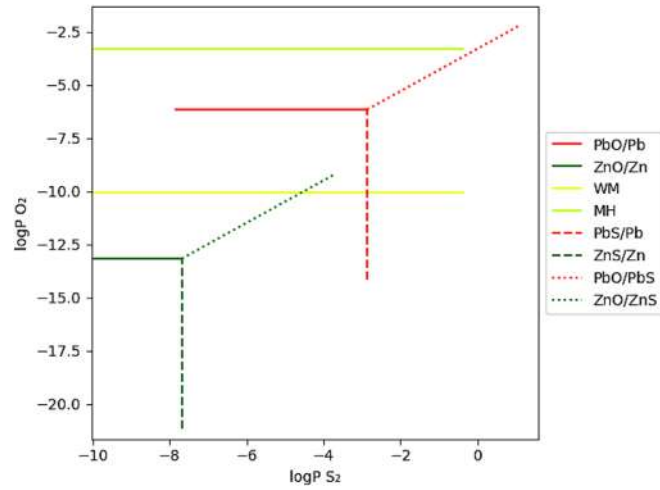

FIGURE 3 Predominance area diagram generated for a temperature of 1150°C using SLAG software.

the conditions at 1200°C may have been more reducing than suggested by the Ellingham Diagram (−4.5 to −9.5 atm). However, most likely due to the lack of appropriate diagrams, this was only possible for a temperature of 1200°C.

Other values

RII is a parameter used to compare slags after iron production regarding oxidation–reduction conditions (Charlton & Humphris, 2019; Zou et al., 2022) and, indirectly, the efficiency of the process. A value equal to 1 indicates that the amount of FeO and SiO_2 in the melt allowed all FeO to be bound within fayalite (Fe_2SiO_4). If the value is below 1, wüstite (FeO) should occur within the slags as the amount of unreduced FeO is too high to be incorporated within the fayalite structure. Values above 1 may indicate a more reductive environment and more efficient process where less FeO entered the slags, resulting in excess SiO_2 in the slags. Only components such as SiO_2, FeO, and MnO are considered during the calculation (Charlton et al., 2010; Crabb, 2018). This value only roughly describes the oxidation–reduction conditions during smelting. Differences in the amount of SiO_2, FeO, and MnO may be due to the type of deposit or fluxes used. Nonetheless, it can be used effectively for slags produced by a similar process and using similar deposits (Crabb, 2018). Although RII is a value relating to oxidation–reduction conditions, it depends on the chemical composition; thus, it was decided to include it in the tab with the chemical composition of slags.

Glass transition temperature (Tg) is the temperature separating the liquid (relaxed) from the glassy (unrelaxed) state. In the SLAG software, Tg is the temperature at which the melt reaches a viscosity of 10^{12} Pa·s (Debenedetti & Stillinger, 2001; Giordano et al., 2008; Woźniak & Skorek, 2017). Melt fragility is a measure of the sensitivity of liquid structure and flow properties to changes in temperature (Giordano et al., 2008). Based on fragility, liquids are divided into strong and fragile (Debenedetti & Stillinger, 2001). Tg and melt fragility can be applied to reconstruct historical glass production processes. Because glass annealing is necessary to eliminate stresses that could damage or destroy glass, it also had to be used in historical times. The annealing process is conducted at a temperature high enough to eliminate stresses and yet low enough to prevent the deformation of the final product (Woźniak & Skorek, 2017). To

determine at what temperature this production stage was carried out, we can use glass transition temperature because, at this temperature, the viscosity of the melt is sufficiently high to remodel the crystal lattice (Woźniak & Skorek, 2017). Because the ability to produce glass also depends on melt fragility (Debenedetti & Stillinger, 2001), it should also be determined when reconstructing the historical glass production processes.

SUMMARY

The SLAG software is an easy-to-use tool for precise and efficient recreations of conditions during historical smelting processes based on the slag properties. The software calculates the most important parameters during smelting. The comparison of the results derived from the SLAG software and the data presented by the authors validates the efficacy of this tool in assessing parameters like liquidus temperature, melt viscosity, and oxidation–reduction conditions. By selecting the appropriate model for calculating temperature and viscosity, we can obtain reliable results, the precision of which is often higher than that obtained using other tools. However, it should be remembered that any deviations may result in erroneous results. Some of the models used in the SLAG software are very sensitive to any deviation from their range of applicability regarding chemical composition. The advantage of SLAG software is also the ability to create PAD for any temperature, which eliminates limitations related to the availability of diagrams in the literature. Moreover, The included viscosity model designed for natural rocks allows SLAG to calculate the viscosity of natural melts.

ACKNOWLEDGEMENTS

This study was supported by the National Science Center (NCN) grant no. 2019/35/O/ST10/00313.

DATA AVAILABILITY STATEMENT

The data that support the findings of the study are given in the tables and figures within the main text. This study brought together existing data from several different sources, which are cited throughout.

ORCID

Krzysztof Kupczak https://orcid.org/0000-0002-3395-9547
Rafał Warchulski https://orcid.org/0000-0002-0508-347X

REFERENCES

Addis, A., Angelini, I., Nimis, P., & Artioli, G. (2016). Late Bronze Age copper smelting slags from Luserna (Trentino, Italy): Interpretation of the metallurgical process. *Archaeometry*, *58*(1), 96–114. https://doi.org/10.1111/arcm.12160

Altman, R., Stavropoulos, G., Parameswaran, K., & Goel, R. P. (1985). Viscosity measurements of industrial lead blast furnace slags. In *Physical Chemistry of Extractive Metallurgy. Proceedings of an International Symposium held at the AIME Annual Meeting* (pp. 97–116).

Bachmann, H. G., Lutz, C., & Thiemann, U. (1989). Schlackenviskositäten. In A. Hauptmann, E. Pernicka, & G. A. Wagner (Eds.), *Archäometallurgie in der Alten Welt – Old World archaeometallurgy. Der Anschnitt, Beiheft 7* (pp. 137–140). Bochum::Verlag Glückauf GmbH.

Barin, I. (1993). *Thermochemical data of pure substances* (Vol. 2) (p. 1523). VCH.

Bassiakos, Y., & Catapotis, M. (2006). Reconstruction of the copper smelting process based on the analysis of ore and slag samples. *Hesperia Supplements*, *36*, 329–353.

Berger, D., Brügmann, G., Friedrich, R., Lutz, J., Meyer, H.-P., & Pernicka, E. (2022). Shiny bronze in glassy matter: An inconspicuous piece of slag from the Bronze Age mining site of Mušiston (Tajikistan) and its significance for the development of tin metallurgy in Central Asia. *Archaeological and Anthropological Sciences*, *14*(8), 150. https://doi.org/10.1007/s12520-022-01606-2

Bielenin, K. (1992). *Starożytne górnictwo i hutnictwo żelaza w Górach Świętokrzyskich* (Wyd II ed.). Kieleckie Towarzystwo Naukowe.

Cadet, M., Tereygeol, F., Sayavongkhamdy, T., Souksavatdy, V., Luangkhoth, T., Chang, N., Dillmann, P., & Pryce, T. O. (2021). Late prehistoric copper smelting in the Lao PDR: Experimental reconstruction based on the Vilabouly Complex evidence. *Journal of Archaeological Science: Reports*, *37*, 102932. https://doi.org/10.1016/j.jasrep.2021.102932

Charlton, M., & Humphris, J. (2019). Exploring ironmaking practices at Meroe, Sudan—A comparative analysis of archaeological and experimental data. *Archaeological and Anthropological Sciences*, *11*, 895–912. https://doi.org/10.1007/s12520-017-0578-2

Charlton, M. F., Crew, P., Rehren, T., & Shennan, S. J. (2010). Explaining the evolution of ironmaking recipes—An example from northwest Wales. *Journal of Anthropological Archaeology*, *29*(3), 352–367. https://doi.org/10.1016/j.jaa.2010.05.001

Chevrel, M. O., Giordano, D., Potuzak, M., Courtial, P., & Dingwell, D. B. (2013). Physical properties of CaAl2Si2O8–CaMgSi2O6–FeO–Fe2O3 melts: Analogues for extra-terrestrial basalt. *Chemical Geology*, *346*, 93–105. https://doi.org/10.1016/j.chemgeo.2012.09.004

Crabb, S. (2018). How did the iron industry in Southern Britain change from the Iron Age to the Roman period? (PhD Thesis). University of Oxford.

Craddock, P. T. (1995). *Early metal mining and production*. Edinburgh University Press.

Davenport, W. G., King, M. J., Schlesinger, M. E., & Biswas, A. K. (2002). *Extractive metallurgy of copper*. Elsevier.

de Capitani, C., & Petrakakis, K. (2010). The computation of equilibrium assemblage diagrams with Theriak/Domino software. *American Mineralogist*, *95*(7), 1006–1016. https://doi.org/10.2138/am.2010.3354

Debenedetti, P. G., & Stillinger, F. H. (2001). Supercooled liquids and the glass transition. *Nature*, *410*(6825), 259–267. https://doi.org/10.1038/35065704

Derkowska, K., Świerk, M., & Nowak, K. (2021). Reconstruction of copper smelting technology based on 18–20th-century slag remains from the Old Copper Basin, Poland. *Minerals*, *11*(9), 926. https://doi.org/10.3390/min11090926

Dong, J., Zhang, D., & Gan, L. (2019). An empirical formula for accurate calculation of liquidus temperature of blast furnace slags in SiO2–Al2O3–CaO–MgO system. *Ironmaking & Steelmaking*, *46*(1), 71–74. https://doi.org/10.1080/03019233.2017.1340545

Ettler, V., Červinka, R., & Johan, Z. (2009). Mineralogy of medieval slags from lead and silver smelting (Bohutín, Příbram district, Czech Republic): Towards estimation of historical smelting conditions. *Archaeometry*, *51*(6), 987–1007. https://doi.org/10.1111/j.1475-4754.2008.00455.x

Ghiorso, M. S., & Gualda, G. A. (2015). An H_2O–CO_2 mixed fluid saturation model compatible with rhyolite-MELTS. *Contributions to Mineralogy and Petrology*, *169*, 1–30. https://doi.org/10.1007/s00410-015-1141-8

Giacometti, F., Rebay, G., Riccardi, M. P., Tarantino, S. C., Tizzoni, C. C., & Tizzoni, M. (2014). Iron Age silicate slags from Val Malenco (Italy): The role of textural and compositional studies in the reconstruction of smelting conditions. *Periodico di Mineralogia*, *83*(3), 329–344. https://doi.org/10.2451/2014PM0018

Giordano, D., Mangiacapra, A., Potuzak, M., Russell, J. K., Romano, C., Dingwell, D. B., & Di Muro, A. (2006). An expanded non-Arrhenian model for silicate melt viscosity: A treatment for metaluminous, peraluminous and peralkaline liquids. *Chemical Geology*, *229*(1–3), 42–56. https://doi.org/10.1016/j.chemgeo.2006.01.007

Giordano, D., Russell, J. K., & Dingwell, D. B. (2008). Viscosity of magmatic liquids: A model. *Earth and Planetary Science Letters*, *271*(1–4), 123–134. https://doi.org/10.1016/j.epsl.2008.03.038

Github. (2023). slagKupczak. Available at https://github.com/slagKupczak/SLAG.git [Accessed March 23, 2023].

Gualda, G. A., Ghiorso, M. S., Lemons, R. V., & Carley, T. L. (2012). Rhyolite-MELTS: A modified calibration of MELTS optimized for silica-rich, fluid-bearing magmatic systems. *Journal of Petrology*, *53*(5), 875–890. https://doi.org/10.1093/petrology/egr080

Hasegawa, M. (2014). Ellingham diagram. In *Seetharaman, S., Treatise on process metallurgy* (pp. 507–516). Oxford: Elsevier. https://doi.org/10.1016/B978-0-08-096986-2.00032-1

Kądziołka, K., Pietranik, A., Kierczak, J., Potysz, A., & Stolarczyk, T. (2020). Towards better reconstruction of smelting temperatures: Methodological review and the case of historical K-rich Cu-slags from the Old Copper Basin, Poland. *Journal of Archaeological Science*, *118*, 105142. https://doi.org/10.1016/j.jas.2020.105142

Khatibi, A. (2008). Distribution of elements in slag, matte, and speiss during settling operation. Independent thesis Advanced level.

Kupczak, K., Warchulski, R., Dulski, M., & Środek, D. (2020). Chemical and phase reactions on the contact between refractory materials and slags, a case from the 19th century Zn-Pb smelter in Ruda Śląska, Poland. *Minerals*, *10*(11), 1006. https://doi.org/10.3390/min10111006

Kupczak, K., Warchulski, R., & Gawęda, A. (2023). Reconstruction of smelting conditions during 16th-to 18th-century copper ore processing in the Kielce region (Old Polish Industrial District) based on slags from Miedziana Góra, Poland. *Archaeometry*, *65*, 547–569. https://doi.org/10.1111/arcm.12837

Lindsley, D. H. (Ed.). (2018). *Oxide minerals: Petrologic and magnetic significance* (Vol. 25). Berlin: Walter de Gruyter GmbH & Co KG.

Mantha, D., & Reddy, R. G. (2005). Viscosities of lead-copper converter slags. *High Temperature Materials and Processes*, *24*(3), 153–158. https://doi.org/10.1515/HTMP.2005.24.3.153

Milisauskas, S. (2011). *European prehistory: A survey*. Springer Science & Business Media. https://doi.org/10.1007/978-1-4419-6633-9

Mills, K. (2011). The estimation of slag properties. *Southern African Pyrometallurgy*, *7*(3), 35–42.

Mills, K. C., Fox, A. B., Li, Z., & Thackray, R. P. (2005). Performance and properties of mould fluxes. *Ironmaking & Steelmaking*, *32*(1), 26–34. https://doi.org/10.1179/174328105X15788

Myers, J., & Eugster, H. P. (1983). The system Fe-Si-O: Oxygen buffer calibrations to 1,500K. *Contributions to Mineralogy and Petrology*, *82*, 75–90. https://doi.org/10.1007/BF00371177

Pater, Z. (2014). *Podstawy metalurgii i odlewnictwa*. Politechnika Lubelska.

Patterson, C. C. (1971). Native copper, silver, and gold accessible to early metallurgists. *American Antiquity*, *36*(3), 286–321. https://doi.org/10.2307/277716

Potysz, A., & Kierczak, J. (2019). Prospective (bio) leaching of historical copper slags as an alternative to their disposal. *Minerals*, *9*(9), 542. https://doi.org/10.3390/min9090542

Potysz, A., van Hullebusch, E. D., Kierczak, J., Grybos, M., Lens, P. N., & Guibaud, G. (2015). Copper metallurgical slags—Current knowledge and fate: A review. *Critical Reviews in Environmental Science and Technology*, *45*, 2424–2488. https://doi.org/10.1080/10643389.2015.1046769

Rehren, T., Boscher, L., & Pernicka, E. (2012). Large scale smelting of speiss and arsenical copper at Early Bronze Age Arisman, Iran. *Journal of Archaeological Science*, *39*(6), 1717–1727. https://doi.org/10.1016/j.jas.2012.01.009

Roberts, B. W., Thornton, C. P., & Pigott, V. C. (2009). Development of metallurgy in Eurasia. *Antiquity*, *83*(322), 1012–1022. https://doi.org/10.1017/S0003598X00099312

Schriner, D. (2018). *Experimental investigation of fundamental viscosity, density, and leaching characteristics of sodium-iron-silicate slags*. Colorado School of Mines.

Seyrankaya, A., & Canbazoğlu, M. (2021). Recovery of cobalt, copper and zinc from Küre-Kastamonu historical copper slag by high pressure oxidative acid leaching. *Russian Journal of Non-Ferrous Metals*, *62*, 390–402. https://doi.org/10.3103/S1067821221040131

Shatynski, S. R. (1977). The thermochemistry of transition metal sulfides. *Oxidation of Metals*, *11*, 307–320. https://doi.org/10.1007/BF00608014

Song, Q., Guo, M.-Z., Wang, L., & Ling, T.-C. (2021). Use of steel slag as sustainable construction materials: A review of accelerated carbonation treatment. *Resources, Conservation and Recycling*, *173*, 105740. https://doi.org/10.1016/j.resconrec.2021.105740

Turkdogan, E. T. (2000). Assessment of P_2O_5 activity coefficients in molten slags. *ISIJ International*, *40*(10), 964–970. https://doi.org/10.2355/isijinternational.40.964

Tylecote, R. F. (1987). *The early history of metallurgy in Europe*. Longman.

Utigard, T. A., & Warczok, A. (1995). Density and viscosity of copperhickel sulphide smelting and converting slags. In W. J. Chen, C. Dim, A. Luraschi, & P. J. Mackey (Eds.), *Copper 95-Cobre 95 proceedings of the third international conference, Vol. l V Pyrometallurgy of copper* (pp. 423–437). The Metallurgical Society of CIM.

Wang, G. C. (2016). *The utilization of slag in civil infrastructure construction*. Sawston, UK: Woodhead Publishing. https://doi.org/10.1016/B978-0-08-100381-7.00006-9

Wang, X., Geysen, D., Padilla Tinoco, S. V., D'Hoker, N. V. G. T., Van Gerven, T., & Blanpain, B. (2015). Characterisation of copper slag in view of metal recovery. *Minerals Processing and Extractive Metallurgy*, *124*(2), 83–87. https://doi.org/10.1179/1743285515Y.0000000004

Warchulski, R. (2016). Zn-Pb slag crystallization: Evaluating temperature conditions on the basis of geothermometry. *European Journal of Mineralogy*, *28*(2), 375–384. https://doi.org/10.1127/ejm/2015/0027-2496

Warchulski, R., Kupczak, K., Gawęda, A., & Sitko, R. (2022). Complete reconstruction of the process and conditions during gold smelting in the 15th–17th centuries in Złoty Stok based on metallurgical slags. *Archaeometry*, *64*(4), 916–934. https://doi.org/10.1111/arcm.12752

Warchulski, R., Szczuka, M., & Kupczak, K. (2020). Reconstruction of 16th–17th century lead smelting processes on the basis of slag properties: A case study from Sławków, Poland. *Minerals*, *10*(11), 1039. https://doi.org/10.3390/min10111039

Westner, K. J., Klein, S., Sergeev, D., & Müller, M. (2022). Temperature estimates of historical Pb-Ag smelting slags: A multi-methodological approach. *Journal of Archaeological Science: Reports*, *46*, 103654. https://doi.org/10.1016/j.jasrep.2022.103654

Woźniak, M., & Skorek, A. (2017). Optymalizacja procesu odprężania wyrobów szklanych formowanych ręcznie w odprężarce komorowej elektrycznej. *Szkło i Ceramika*, *68*, 11–14.

Xie, F. C., Yin, Z. L., Tan, J., Liu, C. Q., & Zhang, P. M. (2016). Plotting and application of predominance area diagram of Me-SO system based on topological rules. *Journal of Central South University*, *23*(6), 1332–1338. https://doi.org/10.1007/s11771-016-3184-z

Zhang, Z., & Reddy, R. G. (2002). Viscosities of lead silicate slags. *Mining, Metallurgy & Exploration*, *19*, 37–42. https://doi.org/10.1007/BF03402899

Zhao, D., Essene, E. J., & Zhang, Y. (1999). An oxygen barometer for rutile–ilmenite assemblages: oxidation state of metasomatic agents in the mantle. *Earth and Planetary Science Letters*, *166*(3–4), 127–137. https://doi.org/10.1016/s0012-821x(98)00281-7

Zou, G., Meng, Z., Li, Y., Huang, Q., & Cui, C. (2022). From bowl furnaces to small shaft furnaces: New evidence from ancient bloomery iron smelting site at Liuzhuoling in Guangxi, Southern China, ca. 400 to 700 AD. *Archaeological and Anthropological Sciences*, *14*(3), 54. https://doi.org/10.1007/s12520-022-01531-4

SUPPORTING INFORMATION

Additional supporting information can be found online in the Supporting Information section at the end of this article.

How to cite this article: Kupczak, K., & Warchulski, R. (2024). SLAG—software for reconstruction of historical smelting processes based on slag properties. *Archaeometry*, 1–21. https://doi.org/10.1111/arcm.12940

Załącznik nr 9
do pisma okólnego nr 2
Prorektora ds. nauki i finansów
z dnia 19 lutego 2024 r.

Sosnowiec, 20.12.2024
miejscowość, data

Krzysztof Kupczak

imię i nazwisko kandydata

ul. Żywiecka 255, 34-382 Wieprz
adres do korespondencji

506559602
nr telefonu

krzysztof.kupczak@us.edu.pl
adres e-mail

OŚWIADCZENIE OSOBY UBIEGAJĄCEJ SIĘ O WŁASNYM WKŁADZIE W POWSTAWANIE PRACY

Oświadczam, że w pracy:

Kupczak Krzysztof, Warchulski Rafał, Dulski Mateusz, Środek Dorota. 2020. Chemical and phase reactions on the contact between refractory materials and slags, a case from the 19th century Zn-Pb smelter in Ruda Śląska, Poland; Minerals; 10(11)

Mój udział polegał na poborze prób, studium literaturowym, przygotowaniu prób do analiz, wykonaniu obserwacji mikroskopowych, analizie i interpretacja danych XRD, XRF, ICP-MS, EPMA, większościowym autorstwie tekstu publikacji oraz przygotowaniu figur i tabel.

Oświadczam, że w pracy:

Warchulski Rafał, Szczuka Monika, **Kupczak Krzysztof.** 2020. Reconstruction of 16th–17th century lead smelting processes on the basis of slag properties: A case study from Sławków, Poland; Minerals; 10(11)

Mój udział polegał na studium literaturowym, przygotowaniu prób do analiz, interpretacji wyników analiz XRD, rekonstrukcji pieca w programie AutoCAD oraz mniejszościowym autorstwie tekstu publikacji.

Oświadczam, że w pracy:

Warchulski Rafał, **Kupczak Krzysztof,** Gawęda Aleksandra, Sitko Rafał. 2022. Complete reconstruction of the process and conditions during gold smelting in the 15th–17th centuries in Złoty Stok based on metallurgical slags; Archaeometry; 64(4); 916-934

Mój udział polegał na poborze prób, studium literaturowym, przygotowaniu prób do analiz, interpretacji danych EPMA, mniejszościowym autorstwie tekstu publikacji, oraz współautorstwie grafik.

Oświadczam, że w pracy:

Kupczak Krzysztof, Warchulski Rafał, Gawęda Aleksandra. 2023. Reconstruction of smelting conditions during 16th-to 18th-century copper ore processing in the Kielce region (Old Polish Industrial District) based on slags from Miedziana Góra, Poland; Archaeometry; 65(3); 547-569

Mój udział polegał na poborze prób, studium literaturowym, przygotowaniu prób do analiz, wykonaniu obserwacji mikroskopowych, analizie i interpretacji danych XRD, XRF, ICP-MS, EPMA, współprowadzeniu eksperymentów wysokotemperaturowych, większościowym autorstwie tekstu publikacji oraz przygotowaniu grafik oraz tabel.

Oświadczam, że w pracy:

Kupczak Krzysztof, Warchulski Rafał, Gawęda Aleksandra, Ślęzak Marta, Migas Piotr. 2024. The use of predominance area diagrams (PAD) to determine the oxygen and sulfur fugacities prevailing during historical metallurgical processes: the case of fifteenth to seventeenth century copper slags from Polichno (Old Polish industrial district); Heritage Science; 2024; 12(1); 49

Mój udział polegał na poborze prób, studium literaturowym, przygotowaniu prób do analiz, wykonaniu obserwacji mikroskopowych, analizie i interpretacja danych XRF oraz EPMA, współprowadzeniu eksperymentów wysokotemperaturowych w piecu laboratoryjnym, większościowym autorstwie tekstu publikacji oraz przygotowaniu grafik i tabel.

Oświadczam, że w pracy:

Kupczak Krzysztof, Warchulski Rafał, Gawęda Aleksandra, Janiec Jan. 2024. Bloomery iron production in the Holy Cross Mountains (Poland) area during the Roman period: conditions during the metallurgical process and their uniformity between locations. Heritage Science; 12(1), 147

Mój udział polegał na studium literaturowym, przygotowaniu prób do analiz, wykonaniu obserwacji mikroskopowych, analizie i interpretacja danych XRD, XRF, EPMA, większościowym autorstwie tekstu publikacji oraz przygotowaniu grafik i tabel

Oświadczam, że w pracy:

Kupczak Krzysztof, Warchulski Rafał. 2024. SLAG—software for reconstruction of historical smelting processes based on slag properties. Archaeometry; 66(4); 803-823

Mój udział polegał na studium literaturowym, przygotowaniu kodu w języku Python, testowaniu oprogramowania, większościowym autorstwie tekstu publikacji oraz przygotowaniu grafik i tabel.

Krzysztof Kupczak

.....

podpis

Załącznik nr 10
do pisma okólnego nr 2
Prorektora ds. nauki i finansów
z dnia 19 lutego 2024 r.

OŚWIADCZENIE

WSPÓŁAUTORA OSOBY UBIEGAJĄCEJ SIĘ O WŁASNYM WKŁADZIE W POWSTAWANIE PRACY

Sosnowiec, dnia 20.12.2024

dr Rafał Warchulski, prof. UŚ
Imię i nazwisko współautora publikacji

Uniwersytet Śląski, Wydział Nauk Przyrodniczych, Instytut Nauk o Ziemi, Będzińska 60, Sosnowiec
Afiliacja

OŚWIADCZENIE

Oświadczam, że w pracy:
Kupczak Krzysztof, **Warchulski Rafał,** Dulski Mateusz, Środek Dorota. 2020. Chemical and phase reactions on the contact between refractory materials and slags, a case from the 19th century Zn-Pb smelter in Ruda Śląska, Poland; Minerals; 10(11); 1006

Mój udział polegał na prowadzeniu prac terenowych, konsultacjach podczas prac laboratoryjnych i interpretacji wyników, nadzorowaniu prac oraz pomocy przy opracowaniu końcowego manuskryptu do publikacji w czasopiśmie naukowym.

Oświadczam, że w pracy:
Warchulski Rafał, Szczuka Monika, Kupczak Krzysztof. 2020. Reconstruction of 16th–17th century lead smelting processes on the basis of slag properties: A case study from Sławków, Poland; Minerals; 10(11)

Mój udział polegał na administracji projektu, nadzorem nad pracami, opracowaniu metodyki prac, współrealizacji prac terenowych, współrealizacji prac laboratoryjnych, interpretacji wyników i większościowym autorstwie finalnego tekstu publikacji, oraz korekcie tekstu po recenzjach.

Oświadczam, że w pracy:
Warchulski Rafał, Kupczak Krzysztof, Gawęda Aleksandra Sitko Rafał. 2022. Complete reconstruction of the process and conditions during gold smelting in the 15th–17th centuries in Złoty Stok based on metallurgical slags; Archaeometry; 64(4); 916-934

Mój udział polegał na administracji projektu, nadzorem nad pracami, opracowaniu metodyki prac, współrealizacji prac terenowych, współrealizacji prac laboratoryjnych, interpretacji wyników i większościowym autorstwie finalnego tekstu publikacji, oraz korekcie tekstu po recenzjach.

Oświadczam, że w pracy:
Kupczak Krzysztof, **Warchulski Rafał,** Gawęda Aleksandra. 2023. Reconstruction of smelting conditions during 16th-to 18th-century copper ore processing in the Kielce region (Old Polish Industrial District) based on slags from Miedziana Góra, Poland; Archaeometry; 65(3); 547-569

Mój udział polegał na prowadzeniu prac terenowych, realizacji części prac laboratoryjnych i interpretacji wyników, oraz mniejszościowym autorstwie końcowego manuskryptu do publikacji w czasopiśmie naukowym.

Oświadczam, że w pracy:
Kupczak Krzysztof, **Warchulski Rafał,** Gawęda Aleksandra, Ślęzak Marta, Migas Piotr. 2024. The use of predominance area diagrams (PAD) to determine the oxygen and sulfur fugacities prevailing during historical metallurgical processes: the case of fifteenth to seventeenth century copper slags from Polichno (Old Polish industrial district); Heritage Science; 2024; 12(1); 49

Mój udział polegał na prowadzeniu prac terenowych, realizacji części prac laboratoryjnych i interpretacji wyników, oraz mniejszościowym autorstwie końcowego manuskryptu do publikacji w czasopiśmie naukowym.

Oświadczam, że w pracy:
Kupczak Krzysztof, **Warchulski Rafał,** Gawęda Aleksandra, Janiec Jan. 2024. Bloomery iron production in the Holy Cross Mountains (Poland) area during the Roman period: conditions during the metallurgical process and their uniformity between locations. Heritage Science; 12(1), 147

Mój udział polegał na prowadzeniu prac terenowych, realizacji części prac laboratoryjnych i interpretacji wyników, oraz mniejszościowym autorstwie końcowego manuskryptu do publikacji w czasopiśmie naukowym.

Oświadczam, że w pracy:
Kupczak Krzysztof, **Warchulski Rafał.** 2024. SLAG—software for reconstruction of historical smelting processes based on slag properties. Archaeometry; 66(4); 803-823

Mój udział polegał na konsultacji wyników i pomocy przy opracowaniu końcowego manuskryptu do publikacji w czasopiśmie naukowym.

.....

Podpis współautora publikacji

Załącznik nr 10
do pisma okólnego nr 2
Prorektora ds. nauki i finansów
z dnia 19 lutego 2024 r.

OŚWIADCZENIE

WSPÓŁAUTORA OSOBY UBIEGAJĄEJ SIĘ O WŁASNYM WKŁADZIE W POWSTAWANIE PRACY

Sosnowiec, dnia 20.12.2024

prof. dr hab. Aleksandra Gawęda
Imię i nazwisko współautora publikacji

Uniwersytet Śląski, Wydział Nauk Przyrodniczych, Instytut Nauk o Ziemi, Będzińska 60, Sosnowiec
Afiliacja

OŚWIADCZENIE

Oświadczam, że w pracy:
Warchulski Rafał, Kupczak Krzysztof, **Gawęda Aleksandra,** Sitko Rafał. 2022. Complete reconstruction of the process and conditions during gold smelting in the 15th–17th centuries in Złoty Stok based on metallurgical slags; Archaeometry; 64(4); 916-934

Mój udział polegał na prowadzeniu badań terenowych, nadzorowaniu prac laboratoryjnych oraz pomocy przy opracowaniu końcowego manuskryptu do publikacji w czasopiśmie naukowym.

Oświadczam, że w pracy:
Kupczak Krzysztof, Warchulski Rafał, **Gawęda Aleksandra.** 2023. Reconstruction of smelting conditions during 16th-to 18th-century copper ore processing in the Kielce region (Old Polish Industrial District) based on slags from Miedziana Góra, Poland; Archaeometry; 65(3)

Mój udział polegał na prowadzeniu badań terenowych, nadzorowaniu prac laboratoryjnych oraz pomocy przy opracowaniu końcowego manuskryptu do publikacji w czasopiśmie naukowym.

Oświadczam, że w pracy:
Kupczak Krzysztof, Warchulski Rafał, **Gawęda Aleksandra,** Ślęzak Marta, Migas Piotr. 2024. The use of predominance area diagrams (PAD) to determine the oxygen and sulfur fugacities prevailing during historical metallurgical processes: the case of fifteenth to seventeenth century copper slags from Polichno (Old Polish industrial district); Heritage Science; 2024; 12(1); 49

Mój udział polegał na prowadzeniu badań terenowych, nadzorowaniu prac laboratoryjnych oraz pomocy przy opracowaniu końcowego manuskryptu do publikacji w czasopiśmie naukowym

Oświadczam, że w pracy:
Kupczak Krzysztof, Warchulski Rafał, **Gawęda Aleksandra,** Janiec Jan. 2024. Bloomery iron production in the Holy Cross Mountains (Poland) area during the Roman period: conditions during the metallurgical process and their uniformity between locations. Heritage Science; 12(1), 147

Mój udział polegał na nadzorowaniu prac laboratoryjnych oraz pomocy przy opracowaniu końcowego manuskryptu do publikacji w czasopiśmie naukowym

.....

Podpis współautora publikacji

Załącznik nr 10
do pisma okólnego nr 2
Prorektora ds. nauki i finansów
z dnia 19 lutego 2024 r.

OŚWIADCZENIE

WSPÓŁAUTORA OSOBY UBIEGAJĄCEJ SIĘ O WŁASNYM WKŁADZIE W POWSTAWANIE PRACY

Sosnowiec, dnia 20.12.2024

mgr inż. Monika Szczuka
Imię i nazwisko współautora publikacji

Akademia Górniczo-Hutnicza w Krakowie, Wydział Geologii, Geofizyki i Ochrony Środowiska, Katedra Geologii Ogólnej i Geoturystyki, Al. A. Mickiewicza 30, 30-059 Kraków
Afiliacja

OŚWIADCZENIE

Oświadczam, że w pracy:

Warchulski Rafał, **Szczuka Monika**, Kupczak Krzysztof. 2020. Reconstruction of 16th–17th century lead smelting processes on the basis of slag properties: A case study from Sławków, Poland; Minerals; 10(11)

Mój udział polegał na współrealizacji prac terenowych, współrealizacji prac laboratoryjnych, interpretacji wyników i mniejszościowym autorstwie finalnego tekstu publikacji.

Podpis współautora publikacji

Załącznik nr 10
do pisma okólnego nr 2
Prorektora ds. nauki i finansów
z dnia 19 lutego 2024 r.

OŚWIADCZENIE

WSPÓŁAUTORA OSOBY UBIEGAJĄEJ SIĘ O WŁASNYM WKŁADZIE W POWSTAWANIE PRACY

Sosnowiec, dnia 20.12.2024

dr Dorota Środek
Imię i nazwisko współautora publikacji

Uniwersytet Śląski, Wydział Nauk Przyrodniczych, Instytut Nauk o Ziemi, Będzińska 60, Sosnowiec
Afiliacja

OŚWIADCZENIE

Oświadczam, że w pracy:
Kupczak Krzysztof, Warchulski Rafał, Dulski Mateusz, **Środek Dorota.** 2020. Chemical and phase reactions on the contact between refractory materials and slags, a case from the 19th century Zn-Pb smelter in Ruda Śląska, Poland; Minerals; 10(11); 1006

Mój udział polegał na współudziale podczas wykonywania analiz z wykorzystaniem mikroskopu skaningowego i interpretacji otrzymanych wyników.

Dorota Środek

Podpis współautora publikacji

Załącznik nr 10
do pisma okólnego nr 2
Prorektora ds. nauki i finansów
z dnia 19 lutego 2024 r.

OŚWIADCZENIE

WSPÓŁAUTORA OSOBY UBIEGAJĄEJ SIĘ O WŁASNYM WKŁADZIE W POWSTAWANIE PRACY

Sosnowiec, dnia 18.11.2024

dr hab. Mateusz Dulski, prof. UŚ
Imię i nazwisko współautora publikacji

Uniwersytet Śląski, Wydział Nauk Ścisłych i Technicznych
Afiliacja

OŚWIADCZENIE

Oświadczam, że w pracy:
Kupczak Krzysztof, Warchulski Rafał, **Dulski Mateusz,** Środek Dorota. 2020. Chemical and phase reactions on the contact between refractory materials and slags, a case from the 19th century Zn-Pb smelter in Ruda Śląska, Poland; Minerals; 10(11); 1006

Mój udział polegał na wykonaniu analiz z wykorzystaniem spektroskopii Ramana i interpretacji otrzymanych wyników.

.....

Podpis współautora publikacji

Załącznik nr 10
do pisma okólnego nr 2
Prorektora ds. nauki i finansów
z dnia 19 lutego 2024 r.

OŚWIADCZENIE

WSPÓŁAUTORA OSOBY UBIEGAJĄCEJ SIĘ O WŁASNYM WKŁADZIE W POWSTAWANIE PRACY

Kraków, dnia 17.12.2024 r.

dr inż. Marta Ślęzak
Imię i nazwisko współautora publikacji

Akademia Górniczo-Hutnicza im. Stanisława Staszica w Krakowie, Wydział Inżynierii Metali i Informatyki Przemysłowej
Afiliacja

OŚWIADCZENIE

Oświadczam, że w pracy:
Kupczak Krzysztof, Warchulski Rafał, Gawęda Aleksandra, **Ślęzak Marta,** Migas Piotr. 2024. The use of predominance area diagrams (PAD) to determine the oxygen and sulfur fugacities prevailing during historical metallurgical processes: the case of fifteenth to seventeenth century copper slags from Polichno (Old Polish industrial district); Heritage Science; 2024; 12(1); 49

Mój udział polegał na wykonaniu eksperymentów z wykorzystaniem mikroskopu wysokotemperaturowego oraz interpretacji otrzymanych wyników.

.....

Podpis współautora publikacji

Załącznik nr 10
do pisma okólnego nr 2
Prorektora ds. nauki i finansów
z dnia 19 lutego 2024 r.

OŚWIADCZENIE

WSPÓŁAUTORA OSOBY UBIEGAJĄCEJ SIĘ O WŁASNYM WKŁADZIE W POWSTAWANIE PRACY

Kraków, dnia 17.12.2024 r.

dr hab. inż. Piotr Migas
Imię i nazwisko współautora publikacji

Akademia Górniczo-Hutnicza im. Stanisława Staszica w Krakowie, Wydział Inżynierii Metali i Informatyki Przemysłowej
Afiliacja

OŚWIADCZENIE

Oświadczam, że w pracy:
Kupczak Krzysztof, Warchulski Rafał, Gawęda Aleksandra, Ślęzak Marta, **Migas Piotr**. 2024. The use of predominance area diagrams (PAD) to determine the oxygen and sulfur fugacities prevailing during historical metallurgical processes: the case of fifteenth to seventeenth century copper slags from Polichno (Old Polish industrial district); Heritage Science; 2024; 12(1); 49

Mój udział polegał na wykonaniu eksperymentów z wykorzystaniem mikroskopu wysokotemperaturowego oraz interpretacji otrzymanych wyników.

Piotr Migas
.....
Podpis współautora publikacji

Załącznik nr 10
do pisma okólnego nr 2
Prorektora ds. nauki i finansów
z dnia 19 lutego 2024 r.

OŚWIADCZENIE

WSPÓŁAUTORA OSOBY UBIEGAJĄEJ SIĘ O WŁASNYM WKŁADZIE W POWSTAWANIE PRACY

Sosnowiec, dnia 17.12.2024

Jan Janiec
Imię i nazwisko współautora publikacji

.....
Afiliacja

OŚWIADCZENIE

Oświadczam, że w pracy:
Kupczak Krzysztof, Warchulski Rafał, Gawęda Aleksandra, **Janiec Jan**. 2024. Bloomery iron production in the Holy Cross Mountains (Poland) area during the Roman period: conditions during the metallurgical process and their uniformity between locations. Heritage Science; 12(1), 147

Mój udział polegał na przygotowaniu materiału do badań oraz pomocy w studium literaturowym dotyczącym złóż żelaza występujących w rejonie Gór Świętokrzyskich.

.....
Podpis współautora publikacji

Załącznik nr 10
do pisma okólnego nr 2
Prorektora ds. nauki i finansów
z dnia 19 lutego 2024 r.

OŚWIADCZENIE

WSPÓŁAUTORA OSOBY UBIEGAJĄEJ SIĘ O WŁASNYM WKŁADZIE W POWSTAWANIE PRACY

Sosnowiec, dnia 20.12.2024

prof. dr hab. Rafał Sitko
Imię i nazwisko współautora publikacji

Uniwersytet Śląski, Wydział Nauk Ścisłych i Technicznych, Instytutu Chemii
Afiliacja

OŚWIADCZENIE

Oświadczam, że w pracy:
Warchulski Rafał, Kupczak Krzysztof, Gawęda Aleksandra, **Sitko Rafał.** 2022. Complete reconstruction of the process and conditions during gold smelting in the 15th–17th centuries in Złoty Stok based on metallurgical slags; Archaeometry; 64(4); 916-934

Mój udział polegał na wykonaniu analiz zawartości złota w próbkach żużli

.....

Podpis współautora publikacji